

The Pore Pressure, Bulk Density and Lithology Prediction

By

©Olalere Sunday Oloruntobi

A thesis submitted to the School of Graduate Studies
In partial fulfillment of the requirements for the degree of

Doctor of Philosophy
Faculty of Engineering and Applied Science
Memorial University of Newfoundland
St John's, Newfoundland, Canada

October 2019

DEDICATION

This work is dedicated to Almighty God who made heaven and earth. Special thanks to my wife Patience Lucy Oloruntobi who is the solid rock behind my achievement.

ABSTRACT

The pore and fracture pressures are the two most important parameters required for the effective well design. In general, the difference between the two parameters at any given depth dictates the drilling window with no consideration for wellbore stability. While pore pressure prediction from the drilling parameters started in the mid-nineties, very few improvements have been made in these areas when compared to other pore pressure prediction techniques such as seismic and well logs. Pore pressure prediction using the d-exponent method does not consider the effect of bit hydraulic energy on the rate of penetration (ROP). This limits the application of the d-exponent to mostly hard rock environments. Under downhole conditions where the bit hydraulic energy has a significant influence on the ROP (soft rock environments), the d-exponent method may produce inaccurate results. Hence, the primary goal of this research is to develop new pore pressure prediction models from the drilling parameters that incorporate the bit hydraulic energy, making them suitable for any subsurface drilling conditions. The new pore pressure prediction models use the concept of specific energy to predict the onset of overpressure. The concept of specific energy is then extended to the real-time identification of subsurface lithology.

Furthermore, overburden pressure is an important input parameter in pore pressure prediction. Inaccurate prediction of overburden pressure may result in the erroneous prediction of pore pressure which can lead to well control and process safety incidents. In areas where density logs are not available, synthetically derived density logs are used for overburden pressure computations. In this research, an attempt is also made to improve the accuracy of pore pressure prediction by improving the accuracy of overburden pressure computation via improvement in density logs prediction. Finally, since pore and fracture pressures are closely related, an attempt is made to develop a new fracture pressure prediction model for the Niger Delta basin.

ACKNOWLEDGMENTS

I sincerely express my profound gratitude to my supervisor, Dr. Stephen Butt for his care, patience and guidance during my doctoral degree program at the Memorial University of Newfoundland, St John's, Canada. I count it as a great privilege to have worked under his supervision. I will like to acknowledge my co-supervisor Dr. Raghu Chunduru of Shell Exploration and Production Company, Houston, USA for providing great support and encouragement throughout the research work. I also thankfully acknowledge Shell Petroleum Development Company, Port Harcourt, Nigeria for granting me leave of absence to complete the Doctoral degree and providing the necessary field data used in my research. Great appreciation to the Department of Petroleum Resources, Nigeria for approving the field data used in this research. Special thanks to Mr. Richard Ebisike of Shell Petroleum Development Company, Nigeria for his support and mentoring.

TABLE OF CONTENTS

ABSTRACT.....	iii
ACKNOWLEDGMENTS.....	iv
TABLE OF CONTENTS.....	v
List of Tables	viii
List of Figures	ix
List of Acronyms and Symbols	xi
Chapter 1.....	1
1.0 Introduction and Overview	1
1.1 Formation Pore Pressure.....	1
1.2 Formation Pore Pressure Regimes	2
1.2.1 Compaction Disequilibrium (Under-compaction).....	4
1.2.2 Tectonic Activities.....	5
1.2.3 Clay Diagenesis.....	6
1.2.4 Aqua-thermal Expansion	6
1.2.5 Hydrocarbon Generation	6
1.3 Pore Pressure Prediction Techniques	8
1.3.1 Pore Pressure Prediction from Seismic Data.....	11
1.3.2 Pore Pressure Prediction from Well Logs	12
1.3.3 Pore Pressure Prediction from Drilling Parameters.....	21
1.4 Research Objectives.....	28
1.5 Connectivity among the Research Papers	28
1.6 Organization of the Thesis	30
1.7 Reference	30
Chapter 2.....	43
2.0 Overpressure Prediction Using the Hydro-Rotary Specific Energy Concept	43
Preface.....	43

Abstract.....	43
2.1 Introduction.....	44
2.2 Theoretical Background	51
2.3 Methodology	56
2.4 Field Example.....	59
2.5 Discussion.....	66
2.6 Conclusions.....	72
2.7 Reference	73
Chapter 3.....	79
3.0 Energy-based Formation Pressure Prediction	79
Preface.....	79
Abstract.....	79
3.1 Introduction.....	80
3.2 Model Development	92
3.3 Methodology	96
3.4 Field Example.....	97
3.5 Discussion.....	102
3.6 Conclusions.....	105
3.7 Reference	106
Chapter 4.....	114
4.0 The New Formation Bulk Density Predictions for Siliciclastic Rocks	114
Preface.....	114
Abstract.....	114
4.1 Introduction.....	115
4.2 Methodology	120
4.3 Field Examples	122
4.4 Results and discussions.....	126
4.5 Conclusions.....	137

4.6 Reference	138
Chapter 5.....	144
5.0 A New Fracture Pressure Prediction Model for The Niger Delta Basin.....	144
Preface.....	144
Abstract.....	144
5.1 Introduction.....	145
5.2 Field Data.....	155
5.3 Model Development	158
5.4 Model Validation.....	162
5.5 Conclusion	165
5.6 Appendix.....	166
5.7 Reference	168
Chapter 6.....	174
6.0 Real-time Lithology Prediction Using Hydromechanical Specific Energy	174
Preface.....	174
Abstract.....	174
6.1 Introduction.....	175
6.2 Methodology	179
6.3 Field Example.....	184
6.4 Discussion.....	191
6.5 Conclusions	193
6.6 Reference	194
Chapter 7.....	200
7.0 Summary and Recommendations.....	200
7.1 Summary.....	200
7.2 Recommendations	201

List of Tables

Table 2. 1 Merits and limitations of pore pressure prediction methods.....	46
Table 2. 2 The well data summary.....	60
Table 2. 3 The bit data summary.	62
Table 2. 4 Main differences between HRSE and d – exponent.	70
Table 3. 1 The well and bit data summary.....	98
Table 3. 2 Comparison of pore pressure prediction models from drilling parameters.	104
Table 4. 1 The comparison of RMSEs for models under consideration.....	131
Table 5. 1 The pore pressure data for the W 110 well.	163
Table 5. 2 Well data summary	166

List of Figures

Figure 1. 1 The pressure profiles of an onshore well in the Niger Delta.....	7
Figure 1. 2 The acoustic-depth and resistivity-depth plots (Hottmann and Johnson, 1965).	14
Figure 1. 3 The connectivity among the research papers.....	29
Figure 2. 1 Illustration of the HRSE method for pore pressure prediction.....	57
Figure 2. 2 The work flow for the proposed methodology.....	58
Figure 2. 3 Location map for well A.....	59
Figure 2. 4 The well configuration and lithology.	61
Figure 2. 5 The plots of drilling parameters versus depth for well A.....	64
Figure 2. 6 The plots of formation bulk densities, overburden pressure and overburden gradient versus depth for well A.	65
Figure 2. 7 The plots of HRSE, dc – exponent, gamma ray, and shale compressional sonic velocity versus depth for well A.	67
Figure 2. 8 Measured and estimated pore pressure profiles for Well A.	71
Figure 3. 1 Location map for Well A.....	97
Figure 3. 2 The plots of drilling parameters against depth for Well A.	100
Figure 3. 3 The formation bulk density and overburden pressure/gradient profiles for Well A.	101
Figure 3. 4 The HMSE and pore pressure profile for well A	103
Figure 4. 1 The location map for Wells A and B.....	123
Figure 4. 2 The well logs for Well A showing the petrophysical properties of penetrated rocks.	124
Figure 4. 3 The well logs for Well B showing the petrophysical properties of penetrated rocks.	125

Figure 4. 4 The comparison of predicted and measured formation bulk density for various models under consideration (Well A).....	128
Figure 4. 5 The comparison of predicted and measured formation bulk density for various models under consideration (Well B).	129
Figure 4. 6 The residual-depth plots for Wells A and B showing the error profiles.	130
Figure 4. 7 The histograms of the residuals showing the error distributions for various models under consideration (Well A).....	132
Figure 4. 8 The histograms of the residuals showing the error distributions for various models under consideration (Well B).....	133
Figure 4. 9 The overburden gradient profiles using formation bulk density outputs from the new models for Well A.....	135
Figure 4. 10 The overburden gradient profiles using formation bulk density outputs from the Gardner's and Brocher's models for Well A.....	136
Figure 5 1: Location map for some wells used in model development.	157
Figure 5 2: The plot of formation fracture pressure against depth	159
Figure 5 3: Fracture pressure differential versus pore pressure differential.	161
Figure 5 4: Comparison of predicted and measured fracture pressure for well W110	164
Figure 6 1: The location map for Well A.....	185
Figure 6 2: The plots of drilling parameters and wellbore pressures versus depth for Well A (Interval 1).	186
Figure 6 3: The plots of drilling parameters and wellbore pressures versus depth for Well A (Interval 2).	187
Figure 6 4: The offset well data used to calibrate ϕ_o and k	189
Figure 6 5: The GR-depth, VR-depth and HMSE-depth plots for Well A.....	192

List of Acronyms and Symbols

ϕ_o	surface/mudline clay porosity
ΔP_b	bit pressure drop
Δt_m	shale matrix compressional transit time with zero porosity
Δt_{ml}	mudline compressional transit time
Δt_n	normal compaction shale travel time at a given depth
Δt_o	observed shale travel time at a given depth
Δt_{on}	observed compressional transit time in the normally pressured intervals
ρ_b	formation bulk density
ρ_{fl}	saturating fluid density
ρ_{ma}	sand matrix density
ρ_{sh}	shale matrix density
σ_e	vertical effective stress
σ_H	maximum horizontal stress
σ_h	minimum horizontal stress
σ_{max}	vertical effective stress at the onset of unloading
σ'_{max}	vertical effective stress at the onset of unloading
σ'_v	vertical effective stress
σ_t	horizontal tectonic stress term
\emptyset	formation porosity
ΔP	confining/mud pressure minus pore pressure

Δt	shale compressional travel time at a given
A_b	bit Area
BHA	bottom-hole assembly
BHP	bottom-hole pressure
C_b	bulk compressibility
C_b	bulk compressibility
C_g	grain compressibility
C_p	pore compressibility
D_b	bit diameter
d_c – exponent	corrected d – exponent
d_{cn}	d_c – exponent from the normal compaction trend at a given depth
d_{co}	computed d_c – exponent from the measured data at a given depth
ECD	equivalent circulating density
F_j	jet impact force
FP	fracture pressure
FP_{NPT}	normally pressured trendline fracture pressure
ft	feet
G_{FP}	fracture gradient
G_{np}	normal pore pressure gradient at a given depth
G_{ob}	overburden pressure gradient at a given depth
G_{pp}	pore pressure gradient at a given depth
GR_{log}	gamma ray reading

GR_{max}	shale line gamma ray reading
GR_{min}	sand line gamma ray reading
HMSE	hydro-mechanical specific energy
$HMSE_n$	HMSE from the normal compaction trend at a given depth
$HMSE_o$	computed HMSE from the measured data at a given depth
HRSE	hydro-rotary specific energy
$HRSE_n$	HRSE from the normal compaction trend at a given depth
$HRSE_o$	computed HRSE from the measured data at a given depth
I_{GR}	gamma ray index
IP_{min}	minimum injection pressure
JSA	junk slot area
K	hydraulic energy reduction factor
K_i	matrix stress ratio
Ko	effective stress ratio
LWD	logging while drilling
m	specific energy (HRSE or HMSE) exponent
MSE	mechanical specific energy
MW	mud weight
MWD	measurement while drilling
N	rotary speed
NCT	normal compaction trend
NPP	normal pore pressure

NPPG	normal pore pressure gradient
°C	degree centigrade
P _{atm}	atmospheric pressure
P _c	confining pressure
PDC	polycrystalline diamond compact
PP	pore pressure
PP _a	actual pore pressure
PP _n	normal pore pressure
psi	pounds per square inch
psi/ft	pounds per square inch per foot
Q	flow rate
R _n	normal compaction trend shale resistivity at a given depth
R _o	observed shale resistivity at a given depth
RCB	roller cone bit
ROP	rate of penetration
STFR	speed to flow ratio
S _v	overburden pressure
SWD	seismic while drilling
T	torque on bit
T & D	torque and drag
TFA	total flow area
TOB	torque on bit

TVD	true vertical depth
U	unloading parameters
UCS	uniaxial compressive strength
v	Poisson's ratio
V_j	nozzle/jet velocity
V_{\max}	compressional velocity at the onset of unloading
V_n	normal compaction trend shale compressional velocity at a given depth
V_o	observed shale compressional velocity at a given depth
V_p	compressional wave velocity
V_s	shear wave velocity
V_{sh}	shale volume
WOB	downhole weight on bit
WOBe	effective weight on bit
Z	true vertical depth
α	Biot's coefficient
η	hydraulic energy reduction factor
μ	bit coefficient of sliding friction
θ	angle of internal friction

Chapter 1

1.0 Introduction and Overview

1.1 Formation Pore Pressure

The formation pore pressure is the pressure exerted by the pore fluids on the surrounding rocks. The pore pressures of sedimentary rocks are extremely important in oil and gas exploration (Mann and Mackenzie, 1990). At the planning stage, pore pressure is required for well construction, equipment selection, production forecasting, and reservoir simulation. During the actual drilling operations, information about the formation pore pressure is required for improving the drill-ability of the well, maintaining primary well control, reducing the drilling problems and minimizing formation damage. At the completion phase, accurate knowledge of pore pressure is required for specifying completion fluid requirements. At the production phase, information about reservoir pressure is required for well performance analysis, production forecasting, compaction and subsidence analysis, and determination of reservoir drive mechanism. During the workover phase, formation pore pressure will dictate the kill fluid requirements. At the abandonment stage, pore pressure regimes will dictate the isolation requirements. The formation pore pressure and fracture pressure are considered as the most important parameters used in well engineering communities. From a safety point of view, it is necessary to know the subsurface pressure regimes that will be encountered along the well path before drilling into them. This will help to avoid drilling accidentally into overpressure intervals which can lead to catastrophic and process safety incidents. Recognizing the existence of subsurface overpressure conditions is an essential first step in overall well control. The occurrence of subsurface overpressure conditions poses major problems for safety and cost-

effective well design (Gutierrez et al., 2006). In general, the subsurface pressure regimes that will be encountered while drilling will dictate the overall well cost.

1.2 Formation Pore Pressure Regimes

The formation pore pressure can be described as normal, subnormal and overpressure. The normal pore pressure can be defined as the pressure exerted by the column of seawater containing 80,000 ppm total solids (Dickinson, 1953). The normal pore pressure at any given depth is equal to the vertical height of a column of formation water extending from the surface to that depth. In the US Gulf Coast, the average normal pore pressure gradient is 0.465 psi/ft (Harkins and Baugher, 1969). In the North Sea, the average normal pore pressure gradient is 0.452 psi/ft. In the Niger Delta basin, the normal pore pressure gradient varies between 0.433 psi/ft and 0.472 psi/ft. The normal pore pressure gradient is a function of the concentration of dissolved salts, temperature and content of dissolved gases (Serebryakov et al., 2002). Hence, there is a variation in the normal pore pressure gradient at different locations and depths. In ideal environments, pore pressure is expected to be normal from the surface to the depth of interest. Unfortunately, there are various geological and chemical processes that conspire to produce pore pressure values that are higher or lower than the normal. In subnormal pressure zones, the formation pore pressures are lower than the normal at the given depths. In overpressure intervals, the formation pore pressures are higher than the normal at the given depths.

The origins of subsurface subnormal pressure conditions can be geologic or artificial. The geologic origins can be tectonic, stratigraphic or geochemical in nature while the artificial origins are usually related to hydrocarbons withdrawal from porous and permeable rocks. In regions where erosions have removed a significant amount of the overburden loads, the underlying rocks

may relax sufficiently to undergo an increase in pore volume, resulting in the reduction of formation pore pressure (Barker, 1972; Dickey & Cox, 1977; Serebryakov & Chilingar, 1994). Many subnormal pressure conditions are artificially induced by reservoir fluids (oil, water, and gas) withdrawal from subsurface reservoirs during production. For subnormal pressure conditions to occur, either the reservoirs are completely isolated with no communication with the surrounding strata or the reservoirs do not operate under active water drive (when the influx rate of support water is not enough to compensate for the rate of reservoir fluids withdrawal). Drilling through subnormal pressure intervals can cause severe drilling problems such as lost circulation, differential sticking and underground blowout. In extremely cases, reduction in reservoir pressure can lead to compaction and subsidence during production, which can lead to casing collapse and damage to surface structures (Sulak and Danielsen, 1988; Vudovich et al., 1988; Wooley and Prachner, 1988; Bickley and Curry, 1992; Bruno, 1992; Schwall et al., 1996; Schwall and Denney, 1994; Bruno, 2001; Nagel, 2001; Doornhof et al., 2006).

Two conditions must exist for subsurface overpressure conditions to occur: (1) there must be permeability barriers and (2) there must be mechanisms that generate the overpressure. The permeability barriers (seals) restrict the movement of the pore fluids such that overburden loads are partially supported by the pore fluids. The seals are not necessarily impermeable but must be of low permeability with high capillary entry pressure (Pickering and Indelicato, 1985). Typically, the processes that generate subsurface overpressure conditions are very similar to processes involved in the generation, expulsion, migration, accumulation, and entrapment of hydrocarbons. Subsurface overpressure conditions have been encountered throughout the world (Fertl, 1972; Bradley, 1975; Carstens, 1978; Singh & Ford, 1982; Hunt, 1990; Kader, 1994; Gurevich & Chilingar, 1995; Serebryakov & Chilingar, 1995; Swarbrick, 1995; Belonin and

Slavin, 1998; Holm, 1998; Heppard et al., 1998; Nashaat, 1998; Wilson et al., 1998; Slavin & Smirnova, 1998; Schneider, 2000; O'Connor et al., 2012). Several mechanisms have been proposed as possible causes of overpressure generations in sedimentary basins. The five major overpressure generation mechanisms are: (1) compaction disequilibrium (under-compaction); (2) tectonic forces; (3) clay diagenesis; (4) aqua-thermal expansion; and (5) hydrocarbon generation. There are other minor causes of subsurface overpressure conditions. These include charging, artesian effects, centroid effects, and buoyancy/gravity effects. Carstens (1978) suggested that the overpressure conditions found in the argillaceous sediments in the Lower Tertiary of Central North Sea were caused by a self-sealing mechanism provided by small grain size, clay mineralogy, discontinuous limestone stingers and presence of gas.

1.2.1 Compaction Disequilibrium (Under-compaction)

Compaction disequilibrium occurs when the rate of deposition of sediments is greater than the rate of expulsion of interstitial fluids (usually water). The pore fluids become trapped and begin to support the weight of the overlying sediments (overburden loads), leading to subsurface overpressure conditions. Compaction disequilibrium is often considered as the chief cause of subsurface overpressure conditions usually found in young (tertiary) sedimentary basins where the favorable condition of rapid deposition of sediments containing a large quantity of clay minerals exists (Hart et al., 1995; Carlin and Dainelli, 1998; Law and Spencer, 1998; Katahara, 2003; Sayers et al., 2005). In most cases, other causes of overpressure generation mechanisms are generally small compared to compaction disequilibrium (Burrus, 1998). If the rate of deposition of sediments is equal to the rate of expulsion of interstitial fluids, the excess fluid pressure created by the increasing overburden loads will be dissipated and normal pore pressure

will be maintained throughout the sediments at all depths. The greater the degree of under-compaction, the higher the porosity, and the lower the vertical effective stresses when compared to normally pressured intervals at the same depths. Slavin and Smirnova (1998) reported that with the same magnitude of formation pore pressure, the porosity values of the overpressure zones caused by compaction disequilibrium are substantially higher than the porosity values of the overpressure zones caused by post sedimentary or fluid expansion origins

1.2.2 Tectonic Activities

Tectonic activities such as folding, faulting, and diapirism can cause an increase in formation pore pressure (Dickey et al., 1968; Harkins and Baugher, 1969; Finch, 1969; Law et al., 1998). Rock compaction takes place when subsurface formation is compressed (folded), leading to pore fluids being expelled from the formation pore spaces. If the pore fluids cannot escape during the compression-compaction process, the formation can become over-pressured as the pore fluids begin to support parts of the compressional and overburden loads. Faulting can create subsurface overpressure conditions in several ways. The permeable beds can be moved against the impermeable beds thereby preventing further fluid expulsion with compaction. Faults can create a leaking pathway for the migration of pore fluids from deeper overpressure intervals to shallower horizons thereby causing the shallower formations to be over-pressured (charging). A reverse fault can result in permeable formations being moved up to shallower depths resulting in subsurface overpressure conditions. Diapirism occurs when salt or shale becomes ductile and flows like a viscous plastic material under pressure and at elevated temperatures, rising through the entire thickness of the overlying sediments.

1.2.3 Clay Diagenesis

During the sedimentation process, montmorillonite adsorbs water into its lattice structure. Further burial exposes the montmorillonite to higher temperature and pressure. Clay diagenesis usually occurs at a temperature between 90 – 150°C. At this temperature range, the montmorillonite undergoes a transformation and is converted into illite, releasing a large amount of water in the process (Powers, 1967; Burst, 1969; Rieke and Chilingarian, 1974; Burst, 1976; Freed & Peacor, 1989; Buryakovskiy et al., 1995). Due to the compressive forces resulting from the increasing depth of burial, formation water can be squeezed and expelled from the shales into the adjacent porous and permeable rocks, giving rise to subsurface overpressure conditions.

1.2.4 Aqua-thermal Expansion

As the degree of rock compaction increases due to increasing depth of burial, the formation temperature will increase. This causes the expansion of pore fluids with a subsequent increase in formation pore pressure. If a normally pressured rock is effectively isolated and then subjected to a temperature increase, the reservoir fluid pressure will rise above the normal (Lewis & Rose, 1970; Barker, 1972; Magara, 1975; Barkers & Horsfield 1982; Daines, 1982; Sharp Jr, 1983; Luo and Vasseur, 1992; Miller and Luk, 1993; Chen & Huang, 1996; Polutranko, 1998).

1.2.5 Hydrocarbon Generation

Hydrocarbon generation involves the transformation of kerogen into liquid and gaseous hydrocarbons. This can result in a significant increase in pore volume leading to subsurface overpressure conditions (Law & Dickinson, 1985; Spencer, 1987; Holm, 1998; Hunt et al., 1998; Guo et al., 2010; Tingay et al., 2013). It can also involve thermal cracking of liquid

hydrocarbons into gaseous hydrocarbons. Most subsurface overpressure conditions associated with petroleum source rocks are caused by hydrocarbon generation (Stainforth, 1984).

Nevertheless, field observations have shown that the combination of the above overpressure generation mechanisms can create subsurface overpressure conditions within the same sedimentary basin (Plumley, 1980; Kadri, 1991; Luo et al., 1994; Ward et al., 1994; Law et al., 1998; Freire et al., 2010; Ramdhan and Goult, 2011; Satti et al., 2015; Liu et al., 2016).

Figure 1.1 shows the pressure profiles of a well located in the onshore region of the Niger Delta.

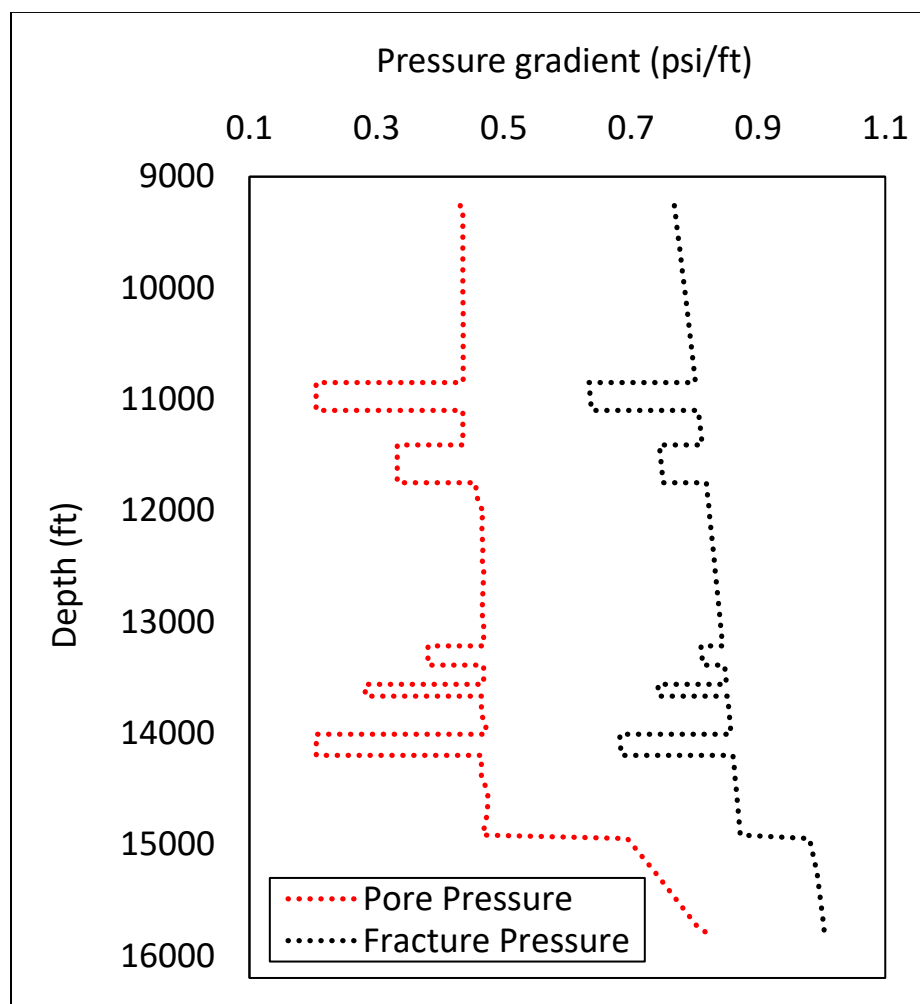


Figure 1.1 The pressure profiles of an onshore well in the Niger Delta.

The initial formation pore pressures in the field are normal from the surface down to 14,917 ft (onset of overpressure) with pore pressure gradient varying between 0.433 psi/ft and 0.472 psi/ft. The formation pore pressure ramps occur just below 14,917 ft. The formation pore pressure increases from 0.472 psi/ft at 14,917 ft to 0.828 psi/ft at 15,831 ft (pressure transition zones and overpressure intervals). No reservoir depletion has ever occurred below the pressure transition zones. However, fluids withdraw from five reservoirs have caused a reduction in formation pore pressures below the normal (subnormal). In the subnormal intervals, the formation pore pressure gradients are less than 0.433 psi/ft. It will be extremely challenging to drill the depleted and overpressure intervals in the same hole sections with conventional drilling techniques without the application of stress caging.

1.3 Pore Pressure Prediction Techniques

Most indirect methods of pore pressure detection techniques assume that subsurface overpressure conditions are associated with under-compaction/compaction disequilibrium. In young, rapidly subsiding basin, transiting from normal pore pressure regimes to overpressure intervals will cause changes in the rock geophysical properties and drilling parameters. These changes are generally seen as reversals in trends when the compaction-dependent geophysical properties are plotted against depth in a uniform lithology (Bowers, 2002). Shale formations are the preferred lithology for pore pressure prediction because they are more responsive to effective stresses than most rock types. Most pore pressure prediction methods require a normal compaction trend (NCT) of the rock properties to be established. Under normal pore pressure conditions, the density, resistivity, compressional wave velocity, and degree of rock compaction are all expected to be increasing with depth while the formation porosity will exponentially decrease with depth.

When drilling through the overpressure zones, the rock density, resistivity and compressional wave velocity are expected to decrease while the formation porosity will increase. However, lithologic variations can create difficulty in defining the appropriate normal compaction trends (NCT) (Swarbrick, 2001). Variations in rock bulk and pore compressibility values have been used to detect the onset of abnormally high formation pressure in carbonate rocks (Atashbari and Tingay, 2012). Pulsed neutron capture logs can also be used to detect and quantitatively evaluate overpressure environments, allowing pore pressure depletion to be monitored behind the casing (Fertl and Chilingarian, 1987). Serebryakov et al. (1995) reported that the natural radioactivity values in the uniform shale layers can be used to identify the onset of abnormally-high pressured zones. In normally pressure conditions, gamma ray values will increase with depth. Departures from the normal compaction trends may signify changes in formation pore pressure regimes (Zoeller, 1983). Satti and Yusoff (2015) used the acoustic impedance principle to analyze the origin of overpressure mechanisms in the Malay Basin. Shear wave velocity can also be used to estimate the formation pore pressure and are more sensitive to pressure variations than the compressional wave velocity (Ebrom et al., 2002; Ebrom et al., 2004). However, subsurface overpressure conditions have been reported to occur in rocks with low porosity and high density especially if the origin of the overpressure mechanism is not compaction disequilibrium. Carstens and Dypvik (1981) found that the Jurassic overpressure shale from the North Sea Viking graben was associated with low porosity and high density. Therefore, it is possible not to have any trend reversal between the normally compacted series and overpressure intervals when porosity indicators such as resistivity, compressional wave velocity and density are plotted against depth (Hermanrud et al., 1998; Teige et al., 1999). Most pore pressure prediction

techniques currently employed in the oil and gas industry may not be applicable to unconventional plays (Couzens-Schultz et al., 2013).

All the pore pressure prediction techniques from geophysical and drilling parameters have their limitations. The formation resistivity is affected by other factors such as rock permeability, pore fluids, temperature and concentration of dissolved salts. Care must be taken when using resistivity data to estimate the formation pore pressure as the reversal in resistivity trend may have nothing to do with subsurface overpressure conditions (Lane and Macpherson, 1976). The compressional wave velocity is affected by the presence of gas and microcracks/fractures in the formation. The effects of gas and microcracks on compressional wave velocity are similar to that of overpressure conditions (Gardner et al., 1974; Tatham and Stoffa, 1976; Ensley, 1985; Williams, 1990; Brie et al., 1995; Hamada, 2004; Kozlowski et al., 2017). Combining shear and compressional wave velocities will help to differentiate the gas effect from the overpressure effect (Dvorkin et al. 1999). The shale radioactivity values (gamma ray) may also be affected by the presence of other minerals in the shales which may have nothing to do with the overpressure conditions. The drilling parameters are affected by bit hydraulics, lithologies, bit wears, bit sizes, shocks, and vibrations. The seismic responses are affected by changes in lithology and pore fluid type. Huffman (2002) summarizes the applications and limitations of various geophysical methods used for pore pressure predictions. The best approach to pore pressure prediction is to examine the combination of all the available measured data (geophysical and drilling parameters) since relying on only one type of data can result in misinterpretations (Fertl and Timko, 1971). Even direct measurements (repeat formation tester, modular formation dynamics tester, reservoir characterization explorer, drill stem test, bottom-hole pressure survey, permanent downhole gauge, and drilling kick) of formation pore pressure

have their own limitations. These measurements are usually made only after the well must have been drilled and possible overpressure zones have been penetrated. Thus, direct measurements have limitations in terms of real-time monitoring and predicting formation pore pressure ahead of the bit. A recently developed logging while drilling (LWD) tool (formation pore pressure while drilling tool) in the bottom-hole assembly (BHA) can measure the reservoir pressures of penetrated rocks while drilling. This does not still change the fact that the rocks must be penetrated before taking the pressure measurements since the tool sensor is placed some feet behind the bit. Direct pore pressure measurements using drilling kick and LWD tool may not be suitable for low permeability reservoirs because the time required for such reservoirs to reach the final pressure build up make cause the BHA to get stuck in the hole. The data used to estimate the formation pore pressure can be classified into three categories: (1) seismic data, (2) well log data and (3) drilling parameters.

1.3.1 Pore Pressure Prediction from Seismic Data

The seismic reflections are functions of acoustic impedance and they are affected by formation pore pressure. The formation interval velocity can be obtained from conventional surface seismic, borehole seismic and seismic while drilling (SWD). The conventional surface seismic method is the only method available to estimate the formation pore pressure when no drilling activities have occurred in a field. Pennebaker (1968) was the first to develop a methodology that uses seismic interval velocity for pore pressure prediction. Dutta and Ray (1997) used the velocity and acoustic impedance inversion of seismic reflections to obtain the formation pore pressure. In normally compacted series with no hydrocarbon saturation, seismic wave propagation velocity will increase with depth in a uniform lithology. Deviation from the

increasing velocities with depth to lower values can be directly related to the increase in formation pore pressure if the rock type and pore fluid remain constant. The quality of the seismic data will affect its accuracy. Seismic wave velocities can be affected by other factors that are not related to overpressure conditions. This can make the estimation of formation pore pressure from seismic sources very difficult. These factors include lithology, degree of rock cementation and the type of pore fluids (Scott and Thomsen, 1993). Several applications of seismic data for pre-drill pore pressure predictions have been reported in the literature (Weakley, 1989; Sayers et al., 2000; Dutta et al., 2001; Huffman, 2002; Dutta, 2002; Sayers et al., 2002; Soleymani & Riahi, 2012; Etminan et al., 2012; Banik et al., 2013). Once the interval velocities at any given depths are obtained from the seismic data, empirical relationships can be used to compute the formation pore pressure (Eaton, 1975; Bower, 1995).

1.3.2 Pore Pressure Prediction from Well Logs

Based on the modification to the porosity model proposed by Athy (1930), an exponential relationship was established between shale porosity and vertical effective stress. This relationship is given by (Rubey & Hubber, 1959; Flemings et al., 2002):

$$\phi = \phi_0 e^{-k\sigma'_v}, \quad (1.1)$$

where ϕ is the formation porosity (fraction); σ'_v is the vertical effective stress (psi); ϕ_0 surface/mudline clay porosity (fraction); k is the stress compaction constant. The vertical effective stress is defined by Terzaghi (1927) as the vertical stress minus pore pressure and is given by:

$$\sigma'_v = \sigma_v - PP, \quad (1.2)$$

where σ_v is the vertical stress (psi); PP is the pore pressure (psi). Burrus (1998) suggested that the pore pressure predictions using the vertical effective stress defined by (Biot, 1941) provided better agreement with the field observations and is given by:

$$\sigma'_v = \sigma_v - \alpha PP, \quad (1.3)$$

where α is the Biot's coefficient. The expression for Biot's coefficient is given by:

$$\alpha = 1 - \frac{C_g}{C_b}, \quad (1.4)$$

where C_g is the grain compressibility (psi^{-1}); C_b is the bulk compressibility (psi^{-1}). In normally compacted series, as vertical effective stress increases, shale porosity will decrease. In pressure transition and overpressure intervals, a decrease in effective stress will be accompanied by an increase in shale porosity if the origin of overpressure mechanism is mainly due to compaction disequilibrium. Mathematical manipulation of equation 1.1 by Hart et al. (1995) is given by:

$$PP = \sigma_v - \left[\frac{1}{k} \ln \left[\frac{\phi_0}{\phi} \right] \right]. \quad (1.5)$$

Equation 1.5 implies that if shale porosities and vertical stresses at various depths are known, the pore pressures can be easily determined. The formation porosities and the vertical stresses can be obtained from density logs. (Burrus, 1998) concluded that the compaction model based on the vertical effective stress – porosity relation sufficiently explained the overpressure conditions in rapidly subsiding basins such as Mahakam Delta, Indonesia, and Gulf Coast, U.S.A.

Hottmann and Johnson (1965) were the first to directly correlate well log data (resistivity and sonic transit time) to subsurface overpressure conditions encountered in the Miocene and

Oligocene shales in Upper Texas and Southern Louisiana Gulf Coast. The methodology involves establishing the normal compaction trend (NCT) that corresponds to the normal pore pressure regime when shale resistivity or sonic transit time is plotted against depth on the semi-log. The divergence of observed sonic transit time or resistivity from the NCT is a measure of the formation pore pressure (Figure 1.2).

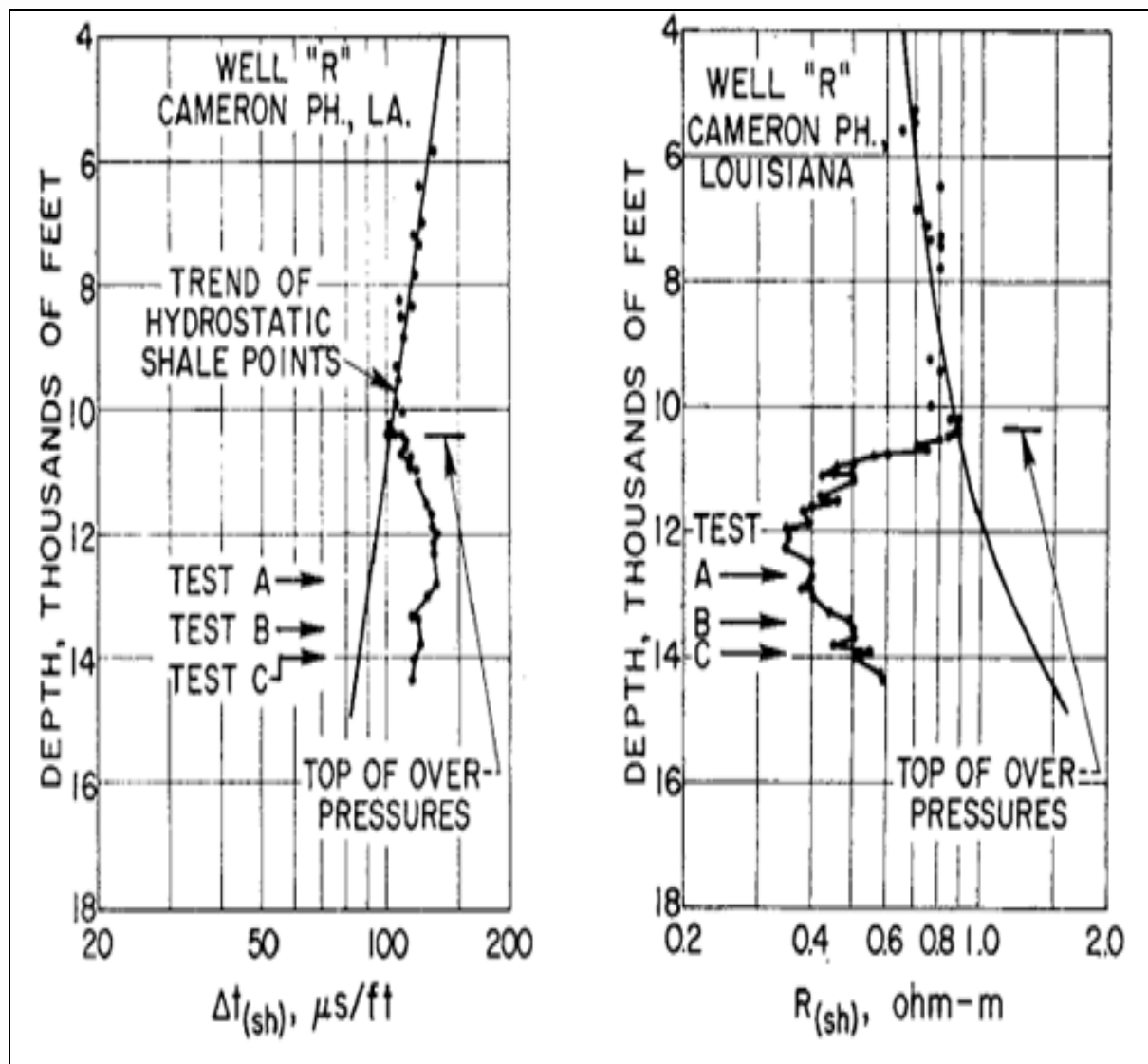


Figure 1.2 The acoustic-depth and resistivity-depth plots (Hottmann and Johnson, 1965).

Based on the shale formation resistivity factor, Foster and Whalen (1966) established a relationship among pore pressure, depth, and the ratio of normal shale resistivity to observed shale resistivity for regions with varying salinity. Foster and Whalen's model is given by:

$$PP = 0.465 * Z + \frac{0.535}{\log b} * \log \left[\frac{R_n}{R_o} \right], \quad (1.6)$$

where PP is the formation pore pressure (psi); Z is the true vertical depth (ft); R_n is the normal shale resistivity (ohm-m); R_o is the observed (abnormal) shale resistivity (ohm-m). The $\log b$ can be obtained from the slope of formation factor versus depth plot.

Based on the data presented by Hottmann and Johnson (1965), Gardner et al. (1974) provided a relationship among vertical effective stress, difference between overburden and normal pore pressure gradients, interval travel time and depth. Gardner's model is given by:

$$\left[\frac{\sigma_v - PP}{G_{ob} - G_{np}} \right]^{\frac{1}{3}} * Z^{\frac{2}{3}} = A - B \log_e \Delta t, \quad (1.7)$$

where σ_v is the vertical stress (psi); PP is the pore pressure (psi); Z is the true vertical depth (ft); G_{ob} is the overburden gradient (psi/ft); G_{np} is the normal pore pressure gradient (psi/ft); Δt is the interval travel time (μ s/ft); A and B are constant parameters. The values of A and B can be obtained by calibration equation 1.7 to any known normally pressured intervals in the region.

Eaton (1975) developed a correlation that relates formation pore pressure gradient to overburden gradient, normal pore pressure gradient and resistivity or velocity ratio. Eaton's models are given by:

$$G_{pp} = G_{ob} - \{G_{ob} - G_{np}\} \left[\frac{R_o}{R_n} \right]^a \quad (1.8)$$

and

$$G_{pp} = G_{ob} - \{G_{ob} - G_{np}\} \left[\frac{\Delta t_n}{\Delta t_o} \right]^b, \quad (1.9)$$

where G_{pp} is the pore pressure gradient (psi/ft); G_{ob} is the overburden gradient (psi/ft); G_{np} is the normal pore pressure gradient (psi/ft); R_o is the observed shale resistivity (ohm-m); R_n is the normal compaction trend shale resistivity (ohm-m); a is the resistivity exponent coefficient (usually 1.5 but can range from 1.0 – 2.0); Δt_n is the normal compaction shale travel time (μ s/ft); Δt_o is the observed shale travel time (μ s/ft); b is the sonic exponent coefficient (usually 3.0 but can range from 2.0 – 4.0). The overburden gradient, formation resistivity and interval travel time are usually obtained from density, resistivity and sonic logs respectively. Eaton's models are probably the most widely used empirical models for pore pressure prediction, especially in under-compacted series.

Eberhart-Phillips et al. (1989) developed empirical relations between measured sonic velocities, effective stress, porosity, and clay contents for shaly sandstone rocks after conducting experimental studies on 64 rock samples. Eberhart-Phillips's models are given by:

$$V_p = 5.77 - 6.94\phi - 1.73\sqrt{C} + 0.446(\sigma'_v - e^{-16.7\sigma'_v}) \quad (1.10)$$

and

$$V_s = 3.70 - 4.94\phi - 1.57\sqrt{C} + 0.361(\sigma'_v - e^{-16.7\sigma'_v}), \quad (1.11)$$

where V_p is the compressional wave velocity (km/s); V_s is the shear wave velocity (km/s); ϕ is the formation porosity; C is the clay volume (fraction); σ' is the effective pressure (kbar).

Equations 1.10 and 1.11 can be adapted for shale by equating the value of clay volume (C) to one. Given the values of V_p , V_s , and porosity as a function of depth from well logs and/or seismic data in shale formations, the vertical effective stress (σ'_v) can be determined. Subtracting the overburden stress from the calculated vertical effective stress at any given depth will give the corresponding value of the formation pore pressure.

Holbrook et al. (1995) expressed vertical effective stress as a function of formation porosity given by:

$$\sigma'_v = A[1 - \emptyset]^B, \quad (1.12)$$

where σ'_v is the vertical effective stress (psi); \emptyset is the formation porosity (fraction); A and B are the fitting parameters relating to the compaction resistance properties of the rocks. The values of A and B can be obtained by calibrating equation 1.12 to the normally pressured intervals in the field. The formation pore pressure at any given depth can be obtained from

$$PP = \sigma_v - A[1 - \emptyset]^B, \quad (1.13)$$

where PP is the formation pore pressure (psi); σ_v is the vertical stress (psi).

Since, most pore pressure prediction techniques fail to take into account the origins of overpressure mechanisms, Bowers (1995) proposed new techniques of predicting the formation pore pressure from compressional sonic velocity based on the principle of effective stress. Bower's models consider the excess pore pressure generated by both under-compaction and fluid expansion mechanisms. The technique involves estimating the vertical effective stress from the compressional sonic velocity. The pore pressure is then computed by subtracting the overburden

pressure from effective stress. Bower's first relation accounts for normal pore pressure regime and overpressure conditions caused by under-compaction (virgin curve) and is given by:

$$V = 5000 + A\sigma_e^B, \quad (1.14)$$

where V is the compressional sonic velocity (ft/sec); σ_e is the effective vertical stress (psi); A and B are virgin curve parameters. The values of A and B can be obtained by calibrating equation 1.14 to the regional data from the normally pressured intervals. The second Bower's relation accounts for overpressure conditions caused by fluid expansion mechanisms (unloading curve) and is given by:

$$V = 5000 + A \left[\sigma_{\max} \left[\frac{\sigma_e}{\sigma_{\max}} \right]^{\frac{1}{U}} \right]^B, \quad (1.15)$$

$$\sigma_{\max} = \left[\frac{V_{\max} - 5000}{A} \right]^{\frac{1}{B}}, \quad (1.16)$$

where σ_{\max} is the effective vertical stress at the onset of unloading (psi); V_{\max} is the compressional sonic velocity at the onset of unloading (ft/sec); U is the unloading parameter which is a measure of how plastic the sediment is. When U is equal to one, there is no permanent deformation because the unloading curve (equation 1.15) reduces to the virgin curve (equation 1.14). The value of U is obtained by calibrating equation 1.15 to the regional offset well data in the overpressure intervals. Bower's models are another widely used empirical relationships and the models are applicable to many sedimentary basins. However, Bower's model has been reported not to be effective for 3D overpressure prediction using seismic velocity in the deep zones of Malay Basin, Malaysia where fluid expansion mechanism is the dominant cause of

overpressure generation (Satti et al., 2016). Bower's model may also overestimate formation pore pressure in shallow unconsolidated formations because the velocities in such formations are very slow (Zhang, 2011).

The combination of compressional and shear wave velocities can be used to estimate the formation pore pressure (Li et al., 2000; Walls et al., 2000; Ebrom et al., 2006; Kumar et al., 2006; Saleh et al., 2013; Yu and Hilterman, 2013; Ebrom et al., 2006; Kumar et al., 2006). Prasad (2002) suggested that the velocity ratio (V_p/V_s) is very sensitive to an increase in formation pore pressure. Saleh et al., (2013) used the V_p/V_s to predict the pore pressure in subsalt environments.

A locally calibrated velocity-dependent pore pressure prediction model was proposed by Shell using the Tau-effective stress concept (Gutierrez et al., 2006) and is given by:

$$\sigma'_v = A \left[\frac{200 - \Delta t}{\Delta t - 50} \right]^B \quad (1.17)$$

where σ'_v is the vertical effective stress (psi); Δt is the compressional transit time ($\mu\text{s}/\text{ft}$); A and B are fitting constants. The values of A and B can be obtained by calibrating equation 1.17 to the regional data from the normally pressured intervals. The formation pore pressure at any given depth can be obtained using:

$$PP = \sigma_v - A \left[\frac{200 - \Delta t}{\Delta t - 50} \right]^B \quad (1.18)$$

where PP is the formation pore pressure (psi); σ_v is the vertical stress (psi).

Zhang (2011) proposed modified Eaton's sonic model by using depth-dependent normal compaction trend equation as given by:

$$G_{pp} = G_{ob} - \{G_{ob} - G_{np}\} \left[\frac{\Delta t_m + [\Delta t_{ml} - \Delta t_m] e^{-CZ}}{\Delta t_o} \right]^3, \quad (1.19)$$

where G_{pp} is the pore pressure gradient (psi/ft); G_{ob} is the overburden gradient (psi/ft); G_{np} is the normal pore pressure gradient (psi/ft); Δt_m is the shale matrix compressional transit time with zero porosity (approximately 65 μ s/ft); Δt_{ml} is the mudline compressional transit time (approximately 200 μ s/ft); Z is the true vertical depth below the mudline (ft); C is the compaction constant; Δt_o is the observed compressional transit time either from the sonic log or seismic velocity (μ s/ft). In Zang's model, the normal compaction trend decreases exponentially with depth and this is given by

$$\Delta t_{on} = \Delta t_m + [\Delta t_{ml} - \Delta t_m] e^{-CZ}, \quad (1.20)$$

where Δt_{on} is the observed compressional transit time in the normally pressured intervals (μ s/ft). The value of C (compaction constant) can be obtained by calibrating equation 1.20 to the normally pressured intervals. Other modifications to the existing pore pressure prediction models from geophysical parameters are presented by Zhang (2011).

For carbonate rocks, Atashbari and Tingay (2012) proposed a pore pressure prediction model based on compressibility attributes. The model is given by

$$PP = \left[\frac{(1 - \phi) C_b \sigma'_v}{(1 - \phi) C_b - (\phi C_p)} \right]^\gamma, \quad (1.21)$$

where PP is the formation pore pressure (psi); \emptyset is the formation porosity (fraction); C_b is the bulk compressibility (psi^{-1}); C_p is the pore compressibility (psi^{-1}); σ'_v is the vertical effective stress (psi); γ is the empirical constant ranging from 0.9 to 1.0.

Zhang (2013) proposed a pore pressure prediction model for cases without unloading which relates formation pore pressure to vertical stress, depth and compressional transit times. This model is given by

$$\text{PP} = \left[\frac{\sigma_v - \left[\frac{\sigma_v - \alpha \text{NPP}}{CZ} \right] \ln \left[\frac{\Delta t_{ml} - \Delta t_m}{\Delta t_o - \Delta t_m} \right]}{\alpha} \right], \quad (1.22)$$

where PP is the formation pore pressure (psi); σ_v is the vertical stress (psi); NPP is the normal pore pressure (psi); Z is the true vertical depth below the mudline (ft); Δt_m is the shale matrix compressional transit time with zero porosity; Δt_{ml} is the mudline compressional transit time; C is the compaction constant; Δt_o is the observed compressional transit time either from the sonic log or seismic velocity ($\mu\text{s}/\text{ft}$); α is the Biot's coefficient. A similar model for unloading conditions is also available (Zhang, 2013).

1.3.3 Pore Pressure Prediction from Drilling Parameters

This method has the advantage of predicting the formation pore pressure at the bit rather than behind the bit. Under normal pressure conditions, the rate of penetration (ROP) will gradually decrease as we drill deeper into the sedimentary basin due to greater rock compaction and increase in vertical effective stress. In overpressure intervals, the ROP will most likely increase due to higher rock porosity and decrease in the vertical effective stress from increasing pore

pressure. An increase in the formation pore pressure for a given mud weight will cause the ROP to increase due to reduced back pressure on the formations (Cunningham & Eenink, 1959; Combs, 1968; Wardlaw. 1969). The results of the experimental studies conducted by Garnier and Lingen (1959) on permeable rocks of varying strength and permeability showed a reduction in the drilling rate of penetration due to an increase in rock strength governed by the differential pressure between the bottom-hole pressure and the formation pore pressure. Black et al. (1985) conducted experimental studies on four water-saturated sandstone samples using water-based mud and concluded that increase in the differential pressure across the mud filter cake on the bottom of the hole will dramatically reduce the penetration rates. From Black's observations, the rate of penetration decreased by roughly a factor of 3 as the differential pressure across the filter cake increased from 0 to 1,000 psi for the specific muds, rock, bit, and conditions tested. Several other researchers have also reached the same conclusion that the rate of penetration decreases with an increase in differential pressure between the bottom-hole pressure and formation pore pressure (Murray & Cunningham, 1955; Lingen, 1962; Maurer, 1965; Vidrine & Benit, 1968; Wardlaw, 1969; Cheatham et al., 1985). In general, the ROP increases exponentially with a decrease in differential pressure between the bottom-hole hole pressure and formation pore pressure. Therefore, the plot of rate of penetration versus depth will most likely follow an ever-decreasing trend in the normally pressured intervals, and the trend will reverse when entering into the overpressure zones. Forgotson (1969) suggested that a minimum increase of 200% in the rate of penetration is required for overpressure detection in shales. However, excessive overbalance may not show any substantial increase in ROP even with a significant increase in differential pressure. ROP can also be influenced by many other factors than the differential pressure. These factors include lithology, formation compaction, weight on bit (WOB), rotary

speed, bit size, bit type, hydraulics and bit wear (Bourgoyne and Young, 1973). A sudden increase in ROP may not necessarily signify drilling into abnormally high-pressured zones. Therefore, the use of ROP for pore pressure prediction may prove difficult due to several limitations on its application (Rasmus and Stephens, 1995). Combs (1968) proposed a mathematical model that relates ROP in shales to differential pressure, WOB, rotary speed, flow rate, hole size, and bit wear index. Contrary to most publications, Detournay and Atkinson (2000) suggested that the drilling specific energy does not depend on the virgin formation pressure in low-permeability formations such as shales. Laboratory drilling studies conducted by Gray-Stephens et al. (1994) also suggested that differential pressure did not have any strong influence on the drilling response in hard shales. Bingham (1965) developed a mathematical relationship between the rate of penetration, weight on bit, rotary speed and the bit diameter based on the laboratory and field data. Bingham's model is given by

$$\frac{ROP}{N} = a \left[\frac{WOB}{D_b} \right]^d, \quad (1.23)$$

where ROP is the rate of penetration (ft/min); N is the rotary speed in revolution per minute (RPM); WOB is the weight on bit (lbs); D_b is the bit diameter (in); a is the matrix strength constant; d is the formation drill-ability constant. Jorden and Shirley (1966) normalized the Bingham's model by correcting for the effects of WOB, rotary speed and hole size on the rate of penetration resulting in the development of the d-exponent concept. The d-exponent is given by

$$d - \text{exponent} = \frac{\log \left[\frac{ROP}{60N} \right]}{\log \left[\frac{12WOB}{10^6 D} \right]}. \quad (1.24)$$

where ROP is the rate of penetration (ft/hr); N is the rotary speed (rpm); WOB is the weight on bit (lbs); D_b is the bit diameter (in). However, the d-exponent proposed by Jorden and Shirley (1966) did not take into account the hydraulic parameters, mud properties, bit type, bit wear, and most importantly the effect of mud weight changes. Harper (1969) modified the d-exponent equation to include the effect of changes in the mud weight/bottom-hole pressure and is given by

$$d_c - \text{exponent} = d - \text{exponent} \left[\frac{G_{np}}{ECD} \right], \quad (1.25)$$

where $d_c - \text{exponent}$ is the corrected d - exponent; G_{np} is the normal pore pressure gradient (psi/ft or ppg); ECD is the equivalent circulating density (psi/ft or ppg). In the normally pressured intervals, the plot of the d_c - exponent versus depth will show an increasing trend in a constant lithology. Upon penetrating the transition and overpressure zones, the d_c - exponent values will deviate from the normal trend to lower values due to decrease in rock compaction and differential pressure. Provided a uniform lithology (100% of clay formation) is being drilled and the differential pressure is not excessive, the plot of d_c - exponent versus depth can be used to identify the onset of overpressure. The d_c - exponent versus depth graph is displayed on the semi-log to prevent significant variation of d_c - exponent with location and geological age. The vertical axis represents the depth on the linear scale and the horizontal axis represents d_c - exponent on the logarithmic scale (Zamora, 1972). The formation pore pressure can be estimated from the d_c - exponent using Eaton's model as given by

$$G_{pp} = G_{ob} - \{G_{ob} - G_{np}\} \left[\frac{d_{co}}{d_{cn}} \right]^c, \quad (1.26)$$

where G_{pp} is the pore pressure gradient (psi/ft); G_{ob} is the overburden gradient (psi/ft); G_{np} is the normal pore pressure gradient (psi/ft); d_{co} is the calculated d_c from measured data; d_{cn} is the d_c from normal trend line; c is the coefficient (usually 1.2 but can range from 1.0 to 2.0).

The applications of the d-exponent method in the field for pore pressure predictions have produced mixed results. The major drawback to the application of d - exponent concept to pore pressure prediction is that it does not consider the effect of bit hydraulic energy on the rate of penetration (ROP). This greatly limits its application to hard rock environments where bit hydraulic energy has little or no effect on rock breakage. In hard rock environments, the major function of the bit hydraulic energy is to clean the bit face and throw the drill cuttings beneath the bit face into the annulus stream. The bit hydraulic energy becomes important in soft formations where jetting will make a large contribution to the rate of penetration. Whenever the bit hydraulic energy changes (due to changes in flow rate, mud weight, and nozzle sizes), or there is a change in the susceptibility of the formation to jetting (soft rocks), the d_c – exponent will also change. Under downhole conditions where the bit hydraulic energy has a significant influence on the rate of penetration (unconsolidated sediments), the d – exponent method may produce inaccurate estimates of formation pore pressure unless the flow rate, mud weight, and jet velocity can be maintained constant while drilling the transition and overpressure zones. However, maintaining these parameters constant during drilling operations may not be possible.

Cardona (2011) was the first to apply the mechanical specific energy (MSE) concept to predict the formation pore pressure in the sub-salt formations in the GOM based on the adaptation of Eaton (1975) model to include the MSE terms. Teale (1965) defined MSE as the amount of energy (axial + rotary loads) required to remove a unit volume of rock and is given by

$$MSE = \frac{WOB}{A_b} + \frac{120 * \pi * N * T}{A_b * ROP}, \quad (1.27)$$

where MSE is the mechanical specific energy (psi); WOB is the downhole weight on bit (lbs); A_b is the bit area (in^2); N is the rotary speed (rpm); T is the torque on bit (lb-ft); ROP is the rate of penetration (ft/hr). The modified Eaton's model using MSE parameters is given by

$$G_{pp} = G_{ob} - \{G_{ob} - G_{np}\} \left[\frac{MSE_o}{MSE_n} \right]^c, \quad (1.28)$$

where G_{pp} is the pore pressure gradient (psi/ft); G_{ob} is the overburden gradient (psi/ft); G_{np} is the normal pore pressure gradient (psi/ft); MSE_o is the actual MSE calculated using equation 1.28; MSE_n is the hypothetical value of MSE from the normal compaction trend; c is the MSE coefficient (usually ≤ 1.0).

Akbari et al. (2014) experimentally showed the dependency of MSE on formation pore pressure. They established a relationship between MSE, differential pressure, and confining pressure (equation 1.29):

$$MSE = UCS + \left[a + b \frac{\Delta P}{P_c} \right] \ln \frac{P_c}{P_{atm}}, \quad (1.29)$$

where MSE is the mechanical specific energy (psi); UCS is the uniaxial compressive strength (psi); ΔP is the differential pressure between confining pressure and pore pressure (psi); P_c is the confining pressure (psi); P_{atm} is the atmospheric pressure (psi); a is the coefficient that is dependent on rock internal friction angle; b is the coefficient that is dependent on rock permeability, porosity, fluid viscosity, fluid compressibility, rotary speed and depth of the cut.

The last major improvement to pore pressure prediction Majidi et al. (2016) proposed the

concept of drilling efficiency and MSE to estimate the formation pore pressure in a sub-salt deepwater well in the Gulf of Mexico. Majidi's model involves the application of downhole drilling parameters and in-situ rock properties. Majidi's model is given by:

$$PP = ECD - [(DE_{trend} \times MSE) - UCS] \left[\frac{1 - \sin \theta}{1 + \sin \theta} \right], \quad (1.30)$$

$$DE_{trend} = a\phi_n^b, \quad (1.31)$$

$$USC = 0.43V_p^{3.2}, \quad (1.32)$$

$$\theta = 1.532V_p^{0.5148}, \quad (1.33)$$

where PP is the pore pressure (psi); ECD is the equivalent circulating density (psi); MSE is the mechanical specific energy (psi); UCS is the uniaxial compressive strength (psi); θ is the angle of internal friction; ϕ is the formation porosity; V_p is the compressional sonic velocity (ft/sec); a is the coefficient of drilling efficiency trend-line from porosity trend-line; b is the exponent of drilling efficiency trend-line from porosity trend-line.

While the recent advancement in pore pressure prediction from the drilling parameters uses the MSE concept (Cardona, 2011; Majidi et al., 2016), the MSE has similar limitations to d – exponent method because the MSE technique does not consider the effect of bit hydraulic energy on the ROP. This will certainly make the MSE method to produce erroneous results under certain drilling conditions where bit hydraulic energy has an effect on ROP. For example, if the driller decides to increase the flow rate to clean the hole or reduce the flow rate to minimize the equivalent circulating density while drilling the pressure transition zones in unconsolidated formations, the MSE may produce inaccurate estimates of formation pore pressure.

1.4 Research Objectives

1. To develop a new pore pressure prediction technique from drilling parameters that incorporates the bit hydraulic energy term based on the concept of total energy consumed while drilling using downhole measurements.
2. To develop a new pore pressure prediction technique from drilling parameters that incorporates the bit hydraulic energy term based on the concept of total energy consumed while drilling using only surface measurements.
3. To improve the accuracy of pore pressure prediction by improving the accuracy of overburden pressure computation via improvement in density logs prediction.
4. To extend the application of total energy concept to real-time lithology identification.
5. To develop a new fracture pressure prediction model that can be applied to normal and overpressure intervals in the Niger Delta.

1.5 Connectivity among the Research Papers

The primary objective of this research is to develop hydraulic-dependent pore pressure prediction models from the drilling parameters using the concept of specific energy. The application of specific energy to drilling operations is further extended to real-time lithology identification. Accurate knowledge of overburden pressure is required for pore pressure prediction. Inaccurate prediction of overburden pressure may lead to erroneous pore pressure estimates. Usually, overburden pressure is computed from density logs. However, in areas where density logs are not available, synthetically derived density logs are used. In this research, new formation bulk density prediction models that can be applied to a wide range of lithologies in siliciclastic

environments are proposed. Finally, since pore and fracture pressures are closely related, an attempt is also made to develop a new fracture pressure prediction model that can be applied to normal and overpressure intervals in the Niger Delta basin.

Figure 1.3 shows the connectivity among the research papers. The research papers are highly connected. The pressure-depth and lithology-depth plots form the basis of well design. Specific energy is required for lithology and pore pressure predictions. Overburden and pore pressures are required for fracture pressure determination. Formation of bulk density and overburden pressure are required for pore pressure prediction. Formation bulk density is required for overburden pressure computation.

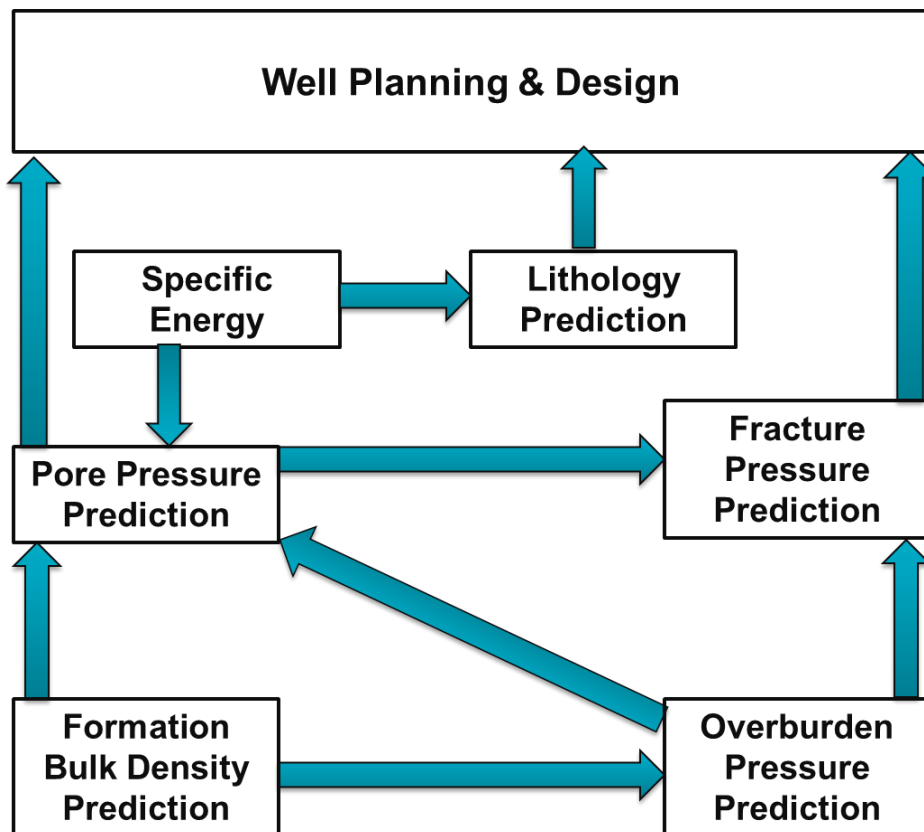


Figure 1.3 The connectivity among the research papers.

1.6 Organization of the Thesis

The thesis is prepared in manuscript style and consists of six main chapters. The outlines of the chapters (research papers) are presented below:

1. Chapter 2 presents an innovative pore pressure prediction technique from drilling parameters based on the concept of hydro-rotary specific energy using downhole measurements. This chapter is published in the *Journal of Natural Gas Science and Engineering*.
2. Chapter 3 presents a pore pressure prediction method from drilling parameters based on the hydro-mechanical specific energy concept using only surface measurements. This chapter is published in the *Journal of Petroleum Science and Engineering*.
3. Chapter 4 presents the new formation bulk density prediction models that can be applied to a wide range of lithologies in siliciclastic environments. This chapter is published in the *Journal of Petroleum Science and Engineering*.
4. Chapter 5 presents a new fracture pressure prediction model that can be applied to normal and overpressure intervals in the Niger Delta. This chapter is submitted to the *Journal of Environmental Earth Sciences*.
5. Chapter 6 presents a new method of identifying subsurface lithology using specific energy concept. This chapter is published in the *Journal of Petroleum Science and Engineering*.

1.7 Reference

Akbari, B., Miska, S., Yu, M., Ozbayoglu, M., 2014. Experimental Investigations of the Effect of the Pore Pressure on the MSE and Drilling Strength of a PDC Bit. Soc. Pet. Eng. (SPE

- 169488). <https://doi.org/10.2118/169488-MS>
- Atashbari, V., Tingay, M.R., 2012. Pore pressure prediction in carbonate reservoirs, in: SPE Latin America and Caribbean Petroleum Engineering Conference. Society of Petroleum Engineers.
- Athy, L.F., 1930. Density, Porosity, and Compaction of Sedimentary Rocks. Am. Assoc. Pet. Geol. Bull. 14, 194–200. <https://doi.org/10.1306/3D93289E-16B1-11D7-8645000102C1865D>
- Banik, N., Koesoemadinata, A., Wagner, C., Inyang, C., Bui, H., 2013. Predrill pore-pressure prediction directly from seismically derived acoustic impedance. 2013 SEG Annu. Meet. 2905–2909. <https://doi.org/10.1190/segam2013-0137.1>
- Barker, C., 1972. Aquathermal Pressuring--Role of Temperature in Development of Abnormal-Pressure Zones: GEOLOGICAL NOTES. Am. Assoc. Pet. Geol. Bull. 10, 2068–2071. <https://doi.org/10.1306/819A41B0-16C5-11D7-8645000102C1865D>
- Barkers, C., Horsfield, B., 1982. Mechanical versus thermal cause of abnormally high pore pressures in shales. Am. Assoc. Pet. Geol. Bull. 66, 99–100. <https://doi.org/10.1306/2F919760-16CE-11D7-8645000102C1865D>
- Belonin, M.D., Slavin, V.I., 1998. Abnormally high formation pressures in petroleum regions of Russia and other countries of the C.I.S. Law, B.E., G.F. Ulmishek, V.I. Slavin eds., Abnorm. Press. Hydrocarb. Environ. AAPG Mem. 70, 115–121.
- Bickley, M.C., Curry, W.E., 1992. Designing wells for subsidence in the Greater Ekofisk Area, in: European Petroleum Conference. Society of Petroleum Engineers.
- Bingham, M.G., 1965. A New Approach to Interpreting Rock Drillability. Pet. Publ. Co.
- Biot, M.A., 1941. General theory of three-dimensional consolidation. J. Appl. Phys. 12, 155–164. <https://doi.org/10.1063/1.1712886>
- Black, A.D., Dearing, H.L., DiBona, B.G., 1985. Effects of Pore Pressure and Mud Filtration on Drilling Rates in a Permeable Sandstone. J. Pet. Technol. 37, 1671–1681. <https://doi.org/10.2118/12117-PA>
- Bourgoine, J.A.T., Young, J.F.S., 1973. Formation Evaluation and Abnormal Pressure Detection. SPWLA Fourteenth Annu. Logging Symp. MAY 6-9,. <https://doi.org/10.1016/B978-0-323-04184-3.50079-0>
- Bowers, G.L., 2002. Detecting high overpressure. Lead. Edge 21, 174–177.

- Bowers, G.L., 1995. Pore pressure estimation from velocity data: Accounting for overpressure mechanisms besides undercompaction. *SPE Drill. Complet.* 10, 89–95.
<https://doi.org/10.2118/27488-PA>
- Bradley, J.S., 1975. Abnormal formation pressure. *Am. Assoc. Pet. Geol. Bull.* 59, 957–973.
- Brie, A., Pampuri, F., Marsala, A.F., Meazza, O., 1995. Shear sonic interpretation in gas-bearing sands, in: SPE Annual Technical Conference and Exhibition. Society of Petroleum Engineers.
- Bruno, M.S., 2001. Geomechanical analysis and decision analysis for mitigating compaction related casing damage, in: SPE Annual Technical Conference and Exhibition. Society of Petroleum Engineers.
- Bruno, M.S., 1992. Subsidence-induced well failure. *SPE Drill. Eng.* 7, 148–152.
- Burrus, J., 1998. Overpressure models for clastic rocks, their relation to hydrocarbon expulsion: a critical re-evaluation. *Abnorm. Press. Hydrocarb. Environ.* 70, 35–63.
- Burst, J., 1969. Diagenesis of Gulf Coast Clayey Sediments and Its Possible Relation To Petroleum Migration. *Am. Assoc. Pet. Geol. Bull.* 53, 73–93.
<https://doi.org/10.1306/5D25C595-16C1-11D7-8645000102C1865D>
- Burst, J.F., 1976. Argillaceous Sediment Dewatering. *Annu. Rev. Earth Planet. Sci.* 4, 293–318.
<https://doi.org/10.1146/annurev.ea.04.050176.001453>
- Buryakovskiy, L.A., Djevanshir, R.D., Chilingar, G. V., 1995. Abnormally-high formation pressures in Azerbaijan and the South Caspian Basin (as related to smectite ??? illite transformations during diagenesis and catagenesis). *J. Pet. Sci. Eng.* 13, 203–218.
[https://doi.org/10.1016/0920-4105\(95\)00008-6](https://doi.org/10.1016/0920-4105(95)00008-6)
- Cardona, J., 2011. Fundamental Investigation of Pore Pressure Prediction during Drilling from the Mechanical Behaviour of Rocks. PhD Thesis, Texas A&M Univ. Mech. Eng.
- Carlin, S., Dainelli, J., 1998. Pressure regimes and pressure systems in the Adriatic Foredeep (Italy). *Abnorm. Press. Hydrocarb. Environ.* 70, 145–160.
- Carstens, H., 1978. Origin Of Abnormal Formation Pressures In Central North Sea Lower Tertiary Clastics. *Log Anal.* 19, 24–31.
- Carstens, H., Dypvik, H., 1981. Abnormal formation pressure and shale porosity. *Am. Assoc. Pet. Geol. Bull.* 65, 344–350.
- Cheatham, C.A., Nahm*, J.J., Heitkamp, N., 1985. Effects of Selected Mud Properties on Rate

- of Penetration in Full-Scale Shale Drilling Simulations. Soc. Pet. Eng. (SPE/IADC 13465).
- Chen, J., Huang, D., 1996. Formation and mechanism of the abnormal pressure zone and its relation to oil and gas accummulations in the Eastern Jiuquan Basin, Northwest China. Sci. China Earth Sci. 39, 194–204.
- Combs, D.G., 1968. Prediction o Pore Pressure From Penetration Rate. Soc. Pet. Eng. (SPE 2162).
- Couzens-Schultz, B. a., Axon, A., Azbel, A., Hansen, K.S., Haugland, M., Sarker, R., Tichelar, B., Wieseneck, J.B., Wilhelm, R., Zhang, Z., 2013. IPTC 16849: Pore Pressure Prediction in Unconventional Resources. Pap. IPTC 16849 Proc. 2013 Int. Pet. Conf. held Beijing, China, 26-28 March. <https://doi.org/10.2523/16849-ms>
- Cunningham, R. a, Eenink, J.G., 1959. Laboratory Study of Effect of Overburden, Formation and Mud Column Pressures on Drilling Rate of Permeable Formations. Pet. Trans. AIME 217, 9–17.
- Daines, S.R., 1982. Aquathermal Pressuring and Geopressure Evaluation: GEOLOGIC NOTES. Am. Assoc. Pet. Geol. Bull. 66, 931–939.
- Detournay, E., Atkinson, C., 2000. Influence of pore pressure on the drilling response in low-permeability shear-dilatant rocks. Int. J. Rock Mech. Min. Sci. 37, 1091–1101. [https://doi.org/10.1016/S1365-1609\(00\)00050-2](https://doi.org/10.1016/S1365-1609(00)00050-2)
- Dickey, P., Cox, W., 1977. Oil and gas in reservoirs with subnormal pressures. Am. Assoc. Pet. Geol. Bull. 12, 2134–2142.
- Dickey, P.A., Shriram, C.R., Paine, W.R., 1968. Abnormal pressures in deep wells of southwestern Louisiana. Science (80-). 160, 609–615.
- Dickinson, G., 1953. Geological Aspects of Abnormal Reservoir Pressures in Gulf Coast Louisiana. Am. Assoc. Pet. Geol. Bull. 37, 410–432. <https://doi.org/10.1306/5CEADC6B-16BB-11D7-8645000102C1865D>
- Doornhof, D., Kristiansen, T.G., Nagel, N.B., Pattillo, P.D., Sayers, C., 2006. Compaction and subsidence. Oilf. Rev. 18, 50–68.
- Dutta, N., 2002. Geopressure Detection Using Reflection Seismic Data and Rock Physics Principles: Methodology and Case Histories From Deepwater Tertiary Clastics Basins. Pap. SPE 77820 Proc. 2002 SPE Asia Pacific Oil Gas Conf. Exhib. held Melbourne, Aust. 8–10 October. <https://doi.org/10.2523/77820-MS>

- Dutta, N., Gelinsky, S., Reese, M., Khan, M., 2001. A New Petrophysically Constrained Predrill Pore Pressure Prediction Method for the Deepwater Gulf of Mexico: A Real-Time Case Study. Pap. SPE 71347 Proc. 2001 SPE Annu. Tech. Conf. Exhib. held New Orleans, Louisiana, 30 Sept. Oct. 2001. <https://doi.org/10.2118/71347-MS>
- Dutta, N.C., Ray, A., 1997. Image of Geopressured Rocks Using Velocity And Acoustic Impedance Inversion of Seismic Data. 1997 SEG Annu. Meet.
- Dvorkin, J., Mavko, G., Nur, A., 1999. Overpressure detection from compressional-and shear-wave data. *Geophys. Res. Lett.* 26, 3417–3420.
- Eaton, B.A., 1975. The Equation for Geopressure Prediction from Well Logs. *Soc. Pet. Eng.* (SPE 5544). <https://doi.org/10.2118/5544-MS>
- Eberhart-Phillips, D., Han, D., Zoback, M.D., 1989. Empirical relationships among seismic velocity, effective pressure, porosity, and clay content in sandstone. *Geophysics*. <https://doi.org/10.1190/1.1442580>
- Ebrom, D., Albertin, M., Heppard, P., 2006. Subsalt pressure prediction from multicomponent seismics (and more!). *Lead. Edge* 25, 1540–1542.
- Ebrom, D., Heppard, P., Thomsen, L., 2002. Numerical modeling of PS moveout as a function of pore pressure, in: SEG Technical Program Expanded Abstracts 2002. Society of Exploration Geophysicists, pp. 1634–1637.
- Ebrom, D., Heppard, P., Thomsen, L., Mueller, M., Harrold, T., Phillip, L., Watson, P., 2004. Effective stress and minimum velocity trends, in: SEG Technical Program Expanded Abstracts 2004. Society of Exploration Geophysicists, pp. 1615–1618.
- Ensley, R.A., 1985. Evaluation of direct hydrocarbon indicators through comparison of compressional-wave and shear-wave seismic data - a case study of the Myrnam gas field Alberta. *Geophysics* 50, 37–48. <https://doi.org/10.1190/1.1441834>
- Etminan, M., Jamali, J., Riahi, M.A., 2012. Formation Pore Pressure Prediction Using Velocity Inversion in Southwest Iran. *Pet. Sci. Technol.* 30, 28–34. <https://doi.org/10.1080/10916461003752538>
- Fertl, W.H., 1972. Worldwide Occurrence of Abnormal Formation Pressures, Part 1. Pap. SPE 3844 Proc. 1972 Abnorm. Subsurf. Press. Symp. Soc. Pet. Eng. AIME, to be held Bat. Rouge, La., May 15-16.
- Fertl, W.H., Chilingarian, G. V., 1987. Abnormal formation pressures and their detection by

- pulsed neutron capture logs. *J. Pet. Sci. Eng.* 1, 23–38. [https://doi.org/10.1016/0920-4105\(87\)90012-X](https://doi.org/10.1016/0920-4105(87)90012-X)
- Fertl, W.H., Timko, D., 1971. Parameters for Identification of Overpressure Formations. Pap. SPE 3223 Proc. 1971 Drill. Rock Mech. Conf. <https://doi.org/10.2118/3223-MS>
- Finch, W., 1969. Abnormal Pressure in the Antelope Field, North Dakota. *J. Pet. Technol.* 21. <https://doi.org/10.2118/2227-PA>
- Flemings, P.B., Stump, B.B., Finkbeiner, T., Zoback, M., 2002. Flow focusing in overpressured sandstones: Theory, observations, and applications. *Am. J. Sci.* 302, 827–855. <https://doi.org/10.2475/ajs.302.10.827>
- Forgotson, S.J.M., 1969. Indication of Proximity of High-Pressure Fluid Reservoir, Louisiana and Texas Gulf Coast. *Am. Assoc. Pet. Geol. Bull.* 53, 171–173.
- Foster, J.B., Whalen, H.E., 1966. Estimation of formation pressures from electrical surveys - Offshore Louisiana. *J. Pet. Technol.* 18, 165–171. <https://doi.org/10.2118/1200-PA>
- Freed, R.L., Peacor, D.R., 1989. Geopressured shale and sealing effect of smectite to illite transition. *Am. Assoc. Pet. Geol. Bull.* 73, 1223–1232.
- Freire, H., Falcão, J., Silva, C.F., Barghigiani, L., 2010. Abnormal Pore Pressure Mechanisms In Brazil. Pap. ARMA 10-407 Proc. 2010 44th US Rock Mech. Symp. 5th U.S.-Canada Rock Mech. Symp. held Salt Lake City, UT June 27–30.,
- Gardner, G.H., Gardner, L., Gregory, A., 1974. Formation Velocity and Density - The Diagnostic Basic for Stratigraphic Traps. *Geophysics* 39, 770–780.
- Gardner, G.H.F., Gardner, L.W., Gregory, A.R., 1974. Formation Velocity and Density - The Diagnostic Basics for Stratigraphic Traps. *Geophysics* 39, 770–780.
- Garnier, A.J., Lingen, N.H. van, 1959. Phenomena affecting drilling rates at depth. *Pet. TRANSA CTIONS, A IME (SPE 1097G)* 216, 232–239.
- Gray-Stephens, D., Cook, J.M., Sheppard, M.C., 1994. Influence of Pore Pressure on Drilling Response in Hard Shales. *SPE Drill. Complet.* 9, 263–270. <https://doi.org/10.2118/23414-PA>
- Guo, X., He, S., Liu, K., Song, G., Wang, X., Shi, Z., 2010. Oil generation as the dominant overpressure mechanism in the Cenozoic Dongying depression, Bohai Bay Basin, China. *Am. Assoc. Pet. Geol. Bull.* 94, 1859–1881.
- Gurevich, A.E., Chilingar, G. V., 1995. Abnormal pressures in Azerbaijan: A brief critical

- review and recommendations. *J. Pet. Sci. Eng.* 13, 125–135. [https://doi.org/10.1016/0920-4105\(95\)00007-5](https://doi.org/10.1016/0920-4105(95)00007-5)
- Gutierrez, M.A., Braunsdor, N.R., Couzens, B.A., 2006. Calibration and ranking of pore-pressure prediction models. *Lead. Edge* 25, 1516–1523.
- Hamada, G.M., 2004. Reservoir Fluids Identification Using Vp/Vs Ratio. *Oil Gas Sci. Technol. – Rev. IFP* 59, 649–654.
- Harkins, L.K., Baugher, I.H., 1969. Geological significance of abnormal formation pressures. *J. Pet. Technol.* 961–966. <https://doi.org/10.2118/2228-PA>
- Harper, D., 1969. New Findings From Over Pressure Detection Curves In Tectonically Stressed Beds. *Soc. Pet. Eng. (SPE 2781)*.
- Hart, B.S., Flemings, P.B., Deshpande, A., 1995. Porosity and pressure: Role of compaction disequilibrium in the development of geopressures in a Gulf Coast Pleistocene basin. *Geology* 23, 45–48.
- Heppard, P.D., Cander, H.S., Eggertson, E.B., 1998. Abnormal pressure and the occurrence of hydrocarbons in offshore eastern Trinidad, West Indies. Law, B.E., G.F. Ulmishek, V.I. Slavin eds., *Abnorm. Press. Hydrocarb. Environ. AAPG Mem.* 70, 215–246.
- Hermanrud, C., Wensaas, L., Teige, G.M.G., Bolas, H.M.N., Hansen, S., Vik, E., 1998. Shale porosities from well logs on haltenbanken (offshore mid-Norway) show no influence of overpressuring. Law, B.E., G.F. Ulmishek, V.I. Slavin eds., *Abnorm. Press. Hydrocarb. Environments AAPG Mem.* 70, 65–85.
- Holbrook, P.W., Maggiori, D.A., Hensley, R., 1995. Real-Time Pore Pressure and Fracture Gradient Evaluation in All Sedimentary Lithologies. *SPE Form. Eval.* 10, 215–222.
- Holm, G.M., 1998. Distribution and origin of overpressure in the Central Graben of the North Sea. Law, B.E., G.F. Ulmishek, V.I. Slavin eds., *Abnorm. Press. Hydrocarb. Environ. AAPG Mem.* 70, 123–144.
- Hottmann, C.E., Johnson, R.K., 1965. Estimation of formation pressures from log-derived shale properties. *J. Pet. Technol. SPE* 1110, 717–722. <https://doi.org/10.2118/1110-PA>
- Huffman, a. R., 2002. The future of pore-pressure prediction using geophysical methods. Pap. OTC 13041 Proc. e 2001 Offshore Technol. Conf. held Houston, Texas, 30 April. May.
- Hunt, J.M., 1990. Generation and migration of petroleum from abnormally pressured fluid compartments. *Am. Assoc. Pet. Geol. Bull.* <https://doi.org/10.1306/0C9B27E5-1710-11D7->

8645000102C1865D

- Hunt, J.M., Whelan, J.K., Eglinton, L.B., Cathles, L.M. ll., 1998. Relation of shale porosities, gas generation, and compaction to deep overpressures in the US. Gulf coast. Law, B.E., G.F. Ulmishek, V.I. Slavin eds., Abnorm. Press. Hydrocarb. Environ. AAPG Mem. 70 87–104.
- Jorden, J.R., Shirley, O.J., 1966. Application of Drilling Performance Data to Overpressure Detection. *J. Pet. Technol.* 18, 1387–1394. <https://doi.org/10.2118/1407-PA>
- Kader, M.S. Bin, 1994. Abnormal pressure occurrence in the Malay and Penyu basins, offshore Peninsular Malaysia - a regional understanding. *Geol. Soc. Malaysia Bull.* 36, 81–91.
- Kadri, I.B., 1991. Abnormal Formation Pressures in Post-Eocene Formation, Potwar Basin, Pakistan. Pap. SPE/IADC 21920 Proc. 1991 SPE/IADC Drill. Conf. held Amsterdam, 11-14 March. <https://doi.org/10.2523/21920-MS>
- Katahara, K., 2003. Analysis of overpressure on the Gulf of Mexico Shelf, in: Offshore Technology Conference. Offshore Technology Conference.
- Kozlowski, M., Quirein, J., Engelmann, B., Wolanski, K., Ochalik, S., 2017. Quantitative Interpretation of Sonic Compressional and Shear Logs for Gas Saturation in Medium Porosity Sandstone, in: SPWLA 58th Annual Logging Symposium. Society of Petrophysicists and Well-Log Analysts.
- Kumar, K.M., Ferguson, R.J., Ebrom, D., Heppard, P., 2006. Pore pressure prediction using an Eaton's approach for PS-waves, in: SEG Technical Program Expanded Abstracts 2006. Society of Exploration Geophysicists, pp. 1550–1554.
- Lane, R.A., Macpherson, L.A., 1976. A Review of Geopressure Evaluation From Well Logs - Louisiana Gulf Coast. *J. Pet. Technol.* 28, 963–971. <https://doi.org/10.2118/5033-PA>
- Law, B.E., Dickinson, W.W., 1985. Conceptual Model for Origin of Abnormally Pressured Gas Accumulations in Low-Permeability Reservoirs. *Am. Assoc. Pet. Geol. Bull.* 69, 1295–1304. <https://doi.org/10.1306/AD462BD7-16F7-11D7-8645000102C1865D>
- Law, B.E., Shah, S.H. a, Malik, M. a, 1998. Abnormally high formation pressures, Potwar Plateau, Pakistan. Law, B.E., G.F. Ulmishek, V.I. Slavin eds., Abnorm. Press. Hydrocarb. Environ. AAPG Mem. 70 247–358. <https://doi.org/10.1306/F4C8E6B6-1712-11D7-8645000102C1865D>
- Law, B.E., Spencer, C.W., 1998. Abnormal Pressure in Hydrocarbon Environments. Law, B.E.,

- G.F. Ulmishek, V.I. Slavin eds., Abnorm. Press. Hydrocarb. Environ. AAPG Mem. 70 1–11. [https://doi.org/10.1016/S0264-8172\(99\)00059-8](https://doi.org/10.1016/S0264-8172(99)00059-8)
- Lewis, C., Rose, S., 1970. A theory relating high temeperatures and overpressures. *J. Pet. Technol.* 22, 11–16.
- Li, Q., Heliot, D., Zhao, L., Chen, Y., 2000. Abnormal pressure detection and wellbore stability evaluation in carbonate formations of east Sichuan, China, in: IADC/SPE Drilling Conference (IADC / SPE 59125). Society of Petroleum Engineers.
- Lingen, N.H. Van, 1962. Bottom Scavenging-A Major Factor Governing Penetration Rates at Depth. *J. Pet. Technol. (SPE 165)* 187–196.
- Liu, Y., Qiu, N., Xie, Z., Yao, Q., Zhu, C., 2016. Overpressure compartments in the central paleo-uplift, Sichuan Basin, southwest China. *Am. Assoc. Pet. Geol. Bull.* 100, 867–888.
- Luo, M., Baker, M.R., LeMone, D. V, 1994. Distribution and generation of the overpressure system, eastern Delaware Basin, western Texas and southern New Mexico. *Am. Assoc. Pet. Geol. Bull.* 78, 1386–1405.
- Luo, X., Vasseur, G., 1992. Contributions of compaction and aquathermal pressuring to geopressure and the influence of environmental conditions (1). *Am. Assoc. Pet. Geol. Bull.* 76, 1550–1559.
- Magara, K., 1975. Importance of aquathermal pressuring effect in Gulf Coast. *Am. Assoc. Pet. Geol. Bull.* 59, 2037–2045.
- Majidi, R., Albertin, M.L., Last, N., 2016. Method for Pore Pressure Estimation Using Mechanical Specific Energy and Drilling Efficiency. Pap. IADC/SPE 178842 Proc. 2016 IADC/SPE Drill. Conf. Exhib. held Fort Worth, Texas, USA, 1–3 March.
- Mann, D.M., Mackenzie, A.S., 1990. Prediction of pore fluid pressures in sedimentary basins. *Mar. Pet. Geol.* 7, 55–65. [https://doi.org/10.1016/0264-8172\(90\)90056-M](https://doi.org/10.1016/0264-8172(90)90056-M)
- Maurer, W.C., 1965. Bit-Tooth Penetration Under Simulated Borehole Conditions. *J. Pet. Technol.* 1433–1442.
- Miller, T.W., Luk, C.H., 1993. Contributions of compaction and aquathermal pressuring to geopressure and the influence of environmental conditions: discussion. *Am. Assoc. Pet. Geol. Bull.* 77, 2006–2010.
- Murray, A.S., Cunningham, R.A., 1955. Effect of Mud Column Pressure on Drilling Rates. *Pet. Trans. AIME* 204, 196–204.

- Nagel, N.B., 2001. Compaction and subsidence issues within the petroleum industry: From Wilmington to Ekofisk and beyond. *Phys. Chem. Earth, Part A Solid Earth Geod.* 26, 3–14.
- Nashaat, M., 1998. Abnormally high formation pressure and seal impacts on hydrocarbon accumulations in the Nile Delta and North Sinai basins, Egypt. *Law, B.E., G.F. Ulmishek, V.I. Slavin eds., Abnorm. Press. Hydrocarb. Environ. AAPG Mem.* 70 161–180.
- O'Connor, S., Swarbrick, R., Hoesni, J., Lahann, R., 2012. Deep Pore Pressure Prediction in Challenging Areas, Malay Basin, SE Asia. *Pap. IPA11 - G - 022 Proceedings, Indones. Pet. Assoc. 35th Annu. Conv. Exhib. May 2011* 15.
- Pennebaker, E., 1968. Detection of Abnormal-pressure Formations from Seismic- Field Data. *Am. Pet. Inst.* 184–191.
- Pickering, L.A., Indelicato, G.J., 1985. Abnormal formation pressure: a review. *Mt. Geol.*
- Plumley, J.W., 1980. Abnormally High Fluid Pressure: Survey of Some Basic Principles: ERRATUM. *Am. Assoc. Pet. Geol. Bull.* 64, 414–422.
- Polutranko, A.J., 1998. Causes of Formation and Distribution of Abnormally High Formation Pressure in Petroleum Basins of Ukraine. *Law, B.E., G.F. Ulmishek, V.I. Slavin eds., Abnorm. Press. Hydrocarb. environments AAPG Mem.* 70 181–194.
- Powers, M.C., 1967. Fluid-release mechanisms in compacting marine mudrocks and their importance in oil exploration. *Am. Assoc. Pet. Geol. Bull.* 7, 1240–1254.
- Prasad, M., 2002. Acoustic measurements in unconsolidated sands at low effective pressure and overpressure detection. *Geophysics* 67, 405–412.
- Ramdhani, A.M., Goultby, N.R., 2011. Overpressure and mudrock compaction in the Lower Kutai Basin, Indonesia: A radical reappraisal. *Am. Assoc. Pet. Geol. Bull.* 95, 1725–1744.
- Rasmus, J., Stephens, G.D.M.R., 1995. I; J. *SPE Drill. Eng.* 177, 1066–1075.
- Rieke, H.H., Chilingarian, G. V, 1974. Compaction of argillaceous sediments. Elsevier.
- Rubey, W.W., Hubber, K.M., 1959. Role of Fluid Pressure in Mechanics of Overthrust Faulting. *Bull. Geol. Soc. Am.* 70, 167–206.
- Saleh, S., Williams, K., Rizvi, A., 2013. Predicting Subsalt Pore Pressure with Vp/Vs. *Offshore Technol. Conf. (OTC 24157)*.
- Satti, A.. I., Yusoff, W.W.I., Ghosh, D., 2016. Overpressure in the Malay Basin and prediction methods. *Geofluids* 16, 301–313. <https://doi.org/10.1111/gfl.12149>
- Satti, I.A., Ghosh, D., Yusoff, W.I.W., Hoesni, M.J., 2015. Origin of Overpressure in a Field in

- the Southwestern Malay Basin. SPE Drill. Complet. 30, 198.
- Satti, I.A., Yusoff, W.I.W., 2015. A New Method for Overpressure Mechanisms Analysis. Soc. Pet. Eng. (SPE 176357).
- Sayers, C.M., Boer Den, L.D., Nagy, Z.R., Hooyman, P.J., Ward, V., 2005. Regional trends in undercompaction and overpressure in the Gulf of Mexico. Seg/houst. 2005 Annu. Meet. 1219–1223.
- Sayers, C.M., Johnson, G.M., Denyer, G., 2002. Predrill pore-pressure prediction using seismic data. Geophysics 67, 1286–1292. <https://doi.org/10.1190/1.1500391>
- Sayers, C.M., Johnson, G.M., Denyer, G., 2000. OTC 11984 Pore Pressure Prediction From Seismic Tomography. Pap. OTC 11984 Proc. 2000 Offshore Technol. Conf. held Houston, Texas, 1–4 May.
- Schneider, F.J., 2000. Abnormal Pressures in Hydrocarbon Environments. Mar. Pet. Geol. 17, 559. [https://doi.org/10.1016/S0264-8172\(99\)00059-8](https://doi.org/10.1016/S0264-8172(99)00059-8)
- Schwall, G.H., Denney, C.A., 1994. Subsidence induced casing deformation mechanisms in the Ekofisk field, in: Rock Mechanics in Petroleum Engineering. Society of Petroleum Engineers.
- Schwall, G.H., Slack, M.W., Kaiser, T.M. V, 1996. Reservoir compaction well design for the Ekofisk field, in: SPE Annual Technical Conference and Exhibition. Society of Petroleum Engineers.
- Scott, D., Thomsen, L., 1993. A global algorithm for pore pressure prediction, in: 55th EAEG Meeting.
- Serebryakov, V.A., Chilingar, G. V., 1995. Abnormal pressure regime in the former USSR petroleum basins. J. Pet. Sci. Eng. 13, 65–74.
- Serebryakov, V.A., Chilingar, G. V., 1994. Investigation of underpressured reservoirs in the powder river Basin, Wyoming and Montana. J. Pet. Sci. Eng. 11, 249–259.
- Serebryakov, V.A., Chilingar, G. V., Katz, S.A., 1995. Methods of estimating and predicting abnormal formation pressures. J. Pet. Sci. Eng. 13, 113–123. [https://doi.org/10.1016/0920-4105\(95\)00006-4](https://doi.org/10.1016/0920-4105(95)00006-4)
- Serebryakov, V.A., Robertson Jr, J.O., Chilingarian, G. V, 2002. Origin and prediction of abnormal formation pressures. Gulf Professional Publishing.
- Sharp Jr, J.M., 1983. Permeability controls on aquathermal pressuring. Am. Assoc. Pet. Geol.

- Bull. 67, 2057–2061.
- Singh, I., Ford, C., 1982. The occurrence, Causes and Detection of Abnormal Pressure in the Malay Basin. Proceedings offshore South East Asia Conf. 9 - 12 Febr.
- Slavin, V.I., Smirnova, E.M., 1998. Abnormally high formation pressures: origin, prediction, hydrocarbon field development, and ecological problems. Law, B.E., G.F. Ulmishek, V.I. Slavin eds., Abnorm. Press. Hydrocarb. Environ. AAPG Mem. 70 105–114.
- Soleymani, H., Riahi, M.A., 2012. Velocity based pore pressure prediction-A case study at one of the Iranian southwest oil fields. J. Pet. Sci. Eng. 94–95, 40–46.
- Spencer, C.W., 1987. Hydrocarbon Generation as a Mechanism for Overpressuring in Rocky Mountain Region. Am. Assoc. Pet. Geol. Bull. 71, 368–388.
- Stainforth, J.G., 1984. GIFFSLAND HYDROCARBONS-A PERSPECTIVE FROM THE BASIN EDGE. APPEA J. 24, 91–100.
- Sulak, A.M., Danielsen, J., 1988. Reservoir aspects of Ekofisk subsidence, in: Offshore Technology Conference. Offshore Technology Conference.
- Swarbrick, R.E., 2001. Pore-Pressure Prediction: Pitfalls in Using Porosity. Pap. OTC 13045 Proc. 2001 Offshore Technol. Conf. held Houston, Texas, 30 April. May.
- Swarbrick, R.E., 1995. Distribution and Generation of the Overpressyre System, Eaastern Delaware BAsin, Western Texas and Southern New Mexico: Discussion. Am. Assoc. Pet. Geol. Bull. 12, 1386–1405.
- Tatham, R.H., Stoffa, P.L., 1976. V p/V s—A potential hydrocarbon indicator. Geophysics 41, 837–849.
- Teale, R., 1965. The Concept of Specific Energy in Rock Drilling. Int. J. Rock Mech. Min. Sci. 2, 57–73. [https://doi.org/10.1016/0148-9062\(65\)90022-7](https://doi.org/10.1016/0148-9062(65)90022-7)
- Teige, G.M.G., Hermanrud, C., Wensaas, L., Bolås, H.M.N., 1999. The lack of relationship between overpressure and porosity in North Sea and Haltenbanken shales. Mar. Pet. Geol. 16, 321–335.
- Terzaghi, K., 1927. No Title. Die Beziehungen zwischen Elastizität und Inn. Sitzungsbur Akad. Wiss. Wein. 132 Abt.
- Tingay, M.R.P., Morley, C.K., Laird, A., Limpornpipat, O., Krisadasima, K., Pabchanda, S., Macintyre, H.R., 2013. Evidence for overpressure generation by kerogen-to-gas maturation in the northern Malay Basin. Am. Assoc. Pet. Geol. Bull. 97, 639–672.

- Vidrine, D.J., Benit, E.J., 1968. Field Verification of the Effect of Differential Pressure on Drilling Rate. *J. Pet. Technol.* (SPE 1859) 20, 676–682. <https://doi.org/10.2118/1859-PA>
- Vudovich, A., Chin, L. V, Morgan, D.R., 1988. Casing deformation in Ekofisk, in: Offshore Technology Conference. Offshore Technology Conference.
- Walls, J., Dvorkin, J., Mavko, G., Nur, A., 2000. Use of Compressional and Shear Wave Velocity for Overpressure Detection. *Offshore Technol. Conf.* (OTC 11912).
- Ward, C.D., Coghill, K., Broussard, M.D., 1994. The application of petrophysical data to improve pore and fracture pressure determination in North Sea Central Graben HPHT wells, in: SPE Annual Technical Conference and Exhibition. Society of Petroleum Engineers.
- Wardlaw, H.W.R., 1969. Drilling Performance Optimization and Identification of Overpressure. *Soc. Pet. Eng. AIME SPE* 2388, 67–78.
- Williams, D.M., 1990. The acoustic log hydrocarbon indicator, in: SPWLA 31st Annual Logging Symposium. Society of Petrophysicists and Well-Log Analysts.
- Wilson, M.S., Gunneson, B.G., Peterson, K.E., Honore, R., 1998. Abnormal pressures encountered in a deep wildcat well, southern Piceance Basin, Colorado. Law, B.E., G.F. Ulmishek, V.I. Slavin eds., *Abnorm. Press. Hydrocarb. Environ.* AAPG Mem. 70 195–214.
- Wooley, G.R., Prachner, W., 1988. Reservoir compaction loads on casings and liners. *SPE Prod. Eng.* 3, 96–102.
- Yu, H., Hilterman, F.J., 2013. Shear wave sensitivity to pore pressure prediction, in: SEG Technical Program Expanded Abstracts 2013. Society of Exploration Geophysicists, pp. 600–604.
- Zamora, M., 1972. Slide Rule Correlation Aids D-exponent. *Oil Gas J.* 70, 68–72.
- Zhang, J., 2013. Effective stress, porosity, velocity and abnormal pore pressure prediction accounting for compaction disequilibrium and unloading. *Mar. Pet. Geol.* 45, 2–11.
- Zhang, J., 2011. Pore pressure prediction from well logs: Methods, modifications, and new approaches. *Earth-Science Rev.* 108, 50–63. <https://doi.org/10.1016/j.earscirev.2011.06.001>
- Zoeller, W.A., 1983. Pore Pressure Detection From the MWD Gamma Ray. Pap. SPE 12166 Proc. 1983 58th Annu. Tech. Conf. Exhib. held San Fr. CA, Oct. 5-8.

Chapter 2

2.0 Overpressure Prediction Using the Hydro-Rotary Specific Energy Concept

Preface

A version of this chapter has been published in the Journal of Natural Gas Science and Engineering, 2018. I am the primary author. Co-author Dr. Sunday Adedigba provided much-needed support in completing the manuscript. Co-author Dr. Faisal Khan reviewed the manuscript and provided valuable insight into the model development. Co-author Dr. Raghu Chunduru reviewed the manuscript and provided technical support in model analysis. Co-author Dr. Stephen Butt reviewed the manuscript and assisted in the development of the concept. I developed the initial concept and carried out most of the data analysis. I prepared the first draft of the manuscript and revised the manuscript based on the feedback from the co-authors and peer review process. The co-authors also helped to refine the concept.

Abstract

Pore pressure predictions from the drilling parameters have experienced little improvement since the inception of the d-exponent concept. Applications of the d-exponent method to pore pressure predictions have produced mixed results, especially in deviated wells and under drilling conditions where bit hydraulic energy has a significant influence on the rate of penetration (ROP). In this paper, a new energy-based pore pressure prediction technique using the concept of hydro-rotary specific energy (HRSE) is presented. The HRSE approximates the total energy required to break and remove a unit volume of rock. Overpressure prediction using the HRSE method is based on the principle that overpressure intervals with lower effective stress will

require less energy to drill than the normally pressured intervals at the same depth. The new technique is tested using a recently drilled deep vertical exploratory gas well in the Tertiary Deltaic System in the central swamp region of the Niger Delta in Nigeria. The pore pressure estimates from the HRSE concept are compared to: (1) the pore pressure estimates derived from the d-exponent and shale compressional velocity, (2) the actual pore pressure measurements taken in the reservoir sands of interest. An excellent agreement is observed in magnitude and trend between the pore pressure estimates derived from the HRSE concept and the actual pore pressure measurements. This clearly demonstrates the applicability of the HRSE concept in predicting the onset of overpressure and estimating the formation pore pressure. The HRSE method of overpressure prediction has the potential to be more accurate in some drilling environments where the d-exponent method may have produced erroneous results.

Keywords: Pore pressure; Overpressure; Mechanical Specific Energy; Hydro-rotary Specific Energy, d-exponent; Normal Compaction Trend

2.1 Introduction

The formation pore pressure is of great importance in the oil and gas industry. It provides the necessary energy required to drive liquid and gaseous hydrocarbons to the surface. It also represents a potential hazard during drilling, completion, and production if not properly managed. Accurate knowledge of the formation pore pressure is very useful in all stages of oil and gas exploration and production. Exploration engineers use pore pressure data to determine subsurface trap integrity. The occurrence of hydrocarbons in some sedimentary basins is also believed to be related to the subsurface pore pressure regime (Belonin & Slavin, 1998).

Information about the formation pressure helps the reservoir engineers in reservoir modeling. Production engineers use pore pressure data for well performance analysis. Drilling engineers use pore pressure data to optimize rig selection, casing depths determination, drilling, and completion fluid design, wellheads design, casing and tubing design, cement design and material selection. Facility engineers also use pore pressure data for surface installation designs. From a business perspective, subsurface pressure regimes will dictate the overall well cost.

The formation pore pressure can be normal (hydrostatic), subnormal or overpressure. It is normal if it is able to support a continuous column of static formation water from the surface to the reservoir depth of interest (Swarbrick & Osborne, 1998). The normal pore pressure gradient varies between 0.433 – 0.515 psi/ft depending on the location, concentration of dissolved salts, pore fluid type, and temperature. Formations with pore pressure gradient lower than normal pore pressure gradients are termed subnormal. Overpressure intervals have a pore pressure gradient greater than the normal pore pressure gradient. Subsurface overpressure conditions and their origins have been reported in nearly all the hydrocarbon-bearing sedimentary basins around the world (Plumley, 1980; Spencer, 1987; Hunt, 1990; Swarbrick, 1995; Yassir et al., 1996; Nashaat, 1998; Polutranko, 1998; Slavin & Smirnova, 1998; Holm, 1998; Kumar et al., 2016). The Normal, subnormal and overpressure conditions can co-exist in a sedimentary basin provided they are separated by permeability barriers. Conventionally, pore pressure predictions have been carried out using seismic, drilling and well log data. However, the best approach to pore pressure prediction is to examine the combination of all the available data. Relying on only one type of data can lead to misinterpretations. For example, under poor borehole conditions such as breakouts or washouts, the well log data may produce inaccurate estimates of pore pressure. The same poor borehole conditions may have little or no effect on the drilling parameters.

Table 2. 1 Merits and limitations of pore pressure prediction methods.

Method	Merits	Limitations
Seismic Data	The conventional seismic data can provide pre-drill pore pressure predictions for well planning purposes, especially in exploration drilling. Formation pressure can be predicted real-time ahead of the bit (seismic while drilling).	The seismic responses can be affected by changes in lithology and pore fluid type. The pore pressure prediction accuracy from the seismic data can be very low. The geology of the application basin must be known.
Well log data	Real-time pore pressure prediction using logging while drilling (LWD) data. Under suitable conditions, pore pressure estimates from the well log data provide the most accurate results when compared to other methods of pore pressure prediction.	Well logs can be affected by borehole conditions. Formation pressure is predicted a few feet behind the bit for real-time applications. They cannot be acquired before the well is drilled. For LWD measurements, data quality may be affected by the drilling rate. Rock properties can be affected by other factors than the formation pore pressure.
Drilling parameters	Formation pressure can be estimated real-time at the bit. May provide good pore pressure estimates under suitable conditions. It is relatively inexpensive. Drilling parameter data are readily available.	Not suitable for pre-drill pore pressure predictions along the well path. Data qualities are affected by shocks/vibrations. Drilling parameters are affected by lithology, rock strength, bit type, bit wear, BHA sticking and excessive overbalance.

This can make the pore pressure estimates from the drilling parameters to be more accurate than pore pressure estimates from well logs under such conditions. Similarly, pore pressure estimates from well log data under excessive bit wear conditions are more likely to be more accurate than

the pore pressure estimates derived from the drilling parameters. Table 2.1 summarizes the merits and limitations of each method.

Hottmann & Johnson (1965) proposed a method for predicting the onset of overpressure from the resistivity and sonic logs by correlating the amount of deviation from the normal compaction trend (NCT) at a given depth to the observed pressure in adjacent reservoir formations. Foster & Whalen (1966) developed a pore pressure prediction model based on the concept of the shale formation resistivity factor for regions with varying salinity. Pennebaker (1968) provided a methodology for estimating the formation pore pressure from the seismic data. Seismic data (velocity and acoustic impedance) have been used in several sedimentary basins for pre-drill pore pressure predictions (Sayers et al., 2002; Soleymani & Riahi, 2012; Brahma et al., 2013; El-Werr et al., 2017). Gardner et al. (1974) developed an empirical correlation among vertical effective stress, depth of burial and interval travel time.

Eaton (1975) proposed three sets of empirical relations based on resistivity, sonic and d-exponent data. Eaton's models are given by:

$$G_{pp} = G_{ob} - \{G_{ob} - G_{np}\} \left[\frac{R_o}{R_n} \right]^{1.2}, \quad (2.1)$$

$$G_{pp} = G_{ob} - \{G_{ob} - G_{np}\} \left[\frac{V_o}{V_n} \right]^3, \quad (2.2)$$

$$G_{pp} = G_{ob} - \{G_{ob} - G_{np}\} \left[\frac{d_{co}}{d_{cn}} \right]^{1.2}, \quad (2.3)$$

where G_{pp} is the pore pressure gradient (psi/ft); G_{ob} is the overburden gradient (psi/ft); G_{np} is the normal pore pressure gradient (psi/ft); R_o is the observed shale resistivity (ohm-m); R_n is the normal compaction trend shale resistivity (ohm-m); V_n is the normal compaction shale

compressional velocity (m/s); V_o is the observed shale compressional velocity (m/s); d_{co} is the calculated d_c from measured data; d_{cn} is the d_c from the normal trend line. Eaton's models are the most widely used pore pressure prediction methods for loading conditions where the main origin of overpressure mechanism is compaction disequilibrium, especially in young tertiary sediments.

Bowers (1995) proposed empirical relations between effective stress and compressional sonic velocity to predict the degree of overpressure generated by compaction disequilibrium and fluid expansion mechanisms. Bower's method is applicable to loading and unloading conditions. Bowers' method is also applicable to many sedimentary basins. However, Bower's method may over-predict the formation pore pressure in shallow unconsolidated formations due primarily to very slow compression sonic velocity in such formations (Zhang, 2011). Zhang (2011) adapted the Eaton's model for the resistivity and sonic transit time data using depth-dependent normal compaction equations. Zhang (2013) proposed a theoretical model to estimate the effective stress and formation pore pressure using porosity and compressional sonic velocity data. Rock properties such as bulk and pore compressibility (Atashbari & Tingay, 2012), natural radioactivity (Serebryakov et al., 1995), acoustic impedance (Satti & Yusoff, 2015) and the ratio of compressional to shear velocities (Li et al., 2000; Walls et al., 2000; Ebrom et al., 2006; Saleh et al., 2013) have also been used to predict the onset of overpressure and to estimate the formation pore pressure.

From the field and laboratory observations, the dependency of the ROP on the differential pressure between the bottom-hole pressure and the formation pore pressure has long been established (Murray & Cunningham, 1955; Cunningham & Eenink, 1959; Garnier & Lingen, 1959; Vidrine & Benit, 1968; Combs, 1968; Wardlaw, 1969; Black et al., 1985; Cheatham et al.,

1985). An increase in the formation pore pressure for a given mud weight will cause the drilling rate to increase due to reduced back pressure on the formations. This is the main reason why the driller must stop the drilling operations and perform a flow check any time a positive drilling break is being observed at the well site and more importantly when drilling exploratory wells. The d-exponent method was the first empirical method of estimating formation pore pressure from drilling parameters (Jorden & Shirley, 1966; Harper, 1969; Rehm & Mcclendon, 1971). The empirical model that relates d_c – exponent to drilling parameters is given by:

$$d_c - \text{exponent} = \frac{\log \left[\frac{\text{ROP}}{60N} \right]}{\log \left[\frac{12\text{WOB}}{10^6 D_b} \right]} * \left[\frac{G_{np}}{\text{ECD}} \right], \quad (2.4)$$

where d_c – exponent is the corrected d – exponent; ROP is the rate of penetration (ft/hr); N is the rotary speed in revolution per minute (rpm); WOB is the weight on bit (lbs); D_b is the bit diameter (in); G_{np} is the normal pore pressure gradient (psi/ft or ppg); ECD is the equivalent circulating density (psi/ft or ppg). The values of the d_c – exponent computed over a uniform lithological column (100% shale) are plotted against depth on the semi-log. Under normal pressure conditions, the d_c – exponent will increase with depth. In overpressure intervals, the d_c – exponent will undergo a trend reversal and the amount of deviation from the normal compaction trend (NCT) at any given depth is directly related to the magnitude of overpressure. However, the d – exponent technique does not consider the effect of hydraulic parameters on the ROP. This can lead to inaccurate estimates of formation pore pressure under certain drilling conditions (soft rock environments/unconsolidated formations). The driller can decide to increase the flow rate to clean the hole or reduce the flow rate to minimize the equivalent circulating density (ECD) while

drilling the pressure transition zones. Under these conditions of altering the bit hydraulic energy, the d – exponent method may fail to detect the onset of overpressure.

The mechanical specific energy (MSE) is the energy required to remove a unit volume of rock (Teale, 1965). The MSE combines the axial and torsional loads. The MSE is given by:

$$MSE = \frac{WOB}{A_b} + \frac{120\pi * N * T}{A_b ROP}, \quad (2.5)$$

where MSE is the mechanical specific energy (psi); WOB is the weight on bit (lbs); A_b is the bit area (in^2); N is the rotary speed (rpm); T is the torque on bit (lb-ft); ROP is the rate of penetration (ft/hr). In the absence of reliable downhole torque measurements, Pessier & Fear (1992) expressed the downhole torque as a function of WOB, bit diameter and a bit specific coefficient of sliding friction to eliminate the torque on bit requirement (equation 2.6):

$$MSE = \frac{WOB}{A_b} + \frac{13.33\mu * N * WOB}{D_b ROP}, \quad (2.6)$$

where MSE is the mechanical specific energy (psi); WOB is the downhole weight on bit (lbs); A_b is the bit area (in^2); N is the rotary speed (rpm); D_b is the bit diameter (in); ROP is the rate of penetration (ft/hr); μ is the bit specific coefficient of sliding friction. For field applications, the value of bit coefficient of sliding friction is usually assumed to be 0.25 for roller cone bits and 0.5 for PDC bits (Armenta, 2008). However, the bit coefficient of sliding friction will depend on lithology, rock confined compressive strength, mud weight, bit wear, and depth of cut (Caicedo et al., 2005). Therefore, using a constant value of bit coefficient of sliding friction for a particular bit over the entire drilled section may produce erroneous results. Armenta (2008) showed the importance of bit hydraulic energy on the MSE. Zhou et al. (2017) established a relationship

between MSE and depth of cut. Most works on the applications of specific energy to drilling operations have focused on drilling optimization and identification of downhole drilling problems such as bit balling, bottom hole balling, bit wear, vibration and hole cleaning issues (Waughman et al., 2003; Dupriest & Koederitz, 2005; Dupriest, 2006; Bevilacqua et al., 2013; Abbas et al., 2014; Pinto & Lima, 2016).

The results of the experimental studies performed by Rafatian et al. (2010) on impermeable and permeable rock samples using a single PDC cutter showed that the MSE increases with the confining pressure. Similar experimental works by Akbari et al. (2013) on the Torrey Buff rock samples concluded that the MSE at the underbalanced conditions were considerably lower than the MSE at the balance conditions. Akbari et al. (2014) established an empirical relationship among MSE, uniaxial compressive strength (UCS), differential pressure and confining pressure. Akbari et al. (2014) then concluded that the effect of pore pressure on MSE is similar to that of confining pressure but to a lesser degree and in the opposite direction. Attempts have been made in recent times to estimate the formation pore pressure from the mechanical specific energy (MSE) concept using the field data (Cardona, 2011; Majidi et al., 2017). However, the applications of the MSE to pore pressure predictions have the same limitations as the d – exponent method because the MSE approach does not consider the effect of hydraulic parameters on the ROP. To overcome these limitations, this paper presents a new pore pressure prediction technique based on the concept of hydro-rotary specific energy (HRSE). It approximates the total energy required to break and remove a unit volume of rock.

2.2 Theoretical Background

The MSE proposed by (Teale, 1965) does not necessarily represent the total energy expended in

breaking and removing a unit volume of rock because it excludes the downhole (bit) hydraulic energy component. The bit hydraulic energy weakens the formation ahead of the bit (especially in medium to soft rock environments) and removes the cuttings from the bit face. The hydro-mechanical specific energy (HMSE) is the actual total energy required to break and remove a unit volume of rock (Mohan et al. 2015; Wei et al. 2016; Chen et al., 2016). The HMSE combines the axial, rotary and hydraulic energy (equation 2.7):

$$HMSE = MSE + \frac{\text{Hydraulic Energy}}{\text{Rock Volume Drilled}}. \quad (2.7)$$

Ideally, not all the jet energy at the bit is available for rock penetration and cuttings removal. Due to the accelerated fluid entrainment below the bit nozzles, only a fraction of the available jet energy will reach the bottom of the hole. Therefore, a hydraulic energy reduction factor is introduced into the hydraulics energy term (equation 2.8):

$$HMSE = \frac{WOB}{A_b} + \frac{120\pi NT}{A_b ROP} + \frac{1154\eta \Delta P_b Q}{A_b ROP}, \quad (2.8)$$

where HMSE is the hydro-mechanical specific energy (psi); WOB is the weight on bit (lbs); A_b is the bit area (in^2); N is the rotary speed (rpm); T is the torque on bit (lb-ft); ROP is the rate of penetration (ft/hr); η is the hydraulic energy reduction factor; ΔP_b is the bit pressure drop (psi); Q is the flow rate (gpm). The bit pressure drop can be expressed as a function of mud weight, flow rate and nozzle total flow area (equation 2.9):

$$\Delta P_b = \frac{MW Q^2}{10858 TFA^2}, \quad (2.9)$$

where ΔP_b is the bit pressure drop (psi); MW is the mud weight (ppg); Q is the flow rate (gpm);

TFA is the total flow area (in^2). The value of η ranges from 25 – 40 % (Warren, 1987). According to Warren (1987), the actual value of η depends on the ratio of jet velocity to return fluid velocity (equation 2.10):

$$\eta = 1 - \left[\frac{\text{Jet Velocity}}{\text{Return Bit Velocity at Bit Face}} \right]^{-0.122}. \quad (2.10)$$

However, η can also be expressed as a ratio of bit return flow area to nozzle total flow area since the flow rate is the same everywhere along the fluid flow path (equation 2.11):

$$\eta = 1 - \left[\frac{\text{Bit Return Flow Area}}{\text{TFA}} \right]^{-0.122}. \quad (2.11)$$

For roller cone bits, the bit return flow area is about 15 % of the bit area (in^2) (equation 2.12):

$$\eta_{\text{Roller Cone Bit}} = 1 - \left[\frac{0.15 \text{ Bit Area}}{\text{TFA}} \right]^{-0.122}. \quad (2.12)$$

For PDC bits, the bit area available for fluid return is equal to the junk slot area (equation 2.13):

$$\eta_{\text{PDC Bit}} = 1 - \left[\frac{\text{JSA}}{\text{TFA}} \right]^{-0.122}, \quad (2.13)$$

where JSA is the junk slot area (in^2); TFA is the total flow area (in^2). Equation 2.13 implies that the amount of PDC bit hydraulic energy that is available at the bottom of the hole will increase with increasing JSA and decreasing TFA for a given bit size. Therefore, for the roller cone bits, the HMSE can be obtained by combining equations 2.8, 2.9 and 2.12 (equation 2.14):

$$\text{HMSE} = \frac{\text{WOB}}{A_b} + \frac{120\pi NT}{A_b ROP} + \frac{0.10628 \text{ MW } Q^3 \left[1 - \left[\frac{0.15 \text{ Bit Area}}{\text{TFA}} \right]^{-0.122} \right]}{A_b ROP \text{ TFA}^2}. \quad (2.14)$$

Similarly, the HMSE for PDC bits is obtained from equations 2.8, 2.9 and 2.13 (equation 2.15):

$$HMSE = \frac{WOB}{A_b} + \frac{120\pi NT}{A_b ROP} + \frac{0.10628 MW Q^3 \left[1 - \left[\frac{JSA}{TFA} \right]^{-0.122} \right]}{A_b ROP TFA^2}, \quad (2.15)$$

In this study, the HMSE for PDC bits is considered as the reference case. Changes in the mud weight/equivalent circulating density (ECD) will result in changes in the values of HMSE. Excessive overbalance increases the strength of the surrounding rocks and the chip hold down pressure at the bottom of the hole. This can cause the ROP to reduce and the HMSE to increase when drilling through the pressure transition and overpressure zones. Hence, the HMSE must be corrected for the effect of changes in the bottom-hole pressure (equation 2.16):

$$HMSE = \left[\frac{WOB}{A_b} + \frac{120\pi NT}{A_b ROP} + \frac{0.10628 MW Q^3 \left[1 - \left[\frac{JSA}{TFA} \right]^{-0.122} \right]}{A_b ROP TFA^2} \right] * \left[\frac{G_{np}}{ECD} \right], \quad (2.16)$$

where G_{np} is the normal pore pressure gradient (psi/ft or ppg) and ECD is the equivalent circulating density (psi/ft or ppg). The contribution of the axial energy due to WOB to the total energy is less than 1% (Menand & Mills, 2017). The rotary and hydraulic energies make up over 99% of the HMSE term. Also, the rotary energy term in the HMSE equation has indirectly accounted for the axial energy term because the downhole torque responds in direct proportion to the WOB (Pessier & Fear, 1992). Hence, the axial energy term in the HMSE equation can be neglected, leading to the concept of hydro-rotary specific energy (HRSE). The HRSE contains only the rotary and hydraulic terms (equation 2.17):

$$HRSE = \left[\frac{120\pi NT}{A_b ROP} + \frac{0.10628 MW Q^3 \left[1 - \left[\frac{JSA}{TFA} \right]^{-0.122} \right]}{A_b ROP TFA^2} \right] * \left[\frac{G_{np}}{ECD} \right]. \quad (2.17)$$

In normally pressured compacted series, rock density and degree of rock compaction will increase with depth as pore fluids are being expelled gradually from the underlying sediments. Under these conditions, rock porosity will decrease and grain – to – grain contact force will increase with depth due to an increase in effective stress. Hence, the energy (HRSE) required to remove a unit volume of rock will increase with depth. However, subsurface overpressure conditions will cause a reversal in the HRSE trend as effective stress decreases. For overpressure conditions associated with under-compaction, rock density and degree of rock compaction will decrease as the formation water becomes trapped and begins to support the weights of the overlying sediments. This will cause the rock porosity to increase and the grain – to – grain contact force to decrease with a decrease in effective stress. The HRSE can also be applicable to overpressure conditions caused by fluid expansion mechanisms because the ease of rock removal is directly related to the differential pressure between the mud pressure and the pore pressure.

For accurate pore pressure prediction, downhole measurements data (torque and rotary speed) from the measurement while drilling sensor (MWD) sensors should be used to compute the HRSE. If surface measurements data are used instead, the HRSE will be grossly overestimated, especially in deviated wells where there can be a significant amount of friction between the drill string and the borehole walls along the well path. In a vertical well, it may be possible to use the surface measurements data to compute HRSE because the friction between the drill string and the borehole walls along the well path is negligible, provided there is no excessive vibration of the bottom-hole assembly (BHA) and bit while drilling. There are various ways in which downhole torque can be determined from the surface measurements if the

downhole sensors data are not available. The torque on bit (TOB) can be determined from the difference between the on-bottom and off-bottom torque while drilling in rotary mode. The TOB can be determined from the WOB value if the coefficient of sliding friction between the bit cutters and the formation is known (Pessier & Fear, 1992). When drilling with the steerable system (mud motor), the TOB can be computed from the differential pressure across the mud motor. The TOB can also be calculated at any given depth using torque and drag (T & D) models by subtracting the estimated drill string torque from the measured surface torque while drilling.

2.3 Methodology

Below are the steps required to estimate the formation pore pressure using HRSE concept. Figure 2.2 provides a simple workflow for the proposed methodology.

1. Compute the HRSE at various depths from the drilling, bit and well parameters using equation 2.17. It is recommended that the HRSE be computed over the clean shale intervals. This will eliminate any lithological effects on the HRSE. However, the HRSE can also be computed over the entire lithological column that consists of several stratigraphic units if the effect of lithology on the HRSE is not pronounced (i.e. no wide variations in HRSE values due to different stratigraphic units being penetrated).
2. Plot the HRSE values against depth on a semi-log (Figure 2.1). Establish the normal compaction trend (NCT) through the known normally pressured intervals. Under normal pressure conditions, the HRSE will increase with depth. When the overpressure intervals are penetrated, the HRSE will start to diminish. The amount of divergence of a given point from the established NCT is proportional to the magnitude of the overpressure.

Figure 2.1 illustrates the application of the HRSE concept to overpressure prediction.

From 8,000 ft-TVD to 13,000 ft-TVD, the HRSE values exhibit a normal compaction trend. However, deviation in HRSE values from the normal compaction trend below 13,000 ft-TVD signifies the onset of overpressure.

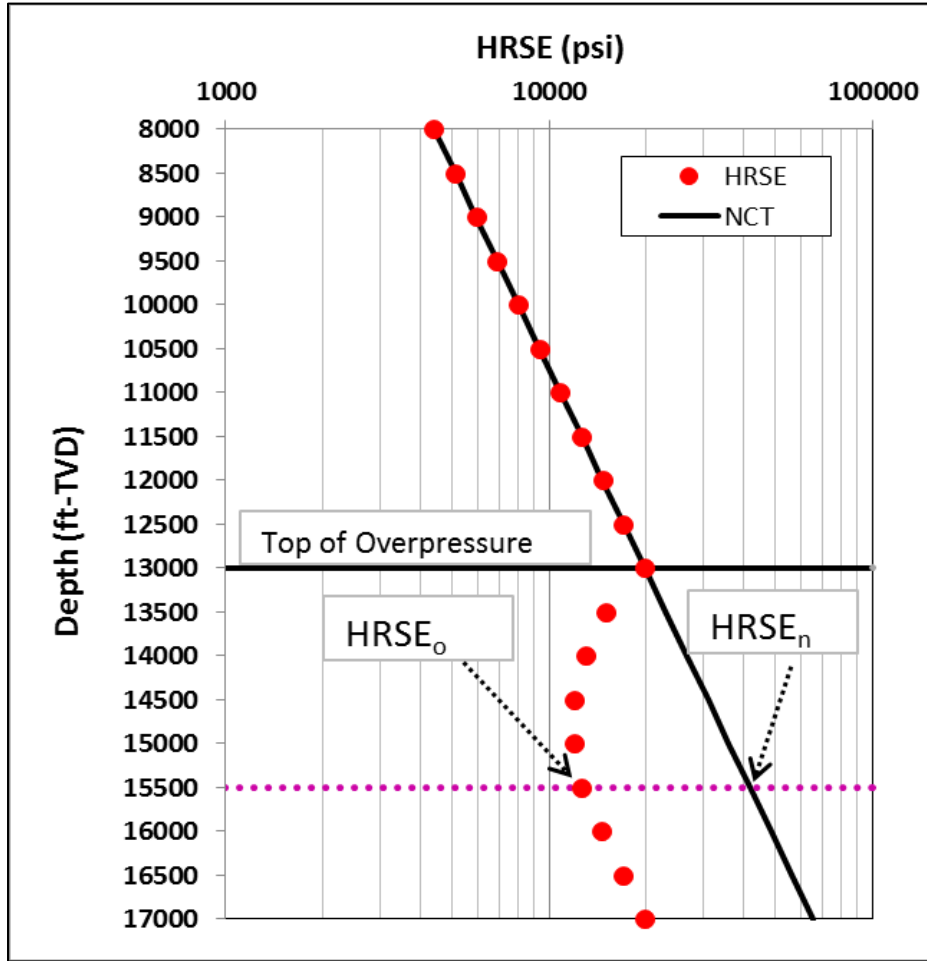


Figure 2. 1 Illustration of the HRSE method for pore pressure prediction.

3. Compute the pore pressure at a given depth using the modified Eaton's model given by:

$$G_{pp} = G_{ob} - \{G_{ob} - G_{np}\} * \left[\frac{HRSE_o}{HRSE_n} \right]^m, \quad (2.18)$$

where G_{pp} is the pore pressure gradient (psi/ft); G_{ob} is the overburden gradient (psi/ft); G_{np} is the normal pore pressure gradient (NPPG) in psi/ft; $HRSE_o$ is the actual HRSE

calculated using equation 2.17; $HRSE_n$ is the hypothetical value of HRSE from the normal compaction trend; m is the HRSE exponent. The value of the HRSE exponent will vary from region to region. The HRSE exponent can be derived by calibrating equation 2.18 to any known overpressure intervals in the offset wells. It can also be determined in the well being drilled by calibrating equation 2.18 to any overpressure intervals predicted by the well log data (shale compressional sonic velocity and resistivity) preferably while drilling the pressure transition zones.

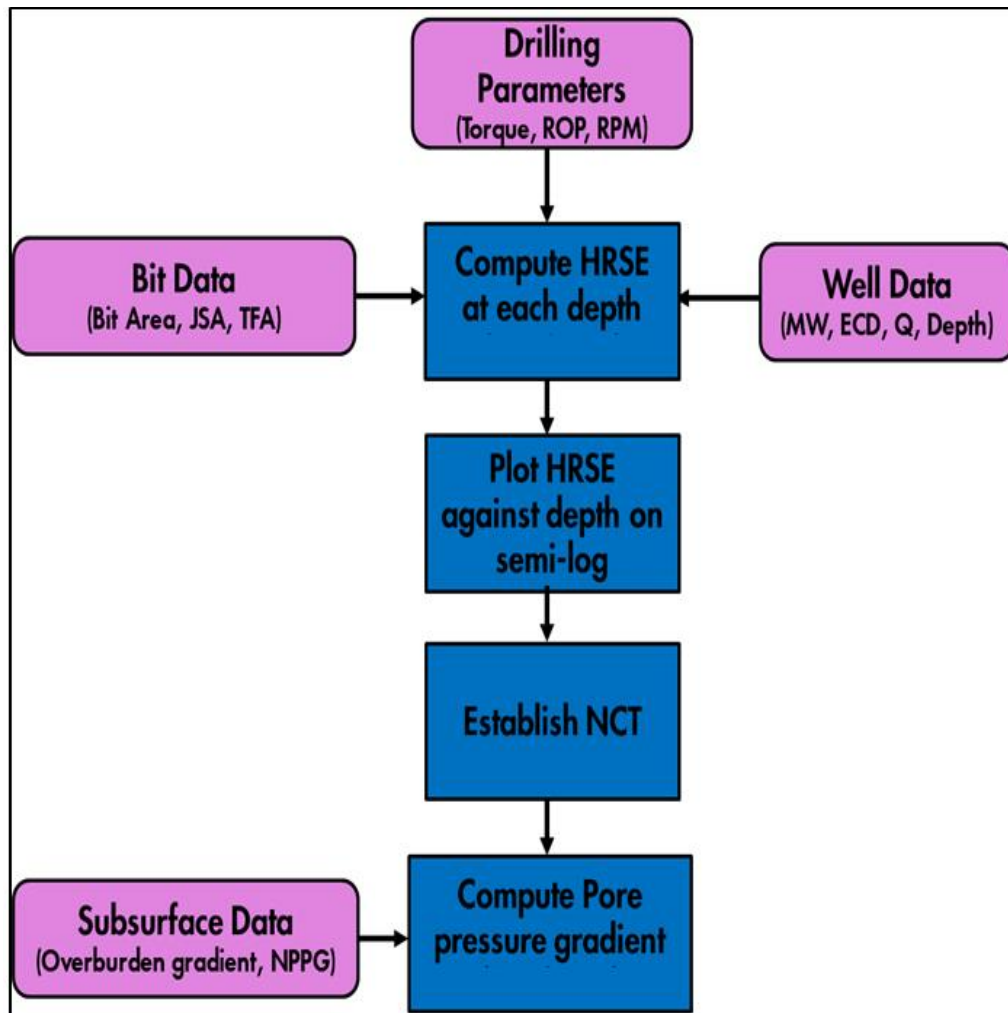


Figure 2. 2 The work flow for the proposed methodology.

2.4 Field Example

To demonstrate the application of the HRSE concept to pore pressure prediction, a recently drilled deep vertical exploratory gas well (well A) is considered as the case study. The well is located about 80 km North-West of Port Harcourt in the Tertiary Deltaic System in the central swamp region of the Niger Delta in Nigeria (Figure 2.3).

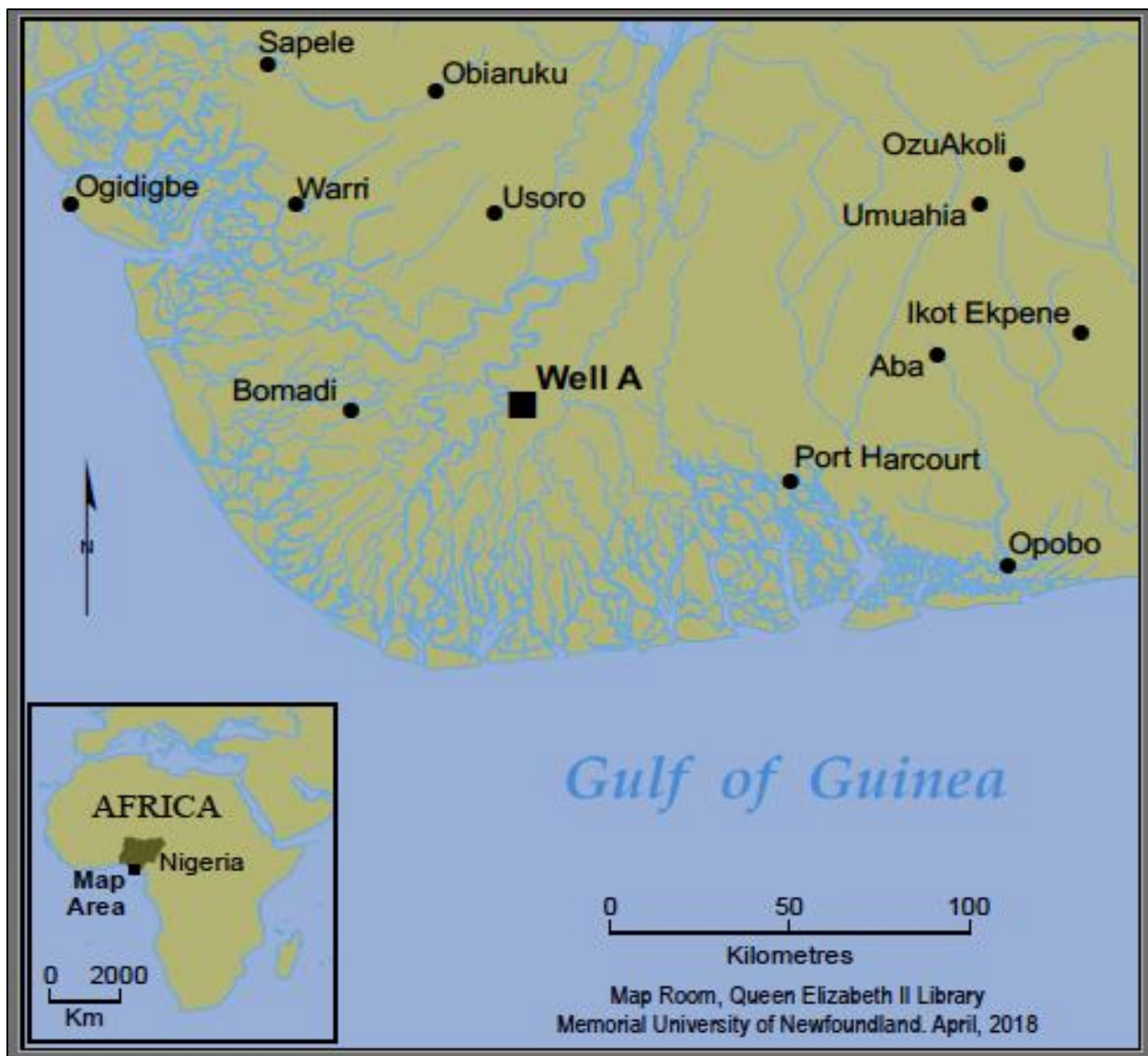


Figure 2.3 Location map for well A.

The Niger Delta Basin is an extensional rift basin that consists of Tertiary clastic sediments up to 12 km thick. The Niger Delta sequence stratigraphy consists of three types of formations in descending order: (1) Benin formations – consist of mainly continental sands, (2) Agbada formations – consist of alternating sequence of sands and shales, and (3) Akata formations – consist of marine shales (Short & Stauble 1967; Avbovbo 1978; Adewole et al. 2016). Well A only penetrates Benin and Agbada formations. The hydrocarbons trapping mechanisms in the Niger Delta are mainly growth faults associated with rollover structures. The primary cause of the subsurface overpressure conditions in the Niger Delta is under-compaction (Daukoru 1975; Ugwu & Nwankwo 2014). The Niger Delta sands have good porosity and permeability. Sands with more than 25% porosity and permeability in the range of 1 – 5 Darcy are not uncommon. In this paper, all depths are with respect to the true vertical depth (TVD) below the rotary table (RT). Table 2.2 and Figure 2.4 provide information about the well configuration, mud type, BHA type, bit type and the formations that were penetrated.

Table 2. 2 The well data summary.

Hole Size (inches)	Casing Size (inches)	Casing Depth (feet)	Lithology	Mud Type	BHA	Bit Type
Piled	30	307	Loose sands	N/A	N/A	N/A
22	18 5/8	4,259	Continental sands	WBM	Steerable	Roller cone
16	13 3/8	10,092	Sand - Shale	WBM	Steerable	Roller cone
12 1/4	9 7/8	15, 224	Sand - Shale	SOBM	RSS & Steerable	PDC
8 1/2	N/A	N/A	Sand - Shale	SOBM	RSS	PDC

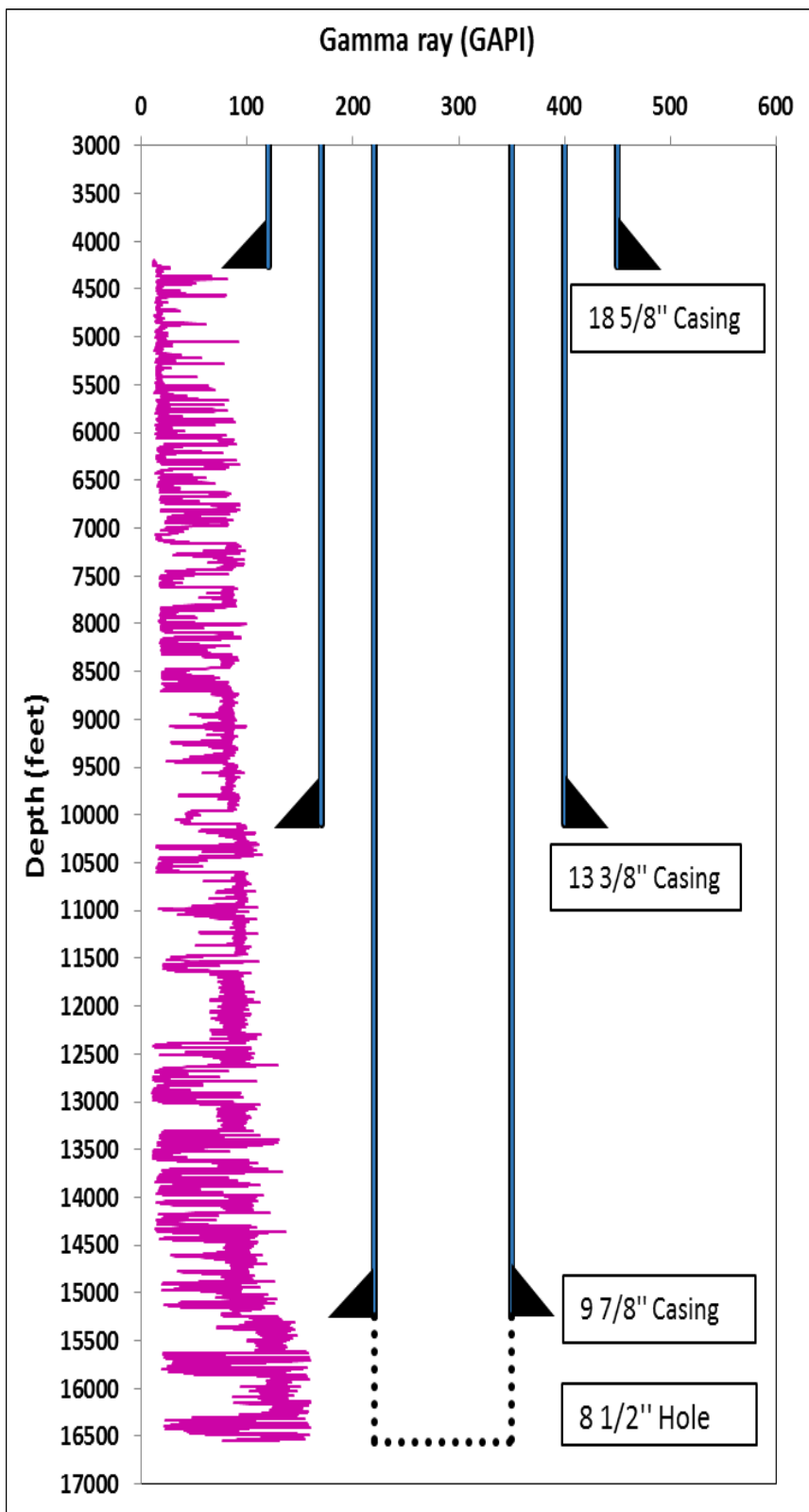


Figure 2. 4 The well configuration and lithology.

The 30" conductor pipe was driven to refusal at 307 ft. After cleaning the conductor pipe, the 22" hole was drilled from 307 ft to 4,269 ft. The 18 5/8" surface casing was run and cemented to surface with the shoe at 4,259 ft. The 16" hole was drilled from 4,269 ft to 10,099 ft. The 13 3/8" intermediate casing was run to 10,092 ft and cemented in place. The 12 1/4" hole section was drilled from 10,099 ft to 15,241 ft. The 9 5/8" production casing was run and cemented with the shoe deep into the pressure transition shale at 15,224 ft to provide the required kick tolerance to drill the 8 1/2" hole overpressure intervals. The 8 1/2" hole section was drilled from 15,241 ft to 15,567 ft and the well was suspended. Table 2.3 provides information about the bits used to drill the hole sections of interest (12 1/4" and 8 1/2"). All the bits used were new bits prior to running in hole except the 12 1/4", HCC, QD 507 FHX, M323 bit that was run as a re-run bit. There was no bit grading for the last bit because it was lost in hole due to a pipe stuck incident that followed well killing operations after taking a gas kick from the bottom of the well.

Table 2. 3 The bit data summary.

Bit Data	Drilled Intervals (ft-TVD)	TFA (in ²)	JSA (in ²)	Bit Dull Grade Out
12 1/4", HCC, Q 506 F, M323	10099 - 15080	1.2824	31.48	2-5-WT-G-X-1-CT-BHA
12 1/4", HCC, QD 507 FHX, M323	15080 - 15241	1.2962	21.28	1-2-CT-S-X-1-NO-TD
8 1/2", HCC, DPD 506, M223	15241 - 16159	0.7777	13.94	1-2-WT-A-X-1-NO-DTF
8 1/2", HCC, QD 408 FHX, M433	16159 - 16567	0.7823	10.97	N/A

The top-hole sections (22" & 16") are excluded from the analysis because data acquisitions in these sections were limited and the sections consist of predominantly unconsolidated sands with no hydrocarbon-bearing or overpressure intervals. The data analysis is focused on the deeper 12 1/4" and 8 1/2" hole sections drilled with mostly rotary steerable system (RSS) assemblies and

polycrystalline diamond compact (PDC) bits. These sections consist of hydrocarbon bearing intervals, normally pressured compacted series, pressure transition zones and overpressure intervals. The drilling parameters were acquired every 1 ft and out of range (unrealistic) data were filtered out. Figure 2.5 shows the plots of the actual drilling parameters acquired while drilling well A. The TOB values were computed from the difference between the measured on-bottom and off-bottom torque (dark-blue colour) and were validated with the TOB values estimated from the T & D model (pink colour).

The overburden pressure (S_v) can be obtained by integrating the formation bulk density from the surface to the depth of interest and it is given by:

$$S_v = 0.433 \int_0^z \rho_b dz , \quad (2.19)$$

$$\rho_b = 0.9526 Z^{0.101}, \quad (2.20)$$

where ρ_b is the formation bulk density as a function of depth (g/cc); Z is the depth of interest (ft). In well A, the density log was only acquired in the 12 ¼" hole. To obtain the overburden pressure at each depth of interest, the density log in the 12 ¼" hole section of this well was integrated with the offset well density log to produce the equation of best fit (equation 2.20). The equation of best fit was then used to compute the formation bulk density values in the intervals where the density log data were not available. The overburden gradient (G_{ob}) was obtained by dividing the overburden pressure by the true vertical depth. Figure 2.6 shows the plots of formation bulk density, overburden pressure and overburden gradient versus depth for well A.

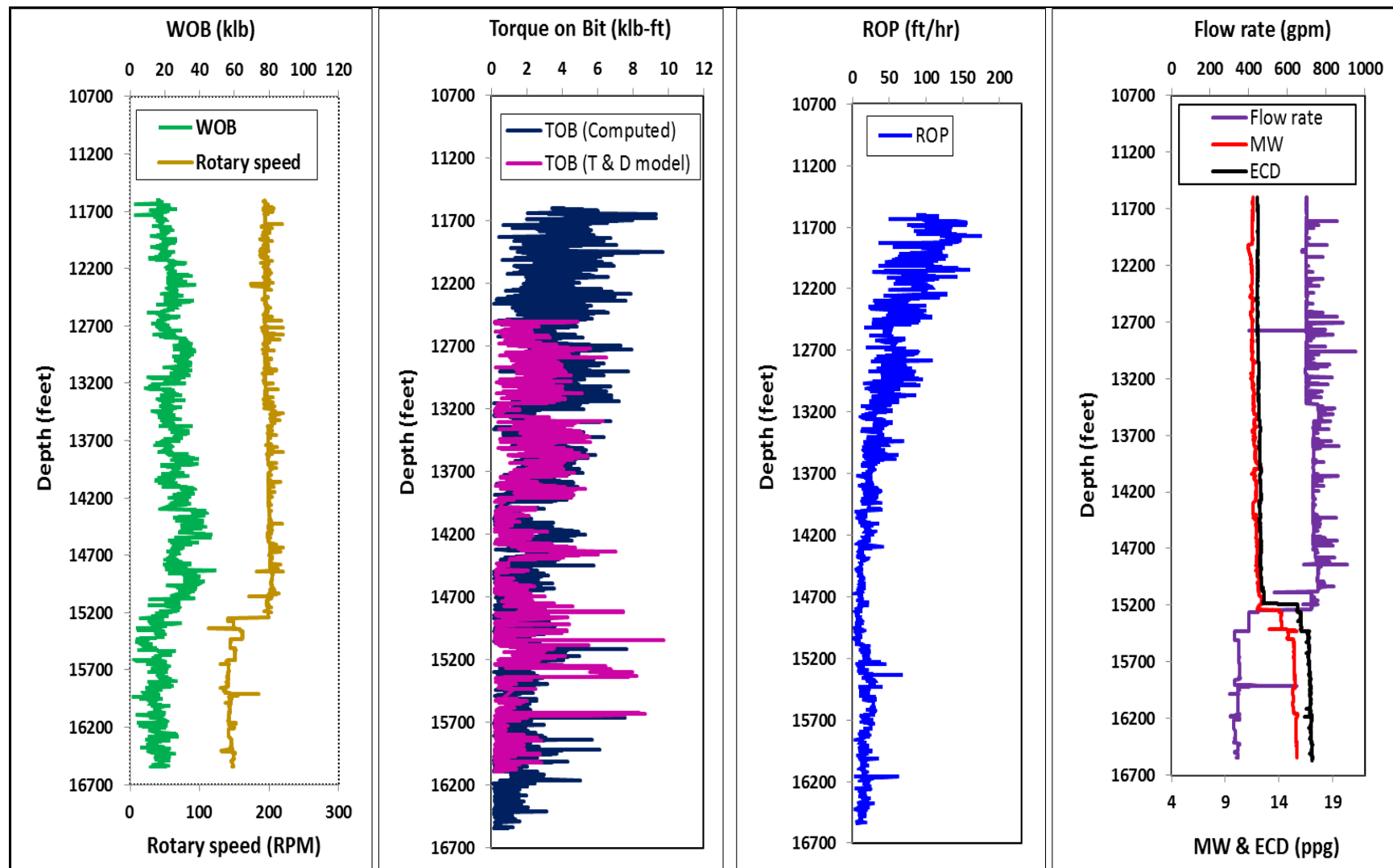


Figure 2. 5 The plots of drilling parameters versus depth for well A.

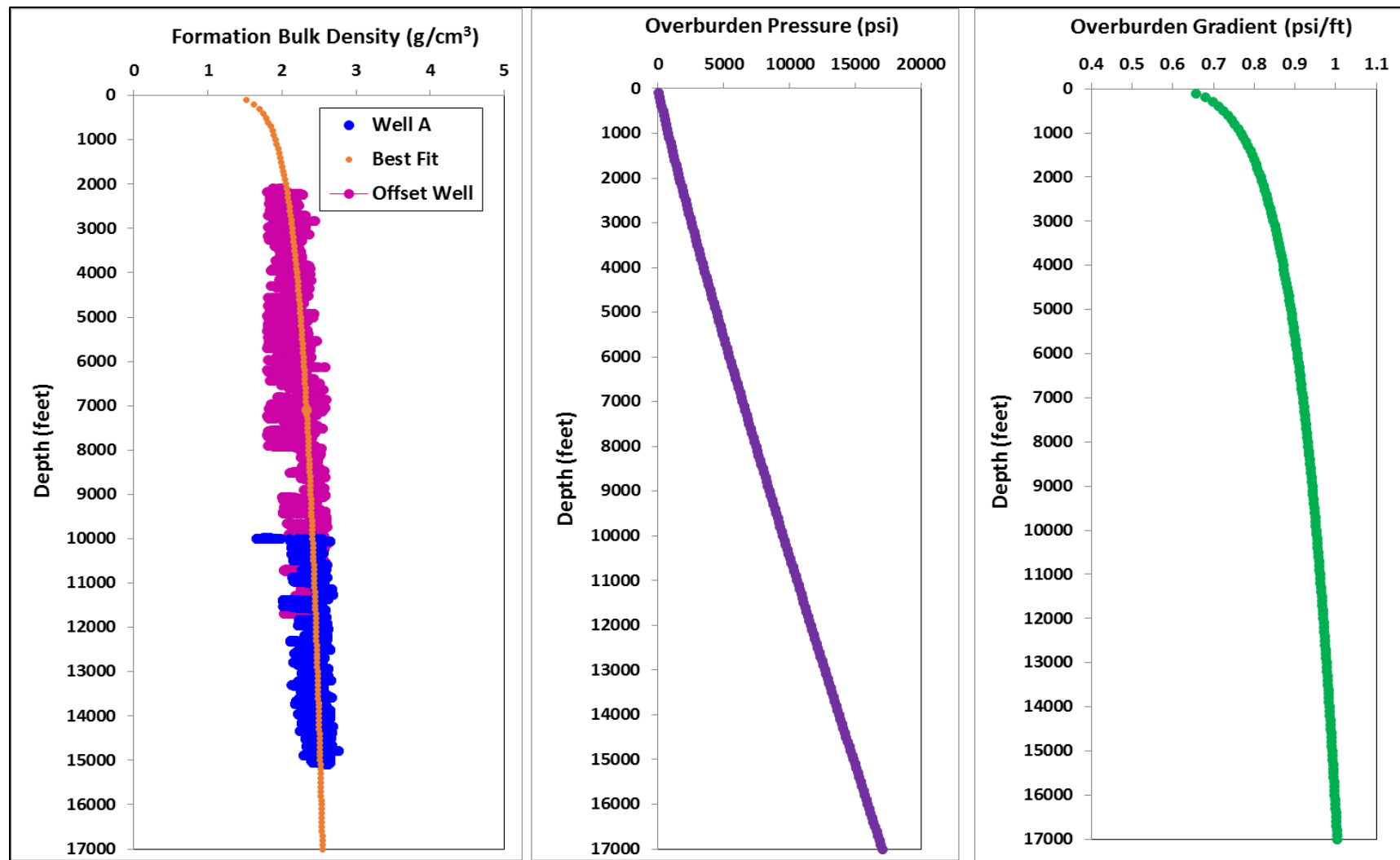


Figure 2. 6 The plots of formation bulk densities, overburden pressure and overburden gradient versus depth for well A.

2.5 Discussion

The plot of HRSE versus depth is shown in Figure 2.7. The HRSE values are computed across the sand and shale intervals because the effect of lithology on the HRSE is not pronounced in this well and the normal compaction trend can be clearly identified. From 11,600 ft to 15,060 ft, the HRSE increases with depth due to an increase in vertical effective stress. These depth intervals correspond to the normally pressured compacted series in the field with a pore pressure gradient of 0.45 psi/ft and they are used to establish the NCT. Below the 15,060 ft (top of overpressure), the HRSE begins to undergo a departure from the NCT to lower values due to the presence of subsurface overpressure conditions. As the formation pore pressure increases in the under-compacted series (decrease in vertical effective stress), the degree of rock compaction decreases. Under these conditions, the energy required to remove a unit volume of rock (HRSE) decreases. Hence, the reversal in the HRSE trend can be used to identify the overpressure intervals. From Figure 2.7, the HRSE clearly identifies the top of overpressure (15,060 ft), the pressure transition intervals (15,060 – 15,400 ft) and the overpressure zones (>15,400 ft).

Figure 2.7 also shows the plots of d_c – exponent, gamma ray (GR) and shale compressional sonic velocity versus depth. The d_c – exponent values are computed using equation 2.4. In the intervals that correspond to the normally pressured zones, the d_c – exponent and shale compressional sonic velocity increase with depth (similar in trend to HRSE). Below the top of overpressure at 15,060 ft, the d_c – exponent, and shale compressional sonic velocity start to deviate from the NCT to lower values in the same manner as HRSE. Increase in formation pore pressure (decrease in vertical effective stress) causes a reversal in the d_c – exponent and shale compressional velocity trends.

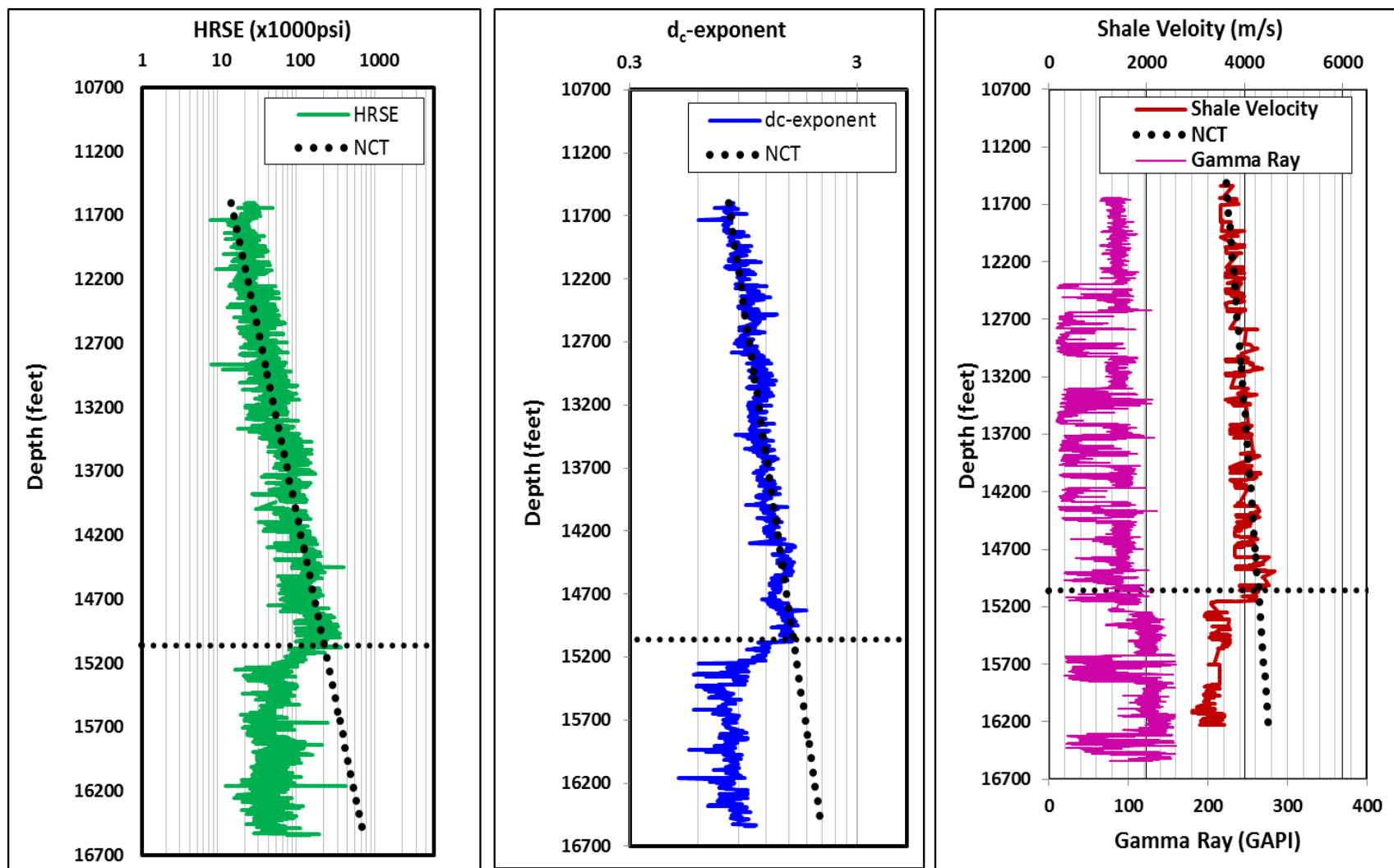


Figure 2. 7 The plots of HRSE, dc – exponent, gamma ray, and shale compressional sonic velocity versus depth for well A.

It is relatively easy to attribute the reversal in the HRSE trend in the 12 $\frac{1}{4}$ " hole to a new bit change. A critical review of the well information suggests otherwise. The first bit (12 $\frac{1}{4}$ ", HCC, Q 506 F, M323) penetrated about 20 ft into the pressure transition zones before being pulled out of hole. The bit was pulled out of hole to change the BHA configuration so that the logging while drilling (LWD) sensors for pore pressure predictions (GR, sonic and resistivity) could be placed closer to the bit. The gradual (not sudden) decrease in the HRSE, with the corresponding decrease in the d_c – exponent and shale compressional sonic velocity below 15,060 ft in the 12 $\frac{1}{4}$ " hole section suggests that the reversal in HRSE trend is most likely due to the presence of subsurface overpressure conditions rather than the bit change. Finally, a drill bit change that occurred in the 8 $\frac{1}{2}$ " hole section at 16,159 ft did not produce any corresponding shift in HRSE and d_c – exponent trends. It should be noted that efficient/improved drilling conditions can also result in the reversal of the HRSE trend. Hence, any reversal in the HRSE trend while drilling should be investigated especially while drilling the exploratory wells. The gradual reversal in the HRSE trend, with corresponding reversal in the shale petrophysical properties (compressional sonic velocity, density and resistivity) will most likely indicate the presence of overpressure. The sudden reversal in the HRSE trend with no corresponding reversal in the shale petrophysical properties will most likely indicate efficient/improved downhole drilling conditions.

Figure 2.8 compares the pore pressure estimates derived from the HRSE, d_c – exponent, and shale compressional velocity to the actual pore pressure measurements taken in the reservoir sands of interest. The actual pore pressure measurements were obtained from the combination of formation pressure while drilling tool (Tes-Trak), wireline pressure sampling tool (RCX - reservoir characterization explorer) and gas kick data. The pore pressure estimates from the shale compressional velocity and d_c – exponent are derived from Eaton's models (equations 2.2 and

2.3 respectively). The pore pressure estimates from the HRSE are derived from equation 2.18 with the value of the HRSE exponent (m) equal to 0.32. The HRSE exponent is obtained by calibrating equation 2.18 to the pore pressure estimates derived from the sonic log data in the upper sections of the pressure transition zones (15,060 – 15,300 ft). A single constant value of 8.66 ppg (0.45 psi/ft) average equivalent density is used for the normal pore pressure gradient (NPPG) based on the formation water density/salinity in the region. From Figure 2.8, The HRSE predicts the formation pore pressure gradient to be normal down to 15,060 ft with an average value of 0.45 psi/ft. In the transition zones, the HRSE predicts a gradual shift from the normal pore pressure regime to overpressure regime (the formation pore pressure gradient increases from 0.45 psi/ft to 0.68 psi/ft). In the overpressure intervals, the formation pore pressure gradient predicted by HRSE increases further from 0.68 psi/ft at 15,400 ft to 0.81 psi/ft at 16,250 ft. The formation pore pressure gradient then remains relatively constant at 0.81 psi/ft from 16,250 ft to the well total depth. There is an excellent agreement in magnitude and trend between the pore pressure estimates derived from the HRSE concept and the actual pore pressure measurements. The shale compressional sonic velocity also provides good estimates of the formation pore pressure. However, the shale compressional sonic velocity is unable to provide the pore pressure estimates at the well TD because of the offset between the bit and the acoustic sensors. The $d -$ exponent method provides good estimates in the deeper sections of the well but over-predicts the formation pore pressure in the intervals immediately below the pressure transition zones, reaching a formation pore pressure of 0.81 psi/ft just below 15,400 ft. From the drilling optimization perspective, using the pore pressure estimates derived from the $d -$ exponent method to design the mud weight (MW) required to drill through the intervals just below the transition zones with an average actual formation pore pressure of 0.72 psi/ft will create an

excessive overbalance, which can result in ROP reduction. If the next casing depth or total depth is to be called off before drilling through the intervals with formation pore pressure of 0.81 psi/ft, using the pore pressure estimates derived from the d – exponent method to design the mud weight may also result in lost circulation and pipe sticking incidents. Although the d – exponent method over-predicts the formation pore pressures in some overpressure intervals, it is relatively accurate in this well (in the deeper sections) because the downhole drilling conditions are suitable to its applications. The well is vertical, the bit hydraulic energy is relatively constant in each hole section and the rocks are consolidated (shale compressional sonic velocity is greater than 3,387 m/s above the overpressure intervals). Table 2.4 summarizes the main differences between HRSE and d – exponent.

Table 2. 4 Main differences between HRSE and d – exponent.

	HRSE	d – exponent
1	Exclude the WOB term	Include WOB term
2	Include the torque term	Exclude torque term
3	Include the bit hydraulic energy term. Consider variations in bit hydraulic energy.	Excluded the bit hydraulic energy term. Does not consider variations in bit hydraulic energy
4	Can be applicable to hard and soft rock environments. Soft rocks are more response to rotary speed and bit hydraulics than WOB.	Mostly suitable for hard rock environments. Hard rocks are more response to WOB.

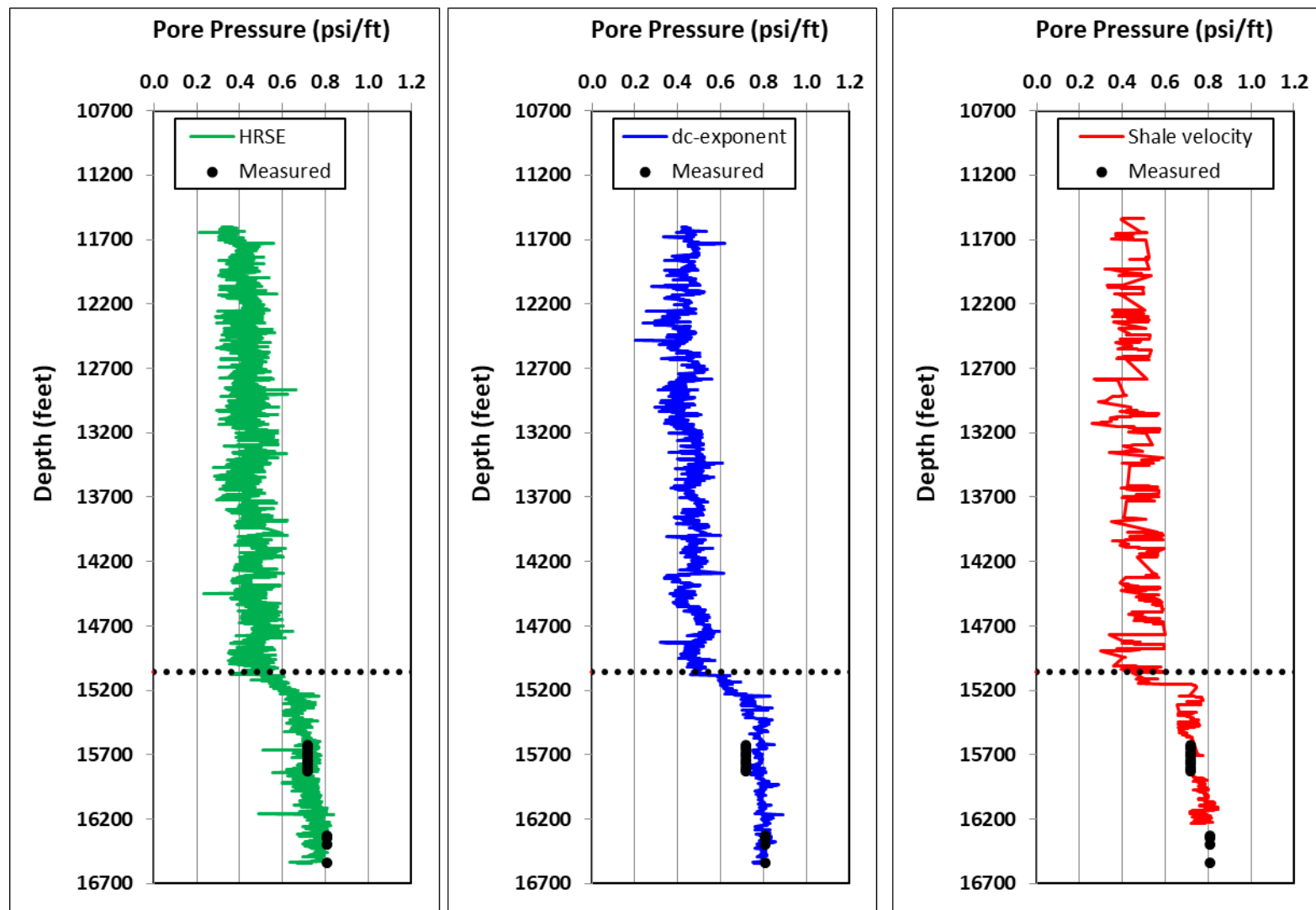


Figure 2. 8 Measured and estimated pore pressure profiles for Well A.

2.6 Conclusions

A new pore pressure prediction technique based on the amount of energy expended while drilling is being proposed. This is based on the principle that overpressure intervals with lower effective stress will require less energy to drill than the normally pressured intervals at the same depth. Under normal pressure conditions, the HRSE will increase with depth as rock compaction and effective stress increase. Drilling through the overpressure zones will cause a reversal in the HRSE trend. The field example presented in this paper demonstrates the applicability of the HRSE method in predicting the onset of overpressure and estimating the formation pore pressure. An excellent agreement is observed in magnitude and trend between the pore pressure estimates derived from the HRSE concept and the actual pore pressure measurements. The formation pore pressure prediction accuracy from the HRSE concept is also comparable to compressional sonic velocity. Unlike the d-exponent method, the HRSE method includes the bit hydraulic energy term, thereby extending its application to some drilling environments (soft rock environments/unconsolidated formations, varying jet hydraulic energy, etc.) where the d-exponent method may not work.

However, the ability of the HRSE method to predict the onset of overpressure and its magnitude will depend greatly on the quality of the input data. TOB measurements from the bit/BHA subjected to vibrations (axial, torsional/stick-slip, whirl) will produce erroneous results. Computed TOB from the surface data will produce inaccurate results if the BHA is subjected to downhole buckling conditions. Excessive bit wear and bit balling can also mask the reversal in the HRSE trend when drilling through the pressure transition zones. To improve the quality of the input data, downhole sensors should be properly calibrated before run in hole. Noise should be minimized in the data transmission system. Shocks and vibrations should be minimized while

drilling (optimize BHA design, bit selection, shock sub application for axial vibration, drilling parameters optimization). Multiple sources of measurements should be made for comparison purposes. For example, the TOB from the downhole sensors should be compared to surface derived TOB. If possible, avoid changing from the bit type in the same hole interval (e.g. from roller cone bit to PDC bit). Compute the HRSE over clean shale intervals only if the effect of lithology is noticed on the HRSE.

2.7 Reference

- Abbas, K.R., Hassanpou, A., Hare, C., Ghadiri, M., 2014. “Instantaneous Monitoring of Drill Bit Wear and Specific Energy as a Criteria for the Appropriate Time for Pulling Out Worn Bits.” Soc. Pet. Eng. (SPE 172269).
- Adewole, E.O., Macdonald, D.I.M., Healy, D., 2016. Estimating density and vertical stress magnitudes using hydrocarbon exploration data in the onshore Northern Niger Delta Basin, Nigeria: Implication for overpressure prediction. J. African Earth Sci. 123, 294–308. <https://doi.org/10.1016/j.jafrearsci.2016.07.009>
- Akbari, B., Miska, S., Mengjiao, Y., Ozbayoglu, E., 2013. Effect of Rock Pore Pressure on Mechanical Specific Energy of Rock Cutting Using Single PDC Cutter. Am. Rock Mech. Assoc. (ARMA 13-205).
- Akbari, B., Miska, S., Yu, M., Ozbayoglu, M., 2014. Experimental Investigations of the Effect of the Pore Pressure on the MSE and Drilling Strength of a PDC Bit. Soc. Pet. Eng. (SPE 169488). <https://doi.org/10.2118/169488-MS>
- Armenta, M., 2008. Identifying Inefficient Drilling Conditions Using Drilling-Specific Energy. Soc. Pet. Eng. (SPE 116667). <https://doi.org/10.2118/116667-MS>
- Atashbari, V., Tingay, M., 2012. Pore Pressure Prediction in a Carbonate Reservoir. Soc. Pet. Eng. (SPE 150836).
- Avbovbo, A.A., 1978. Tertiary lithostratigraphy of the Niger Delta. Am. Assoc. Pet. Geol. Bull. 62, 295–306.
- Belonin, M.D., Slavin, V.I., 1998. Abnormally high formation pressures in petroleum regions of

- Russia and other countries of the C.I.S. Law, B.E., G.F. Ulmishek, V.I. Slavin eds., Abnorm. Press. Hydrocarb. Environ. AAPG Mem. 70, 115–121.
- Bevilacqua, M., Ciarapica, F.E., Marchetti, B., 2013. Acquisition, Processing and Evaluation of Down Hole Data for Monitoring Efficiency of Drilling Processes. *J. Pet. Sci. Res.* 2, 49–56.
- Black, A.D., Dearing, H.L., DiBona, B.G., 1985. Effects of Pore Pressure and Mud Filtration on Drilling Rates in a Permeable Sandstone. *J. Pet. Technol.* 37, 1671–1681. <https://doi.org/10.2118/12117-PA>
- Bowers, G.L., 1995. Pore pressure estimation from velocity data: Accounting for overpressure mechanisms besides undercompaction. *SPE Drill. Complet.* 10, 89–95. <https://doi.org/10.2118/27488-PA>
- Brahma, J., Sircar, A., Karmakar, G.P., 2013. Pre-drill pore pressure prediction using seismic velocities data on flank and synclinal part of Atharamura anticline in the Eastern Tripura, India. *J. Pet. Explor. Prod. Technol.* 3, 93–103. <https://doi.org/10.1007/s13202-013-0055-0>
- Caicedo, H.U., Calhoun, W.M., Ewy, R.T., 2005. Unique ROP Predictor Using Bit-specific Coefficient of Sliding Friction and Mechanical Efficiency as a Function of Confined Compressive Strength Impacts Drilling Performance. *Soc. Pet. Eng. (SPE/IADC 92576)*. <https://doi.org/10.2118/92576-MS>
- Cardona, J., 2011. Fundamental Investigation of Pore Pressure Prediction during Drilling from the Mechanical Behaviour of Rocks. PhD Thesis, Texas A&M Univ. Mech. Eng.
- Chen, X., Gao, D., Guo, B., Feng, Y., 2016. Real-time optimization of drilling parameters based on mechanical specific energy for rotating drilling with positive displacement motor in the hard formation. *J. Nat. Gas Sci. Eng.* 35, 686–694. <https://doi.org/10.1016/j.jngse.2016.09.019>
- Combs, D.G., 1968. Prediction o Pore Pressure From Penetration Rate. *Soc. Pet. Eng. (SPE 2162)*.
- Cunningham, R. a, Eenink, J.G., 1959. Laboratory Study of Effect of Overburden, Formation and Mud Column Pressures on Drilling Rate of Permeable Formations. *Pet. Trans. AIME* 217, 9–17.
- Daukoru, J.W., 1975. PD 4(1) Petroleum Geology of the Niger Delta. *World Pet. Congr.*
- Dupriest, F.E., 2006. Comprehensive Drill-Rate Management Process To Maximize Rate of Penetration. *Soc. Pet. Eng. (SPE 102210)*. <https://doi.org/10.2118/102210-MS>

- Dupriest, F.E., Koederitz, W.L., 2005. Maximizing Drill Rates with Real-Time Surveillance of Mechanical Specific Energy. Soc. Pet. Eng. (SPE/IADC 92194). <https://doi.org/10.2118/92194-MS>
- Eaton, B.A., 1975. The Equation for Geopressure Prediction from Well Logs. Soc. Pet. Eng. (SPE 5544). <https://doi.org/10.2118/5544-MS>
- Ebrom, D., Heppard, P., Albertin, M., 2006. OTC 18399 Travel-Time Methods of V_p / V_s Determination for Pore Pressure Prediction Using Lookahead VSPs. Offshore Technol. Conf. (OTC 18399).
- El-Werr, A., Shebl, A., El-Rawy, A., Al-Gundor, N., 2017. Pre-drill pore pressure prediction using seismic velocities for prospect areas at Beni Suef Oil Field, Western Desert, Egypt. J. Pet. Explor. Prod. Technol. 7, 1011–1021. <https://doi.org/10.1007/s13202-017-0359-6>
- Foster, J.B., Whalen, H.E., 1966. Estimation of formation pressures from electrical surveys - Offshore Louisiana. J. Pet. Technol. 18, 165–171. <https://doi.org/10.2118/1200-PA>
- Gardner, G.H., Gardner, L., Gregory, A., 1974. Formation Velocity and Density - The Diagnostic Basic for Stratigraphic Traps. Geophysics 39, 770–780.
- Harper, D., 1969. New Findings From Over Pressure Detection Curves In Tectonically Stressed Beds. Soc. Pet. Eng. (SPE 2781).
- Holm, G.M., 1998. Distribution and origin of overpressure in the Central Graben of the North Sea. Law, B.E., G.F. Ulmishek, V.I. Slavin eds., Abnorm. Press. Hydrocarb. Environ. AAPG Mem. 70, 123–144.
- Hottmann, C.E., Johnson, R.K., 1965. Estimation of formation pressures from log-derived shale properties. J. Pet. Technol. SPE 1110, 717–722. <https://doi.org/10.2118/1110-PA>
- Hunt, J.M., 1990. Generation and migration of petroleum from abnormally pressured fluid compartments. Am. Assoc. Pet. Geol. Bull. <https://doi.org/10.1306/0C9B27E5-1710-11D7-8645000102C1865D>
- Kumar, A., Gunasekaran, K., Bhardwaj, N., Dutta, J., Banerjee, S., 2016. Technical papers t Origin and distribution of abnormally high pressure in the Mahanadi Basin , east coast of India. Interpretation 4, 303–311. <https://doi.org/10.1190/INT-2015-0087.1>
- Li, Q., Heliot, D., Zhao, L., Chen, Y., 2000. Abnormal Pressure Detection and Wellbore Stability Evaluation in Carbonate Formations of East Sichuan , China. Soc. Pet. Eng. (IADC / SPE 59125).

- Majidi, R., Albertin, M., Last, N., 2017. Pore-Pressure Estimation by Use of Mechanical Specific Energy and Drilling Efficiency. 2017 SPE Drill. Complet. J. (SPE 178842).
- Menand, S., Mills, K., 2017. Use of Mechanical Specific Energy Calculation in Real-Time to Better Detect Vibrations and Bit Wear While Drilling. Am. Assoc. Drill. Eng.
- Mohan, K., Adil, F., Samuel, R., 2015. Comprehensive Hydromechanical Specific Energy Calculation for Drilling Efficiency. J. Energy Resour. Technol. 137, 012904. <https://doi.org/10.1115/1.4028272>
- Nashaat, M., 1998. Abnormally high formation pressure and seal impacts on hydrocarbon accumulations in the Nile Delta and North Sinai basins, Egypt. Law, B.E., G.F. Ulmishek, V.I. Slavin eds., Abnorm. Press. Hydrocarb. Environ. AAPG Mem. 70 161–180.
- Pennebaker, E., 1968. Detection of Abnormal-pressure Formations from Seismic- Field Data. Am. Pet. Inst. 184–191.
- Pessier, R.C., Fear, M.J., 1992. Quantifying Common Drilling Problems With Mechanical Specific Energy and a Bit-Specific Coefficient of Sliding Friction. Soc. Pet. Eng. (SPE 24584). <https://doi.org/10.2118/24584-MS>
- Pinto, C.N., Lima, A.L.P., 2016. Mechanical Specific Energy for Drilling Optimization in Deepwater Brazilian Salt Environments. Soc. Pet. Eng. (IADC/SPE 180646). <https://doi.org/10.2118/180646-MS>
- Plumley, J.W., 1980. Abnormally High Fluid Pressure: Survey of Some Basic Principles: ERRATUM. Am. Assoc. Pet. Geol. Bull. 64, 414–422. <https://doi.org/10.1306/2F919409-16CE-11D7-8645000102C1865D>
- Polutranko, A.J., 1998. Causes of Formation and Distribution of Abnormally High Formation Pressure in Petroleum Basins of Ukraine. Law, B.E., G.F. Ulmishek, V.I. Slavin eds., Abnorm. Press. Hydrocarb. environments AAPG Mem. 70 181–194. [https://doi.org/10.1130/0091-7613\(1998\)026<0911](https://doi.org/10.1130/0091-7613(1998)026<0911)
- Rafatian, N., Miska, S., Ledgerwood III, L.W., Ahmed, R., Yu, M., Takach, N., 2010. Experimental Study of MSE of a Single PDC Cutter Interacting With Rock Under Simulated Pressurized Conditions. SPE Drill. Complet. 25, 10–18. <https://doi.org/10.2118/119302-MS>
- Rehm, B., Mcclendon, R., 1971. Measurement of Formation Pressure from Drilling Data. Soc. Pet. Eng.

- Saleh, S., Williams, K., Rizvi, A., 2013. Predicting Subsalt Pore Pressure with Vp/Vs. Offshore Technol. Conf. (OTC 24157).
- Satti, I.A., Yusoff, W.I.W., 2015. A New Method for Overpressure Mechanisms Analysis. Soc. Pet. Eng. (SPE 176357).
- Sayers, C.M., Johnson, G.M., Denyer, G., 2002. Predrill pore-pressure prediction using seismic data. Geophysics 67, 1286–1292. <https://doi.org/10.1190/1.1500391>
- Serebryakov, V.A., Chilingar, G. V., Katz, S.A., 1995. Methods of estimating and predicting abnormal formation pressures. J. Pet. Sci. Eng. 13, 113–123. [https://doi.org/10.1016/0920-4105\(95\)00006-4](https://doi.org/10.1016/0920-4105(95)00006-4)
- Short, K., Stauble, A., 1967. Outline of Geology of Niger Delta. Am. Assoc. Pet. Geol. Bull. 51, 761–779.
- Slavin, V.I., Smirnova, E.M., 1998. Abnormally high formation pressures: origin, prediction, hydrocarbon field development, and ecological problems. Law, B.E., G.F. Ulmishek, V.I. Slavin eds., Abnorm. Press. Hydrocarb. Environ. AAPG Mem. 70 105–114.
- Soleymani, H., Riahi, M.A., 2012. Velocity based pore pressure prediction-A case study at one of the Iranian southwest oil fields. J. Pet. Sci. Eng. 94–95, 40–46. <https://doi.org/10.1016/j.petrol.2012.06.024>
- Spencer, C.W., 1987. Hydrocarbon Generation as a Mechanism for Overpressuring in Rocky Mountain Region. Am. Assoc. Pet. Geol. Bull. 71, 368–388. <https://doi.org/10.1306/94886EB6-1704-11D7-8645000102C1865D>
- Swarbrick, R.E., 1995. Distribution and Generation of the Overpressyre System, Eaastern Delaware BAsin, Western Texas and Southern New Mexico: Discussion. Am. Assoc. Pet. Geol. Bull. 12, 1386–1405.
- Swarbrick, R.E., Osborne, M.J., 1998. Mechanisms that generate abnormal pressures: an overview. Law, B.E., G.F. Ulmishek, V.I. Slavin eds., Abnorm. Press. Hydrocarb. Environ. AAPG Mem. 70 13–34.
- Teale, R., 1965. The Concept of Specific Energy in Rock Drilling. Int. J. Rock Mech. Min. Sci. 2, 57–73. [https://doi.org/10.1016/0148-9062\(65\)90022-7](https://doi.org/10.1016/0148-9062(65)90022-7)
- Ugwu, S.A., Nwankwo, C.N., 2014. Integrated approach to geopressure detection in the X-field, Onshore Niger Delta. J. Pet. Explor. Prod. Technol. 4, 215–231. <https://doi.org/10.1007/s13202-013-0088-4>

- Vidrine, D.J., Benit, E.J., 1968. Field Verification of the Effect of Differential Pressure on Drilling Rate. *J. Pet. Technol.* (SPE 1859) 20, 676–682. <https://doi.org/10.2118/1859-PA>
- Walls, J., Dvorkin, J., Mavko, G., Nur, A., 2000. Use of Compressional and Shear Wave Velocity for Overpressure Detection. *Offshore Technol. Conf.* (OTC 11912).
- Wardlaw, H.W.R., 1969. Drilling Performance Optimization and Identification of Overpressure. *Soc. Pet. Eng. AIME SPE* 2388, 67–78.
- Warren, T.M., 1987. Penetration Rate Performance of Roller Cone Bits. *SPE Drill. Eng.* 2, 9–18. <https://doi.org/10.2118/13259-PA>
- Waughman, J.R., Kenner, V.J., Moore, A.R., 2003. Real-Time Specific Energy Monitoring Enhances the Understanding of When To Pull Worn PDC Bits. *SPE Drill. Compleat.* (SPE 81822) 59–68.
- Wei, M., Li, G., Shi, H., Shi, S., Li, Z., Zhang, Y., 2016. Theories and Applications of Pulsed-Jet Drilling With Mechanical Specific Energy. *SPE J. (SPE 174550)* 303–310.
- Yassir, N., Bell, J., others, 1996. Abnormally high fluid pressures and associated porosities and stress regimes in sedimentary basins. *SPE Form. Eval.* 11, 5–10. <https://doi.org/10.2118/28139-PA>
- Zhang, J., 2013. Effective stress, porosity, velocity and abnormal pore pressure prediction accounting for compaction disequilibrium and unloading. *Mar. Pet. Geol.* 45, 2–11. <https://doi.org/10.1016/j.marpetgeo.2013.04.007>
- Zhang, J., 2011. Pore pressure prediction from well logs: Methods, modifications, and new approaches. *Earth-Science Rev.* 108, 50–63. <https://doi.org/10.1016/j.earscirev.2011.06.001>
- Zhou, Y., Zhang, W., Gamwo, I., Lin, J.S., 2017. Mechanical specific energy versus depth of cut in rock cutting and drilling. *Int. J. Rock Mech. Min. Sci.* 100, 287–297. <https://doi.org/10.1016/j.ijrmms.2017.11.004>

Chapter 3

3.0 Energy-based Formation Pressure Prediction

Preface

*A version of this chapter has been published in the **Journal of Petroleum Science and Engineering, 2019**. I am the primary author. Co-author Dr. Stephen Butt reviewed the manuscript and provided technical assistance in the development of the concept. I formulated the initial concept and carried out most of the data analysis. I prepared the first draft of the manuscript and revised the manuscript based on the feedback from the co-author and peer review process. The co-author also helped to refine the concept.*

Abstract

Conventionally, pore pressure predictions from the drilling parameters have the advantage of estimating the formation pressure at the bit at relatively low cost. The limitations on the application of the d-exponent concept to pore pressure prediction have long been established. Recent developments in pore pressure prediction from the drilling parameters use the concept of mechanical specific energy (MSE) and hydro-rotary specific energy (HRSE). These energies are usually computed from the downhole measurements. However, the majority of readily available field data in older (offset) and present-day wells are in the form of surface measurements. In this paper, a new pore pressure prediction technique based on the concept of hydro-mechanical specific energy (HMSE) is being proposed. The HMSE is the combination of axial, rotary and hydraulic energies required to break and remove a unit volume of rock. The new technique uses drilling parameters that are obtained only from surface measurements. Pore pressure prediction using the concept of HMSE is based on the theory that total energy consumed in breaking and

removing a unit volume of rock beneath the bit is a function of effective stress: the higher the effective stress, the greater the total energy required to break and remove a unit volume of rocks. Abnormally high formation pressure intervals with lower effective stress will require less energy to drill than the normally compacted series at the same depth. The new technique is tested using a recently drilled near-vertical deep High-Pressure High-Temperature (HPHT) exploratory well in the Tertiary Deltaic System of the Niger Delta basin where the main cause of overpressure mechanism is under-compaction. The well drilled to a total depth of more than 17,000 ft-TVD, covers the normally compacted series, pressure transition zones and overpressure intervals. Pore pressure estimates derived from the HMSE concept are then compared to the actual pore pressure measurements taken from the formations of interest. There is an excellent agreement between the predicted and measured formation pore pressure. The new technique can provide a reliable means of estimating the formation pore pressure from the drilling parameters in the absence of reliable downhole measurements at relatively low cost.

Keywords: Pore pressure, Effective Stress, Hydro-mechanical Specific Energy, Mechanical Specific Energy, Normal Compaction Trend.

3.1 Introduction

Pore pressure is the pressure of the formation fluids contained in the pore spaces of rocks. Accurate knowledge of formation pore pressure is required at all stages of the field development plan. It is perhaps the single most important input parameter used for well planning and design. From a well construction point of view, pore pressure data are used for rig sizing, casing depths determination, cement design, drilling and completion fluid design, wellheads/christmas tree design, casing and tubing design, and equipment selection. Having accurate knowledge of the

formation pore pressure will help to optimize drilling rate, prevent well control incidents (kicks/blowout), reduce the risk of differential sticking of pipes and minimize formation damage. Pore pressure data are also used for production forecast/well performance analysis, reservoir modeling, subsurface trap integrity determination, and geo-mechanical analysis. Pore pressure prediction is very important to exploration, drilling, and production of oil and gas since hydrocarbons distribution around the world is directly related to the subsurface pressure and temperature conditions.

The formation pore pressure is normal if it is able to support a continuous column of static formation water from surface to formation depth of interest without any losses or excess surface pressure (Swarbrick and Osborne, 1998). Louden (1972) defined the normal pore pressure gradient as the lithological gradient for a saltwater basin. The value of the normal pore pressure gradient varies from region to region depending on pore fluid type, formation temperature and concentration of dissolved salts in the formation water. Even within the same geological basin, normal pore pressure gradient may vary from one depth to the other. Generally, normal pore pressure gradient varies between 0.433 – 0.515 psi/ft. For the North Sea, the average normal pore pressure gradient is 0.45 psi/ft (Holm, 1998). In the Gulf Coast, the average normal pore pressure gradient is 0.465 psi/ft (Harkins & Baugher, 1969; Parker, 1973). In the Rocky Mountain regions in Canada and USA, it is approximately 0.433 psi/ft (Finch, 1969). Intervals with pore pressure gradient higher or lower than the normal pore pressure gradient are termed abnormally high (overpressure) or abnormally low (subnormal) respectively.

Subnormal pressure regimes can result from geological and production conditions. The geological conditions can be tectonic, stratigraphic or geochemical in nature. The production condition relates to reservoir depletion that results from fluids withdrawal from a rock where the

rate of fluid influx into the rock is significantly less than the rate of formation fluids withdrawal. Barker (1972) suggested that if a reservoir under normal pressure conditions becomes isolated with permeability barriers and is then subjected to a temperature decrease, the reservoir pressure will fall below the normal hydrostatic pressure causing subnormal pressure conditions. These conditions can occur during sediments erosion and upliftment whereby sediments from the deeper zones are moved to shallower depths. Subnormal pressure conditions have been reported in some sedimentary basins around the world (Serebryakov & Chilingar, 1994; Bachu & Underschultz, 1995; Dickey & Cox, 1977). The presence of subnormal pressure conditions in the subsurface formations can cause drilling problems such as lost circulation, differential sticking, underground blowout, and a potential surface blowout.

There are five main mechanisms of overpressure generation (Yassir et al., 1996). The first mechanism is compaction disequilibrium - this occurs when the rate of deposition of sediments is greater than the rate of expulsion and migration of interstitial fluids (usually water). The water becomes trapped and begins to support the weights of the overlying sediments since there is no enough time for the water to escape. This usually occurs when rapid sedimentation involves large quantities of clay materials (Carlin and Dainelli, 1998). In young sedimentary basins with thick terrigenous rocks, compaction disequilibrium is the dominant cause of abnormally high formation pressure (Law and Spencer, 1998; Tingay et al., 2009). Other causes of overpressure mechanisms are generally small compared to compaction disequilibrium (Burrus, 1998). Most shallow water flows arising from the overpressure conditions near the mud line in the offshore Gulf of Mexico (GOM) were attributed to compaction disequilibrium (Sayers et al., 2005). The second mechanism is tectonic activities – tectonic events such as folding, faulting and diapirism can result in subsurface overpressure conditions (Law et al., 1998). The

third mechanism is clay diagenesis – between 90 – 150°C, montmorillonite undergoes a transformation and is converted into illite, releasing a large amount of water in the process (Powers, 1967; Burst, 1969; Burst, 1976, Freed & Peacor, 1989; Buryakovskiy et al., 1995). The threshold temperature requires for clay diagenesis to occur varies from region to region. It ranges from about 71 °C for Mississippi River sediments in the US to more than 150°C for the Niger Delta sediments in Nigeria (Bruce, 1984). The fourth mechanism is aqua-thermal expansion – formation temperature increases as the depth of burial of sediments increases. This causes fluid expansion with subsequent increase in the formation pore (Barker, 1972; Chen & Huang, 1996; Barkers & Horsfield, 1982; Sharp, 1983; Polutranko, 1998; Lewis & Rose, 1970). The last major overpressure mechanism is hydrocarbon generation – thermal cracking of kerogen into liquid and gaseous hydrocarbons can result in a significant increase in pore volume leading to overpressure conditions by (Law & Dickinson, 1985; Spencer, 1987; Holm, 1998; Hunt et al., 1998). This is also applicable to thermal cracking of liquid hydrocarbons into gaseous hydrocarbons. Other causes of subsurface overpressure conditions include oil and gas occurrence, artesian effect, centroid effects and charging from other zones. Overpressure generation due to buoyancy effect can also occur in thick gas-filled reservoirs (Swarbrick and Osborne, 1998; Aadnoy, 2010). The amount of overpressure within the gas accumulation is a function of the gas gradient and the height of the gas column.

It should be noted that combination of the above mechanisms can create subsurface overpressure conditions within the same sedimentary basin (Plumley, 1980; Kadri, 1991; Freire et al., 2010; Satti et al., 2015; Satti et al., 2016). For example, in a deltaic environment where sedimentation rate is high, compaction disequilibrium may initially be the cause of abnormally high formation pressures. As the formation temperature increases from the increasing depth of

burial, hydrocarbon generation, clay diagenesis, and aqua-thermal expansion may compliment compaction disequilibrium as the main cause of overpressure mechanisms. Drilling into abnormally high formation pressure intervals unexpectedly can lead to catastrophic and process safety incidents such as surface blowouts. This can result in costly drilling expenses, loss of lives and properties, loss of reputations and damage to environments. To minimize the risks of a well blowout, it is therefore extremely important to be able to detect overpressure intervals before drilling into them. The best approach for the detection and evaluation of overpressure intervals is to compare the pore pressure estimates derived from various independent sources (seismic, well logs and drilling parameters) since relying on any single technique can result in misinterpretations especially when drilling exploratory wells (Fertl & Timko, 1971).

Most pore pressure prediction techniques rely on the hypothesis that overpressure intervals have higher porosity than normally pressured intervals for any given depth. However, it is also possible not to have any trend reversal between the normal pressure and overpressure intervals when porosity indicators (resistivity, compressional sonic velocity, and density) are plotted against depth (Carstens & Dypvik, 1981; Hermanrud et al., 1998; Teige et al., 1999). In most cases, pore pressure prediction techniques require a normal compaction trend (NCT) of the shale petrophysical properties to be established. Deviation from the normal compaction trend will likely indicate the onset of abnormally high formation pressure. Formation pore pressures are estimated in shale formations due to distinct variations in the petrophysical properties of shales with respect to pore pressure. In addition, pore pressure prediction in shale formations will give early warning of abnormally high formation pressure in the underlying reservoir rocks prior to drilling into them. Hottmann & Johnson (1965) proposed a method for predicting the onset of abnormally high formation pressure from petrophysical data (resistivity and compressional sonic

travel time) acquired in the Miocene and Oligocene shales in Upper Texas and Southern Louisiana Gulf Coast. They observed that the plots of shale resistivity and sonic transit time against depth in zones with normal pore pressures exhibited a distinctive trend called normal compaction trend (NCT). Reversals in the shale resistivity and sonic transit time were correlated to the onset of overpressure.

Foster and Whalen (1966) developed an empirical relationship between formation pore pressure, depth of burial and the ratio of normal shale resistivity to abnormal shale resistivity for regions with varying salinity (equation 3.1):

$$PP = 0.465 * Z + \frac{0.535}{\log b} * \log \left[\frac{R_n}{R_o} \right], \quad (3.1)$$

where PP is the formation pore pressure (psi); Z is the true vertical depth (ft); R_n is the normal shale resistivity (ohm-m); R_o is the observed (abnormal) shale resistivity (ohm-m). The \log_b can be obtained from the slope of formation factor versus depth plot. Gardner et al. (1974) proposed an empirical relationship among vertical effective stress, sonic travel time and depth of burial based on the data presented by Hottmann and Johnson (1965). Gardner's model is given by:

$$\left[\frac{\sigma_v - PP}{G_{ob} - G_{np}} \right]^{\frac{1}{3}} * Z^{\frac{2}{3}} = A - B \log_e \Delta t \quad (3.2)$$

where σ_v is the vertical stress (psi); PP is the pore pressure (psi); Z is the true vertical depth (ft); G_{ob} is the overburden gradient (psi/ft); G_{np} is the normal pore pressure gradient (psi/ft); Δt is the interval travel time (μ s/ft); A and B are constant parameters. The values of A and B can be obtained by calibration equation 3.2 to any known normally pressured intervals in the region.

Eaton (1975) proposed three sets of pore pressure prediction models based on resistivity

measurements, acoustic measurements, and corrected d-exponent computed from drilling parameters. Eaton's models are given by:

$$G_{pp} = G_{ob} - \{G_{ob} - G_{np}\} \left[\frac{R_o}{R_n} \right]^{1.2}, \quad (3.3)$$

$$G_{pp} = G_{ob} - \{G_{ob} - G_{np}\} \left[\frac{\Delta t_n}{\Delta t_o} \right]^3, \quad (3.4)$$

$$G_{pp} = G_{ob} - \{G_{ob} - G_{np}\} \left[\frac{d_{co}}{d_{cn}} \right]^{1.2}, \quad (3.5)$$

where G_{pp} is the pore pressure gradient (psi/ft); G_{ob} is the overburden gradient (psi/ft); G_{np} is the normal pore pressure gradient (psi/ft); R_o is the observed shale resistivity (ohm-m); R_n is the normal compaction trend shale resistivity (ohm-m); Δt_n is the normal compaction shale travel time (μ s/ft); Δt_o is the observed shale travel time (μ s/ft); d_{co} is the calculated d_c from measured data; d_{cn} is the d_c from the normal trend line. Eaton's models are among the most widely used pore pressure prediction methods. These models are particularly suitable for overpressure conditions caused by compaction disequilibrium. Eaton's models can also be applicable to other forms of overpressure mechanisms caused by unloading conditions with a higher exponent coefficient (Satti et al., 2015).

Bowers (1995) proposed pore pressure prediction models based on the principle of effective stress to predict the degree of overpressure generated by compaction disequilibrium and fluid expansion mechanisms using the virgin and unloading curves concept. The virgin curve model for normal pressure and overpressure generated by compaction disequilibrium is given by:

$$V = 5000 + A\sigma_e^B, \quad (3.6)$$

where V is the compressional sonic velocity (ft/sec); σ_e is the effective vertical stress (psi); A and B are virgin curve parameters. The values of A and B can be obtained by calibrating equation 3.6 to the normally compacted series in the same well or offset wells. The unloading curve model for overpressure generated by fluid expansion mechanisms is given by

$$V = 5000 + A \left[\sigma_{\max} \left[\frac{\sigma_e}{\sigma_{\max}} \right]^{\frac{1}{U}} \right]^B, \quad (3.7)$$

$$\sigma_{\max} = \left[\frac{V_{\max} - 5000}{A} \right]^{\frac{1}{B}}, \quad (3.8)$$

where σ_{\max} is the effective vertical stress at the onset of unloading (psi); V_{\max} is the compressional sonic velocity at the onset of unloading (ft/sec); U is the unloading parameter which measures how plastic the sediment is. The value of U is obtained by fitting equation 3.7 to the regional offset wells. Under normal and overpressure conditions caused by compaction disequilibrium, the plot of compressional sonic velocity against effective stress will follow the virgin curve (equation 3.6). However, subsurface overpressure conditions caused by fluid expansion mechanisms will trail the unloading curve (equation 3.7).

Most current pore pressure prediction models are not applicable to non-clastic rocks. Carbonate rocks are stiffer than shales and their porosity related properties may not be affected by overpressure environments. Atashbari & Tingay (2012) proposed a pore pressure prediction model based on bulk and pore compressibilities for carbonate rocks (equation 3.9):

$$PP = \left[\frac{(1 - \phi)C_b \sigma'_v}{(1 - \phi)C_b - (\phi C_p)} \right]^\gamma, \quad (3.9)$$

where PP is the formation pore pressure (psi); \emptyset is the formation porosity (fraction); C_b is the bulk compressibility (psi^{-1}); C_p is the pore compressibility (psi^{-1}); σ'_v is the vertical effective stress (psi); γ is the empirical constant ranging from 0.9 to 1.0. There are other popular pore pressure prediction models that have been developed but these are based mostly on the modifications to the previous models (Zhang, 2011; Zhang, 2013).

Early application of drilling parameters to pore pressure prediction used the rate of penetration (ROP) as a principal indicator of subsurface overpressure conditions in a uniform lithology (Forgotson, 1969). Field and laboratory observations have shown an inverse relationship between the ROP and differential pressure (Cunningham & Eenink, 1959; Vidrine & Benit, 1968; Wardlaw, 1969; Black et al., 1985; Cheatham et al., 1985). In overpressure formations, the ROP will most likely increase (positive drilling break) due to lower degree of rock compaction, higher porosity and decrease in vertical effective stress especially if the primary cause of overpressure mechanism is compaction disequilibrium. However, ROP is affected by many factors other than the differential pressure. These factors include lithology, degree of compaction, weight on bit (WOB), rotary speed, bit size, bit type, hydraulics excessive overbalance and bit wear (Bourgoyne & Young, 1973). From the operational point of view, it is not always possible to maintain the above factors constant while drilling a well. Hence, a sudden increase in ROP may not necessarily signify drilling into abnormally pressured zones. Normalization of ROP for the effects of WOB, rotary speed and bit size led to the development of d-exponent concept (Jorden & Shirley 1966; Harper 1969; Rehm & McClendon 1971). The d_c – exponent model is given by:

$$d_c - \text{exponent} = \frac{\log \left[\frac{\text{ROP}}{60N} \right]}{\log \left[\frac{12\text{WOB}}{10^6 D_b} \right]} * \left[\frac{G_{np}}{\text{ECD}} \right], \quad (3.10)$$

where $d_c - \text{exponent}$ is the corrected $d - \text{exponent}$; ROP is the rate of penetration (ft/hr); N is the rotary speed in revolution per minute (rpm); WOB is the weight on bit (lbs); D_b is the bit diameter (in); G_{np} is the normal pore pressure gradient (psi/ft or ppg); ECD is the equivalent circulating density (psi/ft or ppg). The corrected d -exponent (equation 3.10) versus depth graph is displayed on the semi-log to prevent significant variation of d -exponent with location and geological age. In normal pressure environments, the corrected d -exponent will show an increasing trend with depth. In overpressure shales, the corrected d -exponent will deviate from the normal compaction trend (NCT) to lower values. The amount of deviation from the NCT at a given depth is correlated to the magnitude of overpressure. One of the major drawbacks to the application of $d - \text{exponent}$ concept to pore pressure prediction is that it does not consider the effect of bit hydraulic energy on the ROP. This limits its application to hard rock environments.

Traditionally, most works on the applications of specific energy to drilling operations have been directed at improving the drilling efficiency (drilling optimization) and identification of abnormal/inefficient drilling conditions (Rabia, 1985; Waughman et al., 2003; Dupriest & Koederitz, 2005; Koederitz & Weis, 2005; Dupriest, 2006; Armenta, 2008; Amadi & Iyalla, 2012; Bevilacqua et al., 2013; Abbas et al., 2014; Mohan et al., 2015; Pinto & Lima, 2016; Wei et al., 2016; Zhou et al., 2017). While the results of experimental investigations on rock samples have shown the dependency of specific energy on confining/differential pressure (Rafatian et al., 2010; Akbari et al., 2013; Akbari et al., 2014), only few (three) attempts have been made to apply energy-based concept to pore pressure prediction using field data. Cardona (2011) was the first to use mechanical specific energy (MSE) concept to estimate the formation pore pressure

from the field data. Just like the d-exponent concept, Cardona's model does not contain the hydraulic energy term, making it suitable to only hard rock environments. Majidi et al. (2017) then proposed a methodology to determine the formation pore pressure from the combination of downhole drilling parameters and in-situ rock properties using the concept of drilling efficiency and mechanical specific energy (DE-MSE). The formation pressure was expressed as a function of equivalent circulating density, MSE, uniaxial compressive strength and angle of internal friction. The Majidi's model is given by:

$$PP = ECD - [(DE_{trend} \times MSE) - UCS] \left[\frac{1 - \sin \theta}{1 + \sin \theta} \right], \quad (3.11)$$

$$DE_{trend} = a\phi_n^b, \quad (3.12)$$

$$USC = 0.43V_p^{3.2}, \quad (3.13)$$

$$\theta = 1.532V_p^{0.5148}, \quad (3.14)$$

where PP is the pore pressure (psi); ECD is the equivalent circulating density (psi); MSE is the mechanical specific energy (psi); UCS is the uniaxial compressive strength (psi); θ is the angle of internal friction; ϕ is the formation porosity; V_p is the compressional sonic velocity (ft/sec); a is the coefficient of drilling efficiency trend-line from porosity trend-line; b is the exponent of drilling efficiency trend-line from porosity trend-line. The major drawback to Majidi's model is that there are so many variables to be considered including the rock petrophysical properties. The empirical equations (equations 3.13 and 3.14) that relate uniaxial compressive strength (UCS) and angle of internal friction to compressional sonic velocity must be validated with core data in the region of application. More so, Majidi's model does not provide an independent means of estimating the formation pore pressure since the compressional sonic velocity which is used to estimate the UCS and angle of internal friction is also a function of the formation pore pressure.

Lastly, Majidi's model ignores the effect of bit hydraulic energy on the ROP.

Oloruntobi et al. (2018) developed a methodology to estimate the formation pore pressure using the concept of hydro-rotary specific energy (HRSE). This model is given by:

$$HRSE = \left[\frac{120\pi NT}{A_b ROP} + \frac{0.10628 MW Q^3 \left[1 - \left[\frac{JSA}{TFA} \right]^{-0.122} \right]}{A_b ROP TFA^2} \right] * \left[\frac{G_{np}}{ECD} \right], \quad (3.15)$$

where HRSE is the hydro-rotary specific energy (psi); A_b is the bit area (in^2); N is the rotary speed (rpm); T is the torque on bit (lb-ft); ROP is the rate of penetration (ft/hr); Q is the flow rate (gpm); MW is the mud weight (ppg); JSA is the junk slot area (in^2); TFA is the total flow area (in^2); G_{np} is the normal pore pressure gradient (psi/ft or ppg) and ECD is the equivalent circulating density (psi/ft or ppg). Oloruntobi's model was derived from the combination of rotary and hydraulic energies with the axial energy being neglected (equation 3.15). While the model can be applied to consolidated (hard) and unconsolidated (soft) sediments due to the inclusion of bit hydraulic energy term, accurate knowledge of torque on bit (TOB) is required. TOB is usually subjected to a lot of fluctuations during drilling and it is perhaps the major source of errors in the computation of specific energies.

Since most readily available field data in older (offset) and present-day wells are in the form of surface measurements especially for marginal field operators, there is a need to develop a pore pressure prediction technique from drilling parameters based on this reality. In this paper, a new energy-based pore pressure prediction model that uses only surface measurements is being proposed based on the concept of hydro-mechanical specific energy (HMSE). The HMSE is the combination of axial, torsional and hydraulic energies required to break and remove a unit volume of rock. The new technique can provide an excellent means of estimating the formation

pore pressure from the drilling parameters in the absence of reliable downhole measurements at relatively low cost.

3.2 Model Development

Teale (1965) defined mechanical specific energy (MSE) as the amount of energy required to remove a unit volume of rock. It amounts to the combination of energies due to axial and torsional loads (equation 3.16):

$$MSE = \frac{WOB}{A_b} + \frac{120 * \pi * N * T}{A_b * ROP}, \quad (3.16)$$

where MSE is the mechanical specific energy (psi); WOB is the downhole weight on bit (lbs); A_b is the bit area (in^2); N is the rotary speed (rpm); T is the torque on bit (lb-ft); ROP is the rate of penetration (ft/hr). However, the MSE does not necessarily represent the total energy consumed in breaking and removing the rock fragments beneath the bit as the bit hydraulic energy term is omitted in the model. The hydro-mechanical specific energy (HMSE) is the combination of axial, torsional and hydraulic energies (Mohan et al., 2015; Chen et al., 2016; Wei et al., 2016).

$$HMSE = \frac{\text{Axial Energy}}{\text{Rock Volume Drilled}} + \frac{\text{Torsional Energy}}{\text{Rock Volume Drilled}} + \frac{\text{Hydraulic Energy}}{\text{Rock Volume Drilled}}, \quad (3.17)$$

The hydro-mechanical specific energy (HMSE) in the expanded form is given by:

$$HMSE = \frac{WOB}{A_b} + \frac{120 * \pi * N * T}{A_b * ROP} + \frac{1154 * \Delta P_b * Q}{A_b * ROP}, \quad (3.18)$$

where WOB is the downhole weight on bit (lbs); A_b is the bit area (in^2); N is the rotary speed (rpm); T is the torque on bit (lb-ft); ROP is the rate of penetration (ft/hr); ΔP_b is the bit pressure

drop (psi); Q is the flow rate (gpm). Pessier and Fear (1992) expressed the downhole torque (T) as a function of weight on bit (WOB), bit specific coefficient of sliding friction (μ) and bit diameter (D_b) as given by:

$$T = \frac{\mu * D_b * WOB}{36}. \quad (3.19)$$

Combination of equations 3.18 and 3.19 will lead to equation 3.20:

$$HMSE = \frac{WOB}{A_b} + \frac{13.33 * \mu * N * WOB}{D_b * ROP} + \frac{1154 * \Delta P_b * Q}{A_b * ROP}, \quad (3.20)$$

Excessive overbalance conditions will increase the confinement of rock and cuttings at the bit face. This can lead to a reduction in ROP and an increase in the amount of energy required to remove a unit volume of rock. Therefore, the HMSE needs to be corrected for changes in bottom-hole pressure (equation 3.21):

$$HMSE = \left[\frac{WOB}{A_b} + \frac{13.33 * \mu * N * WOB}{D_b * ROP} + \frac{1154 * \Delta P_b * Q}{A_b * ROP} \right] * \left[\frac{G_{np}}{ECD} \right], \quad (3.21)$$

where all parameters are as previously defined. This correction follows a similar correction for the effect of mud weight/equivalent circulating density on d-exponent (Rehm & McClendon 1971). Due to accelerated fluid entrainment immediately below the bit nozzles, not all the available hydraulic energy at the bit will reach the bottom of the hole. Therefore, the bit hydraulic energy is converted into the bottom-hole hydraulic energy by introducing a hydraulic energy reduction factor (η) into the bit hydraulic energy (equation 3.22):

$$HMSE = \left[\frac{WOB}{A_b} + \frac{13.33 * \mu * N * WOB}{D_b * ROP} + \frac{1154 * \eta * \Delta P_b * Q}{A_b * ROP} \right] * \left[\frac{G_{np}}{ECD} \right]. \quad (3.22)$$

Due to jet impact of the drilling fluid on the formation, an equal and opposite (pump-off) force is exerted on the bit, leading to a reduction in WOB (equation 3.23):

$$HMSE = \left[\frac{WOB_e}{A_b} + \frac{13.33 * \mu * N * WOB_e}{D_b * ROP} + \frac{1154 * \eta * \Delta P_b * Q}{A_b * ROP} \right] * \left[\frac{G_{np}}{ECD} \right], \quad (3.23)$$

where WOB_e is the effective weight on bit (lbs); all other parameters are as previously defined. The effective weight on bit (WOB_e) is the surface WOB minus the component of jet impact force that reaches the bottom of the hole (equation 3.24):

$$WOB_e = WOB - \eta * F_j, \quad (3.24)$$

where WOB is the surface weight on bit (lbs); (η) is the hydraulic energy reduction factor; F_j is the bit jet impact force (lbs). Equation 3.25 is obtained by combining equations 3.23 and 3.24:

$$HMSE = \left[\frac{[WOB - \eta F_j]}{A_b} + \frac{13.33 \mu N [WOB - \eta F_j]}{D_b ROP} + \frac{1154 \eta \Delta P_b Q}{A_b ROP} \right] * \left[\frac{G_{np}}{ECD} \right]. \quad (3.25)$$

The bit jet impact force is given by:

$$F_j = 0.000516 * MW * Q * V_j, \quad (3.26)$$

where MW is the mud weight (ppg); Q is the flow rate (gpm); V_j is the jet velocity (ft/sec). The jet velocity is given by:

$$V_j = \frac{0.32 * Q}{TFA}, \quad (3.27)$$

where Q is the flow rate (gpm); TFA is the total flow area (in^2). For PDC bits, the hydraulic

energy reduction factor (η) is expressed as a function of junk slot area and total flow area (Oloruntobi et al., 2018) and this is given by:

$$\eta_{PDC\ Bit} = 1 - \left[\frac{JSA}{TFA} \right]^{-0.122}, \quad (3.28)$$

where JSA is the junk slot area (in^2); TFA is the total flow area (in^2). For roller cone bits, the model proposed by Warren (1987) provides good estimates and this is given by:

$$\eta_{Roller\ Cone\ Bit} = 1 - \left[\frac{0.15\ Bit\ Area}{TFA} \right]^{-0.122}. \quad (3.29)$$

The hydraulic energy reduction factor model proposed by Rabia (1989) is more complex and may not be suitable for applications where there are variations in nozzle sizes within the same bit. The pressure drop across the bit is given by:

$$\Delta P_b = \frac{MW Q^2}{10858 TFA^2}, \quad (3.30)$$

where ΔP_b is the bit pressure drop (psi); MW is the mud weight (ppg); Q is the flow rate (gpm); TFA is the total flow area (in^2). For fixed cutter bits, the value of bit specific coefficient of sliding friction (μ) will depend on lithology, rock strength, mud weight, blade count, bit wear and cutter sizes (Caicedo et al. 2005; Guerrero & Kull 2007). However, from field observations, the value of μ often stays within a narrow range: 0.18 – 0.24 for roller cone bits and 0.5 – 0.8 for PDC bits under different operating conditions (Wei et al. 2016). To minimize the errors in the computation of HMSE, it is reasonable to assume average values of 0.21 and 0.65 for roller cone and PDC bit respectively.

As the depth of burial increases in normally compacted series, the energy (HMSE)

required to break and remove a unit volume of rock will also increase. However, subsurface overpressure intervals with lower vertical effective stress will require less energy to drill than the normally compacted series at the same depth, leading to the reversal in the HMSE trend.

3.3 Methodology

1. Compute the HMSE at the depth of interest using equations 3.25 – 3.30. If there are wide variations/fluctuations in HMSE values due to different lithologies being penetrated, the HMSE should be estimated over clean shale intervals only to remove any lithological effects on HMSE.
2. Display the plot of HMSE against depth on a semi-log and establish the normal compaction trend (NCT) over the entire interval.
3. Estimate the formation pore pressure gradient at any given depth using the energy-based Eaton's model given as:

$$G_{pp} = G_{ob} - \{G_{ob} - G_{np}\} * \left[\frac{HMSE_o}{HMSE_n} \right]^m, \quad (3.31)$$

where G_{pp} is the pore pressure gradient (psi/ft); G_{ob} is the overburden gradient (psi/ft); G_{np} is the normal pore pressure gradient (NPPG) in psi/ft; $HMSE_o$ is the actual HMSE calculated using equations 3.25 – 3.30; $HMSE_n$ is the hypothetical value of HMSE from the normal compaction trend; m is the HMSE exponent. The value of the specific energy ratio exponent (m) will vary from one region to another. It can be obtained by calibrating equation 3.31 to any known overpressure intervals in the offset or current wells. If the current well being drilled is used as the calibration well, equation 3.30 should be preferably calibrated to the pressure transition zones where kick intensity is reduced.

3.4 Field Example

To demonstrate the applicability of the new pore pressure prediction technique, a recently drilled High-Pressure High-Temperature exploratory well (Well A) in the tertiary deltaic system of the Niger Delta is considered as the case study. Well A is located approximately 80 km northwest of Port Harcourt in the central region of the basin (Figure 3.1).

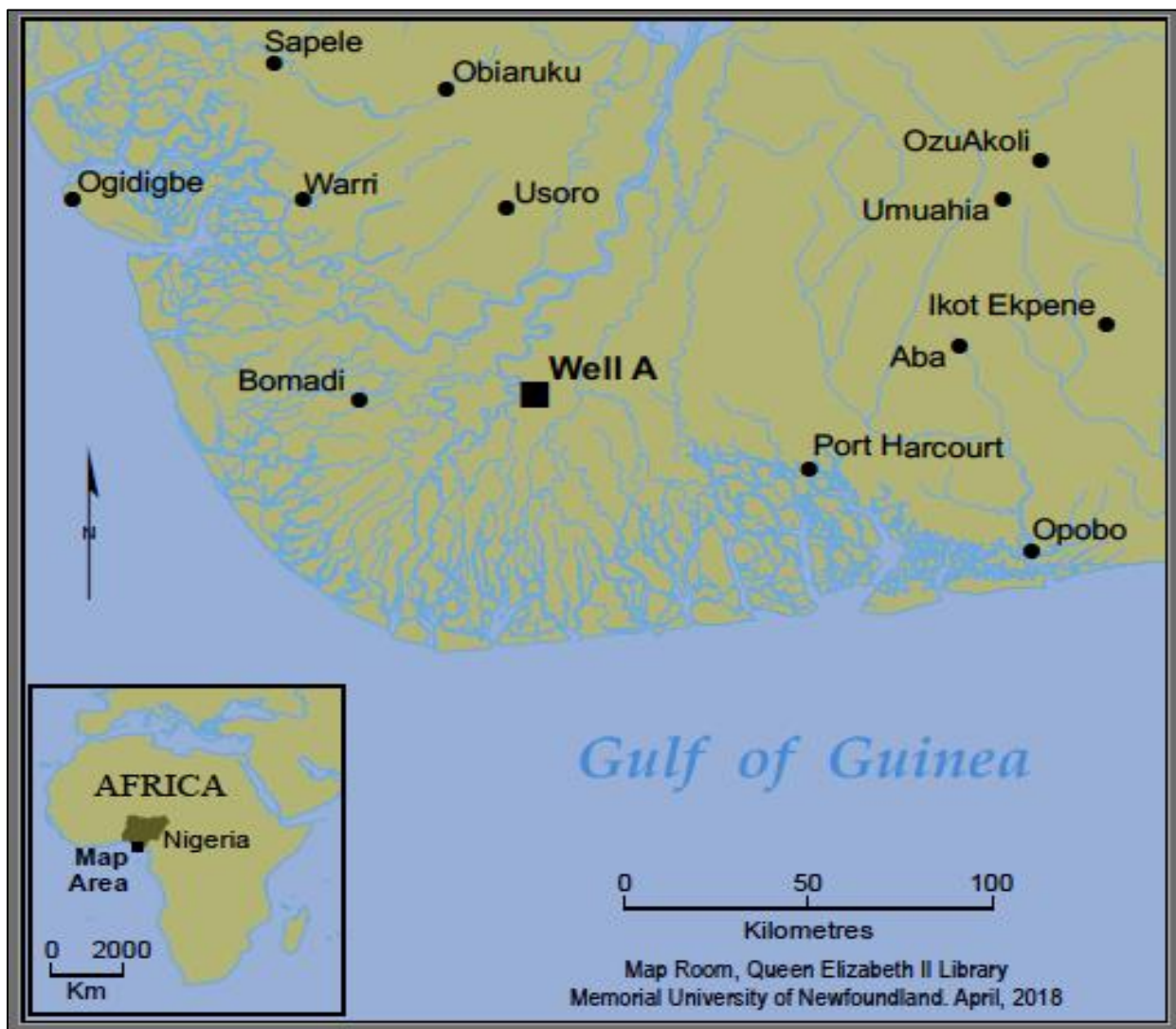


Figure 3. 1 Location map for Well A.

The well is a near-vertical sidetrack well drilled to a total depth of 17,265 ft with a maximum inclination of 6.8 degrees. The Niger Delta is an extensional rift basin that consists of the regressive clastic sequence up 12 km in thickness and covers about 75,000 km² (Evamy et al., 1978). The detailed geology of the basin can be obtained from the literature (Short and Stauble, 1967; Avbovbo, 1978; Doust and Omatsola, 1990; Reijers, 2011). The growth and development of the structural and depositional systems in the basin involves a complex interaction of subsidence, contraction, and extension (Hooper et al., 2002). The structural geology of the area is characterized by growth faults associated with rollover structures (Daukoru, 1975; Weber, 1987). The primary mechanism for overpressure generation in the Niger Delta is under-compaction (Daukoru, 1975; Ugwu & Nwankwo, 2014). In this paper, all depths are referenced to true vertical depth (TVD) below the rotary table (RT)

Table 3. 1 The well and bit data summary.

Hole Size	Bit Data	BHA Type	Intervals (ft)	TFA (in ²)	JSA (in ²)	Bit Dull Grade
12 1/4"	PDC Bit (HCC, Q 506 F)	RSS	10099 - 15080	1.2824	31.48	2-5-WT-G-X-I-CT-BHA
12 1/4"	PDC Bit (HCC, QD 507 FHX)	Steerable	15080 - 15193	1.2962	21.28	1-2-CT-S-X-I-NO-TD
8 1/2"	PDC Bit (HCC, DP 506 F)	RSS	15193 - 15601	0.8399	15.55	1-1-WT-S-X-I-NO-DTF
8 1/2"	PDC Bit (HCC, DP 506 F)	RSS	15601 - 16556	1.0301	15.55	2-2-BU-A-X-I-PN-TD
5 5/8"	PDC Bit (HCC, QD 406 FHX)	Steerable	16556 - 17265	0.8437	4.295	N/A

Table 3.1 provides information about the type of bit and bottom-hole assembly (BHA) used to drill the hole sections of interest. The dull grade for the bit used to drill the 5 5/8" hole was not available because the bit was lost in hole due to a pipe stuck incident following a well killing operation. Only the 12 1/4", 8 1/2" and 5 5/8" hole sections are under considerations in this paper. These intervals contain the normally compacted series, pressure transition zones and

overpressure formations. The top/big hole sections have been excluded from the analysis because of limited data acquisitions and the sections contain loose continental sands with no overpressure or hydrocarbon-bearing intervals. Figure 3.2 displays the plots of the recorded drilling parameters from surface measurements while drilling the well. Where the bottom hole assembly (BHA) contains mud motor (steerable), the total rotary speed is obtained using equation 3.32:

$$\text{Total rotary speed} = \text{Surface string rotation} + [Q * \text{Motor STFR}], \quad (3.32)$$

where Q is the flow rate (gpm); STFR is the speed to flow ratio (rpm/gpm).

To determine the overburden pressure, the formation bulk density data from the offset wells were combined with the formation bulk density data from the current well (Well A) to produce the equation of best fit. The equation of best fit was used to estimate the formation bulk density values in intervals where formation bulk density logs were not acquired. The formation bulk density equation of best fit is given by:

$$\rho_b = 1.136 Z^{0.0833}, \quad (3.33)$$

where ρ_b is the formation bulk density as a function of depth (g/cc); Z is the depth of interest (ft). By integrating the bulk density data, the overburden pressure was computed using:

$$S_v = 0.433 \int_0^Z \rho_b dz, \quad (3.33)$$

where S_v is the overburden pressure (psi); ρ_b is the formation bulk density as a function of depth (g/cc); Z is the depth of interest (ft). The equation of best fit was further constrained by the leak-off test (LOT) data in the field since the Niger Delta basin operates under normal faulting regime such that overburden pressure is the maximum principal stress ($S_v > \sigma_H > \sigma_h$).

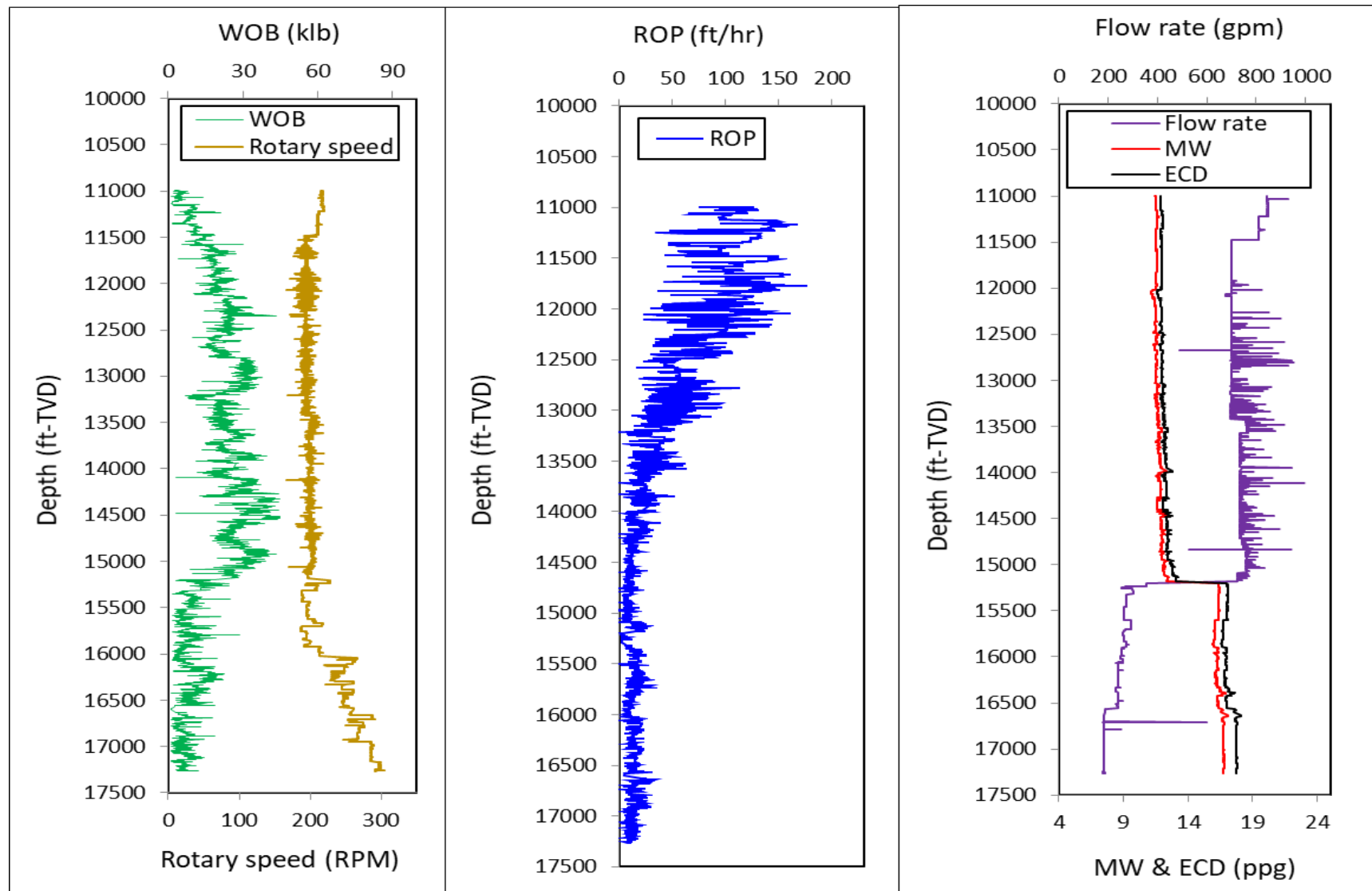


Figure 3. 2 The plots of drilling parameters against depth for Well A.

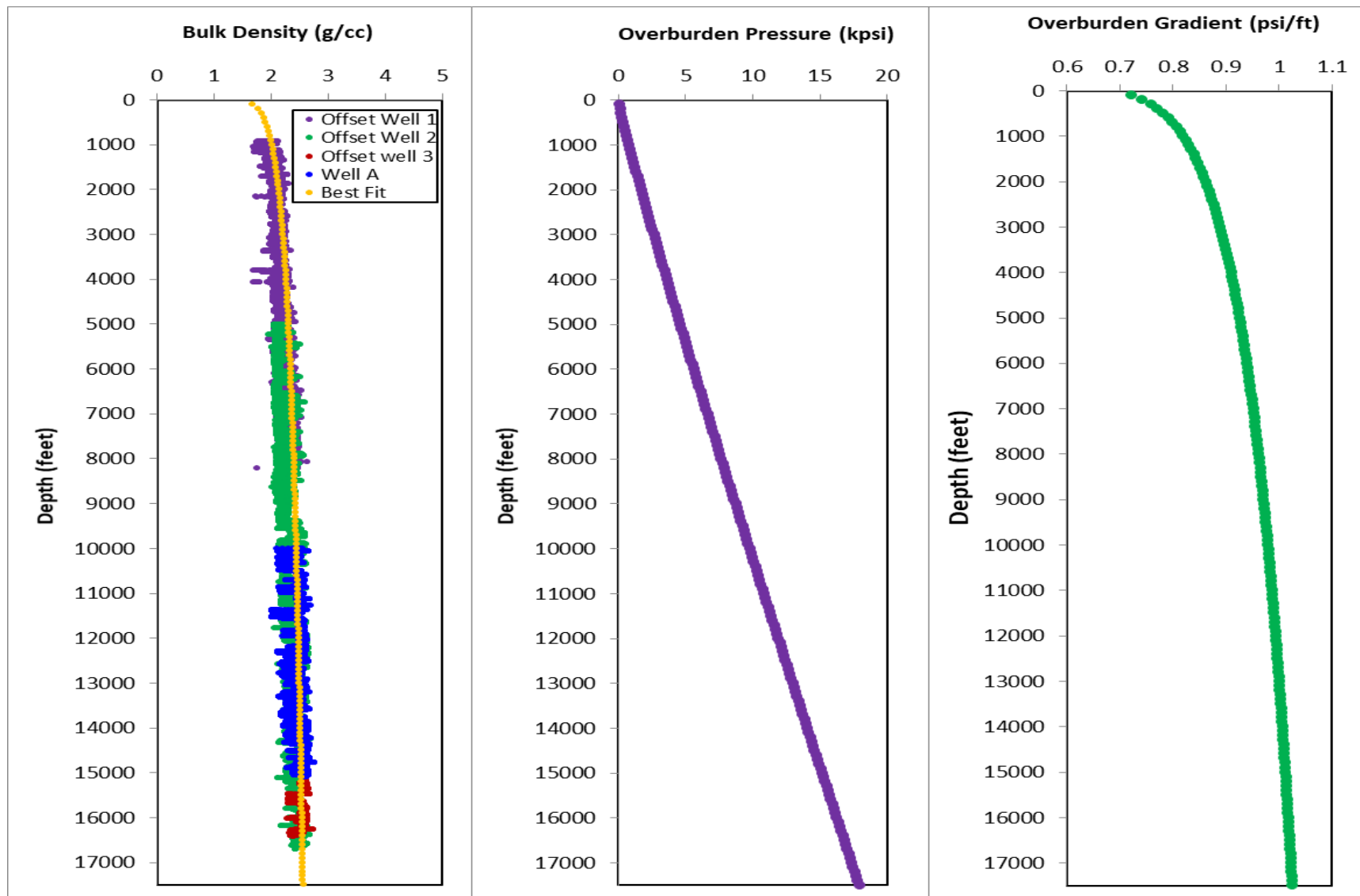


Figure 3. 3 The formation bulk density and overburden pressure/gradient profiles for Well A.

The overburden gradient (G_{ob}) was obtained by dividing the overburden pressure at the depth of interest by the true vertical depth. The plots of formation bulk density, overburden pressure/gradient and equation of best fit are displayed in Figure 3.3. Equation 3.33 is an improvement to the formation bulk density prediction model presented by Oloruntobi et al. (2018) for the central region of the Niger Delta based on a new set of offset well data.

3.5 Discussion

Figure 3.4A shows the plot of HMSE versus depth for Well A. Since the lithological effect on the HMSE is minimal in this well, the HMSE values are estimated across the various stratigraphic units from 10,997 ft to 17,265 ft. From the plot, the normal compaction trend (NCT) can be visibly identified from 10,997 ft to 15,060 ft. In these intervals, the total energy required to break and remove a unit volume of rock beneath the bit (HMSE) increases with depth due to a decrease in rock porosity and an increase in effective stress. Depth intervals that lie on the NCT correspond to the normally compacted series in the field. Based on the salinity of the formation waters in the region, the average normal pore pressure in the intervals that lie on the NCT is 8.66 ppg (0.45 psi/ft). In the intervals just below the 15,060 ft (top of pressure transition zones), subsurface overpressure conditions cause the HMSE to depart from the NCT to lower values. The overpressure intervals with lower effective stress consumed less energy to drill than the normally compacted series at the same depth. The magnitude of overpressure is directly correlated to the amount of deviation from the NCT.

Figure 3.4B shows the comparison between pore pressure estimates derived from HMSE concept (equation 3.31) and actual pore pressure measurements. A close agreement exists between the predicted and measured formation pore pressure.

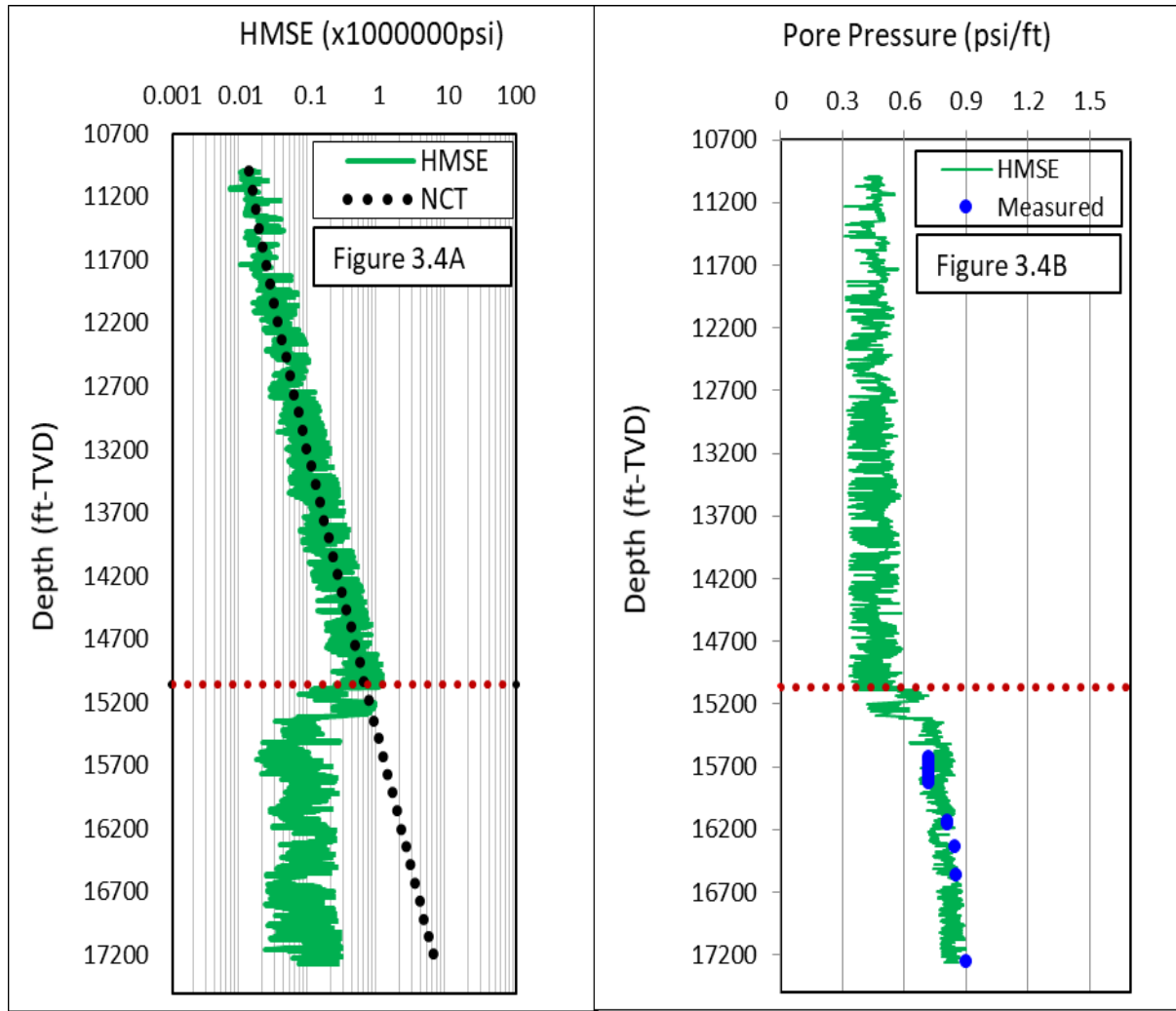


Figure 3.4 The HMSE and pore pressure profile for well A

The actual pore pressure measurements were obtained from the wireline pressure sampling tool and drilling kick data at the formations/depths of interest. Since the actual formation pore pressure in the field is known up to 16,567 ft (from offset wells) prior to drilling the current well, equation 3.31 is calibrated to these intervals to determine the value of the specific energy ratio exponent (m). The value of the specific energy ratio exponent (m) is 0.28. The predicted formation pore pressure is normal from 10,997 ft to 15,060 ft with an average value of 0.45 psi/ft. At the depth just below 15,060 ft (onset of overpressure), the formation pore pressure

increases from 0.45 psi/ft to 0.72 psi/ft at 15,630 ft. The formation pore pressure then increases further from 0.72 psi/ft at 15,630 ft to 0.9 psi/ft at the bottom of the well. The actual formation pore pressure at the bottom of the well was obtained from a gas kick data. While drilling with a mud weight (MW) of 0.87 psi/ft at the bottom of the well (17,265 ft), a gas kick was taken with stabilized shut-in drill pipe pressure (SIDPP) of 530 psi. This results in formation pore pressure of 0.9 psi/ft. Table 3.2 summarizes the main differences between pore pressure prediction technique based on HMSE concept and other pore pressure prediction models derived from drilling parameters.

Table 3. 2 Comparison of pore pressure prediction models from drilling parameters.

Author	Concept	Input Drilling Parameters	Remarks
Jorden & Shirley (1966)	d – exponent	WOB, N, and ROP	Empirically derived. It excludes the bit hydraulic energy term. Suitable mostly to hard rocks.
Cardona (2011)	MSE	WOB, N, T, and ROP	Derived from specific energy concept based on the combination of axial and rotary energies. It excludes the bit hydraulic energy term. Suitable mostly to hard rock.
Majidi et al. (2017)	DE-MSE	WOB, N, T, and ROP	The same as Cardona (2011). It also requires in-situ rock properties to be known.
Oloruntobi et al. (2018)	HRSE	N, T, Q, and ROP	Derived from specific energy concept based on the combination of rotary and hydraulic energies. It includes the bit hydraulic energy term. Suitable to soft and hard rocks. It excludes WOB term.
New Method	HMSE	WOB, N, Q, and ROP	Derived from specific energy concept based on the combination of axial, rotary and hydraulic energies. It includes the bit hydraulic energy term. Suitable to soft and hard rocks. It excludes torque term.

3.6 Conclusions

A new methodology to estimate the formation pore pressure from the drilling parameters is being proposed. The new methodology is based on the concept of total energy (axial, rotary and hydraulic) required to remove a unit volume of rock using only surface measurements. Since downhole measurements are not routinely measured as part of normal drilling parameters, the proposed methodology can provide a reliable means of estimating the formation pore pressure from the drilling parameters at relatively low cost. The HMSE computed from surface measurements can provide a reliable means of identifying the onset of overpressure in low inclination well (inclination < 30 degrees) where there is a good transfer of WOB to the bottom of the hole. In a high angle well (inclination > 30 degrees), hole drag due to friction loss along the wellbore may prevent effective transfer of WOB to the bottom of the hole, especially during sliding operations. In a high angle well, downhole parameters should be used to compute HMSE. Even if downhole measurements are available, a comparison of HMSE computed from downhole measurements with HMSE computed from surface measurements along with the compressional sonic velocity can be useful in identifying the source of a drilling problem. For instance, an increase in HMSE computed from both surface and downhole measurements with a corresponding increase in compressional sonic velocity may indicate drilling into a hard formation for a normal drilling operation. Increase in HMSE computed from both surface and downhole measurements with no corresponding increase in compressional sonic velocity may indicate bit related problems for a normal drilling operation. Increase in HMSE computed from surface measurements with no corresponding increase in HMSE computed from downhole measurements may indicate wellbore related problems such as stabilizer hanging up and cuttings accumulation in the annulus (hole inclination > 30 degrees). However, the proposed

methodology should be applied with care under excessive bit wear, bit balling conditions, excessive vibration and mud motor stalling conditions. The above conditions can mask subsurface overpressure conditions when drilling through the pressure transition zones.

3.7 Reference

- Aadnoy, B.S., 2010. Introduction to Geomechanics in Drilling. Mitchell, Robert F Miska, Stefan Z. Fundam. Drill. Eng. Soc. Pet. Eng. 58–59.
- Abbas, R.K., Hassanpour, A., Hare, C., Ghadiri, M., 2014. Instantaneous Monitoring of Drill Bit Wear and Specific Energy as a Criteria for the Appropriate Time for Pulling Out Worn Bits (Russian), in: SPE Annual Caspian Technical Conference and Exhibition. Society of Petroleum Engineers.
- Akbari, B., Miska, S., Mengjiao, Y., Ozbayoglu, E., 2013. Effect of Rock Pore Pressure on Mechanical Specific Energy of Rock Cutting Using Single PDC Cutter, in: 47th US Rock Mechanics/Geomechanics Symposium. American Rock Mechanics Association.
- Akbari, B., Miska, S., Yu, M., Ozbayoglu, M., 2014. Experimental Investigations of the Effect of the Pore Pressure on the MSE and Drilling Strength of a PDC Bit, in: SPE Western North American and Rocky Mountain Joint Meeting. Society of Petroleum Engineers.
- Amadi, W.K., Iyalla, I., 2012. Application of Mechanical Specific Energy Techniques in Reducing Drilling Cost in Deepwater Development, in: SPE Deepwater Drilling and Completions Conference. Society of Petroleum Engineers.
- Armenta, M., 2008. Identifying inefficient drilling conditions using drilling-specific energy, in: SPE Annual Technical Conference and Exhibition. Society of Petroleum Engineers.
- Atashbari, V., Tingay, M.R., 2012. Pore pressure prediction in carbonate reservoirs, in: SPE Latin America and Caribbean Petroleum Engineering Conference. Society of Petroleum Engineers.
- Avbovbo, A.A., 1978. Tertiary lithostratigraphy of the Niger Delta. Am. Assoc. Pet. Geol. Bull. 62, 295–306.
- Bachu, S., Underschultz, J.R., 1995. Large-scale underpressuring in the Mississippian-Cretaceous succession, southwestern Alberta Basin. Am. Assoc. Pet. Geol. Bull. 79, 989–

1004. <https://doi.org/10.1306/8D2B21A5-171E-11D7-8645000102C1865D>
- Barker, C., 1972. Aquathermal Pressuring--Role of Temperature in Development of Abnormal-Pressure Zones: GEOLOGICAL NOTES. Am. Assoc. Pet. Geol. Bull. 10, 2068–2071. <https://doi.org/10.1306/819A41B0-16C5-11D7-8645000102C1865D>
- Barkers, C., Horsfield, B., 1982. Mechanical versus thermal cause of abnormally high pore pressures in shales. Am. Assoc. Pet. Geol. Bull. 66, 99–100. <https://doi.org/10.1306/2F919760-16CE-11D7-8645000102C1865D>
- Bevilacqua, M., Ciarapica, F.E., Marchetti, B., 2013. Acquisition, processing and evaluation of down hole data for monitoring efficiency of drilling processes. J. Pet. Sci. Res.
- Black, A.D., Dearing, H.L., DiBona, B.G., 1985. Effects of Pore Pressure and Mud Filtration on Drilling Rates in a Permeable Sandstone. J. Pet. Technol. 37, 1671–1681. <https://doi.org/10.2118/12117-PA>
- Bourgoyne Jr, A.T., Young Jr, F.S., 1973. The Use of Drillability Logs for Formation Evaluation and Abnormal Pressure Detection, in: SPWLA 14th Annual Logging Symposium. Society of Petrophysicists and Well-Log Analysts.
- Bowers, G.L., 1995. Pore pressure estimation from velocity data: Accounting for overpressure mechanisms besides undercompaction. SPE Drill. Compleat. 10, 89–95. <https://doi.org/10.2118/27488-PA>
- Bruce, C.H., 1984. Smectite Dehydration-Its Relation to Structural Development and Hydrocarbon Accumulation in Northern Gulf of Mexico Basin. Am. Assoc. Pet. Geol. Bull. 68, 673–683. <https://doi.org/10.1306/AD461363-16F7-11D7-8645000102C1865D>
- Burrus, J., 1998. Overpressure models for clastic rocks, their relation to hydrocarbon expulsion: a critical re-evaluation. Abnorm. Press. Hydrocarb. Environ. 70, 35–63.
- Burst, J., 1969. Diagenesis of Gulf Coast Clayey Sediments and Its Possible Relation To Petroleum Migration. Am. Assoc. Pet. Geol. Bull. 53, 73–93. <https://doi.org/10.1306/5D25C595-16C1-11D7-8645000102C1865D>
- Burst, J.F., 1976. Argillaceous Sediment Dewatering. Annu. Rev. Earth Planet. Sci. 4, 293–318. <https://doi.org/10.1146/annurev.ea.04.050176.001453>
- Buryakovskiy, L.A., Djevanshir, R.D., Chilingar, G. V., 1995. Abnormally-high formation pressures in Azerbaijan and the South Caspian Basin (as related to smectite ??? illite transformations during diagenesis and catagenesis). J. Pet. Sci. Eng. 13, 203–218.

[https://doi.org/10.1016/0920-4105\(95\)00008-6](https://doi.org/10.1016/0920-4105(95)00008-6)

- Caicedo, H.U., Calhoun, W.M., Ewy, R.T., 2005. Unique ROP Predictor Using Bit-specific Coefficient of Sliding Friction and Mechanical Efficiency as a Function of Confined Compressive Strength Impacts Drilling Performance. Soc. Pet. Eng. (SPE/IADC 92576).
<https://doi.org/10.2118/92576-MS>
- Cardona, J., 2011. Fundamental Investigation of Pore Pressure Prediction during Drilling from the Mechanical Behaviour of Rocks. PhD Thesis, Texas A&M Univ. Mech. Eng.
- Carlin, S., Dainelli, J., 1998. Pressure regimes and pressure systems in the Adriatic Foredeep (Italy). Abnorm. Press. Hydrocarb. Environ. 70, 145–160.
- Carstens, H., Dypvik, H., 1981. Abnormal formation pressure and shale porosity. Am. Assoc. Pet. Geol. Bull. 65, 344–350.
- Cheatham, C.A., Nahm*, J.J., Heitkamp, N., 1985. Effects of Selected Mud Properties on Rate of Penetration in Full-Scale Shale Drilling Simulations. Soc. Pet. Eng. (SPE/IADC 13465).
- Chen, J., Huang, D., 1996. Formation and mechanism of the abnormal pressure zone and its relation to oil and gas accumulations in the Eastern Jiuquan Basin, Northwest China. Sci. China Earth Sci. 39, 194–204.
- Chen, X., Gao, D., Guo, B., Feng, Y., 2016. Real-time optimization of drilling parameters based on mechanical specific energy for rotating drilling with positive displacement motor in the hard formation. J. Nat. Gas Sci. Eng. 35, 686–694.
- Cunningham, R. a, Eenink, J.G., 1959. Laboratory Study of Effect of Overburden, Formation and Mud Column Pressures on Drilling Rate of Permeable Formations. Pet. Trans. AIME 217, 9–17.
- Daukoru, J.W., 1975. PD 4(1) Petroleum Geology of the Niger Delta. World Pet. Congr.
- Dickey, P., Cox, W., 1977. Oil and gas in reservoirs with subnormal pressures. Am. Assoc. Pet. Geol. Bull. 12, 2134–2142.
- Dupriest, F.E., 2006. Comprehensive Drill-Rate Management Process To Maximize Rate of Penetration. Soc. Pet. Eng. (SPE 102210). <https://doi.org/10.2118/102210-MS>
- Dupriest, F.E., 2006. Comprehensive Drill Rate Management Process To Maximize ROP, in: SPE Annual Technical Conference and Exhibition. Society of Petroleum Engineers.
- Dupriest, F.E., Koederitz, W.L., 2005. Maximizing drill rates with real-time surveillance of mechanical specific energy, in: SPE/IADC Drilling Conference. Society of Petroleum

Engineers.

- Eaton, B.A., 1975. The Equation for Geopressure Prediction from Well Logs. Soc. Pet. Eng. (SPE 5544). <https://doi.org/10.2118/5544-MS>
- Evamy, B.D., Haremboure, J., Kamerling, P., Knaap, W.A., Molloy, F.A., Rowlands, P.H., 1978. Hydrocarbon habitat of Tertiary Niger delta. Am. Assoc. Pet. Geol. Bull. 62, 1–39.
- Fertl, W.H., Timko, D.J., 1971. Parameters for identification of overpressure formations, in: Drilling and Rock Mechanics Conference. Society of Petroleum Engineers.
- Finch, W., 1969. Abnormal Pressure in the Antelope Field, North Dakota. J. Pet. Technol. 21. <https://doi.org/10.2118/2227-PA>
- Forgotson, S.J.M., 1969. Indication of Proximity of High-Pressure Fluid Reservoir, Louisiana and Texas Gulf Coast. Am. Assoc. Pet. Geol. Bull. 53, 171–173.
- Foster, J.B., Whalen, H.E., 1966. Estimation of formation pressures from electrical surveys - Offshore Louisiana. J. Pet. Technol. 18, 165–171. <https://doi.org/10.2118/1200-PA>
- Freed, R.L., Peacor, D.R., 1989. Geopressured shale and sealing effect of smectite to illite transition. Am. Assoc. Pet. Geol. Bull. 73, 1223–1232. <https://doi.org/10.1306/44B4AA0A-170A-11D7-8645000102C1865D>
- Freire, H., Falcão, J., Silva, C.F., Barghigiani, L., 2010. Abnormal Pore Pressure Mechanisms In Brazil. Pap. ARMA 10-407 Proc. 2010 44th US Rock Mech. Symp. 5th U.S.-Canada Rock Mech. Symp. held Salt Lake City, UT June 27–30.,
- Gardner, G.H., Gardner, L., Gregory, A., 1974. Formation Velocity and Density - The Diagnostic Basic for Stratigraphic Traps. Geophysics 39, 770–780.
- Guerrero, C.A., Kull, B.J., 2007. Deployment Of An SeROP Predictor Tool For Real-Time Bit Optimization. SPE/IADC Drill. Conf. <https://doi.org/10.2118/105201-MS>
- Harkins, L.K., Baugher, I.H., 1969. Geological significance of abnormal formation pressures. J. Pet. Technol. 961–966. <https://doi.org/10.2118/2228-PA>
- Harper, D., 1969. New Findings from Over Pressure Detection Curves in Tectonically Stressed Beds, in: SPE California Regional Meeting. Society of Petroleum Engineers.
- Hermanrud, C., Wensaas, L., Teige, G.M.G., Bolas, H.M.N., Hansen, S., Vik, E., 1998. Memoir 70, Chapter 4: Shale Porosities from Well Logs on Haltenbanken (Offshore Mid-Norway) Show No Influence of Overpressuring.
- Holm, G.M., 1998. Distribution and origin of overpressure in the Central Graben of the North

- Sea. Law, B.E., G.F. Ulmishek, V.I. Slavin eds., Abnorm. Press. Hydrocarb. Environ. AAPG Mem. 70, 123–144.
- Hooper, R.J., Fitzsimmons, R.J., Grant, N., Vendeville, B.C., 2002. The role of deformation in controlling depositional patterns in the south-central Niger Delta, West Africa. *J. Struct. Geol.* 24, 847–859.
- Hottmann, C.E., Johnson, R.K., 1965. Estimation of formation pressures from log-derived shale properties. *J. Pet. Technol.* 17, 717–722.
- Hunt, J.M., Whelan, J.K., Eglinton, L.B., Cathles, L.M. ll., 1998. Relation of shale porosities, gas generation, and compaction to deep overpressures in the US. Gulf coast. Law, B.E., G.F. Ulmishek, V.I. Slavin eds., Abnorm. Press. Hydrocarb. Environ. AAPG Mem. 70 87–104.
- Jorden, J.R., Shirley, O.J., 1966. Application of drilling performance data to overpressure detection. *J. Pet. Technol.* 18, 1–387.
- Kadri, I.B., 1991. Abnormal Formation Pressures in Post-Eocene Formation, Potwar Basin, Pakistan. Pap. SPE/IADC 21920 Proc. 1991 SPE/IADC Drill. Conf. held Amsterdam, 11-14 March. <https://doi.org/10.2523/21920-MS>
- Koederitz, W., Weis, J., 2005. A Real-Time Implementation of MSE, American Association of Drilling Engineers. AADE-05-NTCE-66.
- Law, B.E., Dickinson, W.W., 1985. Conceptual Model for Origin of Abnormally Pressured Gas Accumulations in Low-Permeability Reservoirs. *Am. Assoc. Pet. Geol. Bull.* 69, 1295–1304. <https://doi.org/10.1306/AD462BD7-16F7-11D7-8645000102C1865D>
- Law, B.E., Shah, S.H. a, Malik, M. a, 1998. Abnormally high formation pressures, Potwar Plateau, Pakistan. Law, B.E., G.F. Ulmishek, V.I. Slavin eds., Abnorm. Press. Hydrocarb. Environ. AAPG Mem. 70 247–358. <https://doi.org/10.1306/F4C8E6B6-1712-11D7-8645000102C1865D>
- Law, B.E., Spencer, C.W., 1998. Abnormal Pressure in Hydrocarbon Environments. Law, B.E., G.F. Ulmishek, V.I. Slavin eds., Abnorm. Press. Hydrocarb. Environ. AAPG Mem. 70 1–11. [https://doi.org/10.1016/S0264-8172\(99\)00059-8](https://doi.org/10.1016/S0264-8172(99)00059-8)
- Lewis, C., Rose, S., 1970. A theory relating high temeperatures and overpressures. *J. Pet. Technol.* 22, 11–16.
- Louden, L.R., 1972. Origin and maintenance of abnormal pressures, in: Abnormal Subsurface

- Pressure Symposium. Society of Petroleum Engineers.
- Majidi, R., Albertin, M., Last, N., 2017. Pore-Pressure Estimation by Use of Mechanical Specific Energy and Drilling Efficiency. *SPE Drill. Complet.* 32, 97–104.
- Mohan, K., Adil, F., Samuel, R., 2015. Comprehensive Hydromechanical Specific Energy Calculation for Drilling Efficiency. *J. Energy Resour. Technol.* 137, 012904. <https://doi.org/10.1115/1.4028272>
- Oloruntobi, O., Adedigba, S., Khan, F., Chunduru, R., Butt, S., 2018. Overpressure prediction using the hydro-rotary specific energy concept. *J. Nat. Gas Sci. Eng.* 55, 243–253.
- Parker, C.A., 1973. Geopressures in the deep Smackover of Mississippi. *J. Pet. Technol.* 25, 971–979.
- Pessier, R.C., Fear, M.J., 1992. Quantifying common drilling problems with mechanical specific energy and a bit-specific coefficient of sliding friction, in: SPE Annual Technical Conference and Exhibition. Society of Petroleum Engineers.
- Pinto, C.N., Lima, A.L.P., 2016. Mechanical Specific Energy for Drilling Optimization in Deepwater Brazilian Salt Environments. *Soc. Pet. Eng. (IADC/SPE 180646).* <https://doi.org/10.2118/180646-MS>
- Plumley, J.W., 1980. Abnormally High Fluid Pressure: Survey of Some Basic Principles: ERRATUM. *Am. Assoc. Pet. Geol. Bull.* 64, 414–422. <https://doi.org/10.1306/2F919409-16CE-11D7-8645000102C1865D>
- Polutranko, A.J., 1998. Causes of Formation and Distribution of Abnormally High Formation Pressure in Petroleum Basins of Ukraine. Law, B.E., G.F. Ulmishek, V.I. Slavin eds., *Abnorm. Press. Hydrocarb. environments AAPG Mem.* 70 181–194. [https://doi.org/10.1130/0091-7613\(1998\)026<0911](https://doi.org/10.1130/0091-7613(1998)026<0911)
- Powers, M.C., 1967. Fluid-release mechanisms in compacting marine mudrocks and their importance in oil exploration. *Am. Assoc. Pet. Geol. Bull.* 7, 1240–1254.
- Rabia, H., 1989. Rig Hydraulics Entrac Software.
- Rabia, H., 1985. Specific energy as a criterion for bit selection. *J. Pet. Technol.* 37, 1225–1229. <https://doi.org/10.2118/12355-PA>
- Rafatian, N., Miska, S.Z., Ledgerwood, L.W., Yu, M., Ahmed, R., Takach, N.E., 2010. Experimental study of MSE of a single PDC cutter interacting with rock under simulated pressurized conditions. *SPE Drill. Complet.* 25, 10–18.

- Rehm, B., McClendon, R., 1971. Measurement of formation pressure from drilling data, in: Fall Meeting of the Society of Petroleum Engineers of AIME. Society of Petroleum Engineers.
- Reijers, T., 2011. Stratigraphy and sedimentology of the Niger Delta. *Geologos* 17, 133–162.
- Satti, A.. I., Yusoff, W.W.I., Ghosh, D., 2016. Overpressure in the Malay Basin and prediction methods. *Geofluids* 16, 301–313. <https://doi.org/10.1111/gfl.12149>
- Satti, I.A., Ghosh, D., Yusoff, W.I.W., Hoesni, M.J., 2015. Origin of Overpressure in a Field in the Southwestern Malay Basin. *SPE Drill. Complet.* 30, 198.
- Sayers, C.M., Boer Den, L.D., Nagy, Z.R., Hooymann, P.J., Ward, V., 2005. Regional trends in undercompaction and overpressure in the Gulf of Mexico. *Seg/houst. 2005 Annu. Meet.* 1219–1223.
- Serebryakov, V.A., Chilingar, G. V., 1994. Investigation of underpressured reservoirs in the powder river Basin, Wyoming and Montana. *J. Pet. Sci. Eng.* 11, 249–259. [https://doi.org/10.1016/0920-4105\(94\)90044-2](https://doi.org/10.1016/0920-4105(94)90044-2)
- Sharp, J.M., 1983. Permeability Controls on Aquathermal Pressuring. *Am. Assoc. Pet. Geol. Bull.* 67, 2057–2061.
- Short, K., Stauble, A., 1967. Outline of Geology of Niger Delta. *Am. Assoc. Pet. Geol. Bull.* 51, 761–779.
- Spencer, C.W., 1987. Hydrocarbon Generation as a Mechanism for Overpressuring in Rocky Mountain Region. *Am. Assoc. Pet. Geol. Bull.* 71, 368–388. <https://doi.org/10.1306/94886EB6-1704-11D7-8645000102C1865D>
- Swarbrick, R.E., Osborne, M.J., 1998. Mechanisms that generate abnormal pressures: an overview. Law, B.E., G.F. Ulmishek, V.I. Slavin eds., *Abnorm. Press. Hydrocarb. Environ.* AAPG Mem. 70 13–34.
- Teale, R., 1965. The Concept of Specific Energy in Rock Drilling. *Int. J. Rock Mech. Min. Sci.* 2, 57–73. [https://doi.org/10.1016/0148-9062\(65\)90022-7](https://doi.org/10.1016/0148-9062(65)90022-7)
- Teige, G.M.G., Hermanrud, C., Wensaas, L., Bolås, H.M.N., 1999. The lack of relationship between overpressure and porosity in North Sea and Haltenbanken shales. *Mar. Pet. Geol.* 16, 321–335.
- Tingay, M.R.P., Hillis, R.R., Swarbrick, R.E., Morley, C.K., Damit, A.R., 2009. Origin of overpressure and pore-pressure prediction in the Baram province, Brunei. *Am. Assoc. Pet. Geol. Bull.* 93, 51–74.

- Ugwu, S.A., Nwankwo, C.N., 2014. Integrated approach to geopressure detection in the X-field, Onshore Niger Delta. *J. Pet. Explor. Prod. Technol.* 4, 215–231. <https://doi.org/10.1007/s13202-013-0088-4>
- Vidrine, D.J., Benit, E.J., 1968. Field Verification of the Effect of Differential Pressure on Drilling Rate. *J. Pet. Technol. (SPE 1859)* 20, 676–682. <https://doi.org/10.2118/1859-PA>
- Wardlaw, H.W.R., 1969. Drilling Performance Optimization and Identification of Overpressure. *Soc. Pet. Eng. AIME SPE 2388*, 67–78.
- Warren, T.M., 1987. Penetration Rate Performance of Roller Cone Bits. *SPE Drill. Eng.* 2, 9–18. <https://doi.org/10.2118/13259-PA>
- Waughman, J.R., Kenner, V.J., Moore, A.R., 2003. Real-Time Specific Energy Monitoring Enhances the Understanding of When To Pull Worn PDC Bits. *SPE Drill. Complet. (SPE 81822)* 59–68.
- Weber, K.J., 1987. Hydrocarbon distribution patterns in Nigerian growth fault structures controlled by structural style and stratigraphy. *J. Pet. Sci. Eng.* 1, 91–104.
- Wei, M., Li, G., Shi, H., Shi, S., Li, Z., Zhang, Y., 2016. Theories and applications of pulsed-jet drilling with mechanical specific energy. *SPE J.* 21, 303–310.
- Yassir, N., Bell, J., others, 1996. Abnormally high fluid pressures and associated porosities and stress regimes in sedimentary basins. *SPE Form. Eval.* 11, 5–10. <https://doi.org/10.2118/28139-PA>
- Zhang, J., 2013. Effective stress, porosity, velocity and abnormal pore pressure prediction accounting for compaction disequilibrium and unloading. *Mar. Pet. Geol.* 45, 2–11. <https://doi.org/10.1016/j.marpetgeo.2013.04.007>
- Zhang, J., 2011. Pore pressure prediction from well logs: Methods, modifications, and new approaches. *Earth-Science Rev.* 108, 50–63. <https://doi.org/10.1016/j.earscirev.2011.06.001>
- Zhou, Y., Zhang, W., Gamwo, I., Lin, J.-S., 2017. Mechanical specific energy versus depth of cut in rock cutting and drilling. *Int. J. Rock Mech. Min. Sci.* 100, 287–297.

Chapter 4

4.0 The New Formation Bulk Density Predictions for Siliciclastic Rocks

Preface

*A version of this chapter has been published in the **Journal of Petroleum Science and Engineering, 2019**. I am the primary author. Co-author Dr. Stephen Butt reviewed the manuscript and provided technical assistance in the development of the concept. I formulated the initial concept and carried out most of the data analysis. I prepared the first draft of the manuscript and revised the manuscript based on the feedback from the co-author and peer review process. The co-author also helped to refine the concept.*

Abstract

Accurate determination of the overburden pressure obtained by integrating the formation bulk densities from surface to the depth of interest is very critical to pore pressure prediction. When information about the formation bulk density is not available, the current practice is to estimate the formation bulk density from compressional wave velocity using empirical relationships. There is no single formation bulk density prediction model that considers lithologic variation in siliciclastic settings. This imposes severe limitations on the application of the existing empirical relationships to any lithological column that consists of several stratigraphic units and/or non-clean intervals. In this paper, attempt is made to develop the new formation bulk density prediction models that can be applied to a wide range of lithologies in siliciclastic environments. The new models are validated using wireline log data acquired from two wells in the tertiary deltaic system of the Niger Delta basin. In the new models, formation bulk density is expressed

as a function of compressional wave velocity and shale volume factor. The accuracy of the new models is quantified using statistical analysis. When compared to the existing models, the new models outperform the most widely used empirical relationships. The new models produce the lowest root mean square errors (5 - 6%), excellent error distributions and lowest residual values. Unlike any of the existing empirical relationships, the new formation bulk density prediction models can be applied to clean sands, clean shales and formations that contain a mixture of sands and shales in any proportion. In general, the applications of the new models show an excellent agreement between the predicted and measured formation bulk density.

Keywords: Formation bulk density, Compressional velocity, Empirical relationship, Lithology.

4.1 Introduction

Accurate determination of the rock mechanical properties is very essential for reducing the risks associated with drilling, completion and production operations (Onalo et al., 2018). In addition to compressional and shear wave velocity data, formation bulk density is an important input parameter required to estimate the rock mechanical properties (Tixier et al., 1975; Coates and Denoo, 1980; Onyia, 1988; Potter and Foltinek, 1997; Ohen, 2003; Chang et al., 2006; Fjar et al., 2008; Ameen et al., 2009; Khair et al., 2015; Xu et al., 2016; Najibi et al., 2015; Feng et al., 2019). These properties are required for geo-mechanical analyses such as compaction and subsidence, wellbore stability prediction, perforation strategy, hydraulic fracturing, sand production prediction and reservoir characterization. Formation bulk density data are also required for porosity estimation, lithology determination, pore fluid identification and overburden pressure prediction. Information about the formation bulk density and its derivative

in clean shales can be very useful in estimating the formation pore pressure and predicting the origin of overpressure (Burrus, 1998; Bowers, 2001; Swarbrick, 2001; Zhang, 2011; Zhang, 2013; Hoesni, 2004; Satti et al., 2015). In seismic reflection analysis, information about the formation bulk density is required in determining the elastic impedance of an interface.

Although density logs are among the common well logs acquired while drilling a well or after the well has been drilled, there are several occasions when formation bulk density predictions from other well log data may be required. First and foremost, density logs are usually not run in all the intervals from surface/seabed to well total depth (Zoback, 2010). In most cases, these logs (density) are run only in the intervals of interest (such as intervals that contain hydrocarbon-bearing sands) for a selected number of wells in a certain field. Furthermore, density logs are usually not run in the top/big hole sections (greater than 16 inches) because of the difficulty of acquiring such logs in large diameter boreholes that are prone to excessive washout and the fact that these sections do not normally contain hydrocarbon-bearing sands. Even if density logs are run in a well, comparison with its prediction from other well logs can be a useful quality control tool, especially in a rugose wellbore. More so, it is possible that density tool may fail while drilling or logging at great depth (greater than 17,000 feet) in an offshore environment with a floating rig. Under this condition of extremely high operating cost, operators will not likely pull out of hole to re-run the density tool if other well logs that can be used to accurately predict formation bulk density are available. Finally, accurate determination of overburden pressure for pre-drill pore/fracture pressure predictions and wellbore stability analyses requires information about the formation bulk density over the entire penetrated intervals from surface to the depth of interest. Since density logs are not usually acquired over the entire drilled intervals from surface to the depth of interest, prediction of this property is

highly required in the intervals that do not contain density logs. In general, lack of continuous formation bulk density measurements along the well path necessitates its prediction for overburden pressure estimation. Other possible reasons for the absence of density logs in most wells/intervals may include economic reasons (especially marginal operators) and the risk of losing a radioactive source in the well. In formations/intervals where density logs are not acquired, empirical relationships have been developed to estimate the formation bulk density from the compressional wave velocity. Equations of best fit through the intervals that do not contain formation bulk density data should be used with caution and only if formation bulk density values cannot be predicted due to unavailability of other well log data. In this paper, unless otherwise stated, the compressional velocity and formation bulk density are expressed in kilometers per second (km/s) and grams per cubic centimeter (g/cm^3 or g/cc) respectively.

The relationship between the formation bulk density and compressional wave velocity has long been established. In non-fractured rocks, the formation bulk density is a function of compressional wave velocity (Lobkovsky et al., 1996). Birch (1961) established a linear relationship between the formation bulk density (ρ_b) and compressional wave velocity (V_p) for igneous and metamorphic rocks based on laboratory measurements. The empirical model proposed by Birch (1961) is given by:

$$\rho_b = AV_p + B, \quad (4.1)$$

where A and B are empirical constants. Anderson (1967) then extended and modified Birch's model to be in accordance with theoretical predictions. For most volcanic and granitic rocks, Carroll (1969) concluded that the relationship between formation bulk density and compressional wave velocity is also linear. Based on a large number of laboratory and field observations of

different brine-saturated rock types (excluding evaporites) from a wide variety of basins and depths, Gardner et al. (1974) proposed the most widely used exponential relationship between the formation bulk density (ρ_b) and compressional velocity (V_p). Gardner's relation is given by:

$$\rho_b = 1.74[V_p]^{0.25}. \quad (4.2)$$

Gardner's model is one of the most important empirical relationships used in seismic prospecting (Castagna and Backus, 1993). The model is most reliable when the rocks are well consolidated, water-saturated and under substantial effective stress. Gardner's model and its modifications have been applied to several sedimentary basins around the world (Dey and Stewart, 1997; Potter and Stewart, 1998; Potter, 1999; Quijada and Stewart, 2007; Ojha and Sain, 2014; Nwozor et al., 2017; Akhter et al., 2018). In most cases, Gardner's model tends to overestimate formation bulk density in sandstones and underestimate formation bulk density in shales (Wang, 2001). Lindseth (1979) established an empirical relationship between acoustic impedance ($\rho_b V_p$) and compressional velocity (V_p) based on Gardner et al. (1974) data set (equation 4.3):

$$V_p = 0.308\rho_b V_p + 3460, \quad (4.3)$$

where the compressional wave velocity is expressed in feet per second (ft/s). Although Christensen and Mooney (1995) proposed both linear and nonlinear relationships between formation bulk density (ρ_b) and compressional wave velocity (V_p) for crystalline rocks, they concluded that the nonlinear relationship provides the best correlation. The non-linear model proposed by Christensen and Mooney (1995) is given by:

$$\rho_b = G + \frac{K}{V_p}, \quad (4.4)$$

where G and K are empirical constants that depend on the depth at which the rocks are found. Brocher (2005) proposed a nonlinear (polynomial) relationship between formation bulk density (ρ_b) and compressional velocity (V_p) based on the data provided by Ludwig et al. (1970) for all rock types except mafic crustal and calcium-rich rocks. The model is valid for compressional velocity between 1.5 km/s and 8.5 km/sec (Brocher 2008). Brocher's model is another widely used empirical relationship given by:

$$\rho_b = 1.6612V_p - 0.4721V_p^2 + 0.0671V_p^3 - 0.0043V_p^4 + 0.000106V_p^5. \quad (4.5)$$

Khandelwal (2013) presented another linear relationship between formation bulk density (ρ_b) and compressional wave velocity (V_p) for representative rock mass samples of igneous, sedimentary, and metamorphic rocks. Khandelwal's correlation is given by:

$$\rho_b = 0.202V_p - 1794.7, \quad (4.6)$$

where the compressional wave velocity and formation bulk density are expressed in m/s and kg/m³ respectively. Attempts have also been made to estimate the formation bulk density from the combination of compressional and shear wave velocities (Ursenbach, 2001; Ursenbach, 2002a; Ursenbach, 2002b).

Most of the existing empirical relationships between the formation bulk density and compressional wave velocity were developed mainly for clean formations and they do not consider variations in lithology. Empirical relationships that work very well for clean sandstone formations may perform poorly in clean shale/shaly-sandstone formations and vice versa. In fact, the most recent formation bulk density prediction models proposed by Akhter et al. (2018) are still limited to clean formations containing less than 10 % shale by volume. Based on the

experimental data presented by Han et al. (1986) at 40 MPa differential pressure, Miller & Stewart (1991) determined that the relationships between compressional wave velocity and formation bulk density were scattered for rocks that contain a mixture of sand and shale. However, they observed that the relationships improved significantly when the data were categorized by clay content based on Vernik & Nur (1992) classification. This is the basis of the new formation bulk density predictions. In this paper, an attempt is made to develop new formation density prediction models that can be applied to a wide range of lithologies in siliciclastic environments. The new models intend to consider lithologic variation by incorporating a shale volume factor term. The addition of the shale volume term will normalize the new models for lithology effects.

4.2 Methodology

Laboratory investigations have shown that compressional wave velocity (V_p) can be expressed as functions of effective porosity (ϕ) and clay volume (V_{sh}) (Tosaya 1982; Tosaya and Nur 1982; Kowallis et al., 1984; Castagna et al. 1985; Han et al. 1986). This relationship is given by:

$$V_p = A - B\phi - CV_{sh}, \quad (4.7)$$

where A, B and C are regression coefficients. For liquid-filled non-clean formations in siliciclastic settings, effective porosity (ϕ) can be expressed as functions of formation bulk density (ρ_b), sand matrix density (ρ_{ma}), shale matrix density (ρ_{sh}), saturating fluid density (ρ_{fl}) and shale volume fraction (V_{sh}) as given by:

$$\phi = \left[\frac{\rho_{ma}}{\rho_{ma} - \rho_{fl}} \right] - \left[\frac{1}{\rho_{ma} - \rho_{fl}} \right] \rho_b - \left[\frac{\rho_{ma} - \rho_{sh}}{\rho_{ma} - \rho_{fl}} \right] V_{sh}. \quad (4.8)$$

To a large extent, the quantities in the parentheses in equation 4.8 are approximately constant for liquid-filled porous rocks. The saturating fluid density (ρ_f) is usually approximated as the density of mud filtrate. Hence, equation 4.8 will reduce to equation 4.9:

$$\phi = M - N\rho_b - X V_{sh}, \quad (4.9)$$

where M , X and N are constant parameters. Combination of equations 7 and 9 will lead to:

$$\rho_b = QV_p + ZV_{sh} + P, \quad (4.10)$$

where Q , Z and P are the new coefficients. When applied over clean formations where shale volume factor is zero, equation 4.10 will reduce to Birch's model (equation 4.1). Hence, equation 4.10 is referred to as modified Birch's model. Since Gardner's model is the most widely used empirical relationship, a shale volume factor term is also added to Gardner's model to account for variations in lithology. The modified Gardner's model is given by:

$$\rho_b = k[V_p + GV_{sh}]^m, \quad (4.11)$$

where k , G and m are constant parameters. To determine the values of the constant parameters Q , Z , P , G , k and m , equations 4.10 and 4.11 are calibrated to the experimental data provided by Han et al. (1986). Han et al. (1986) conducted laboratory ultrasonic experiments on brine saturated sandstone cores obtained from quarries in USA and Gulf of Mexico wells. Han's data are selected for calibration because the laboratory experiments were conducted on both clean and non-clean formations with the volume of shale in the core samples ranging from 0 to 51%. By calibrating equations 4.10 and 4.11 to the compressional wave velocity, formation bulk density and shale volume data provided by Han et al. (1986) for the entire 75 samples at 40 MPa

differential pressure, the values of the constant parameters Q, Z, P, G, k and m are determined to be 0.222, 0.361, 1.431, 1.650, 1.351 and 0.390 respectively. Hence, the new formation bulk density prediction model (Model I) based on equation 4.10 is given by:

$$\rho_b = 0.222V_p + 0.361V_{sh} + 1.431. \quad (4.12)$$

Likewise, the new density prediction (Model II) based on equation 4.11 is given by:

$$\rho_b = 1.350[V_p + 1.651V_{sh}]^{0.390}. \quad (4.13)$$

4.3 Field Examples

To demonstrate the applicability of the new bulk density prediction models, two wells from the tertiary deltaic system in the Niger Delta basin are considered as the case studies. The Niger Delta is an extensional rift basin system that consists of clastic sediments up to 12 km in thickness and covers an area of about 75,000 km² (Doust and Omatsola, 1990; Evamy et al., 1978). The Tertiary Niger Delta consists of three types of formations that represent the prograding depositional facies of sands and shales. These formations in descending order are: Benin formation, Agbada formation and Akata formation (Short and Stauble, 1967; Ejedawe et al., 1984; Avbovbo, 1978; Matava et al., 2003; Adewole et al., 2016). The Benin formation consists mainly of continental loose sands. The Agbada formation consists of alternating sands and shales. The hydrocarbon accumulations of the Niger Delta basin are generally confined to various levels of the Agbada formation (Ejedawe, 1981). The Akata formation at the base of the delta consists of thick marine shales (potential source rock), turbidite sand (potential reservoirs in deep water environments), and minor amounts of clay and silt (Abbey et al., 2018).

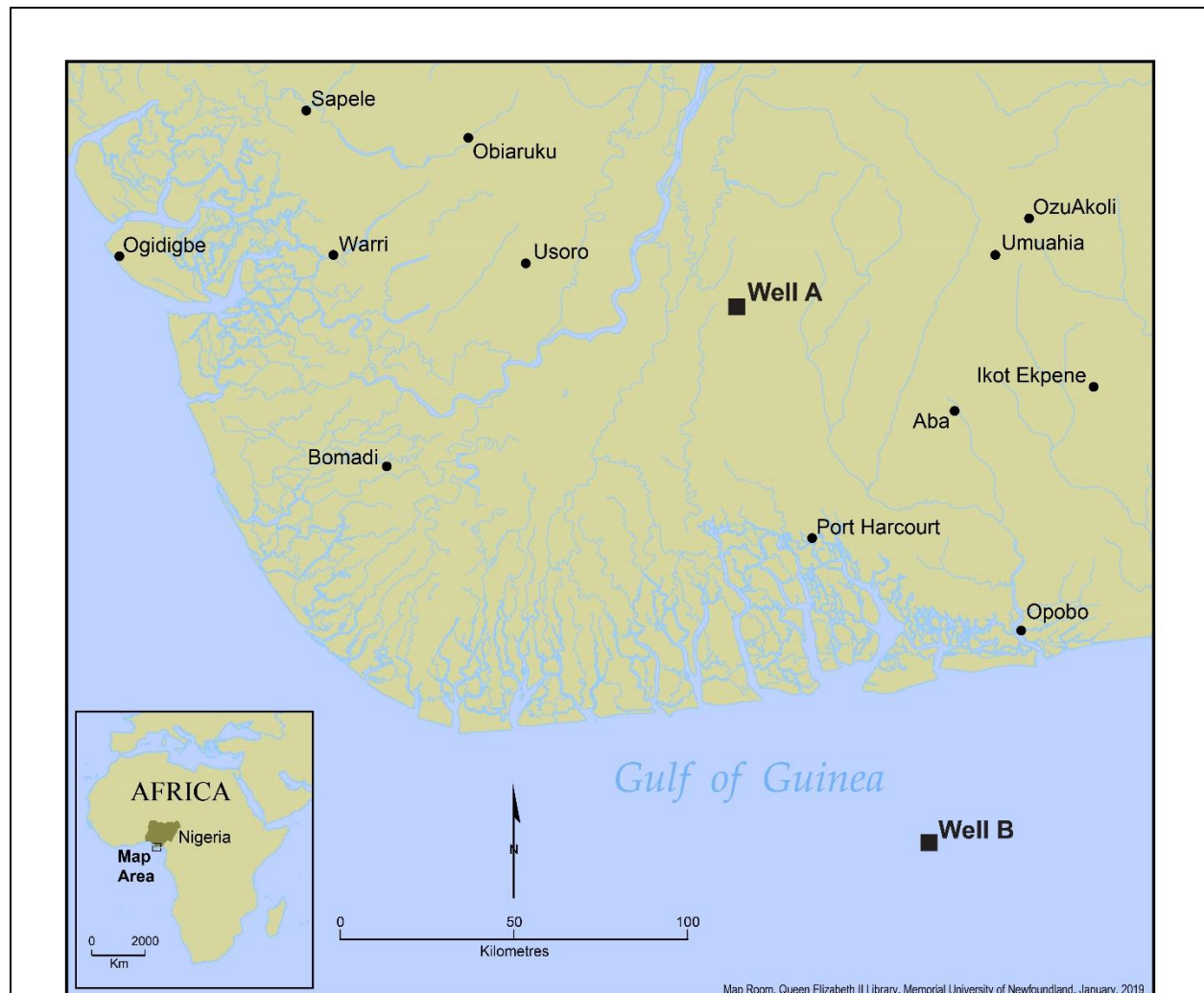


Figure 4. 1 The location map for Wells A and B.

The primary trapping mechanisms in the basin are growth faults associated with rollover structures (Daukoru, 1975; Weber, 1987). At depth shallower than 12,000 ft, the Niger Delta sands have good porosity and permeability (porosity in excess of 20% and permeability in the darcy range). The detailed geology and hydrocarbon system of the Tertiary Niger Delta is presented by Evamy et al. (1978). Figure 4.1 shows the location map of the two wells. Well A is an onshore appraisal well located about 71 km northwest of Port Harcourt. Well B is a shallow offshore exploratory well located about 94 km southeast of Port Harcourt in 215 ft water depth.

Wells A and B only penetrated the Benin and Agbada formations. In this paper, all depths are referenced to true vertical depth below the mean sea level.

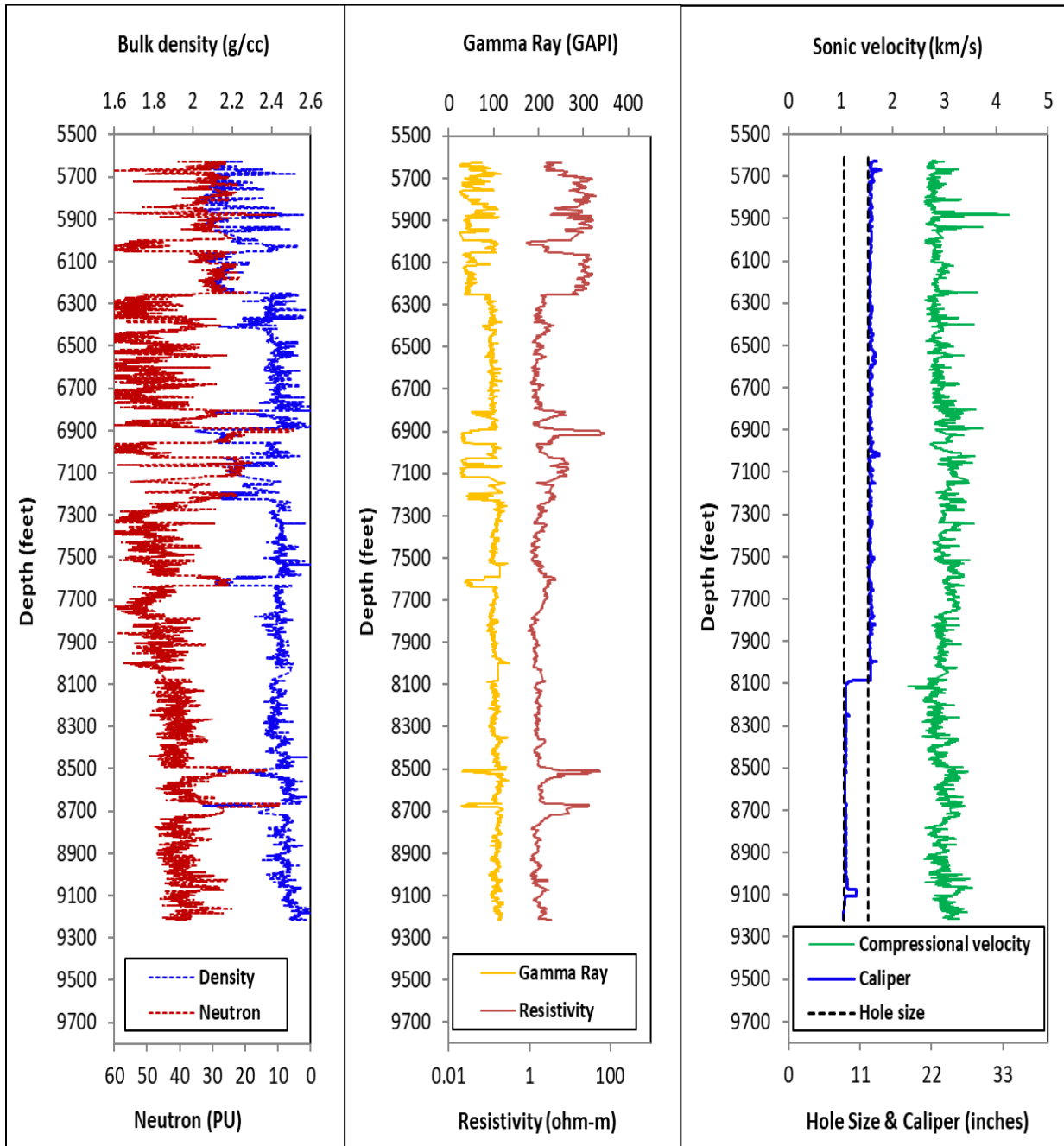


Figure 4. 2 The well logs for Well A showing the petrophysical properties of penetrated rocks.

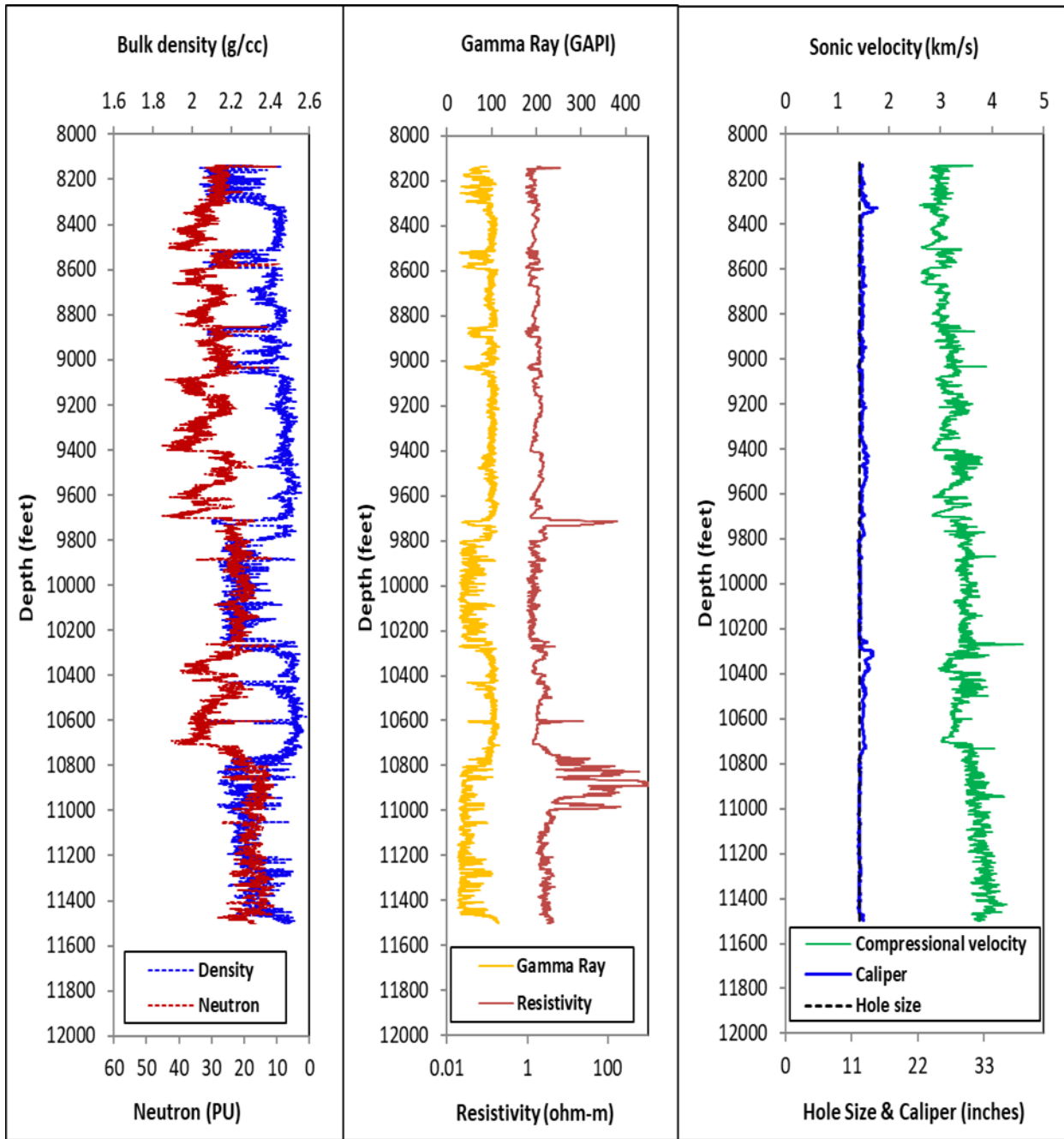


Figure 4. 3 The well logs for Well B showing the petrophysical properties of penetrated rocks.

Figures 4.2 and 4.3 display the wireline log data acquired in the two wells. The measured data include gamma ray, compressional wave velocity, formation bulk density, caliper, neutron porosity, and deep resistivity. Although all the necessary environmental corrections (borehole

size, tool stand-off, mud cake thickness, mud type, mud weight, borehole salinity, pressure, temperature, etc.) have been applied to the log data, the inclusion of the caliper logs will help to identify the likely regions of poor borehole conditions which may result in poor data acquisition. The caliper logs indicate that data acquisitions were carried out in good borehole conditions. Further quality checks on the log data were performed using the compression velocity of seawater (1.61 km/s), compressional velocity of sandstone matrix (5.49 km/s) and shale matrix density in the Niger Delta (2.68 g/cc). The well log data cover a wide range of lithologies (clean sands, clean shales, and a mixture of sands and shales) in siliciclastic environments.

4.4 Results and discussions

Figures 4.4 and 4.5 show the comparison of predicted and measured formation bulk density for the two wells under consideration. The formation bulk density values are computed using equation 4.12 (new model I), equation 4.13 (new model II), equation 4.2 (Gardner's model) and equation 4.5 (Brocher's model). Since Gardner's and Brocher's models are the most widely used empirical relationships developed for a wide range of lithologies, formation bulk density values are also computed using these models for comparison purposes. For tertiary clastic sediments in the Niger Delta basin, field observations have shown that shale volume (V_{sh}) is linearly related to gamma ray index (I_{GR}). Hence, shale volume (in fraction) is computed using equation 4.14:

$$V_{sh} = I_{GR} = \frac{GR_{log} - GR_{min}}{GR_{max} - GR_{min}}, \quad (4.14)$$

where GR_{log} is the gamma ray reading at any given depth; GR_{min} is the sand line gamma ray reading; GR_{max} is the shale line gamma ray reading. However, there are other non-linear

empirical responses between shale volume and gamma ray index depending on the geographic area or formation age (Larionov, 1969; Stieber, 1970; Clavier et al., 1971; Assaad, 2008).

Figures 4.4 and 4.5 clearly highlight the limitations in applying any empirical relationship that is based solely on compressional wave velocity to estimate the formation bulk density. For both wells, the newly developed models (model I and model II) provide accurate estimates of formation bulk density across various stratigraphic units. Reasonable estimates are obtained in clean sands, clean shales, and formations that contain a mixture of sands and shales in any proportion. The addition of the shale volume factor normalizes the new models for lithology effects. Unlike the new models, Gardner's and Brocher's models fail to provide good estimates across all the stratigraphic units. Gardner's model slightly overestimates formation bulk density in clean sands and underestimates formation bulk density in clean shales. Gardner's model provides formation bulk density estimates that fall between the clean sands and clean shales. Gardner's model slightly overestimates bulk density in clean sands because the relationship is basically an average of the fits for sandstones, shales, and carbonates. It also underestimates formation bulk density in clean shales due to lack of shaliness term in the model. While the Brocher's model provides reasonable estimates in clean sand intervals, it underestimates formation bulk density in intervals that contain clean shales due to lack of shaliness term in the model. In clean sands, the accuracy of Brocher's model is higher than that of Gardner's, while in clean shales, the opposite is the case. When applied over a lithological column that consists of several stratigraphic units in siliciclastic environments, any empirical relationship that expresses formation bulk density as a function of only compressional velocity will most likely produce inaccurate estimates in some intervals.

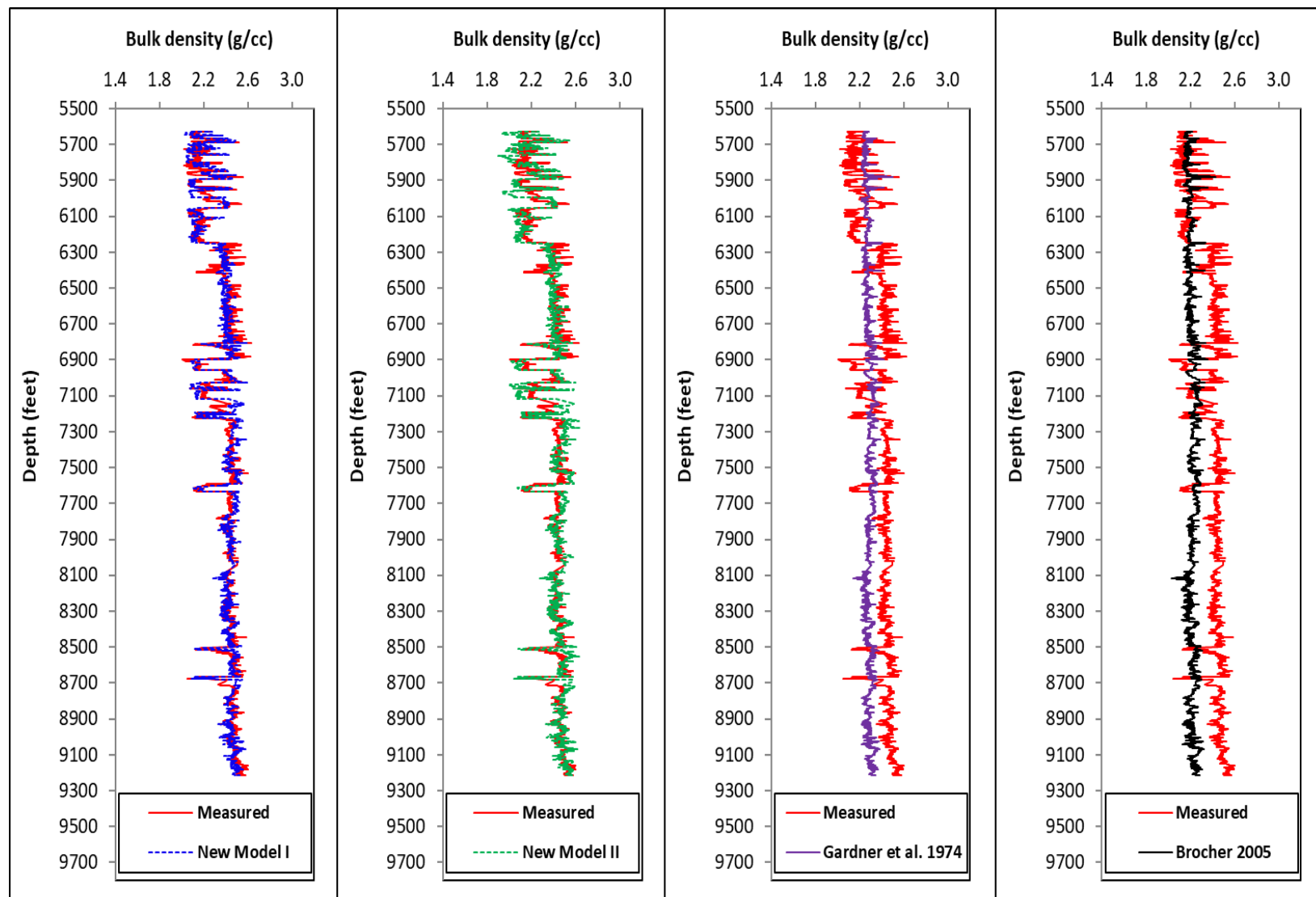


Figure 4.4 The comparison of predicted and measured formation bulk density for various models under consideration (Well A).

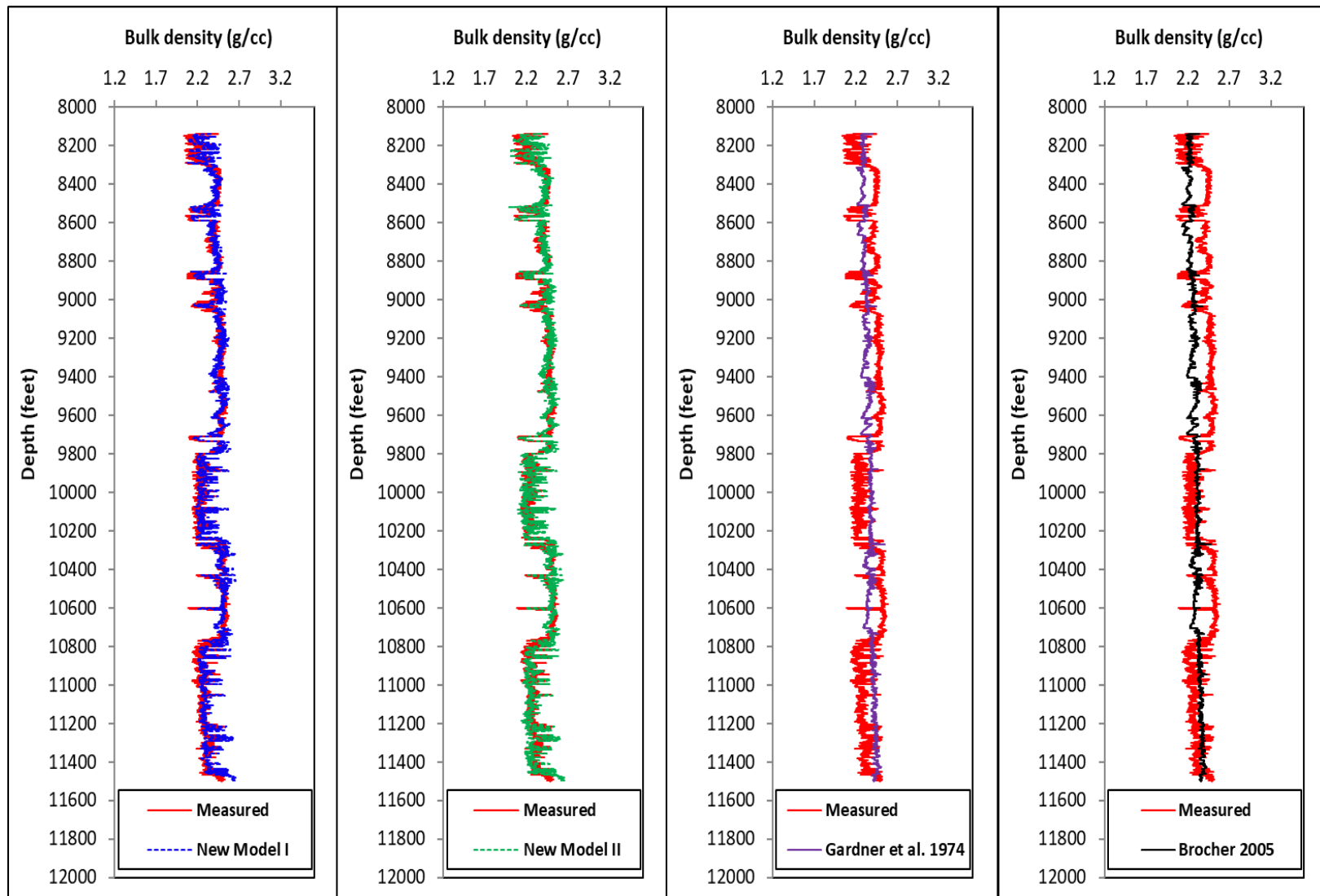


Figure 4. 5 The comparison of predicted and measured formation bulk density for various models under consideration (Well B).

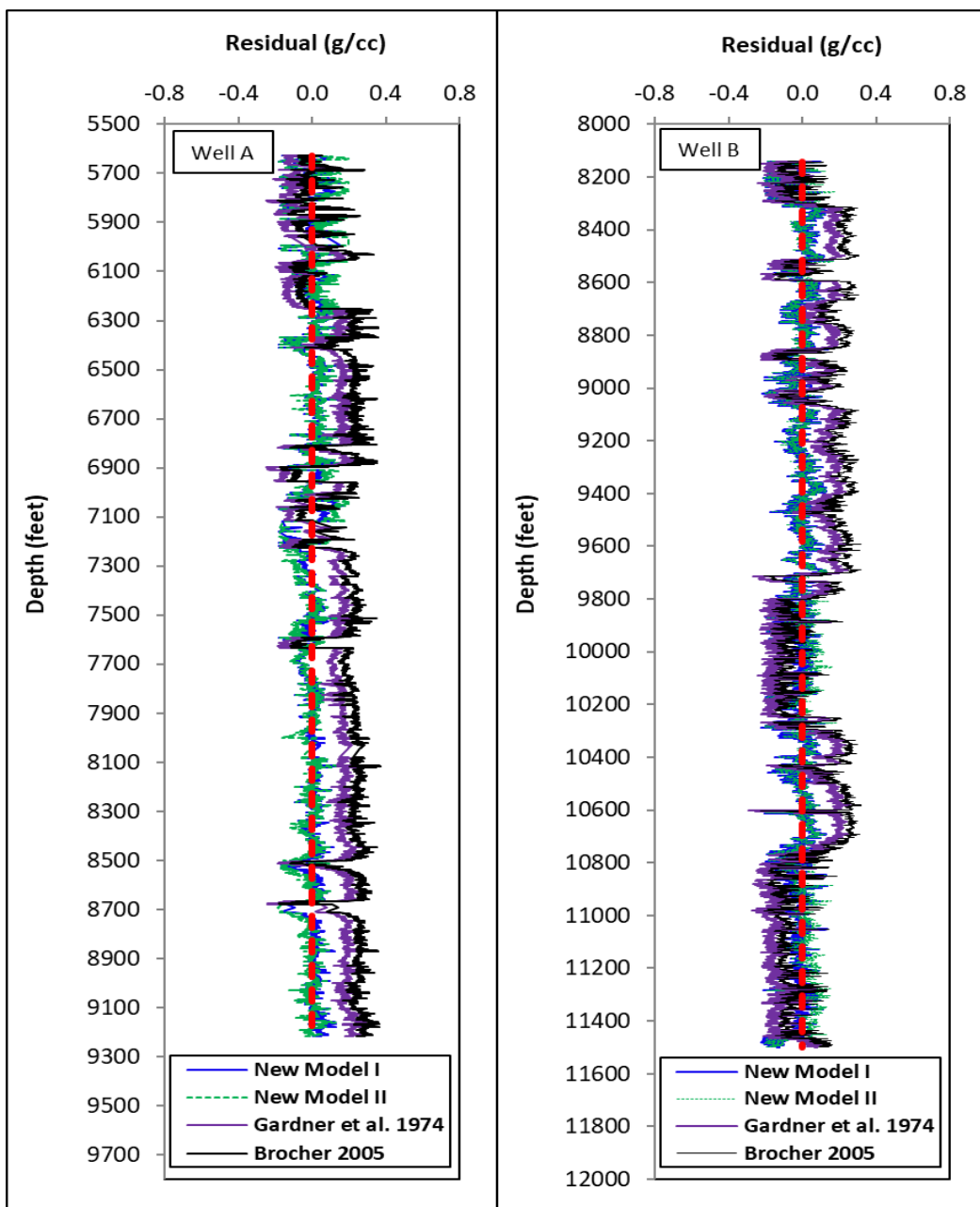


Figure 4.6 The residual-depth plots for Wells A and B showing the error profiles.

In order to compare the accuracy of various methods under consideration, the residual-depth plots are shown in Figure 4.6. The residual value is computed from the difference between measured and predicted value. For all lithologies, the values of residual obtained from the new

models stay close to zero (dotted red line). However, the Gardner's and Brocher's models produce larger residual values especially in clean shale formations. To properly show the error distributions associated with various estimation techniques, the histograms of the residuals are displayed in Figures 4.7 and 4.8. The histograms show that the new models produce lower maximum deviations and better error distributions than the Gardner's and Brocher's models. In Well A, over 92% of the data points fall between the residual range of -0.1g/cc and +0.1g/cc using the new models, whereas less than 22% of the data points fall between the same residual range when Gardner's and Brocher's models are used. In Well B, over 95% of the data points fall between the residual range of -0.1g/cc and +0.1g/cc using the new models, whereas less than 45% of the data points fall between the same residual range when Gardner's and Brocher's models are used.

Table 4. 1 The comparison of RMSEs for models under consideration

Model	Well A	Well B
New model I	5%	6%
New model II	6%	6%
Gardner et al. 1974	16%	15%
Brocher 2005	21%	17%

Table 4.1 shows the comparison of root mean square errors (RMSE) obtained from various models. The new models produce lower RMSE than the most widely used empirical relationships. The statistical analysis clearly shows that the performance of the new models is superior to Gardner's and Brocher's models. The addition of shale volume improves the accuracy of the prediction.

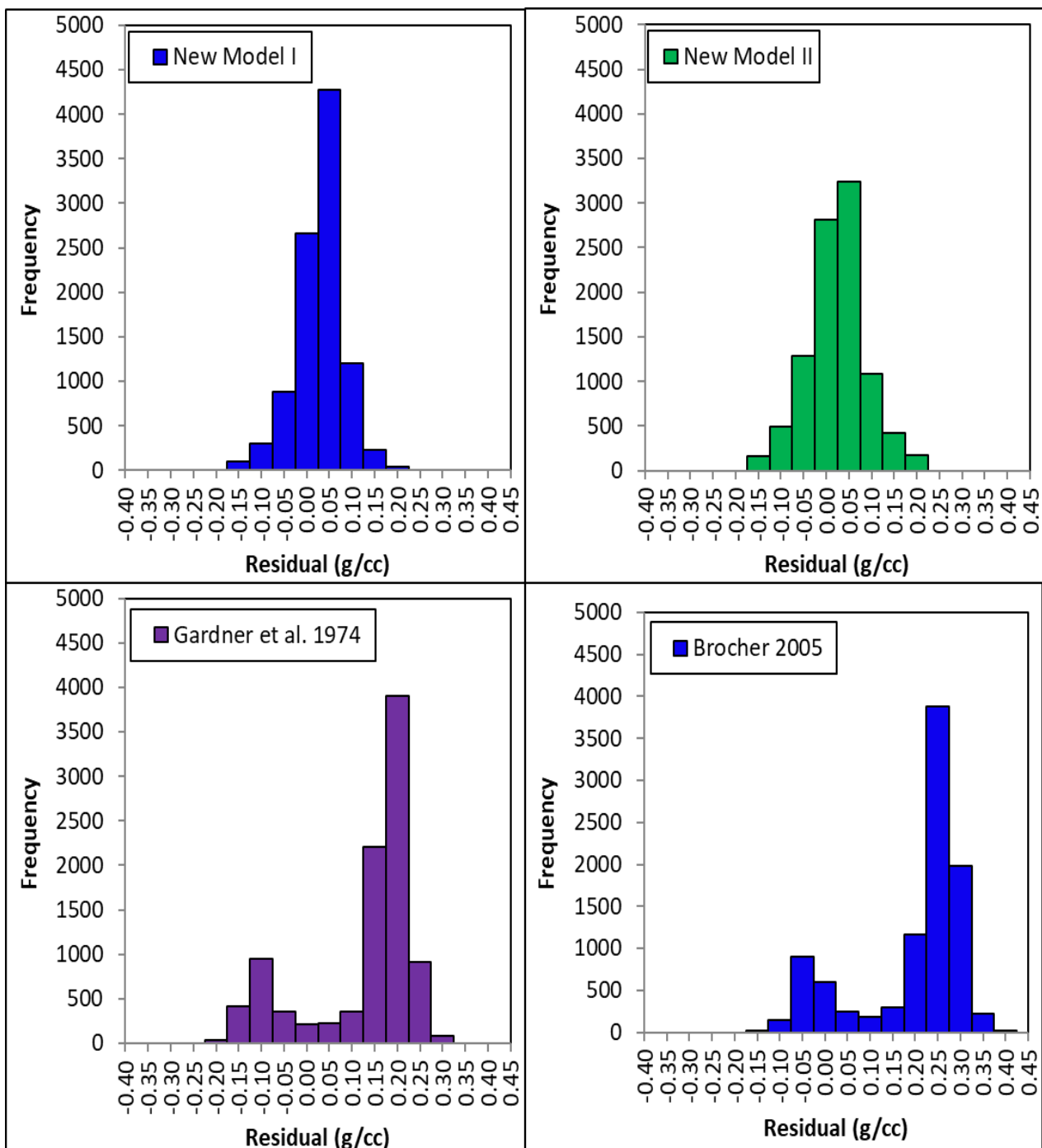


Figure 4. 7 The histograms of the residuals showing the error distributions for various models under consideration (Well A).

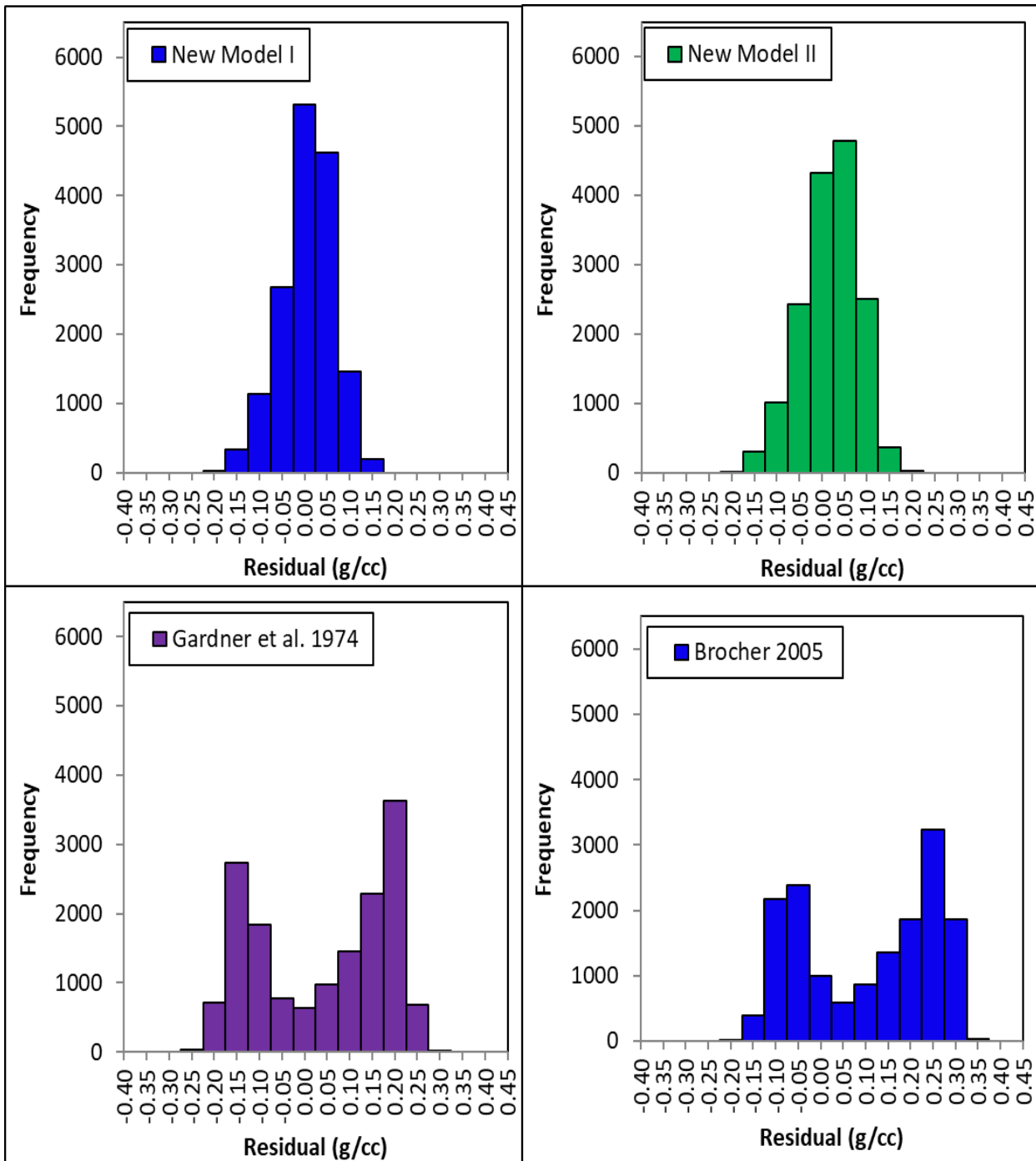


Figure 4. 8 The histograms of the residuals showing the error distributions for various models under consideration (Well B).

If density logs are not available, one has to use synthetically derived formation bulk densities for overburden pressure computation (Kenda et al., 1999; Aminzadeh et al., 2002). Since the

magnitude of overburden pressure is obtained by integrating the formation bulk density values from surface to the depth of interest along the well path (Christman, 1973; Zoback et al., 2003; Aadnoy, 2010; Oloruntobi et al., 2018; Oloruntobi and Butt, 2019), care should be taken in using any model that estimates formation bulk density based solely on compressional wave velocity for overburden pressure computation in areas where the density logs are not available. The knowledge of the overburden pressure is very critical to effective well design. Inaccurate prediction of overburden pressure may result in erroneous prediction of pore pressure, fracture pressure and vertical stress. This in turn can lead to well control, lost circulation and wellbore stability incidents during actual drilling operations especially in very deep wells. To demonstrate the effect of various estimation techniques on overburden gradient computation, Well A is considered as the case study. To estimate the overburden gradient for Well A, a reasonable assumption needs to be made about the average formation bulk density value from surface to the depth where the well log data start (5,627 ft). Based on the overburden gradient curve provided by Oloruntobi et al. (2018) for the onshore region of the Niger Delta, an average sediment bulk density value of 2.08 g/cc is assumed between the ground level and the start of well log data. The overburden pressure (S_v) is computed using:

$$S_v = 0.433 \int_0^Z \rho_b dz, \quad (4.15)$$

where ρ_b is the formation bulk density as a function of depth (g/cc); Z is the depth of interest (ft). The overburden gradient at the depth of interest is obtained by dividing the overburden pressure at any given depth by the true vertical depth. Figures 4.9 and 4.10 compare predicted and measured overburden gradient profiles for the well under consideration along with gamma ray logs. The plots clearly show the limitation of using Gardner's and Brocher's models to

compute formation bulk density values for overburden gradient prediction. While the outputs from the new models provide good estimates of overburden gradient across the entire intervals, the outputs from the Gardner's and Brocher's models underpredict the overburden gradient at the well total depth.

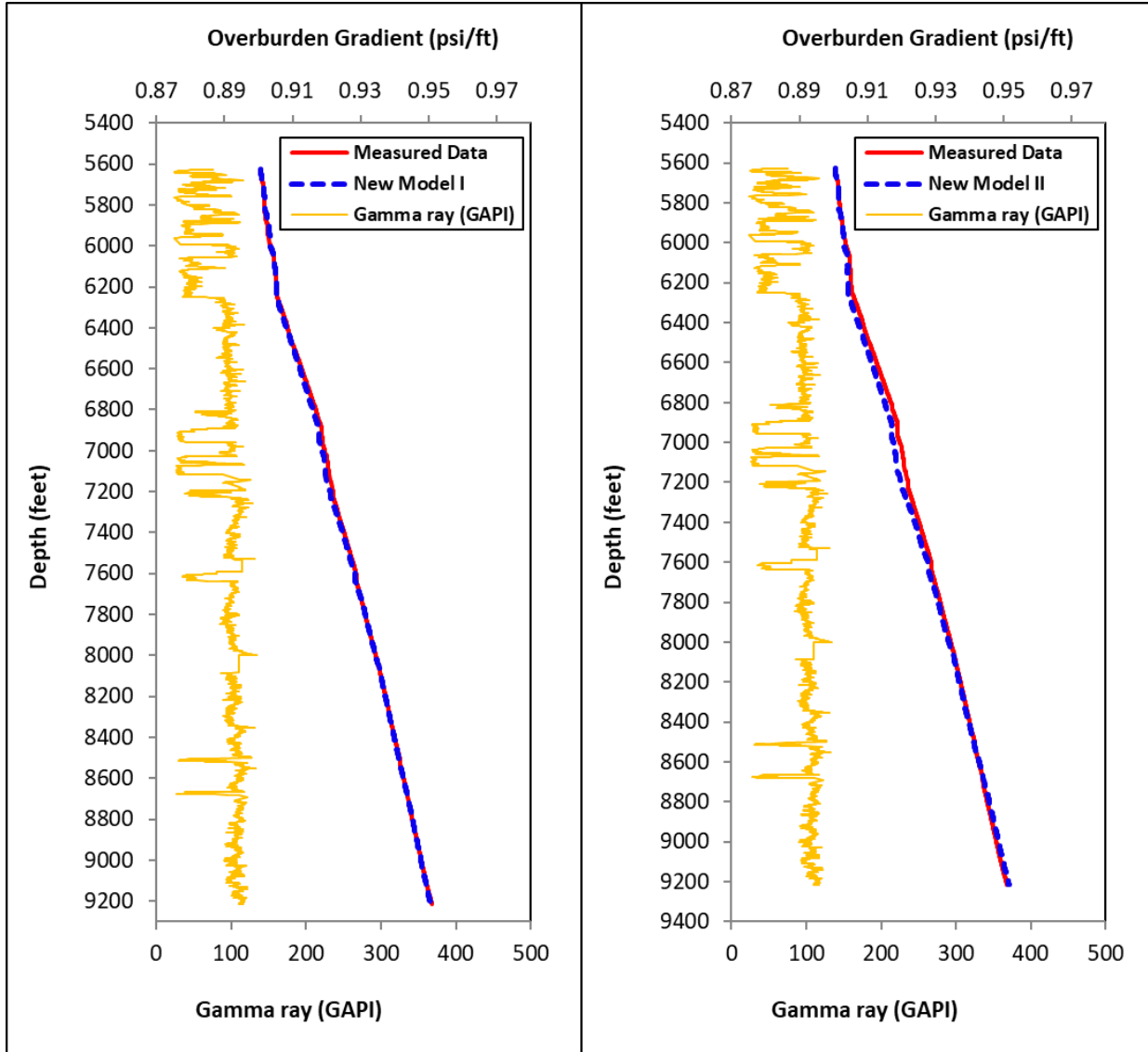


Figure 4. 9 The overburden gradient profiles using formation bulk density outputs from the new models for Well A.

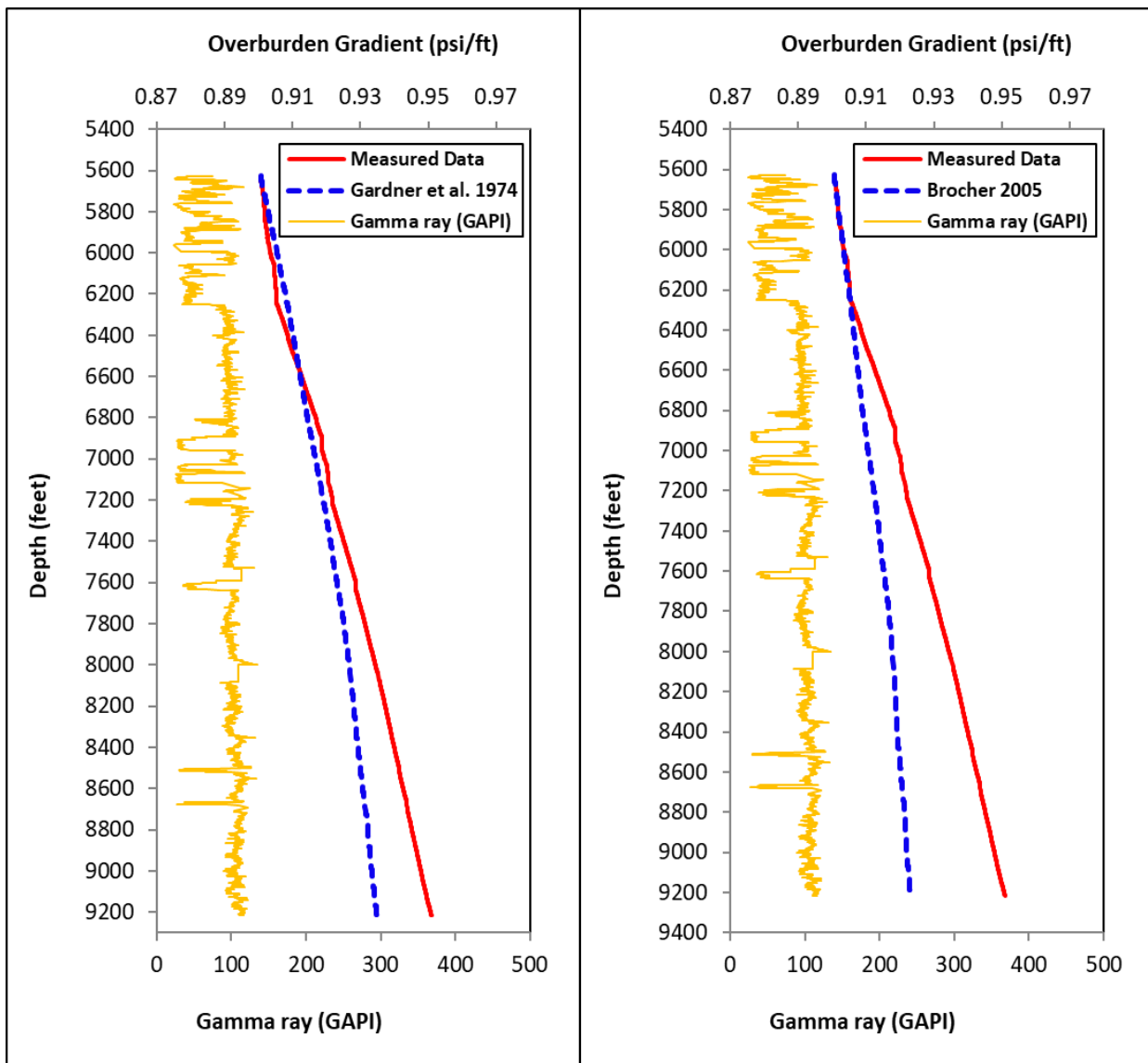


Figure 4. 10 The overburden gradient profiles using formation bulk density outputs from the Gardner's and Brocher's models for Well A.

Between 6,627ft and 6,250ft, the outputs from Brocher's model provide accurate estimates of overburden gradient because the lithologies in these intervals are mostly sands. Below 6,250ft where most lithologies are shales, the outputs from Brocher's model grossly underestimate the overburden gradient. Between 6,627ft and 7,260ft, the outputs from Gardner's model provide reasonable estimates of overburden gradient because the amount of overprediction in sand

intervals negates the amount of underprediction in shale intervals. Below 7,260ft, the outputs from Gardner's model underpredict the overburden gradient because there are no enough sand intervals to negate the massive shale intervals. The accuracy of Gardner's model to estimate formation bulk density for overburden gradient prediction will depend on the shale-to-sand ratio. Outputs from Gardner's model will underpredict the overburden gradient in sedimentary basins that have a very high shale-to-sand ratio. For depositional environments with very low shale-to-sand ratio, outputs from Gardner's model will overpredict the overburden gradient.

4.5 Conclusions

Core samples and well logs from different basins (Gulf of Mexico and Niger Delta) have been used to develop and validate the new formation bulk density prediction models. The new models incorporate the shale volume term, making it suitable for clean and non-clean formations. The application of the new models clearly demonstrates that the existing empirical relationships are simply inadequate for accurate prediction of formation bulk density over a lithological column that consists of several stratigraphic units. For petrophysical evaluations, both Gardner's and Brocher's models are not suitable for formation bulk density prediction. Application of Brocher's model should be limited only to clean sand intervals. Gardner's model provides formation bulk density estimates that fall between the clean sands and clean shales. The outputs from Brocher's model should not be used for overburden gradient computation except the entire lithological column is sand. The outputs from Gardner's model should not be used for overburden gradient computation in sedimentary basins where shale-to-sand ratio is very high or very low. However, the outputs from Gardner's model will provide reasonable estimates of

overburden gradient in sedimentary basins where shale-to-sand ratio approaches unity because the amount of overprediction in sands may negate the amount of underprediction in shales.

Just like all the existing empirical relationships, the new models may not be applicable to gas-filled formations or rocks that contain microcracks/fractures. In consolidated formations that contain microcracks, changes in effective stress will cause substantial changes in compressional wave velocity with little or no changes in formation bulk density until all the microcracks are closed. To be applicable to gas-filled rocks, the generalized forms of the new models are calibrated to any known gas intervals in the regional/field. Although the new models should be applicable to siliciclastic rocks in most sedimentary basins, it will be prudent to calibrate the generalized forms of these models (modified Birch's – equation 4.10 and modified Gardner's – equation 4.11) to regional/field data. In general, a close agreement exists between the predicted and measured formation bulk density using the new models. When compared to the most widely used empirical relationships, the new models produce lower RMSEs, lower residuals, and better error distributions.

The new models are developed primarily for liquid-saturated siliciclastic rocks which include sandstones, siltstones, shales and formations that contain a mixture of sands and shales in any proportion. The models do not cover carbonate and evaporite environments. However, the generalized forms of the new models can be calibrated to carbonate and evaporite rocks to obtain the new set of models for these environments.

4.6 Reference

Aadnoy, B.S., 2010. Introduction to Geomechanics in Drilling. Mitchell, Robert F Miska, Stefan Z. Fundam. Drill. Eng. Soc. Pet. Eng. 57.

Abbey, C.P., Okpogo, E.U., Atueyi, I.O., 2018. Application of rock physics parameters for

- lithology and fluid prediction of ‘TN’ field of Niger Delta basin, Nigeria. *Egypt. J. Pet.*
- Adewole, E.O., Macdonald, D.I.M., Healy, D., 2016. Estimating density and vertical stress magnitudes using hydrocarbon exploration data in the onshore Northern Niger Delta Basin, Nigeria: Implication for overpressure prediction. *J. African Earth Sci.* 123, 294–308. <https://doi.org/10.1016/j.jafrearsci.2016.07.009>
- Akhter, G., Khan, Y., Bangash, A.A., Shahzad, F., Hussain, Y., 2018. Petrophysical relationship for density prediction using V_p & V_s in Meyal oilfield, Potwar sub-basin, Pakistan. *Geod. Geodyn.* 9, 151–155.
- Ameen, M.S., Smart, B.G.D., Somerville, J.M., Hammilton, S., Naji, N.A., 2009. Predicting rock mechanical properties of carbonates from wireline logs (A case study: Arab-D reservoir, Ghawar field, Saudi Arabia). *Mar. Pet. Geol.* 26, 430–444.
- Aminzadeh, F., Chilingar, G. V, Robertson Jr, J.O., 2002. Seismic methods of pressure prediction, in: *Developments in Petroleum Science*. Elsevier, pp. 169–190.
- Anderson, D.L., 1967. A seismic equation of state. *Geophys. J. Int.* 13, 9–30.
- Assaad, F.A., 2008. Field methods for petroleum geologists: A guide to computerized lithostratigraphic correlation charts case study: Northern Africa. Springer Science & Business Media.
- Avbovbo, A.A., 1978. Tertiary lithostratigraphy of the Niger Delta. *Am. Assoc. Pet. Geol. Bull.* 62, 295–306.
- Birch, F., 1961. The velocity of compressional waves in rocks to 10 kilobars: 2. *J. Geophys. Res.* 66, 2199–2224.
- Bowers, G.L., 2001. Determining an appropriate pore-pressure estimation strategy, in: Offshore Technology Conference. Offshore Technology Conference.
- Brocher, T.M., 2008. Key elements of regional seismic velocity models for long period ground motion simulations. *J. Seismol.* 12, 217–221.
- Brocher, T.M., 2005. Empirical Relations between Elastic Wavespeeds and Density in the Earth’s Crust. *Bull. Seismol. Soc. Am.* 95, 2081–2092. <https://doi.org/10.1785/0120050077>
- Burrus, J., 1998. Memoir 70, Chapter 3: Overpressure models for clastic rocks, their relation to hydrocarbon.
- Carroll, R.D., 1969. The determination of the acoustic parameters of volcanic rocks from compressional velocity measurements, in: *International Journal of Rock Mechanics and*

- Mining Sciences & Geomechanics Abstracts. Elsevier, pp. 557–579.
- Castagna, J.P., Backus, M.M., 1993. Offset-dependent reflectivity—Theory and practice of AVO analysis. Society of Exploration Geophysicists.
- Castagna, J.P., Batzle, M.L., Eastwood, R.L., 1985. Relationships between compressional-wave and shear-wave velocities in clastic silicate rocks. *Geophysics* 50, 571–581.
- Chang, C., Zoback, M.D., Khaksar, A., 2006. Empirical relations between rock strength and physical properties in sedimentary rocks. *J. Pet. Sci. Eng.* 51, 223–237.
- Christensen, N.I., Mooney, W.D., 1995. Seismic velocity structure and composition of the continental crust: A global view. *J. Geophys. Res. Solid Earth* 100, 9761–9788.
- Christman, S.A., 1973. Offshore Fracture Gradients. *J. Pet. Technol.* 25, 910–914.
- Clavier, C., Hoyle, W., Meunier, D., 1971. Quantitative interpretation of thermal neutron decay time logs: part I. Fundamentals and techniques. *J. Pet. Technol.* 23, 743–755.
- Coates, G.R., Denoo, S.A., 1980. Log derived mechanical properties and rock stress, in: SPWLA 21st Annual Logging Symposium. Society of Petrophysicists and Well-Log Analysts.
- Daukoru, J.W., 1975. PD 4(1) Petroleum Geology of the Niger Delta. World Pet. Congr.
- Dey, A.K., Stewart, R.R., 1997. Predicting density using Vs and Gardner's relationship. CREWES Res. Rep. 9.
- Doust, H., Omatsola, E., 1990. Niger Delta, in: Divergent / Passive Margin Basins. pp. 201–238.
- Ejedawe, J.E., 1981. Patterns of incidence of oil reserves in Niger Delta Basin. Am. Assoc. Pet. Geol. Bull. 65, 1574–1585.
- Ejedawe, J.E., Coker, S.J.L., Lambert-Aikhionbare, D.O., Alofe, K.B., Adoh, F.O., 1984. Evolution of oil-generative window and oil and gas occurrence in Tertiary Niger Delta Basin. Am. Assoc. Pet. Geol. Bull. 68, 1744–1751.
- Evamy, B.D., Haremboure, J., Kamerling, P., Knaap, W.A., Molloy, F.A., Rowlands, P.H., 1978. Hydrocarbon habitat of Tertiary Niger delta. Am. Assoc. Pet. Geol. Bull. 62, 1–39.
- Feng, C., Wang, Z., Deng, X., Fu, J., Shi, Y., Zhang, H., Mao, Z., 2019. A new empirical method based on piecewise linear model to predict static Poisson's ratio via well logs. *J. Pet. Sci. Eng.* 175, 1–8.
- Fjar, E., Holt, R.M., Raaen, A.M., Risnes, R., Horsrud, P., 2008. Petroleum related rock mechanics. Elsevier.
- Gardner, G.H., Gardner, L., Gregory, A., 1974. Formation Velocity and Density - The

- Diagnostic Basic for Stratigraphic Traps. *Geophysics* 39, 770–780.
- Han, D., Nur, A., Morgan, D., 1986. Effects of porosity and clay content on wave velocities in sandstones. *Geophysics* 51, 2093–2107. <https://doi.org/10.1190/1.1442062>
- Hoesni, M.J., 2004. Origins of overpressure in the Malay Basin and its influence on petroleum systems. (Doctoral Diss. Durham Univ.
- Kenda, W.P., Hobart, S., Doyle, E.F., 1999. Real-time geo-pressure analysis reduces drilling costs. *Oil Gas J.* 97, 52–59.
- Khair, E.M.M., Zhang, S., Abdelrahman, I.M., 2015. Correlation of Rock Mechanic Properties with Wireline Log Porosities through Fulla Oilfield - Muglad Basin -Sudan. SPE North Africa Tech. Conf. Exhib. <https://doi.org/10.2118/175823-MS>
- Khandelwal, M., 2013. Correlating P-wave velocity with the physico-mechanical properties of different rocks. *Pure Appl. Geophys.* 170, 507–514.
- Kowallis, B.J., Jones, L.E.A., Wang, H.F., 1984. Velocity-porosity-clay content systematics of poorly consolidated sandstones. *J. Geophys. Res. Solid Earth* 89, 10355–10364.
- Larionov, V. V, 1969. Radiometry of boreholes. Nedra, Moscow 127.
- Lindseth, R.O., 1979. Synthetic sonic logs—A process for stratigraphic interpretation. *Geophysics* 44, 3–26.
- Lobkovsky, L.I., Ismail-Zadeh, A.T., Krasovsky, S.S., Kuprienko, P.Y., Cloetingh, S., 1996. Gravity anomalies and possible formation mechanism of the Dnieper-Donets Basin. *Tectonophysics* 268, 281–292.
- Ludwig, W., Nafe, J., Drake, C., 1970. No Title. *Seism. Refract. Sea, A. E. Maxwell Vol. 4*, 53–84.
- Matava, T., Rooney, M.A., Chung, H.M., Nwankwo, B.C., Unomah, G.I., 2003. Migration effects on the composition of hydrocarbon accumulations in the OML 67–70 areas of the Niger Delta. *Am. Assoc. Pet. Geol. Bull.* 87, 1193–1206.
- Miller, S.L.M., Stewart, R.R., 1991. The relationship between elastic-wave velocities and density in sedimentary rocks: A proposal. *Crewes Res. Rep.* 260–273.
- Najibi, A.R., Ghafoori, M., Lashkaripour, G.R., Asef, M.R., 2015. Empirical relations between strength and static and dynamic elastic properties of Asmari and Sarvak limestones, two main oil reservoirs in Iran. *J. Pet. Sci. Eng.* 126, 78–82.
- Nwozor, K.K., Onuorah, L.O., Onyekuru, S.O., Egwuachukwu, C.J., 2017. Calibration of Gardner

- coefficient for density–velocity relationships of tertiary sediments in Niger Delta Basin. *J. Pet. Explor. Prod. Technol.* 7, 627–635.
- Ohen, H.A., 2003. Calibrated Wireline Mechanical Rock Properties Model for Predicting and Preventing Wellbore Collapse and Sanding., in: SPE European Formation Damage Conference. Society of Petroleum Engineers.
- Ojha, M., Sain, K., 2014. Velocity-porosity and velocity-density relationship for shallow sediments in the Kerala-Konkan basin of western Indian margin. *J. Geol. Soc. India* 84, 187–191.
- Oloruntobi, O., Adedigba, S., Khan, F., Chunduru, R., Butt, S., 2018. Overpressure prediction using the hydro-rotary specific energy concept. *J. Nat. Gas Sci. Eng.* 55, 243–253.
- Oloruntobi, O., Butt, S., 2019. Energy-based formation pressure prediction. *J. Pet. Sci. Eng.* 173, 955–964
- Onalo, D., Oloruntobi, O., Adedigba, S., Khan, F., James, L., Butt, S., 2018. Static Young's modulus model prediction for formation evaluation. *J. Pet. Sci. Eng.* 171, 394–402.
- Onyia, E.C., 1988. Relationships between formation strength, drilling strength, and electric log properties, in: SPE Annual Technical Conference and Exhibition. Society of Petroleum Engineers.
- Potter, C.C., 1999. Relating density and elastic velocities in clastics: an observation. *CREWES* 1999 Res. Rep. 11.
- Potter, C.C., Foltinek, D.S., 1997. Formation elastic parameters by deriving S-wave velocity logs. *Consort. Res. Elastic Wave Explor. Seismol. Res. Rep.* 9, 1–13.
- Potter, C.C., Stewart, R.R., 1998. Density predictions using V_p and V_s sonic logs. *CREWES* Res 10, 1–10.
- Quijada, M.F., Stewart, R.R., 2007. Density estimations using density-velocity relations and seismic inversion. *CREWES Res Rep* 19, 1–20.
- Satti, I.A., Ghosh, D., Yusoff, W.I.W., Hoesni, M.J., 2015. Origin of Overpressure in a Field in the Southwestern Malay Basin. *SPE Drill. Complet.* 30, 198.
- Short, K., Stauble, A., 1967. Outline of Geology of Niger Delta. *Am. Assoc. Pet. Geol. Bull.* 51, 761–779.
- Stieber, S.J., 1970. Pulsed neutron capture log evaluation-louisiana gulf coast, in: Fall Meeting of the Society of Petroleum Engineers of AIME. Society of Petroleum Engineers.

- Swarbrick, R.E., 2001. Pore-Pressure Prediction: Pitfalls in Using Porosity, in: Offshore Technology Conference. Offshore Technology Conference.
- Tixier, M.P., Loveless, G.W., Anderson, R.A., 1975. Estimation of Formation Strength From the Mechanical-Properties Log (includes associated paper 6400). *J. Pet. Technol.* 27, 283–293.
- Tosaya, C., Nur, A., 1982. Effects of diagenesis and clays on compressional velocities in rocks. *Geophys. Res. Lett.* 9, 5–8. <https://doi.org/10.1029/GL009i001p00005>
- Tosaya, C.A., 1982. Acoustical Properties of Clay-Bearing Rocks. PhD Thesis, Stanford Univ.
- Ursenbach, C.P., 2002a. Generalized Gardner relation for gas-saturated rocks. CREWES 2002 Res. Rep. 14, 1–6.
- Ursenbach, C.P., 2002b. Generalized Gardner Relations. 2002 SEG Annu. Meet.
- Ursenbach, C.P., 2001. A generalized Gardner relation. CREWES 2001 Res. Rep. 13, 77–82.
- Vernik, L., Nur, A., 1992. Petrophysical classification of siliciclastics for lithology and porosity prediction from seismic velocities (1). *Am. Assoc. Pet. Geol. Bull.* 76, 1295–1309.
- Wang, Z., 2001. Fundamentals of seismic rock physics. *Geophysics* 66, 398–412.
- Weber, K.J., 1987. Hydrocarbon distribution patterns in Nigerian growth fault structures controlled by structural style and stratigraphy. *J. Pet. Sci. Eng.* 1, 91–104.
- Xu, H., Zhou, W., Xie, R., Da, L., Xiao, C., Shan, Y., Zhang, H., 2016. Characterization of rock mechanical properties using lab tests and numerical interpretation model of well logs. *Math. Probl. Eng.* 2016.
- Zhang, J., 2013. Effective stress, porosity, velocity and abnormal pore pressure prediction accounting for compaction disequilibrium and unloading. *Mar. Pet. Geol.* 45, 2–11.
- Zhang, J., 2011. Pore pressure prediction from well logs: Methods, modifications, and new approaches. *Earth-Science Rev.* 108, 50–63. <https://doi.org/10.1016/j.earscirev.2011.06.001>
- Zoback, M.D., 2010. *Reservoir geomechanics*. Cambridge University Press.
- Zoback, M.D., Barton, C.A., Brady, M., Castillo, D.A., Finkbeiner, T., Grollimund, B.R., Moos, D.B., Peska, P., Ward, C.D., Wiprut, D.J., 2003. Determination of stress orientation and magnitude in deep wells. *Int. J. Rock Mech. Min. Sci.* 40, 1049–1076.

Chapter 5

5.0 A New Fracture Pressure Prediction Model for The Niger Delta Basin

Preface

A version of this chapter has been submitted to the Journal of Environmental Earth Sciences, 2019. I am the primary author. Co-author Omolola Falugba reviewed the manuscript and provided much-needed support in data acquisition. Co-author Oluchi Ekanem-Attah reviewed the manuscript and provided much-needed support in data acquisition. Co-author Chukwunweike Awa reviewed the manuscript and provided much-needed support in data acquisition. Co-author Dr. Stephen Butt reviewed the manuscript and assisted in the development of the concept. I developed the initial concept and carried out most of the data analysis. I prepared the first draft and subsequently revised the manuscript based on the feedback from the co-authors.

Abstract

Accurate knowledge of formation fracture pressure is very essential to optimizing well design at all stages of the field development. However, erroneous prediction of formation fracture pressure can lead to process safety incidents such as surface and underground blowouts. While fracture pressure prediction models have been developed for some sedimentary basins, it is difficult to transfer these models to areas beyond the regions of study. In the Niger Delta basin, few fracture pressure prediction models have been developed. However, these models were developed primarily from leak-off test data acquired from the normally pressured intervals. Basically, the existing Niger Delta fracture pressure prediction models lack the leak-off test measurements in

the overpressure intervals because such data are not available. In this paper, a new fracture pressure prediction model that can be applied to normally pressured intervals and overpressure zones is being proposed. Model development is based on establishing a relationship between fracture pressure, true vertical depth, and magnitude of overpressure using several leak-off test data acquired from over 100 wells in various fields scattered across the basin. Unlike the previous models, the newly developed model incorporates leak-off test measurements from the overpressure intervals in the basin. In general, the newly proposed model can be used with a high degree of confidence to predict the formation fracture pressure required for safe and economical well planning across the entire basin.

Keywords: Pore pressure, Fracture pressure, Normally pressured, Overpressure, Leak-off test.

5.1 Introduction

Fracture pressure is the pressure required to initiate a crack in a formation. The fracture pressure and pore pressure data are the most important input parameters required for well planning and design. The difference between formation fracture pressure and pore pressure (drilling window) will dictate the overall drilling and completion strategies for the field. Fracture pressure determinations are usually performed as part of pre-drill and wellsite tasks. Pre-drill fracture pressure predictions are very essential for well planning purposes at the “select” and “define” phases of a field development plan. Wellsite fracture pressure determinations are very important for operational decisions. The operational decisions at the wellsite following a formation integrity test (leak-off test, formation break-down test or limit test) may include: (1) performing squeeze cementing jobs; (2) optimizing the flow rate to minimize the annular pressure loss; (3)

reducing the rate of penetration (ROP) to minimize cuttings concentration in the annulus; (4) optimizing tripping in strategy to minimize surge pressure; (5) determining the maximum permissible drilling depth based on the amount of influx (kick tolerance) that can be taken in the open hole sections for a specific kick intensity and circulated out with a Driller's method of well control without fracturing the weakest formations. Decisions can also be made to apply wellbore strengthening/stress caging techniques following a formation integrity test at the wellsite (Alberty & McLean 2004; Aston et al. 2004; Song & Rojas 2006; Bybee 2008; Wang et al. 2009; Kumar et al. 2010; Contreras et al. 2014; Savari et al. 2014; Chellappah et al. 2015; Zhang et al. 2016; Feng & Gray 2017; Chellappah et al. 2018). From well engineering point of view, information about the formation fracture pressures can be used to: (1) determine the maximum allowable equivalent circulating density (ECD) required to drill a well; (2) establish the bottom-hole pressure required for squeeze jobs and hydraulic fracturing; (3) establish the injection pressure required for casing design and equipment selection; (4) select optimum mud properties and additives; and (5) determine the maximum allowable annular surface pressure (MAASP) required to prevent formation breakdown in the event of a kick; (6) establish the bottom-hole pressure required for cuttings reinjection (CRI). From an exploration standpoint, formation fracture pressure data are used for subsurface trap integrity analysis, prospect evaluation and hydrocarbon migration analysis. In intervals where formation pore pressures are greater than the fracture pressures, subsurface traps are likely to leak. Failure to accurately predict the formation fracture pressure can lead to lost circulation and well control incidents (surface and underground blowouts). In general, information about the magnitude of formation fracture pressure is very vital to achieving the overall well objective, especially when drilling into high pressured zones.

To geomechanics specialists, formation fracture pressure is referred to as the minimum principal stress. In well engineering community, formation fracture pressure is referred to as the bottom-hole leak-off pressure (LOP): the bottom-hole pressure at which drilling fluid starts to invade the formation and the relation between mud pressure and volume starts to deviate from linearity (Edwards et al., 1998; Altun et al., 2001; Couzens-Schultz and Chan, 2010). The leak-off test measurements can be conventional or dynamic. Conventional leak-off tests are usually conducted after drilling a few feet of the new formation below the casing shoe. Dynamic leak-off tests can be performed at any depth in the open hole by determining the equivalent circulating density (ECD) required to leak off drilling mud into the formation using the pressure while drilling (PWD) sensors. During the dynamic leak-off tests, bottom-hole pressure (BHP) can be increased either by increasing the flow rate to increase the annular pressure loss or by increasing the annular backpressure while drilling in managed pressure drilling (MPD) mode. However, the magnitude of the minimum principal stress (usually horizontal in the normal faulting regime) can only be determined from micro-fracturing/mini-fracturing/extended leak-off test/lost circulation incidents (Daneshy et al., 1986; De Bree and Walters, 1989; Kunze and Steiger, 1992; Thiercelin et al., 1996; Raaen et al., 2006; Li et al., 2009; Li et al., 2009; Wang et al., 2011; Chan et al., 2015; Feng and Gray, 2016). From field observations, comparison of LOT and hydraulic fracturing (micro-frac/mini-frac/extended leak-off test) data for non-fractured rocks have shown that vast majority of leak-off pressures exceed the minimum principal stresses by an average of 10 - 15%. In this paper, fracture pressure is referred to as the bottom-hole leak-off pressure (pressure at which the pressure versus volume curve starts to deviate from a straight line). The formation fracture pressure is dependent on several factors including formation type, rock strength, permeability, magnitude of the principal stresses, formation pore pressure, wellbore

inclination and azimuth, orientation of the plane of weakness and formation temperature. In most cases, fracture pressures in shale formations are generally higher than that of sand formations. Field experience has shown that increasing water depth reduces the overburden pressure (vertical stress) which can lead to a reduction in apparent fracture pressure (Christman, 1973). Although not in the same proportion, an increase in pore pressure will result in an increase in fracture pressure and a decrease in pore pressure will lead to a decrease in fracture pressure (Salz, 1977; Engelder and Fischer, 1994; Yassir et al., 1998). The magnitude of fracture pressure is affected by wellbore inclination and azimuth (Rai et al., 2014). Generally, fracture pressure reduces as wellbore inclination increases (Aadnoy and Chenevert, 1987). Heating a formation above its undisturbed value (bottom-hole static temperature) will result in higher formation fracture pressure and cooling a formation below its undisturbed temperature will cause a decrease in formation fracture pressure (Perkins & Gonzalez 1984; Gonzalez et al. 2004; Hettema et al. 2004; van Oort & Vargo 2008; Zoback, 2010). The effects of anisotropic elasticity parameters on formation fracture pressure are usually very small Aadnoy, (1988).

When drilling in areas where there are limited or no LOT data (especially rank wildcat) theoretical and empirical relationships have been developed to estimate the formation fracture pressure. Hubbert & Willis (1957) proposed an approximate expression for the minimum injection pressure required to extend a fracture under normal-faulting stress regime (equation 5.1):

$$IP_{min} = \frac{1}{3} [\sigma_v - PP] + PP, \quad (5.1)$$

where IP_{min} is the Minimum injection pressure (psi); σ_v is the vertical stress (psi); PP is the pore pressure (psi). By solving popular Kirch's equation for vertical well at the wellbore wall with no

consideration for temperature effect, Haimson & Fairhurst (1967) suggested that the wellbore pressure required to initiate a fracture in elastic rocks with smooth wellbore wall for non-penetrating wellbore fluid (impermeable case) is a function of the two horizontal principal stresses, the rock tensile strength and the formation pore pressure and it is given by:

$$FP = 3\sigma_h - \sigma_H - PP + T_o, \quad (5.2)$$

where FP is the fracture pressure (psi); σ_h is the minimum horizontal stress (psi); σ_H is the maximum horizontal stress (psi); PP is the pore pressure (psi); T_o is the tensile strength (psi). For porous and permeable rocks, Haimson & Fairhurst (1967) then introduced poroelastic constants into the formation breakdown pressure model to account for the wellbore fluid pressure penetration effect (equation 5.3):

$$FP = \left[\frac{3\sigma_h - \sigma_H + T_o}{2 - \alpha \left(\frac{1 - 2v}{1 - v} \right)} \right] - PP, \quad (5.3)$$

where FP is the fracture pressure (psi); σ_h is the minimum horizontal stress (psi); σ_H is the maximum horizontal stress (psi); PP is the pore pressure (psi); T_o is the tensile strength (psi); v is the Poisson's ratio; α is the Biot's coefficient. When a formation breaks down, the fractures created will propagate in the direction perpendicular to the least principal stress. While theoretical models are helpful, they are difficult to apply in the field (Taylor and Smith, 1970). Matthews and Kelly (1967) proposed a correlation that incorporated a depth-dependent matrix stress coefficient to estimate the fracture pressure of sedimentary formations (equation 5.4).

$$FP = K_i \left[\frac{\sigma_v - PP}{Z} \right] + \frac{PP}{Z}, \quad (5.4)$$

where FP is the fracture pressure (psi); σ_v is the vertical stress (psi); K_i is the matrix stress coefficient; PP is the pore pressure (psi); Z is the true vertical depth (ft). Pennebaker (1968) expressed formation fracture gradient as a function of overburden gradient, pore pressure gradient and effective stress ratio for formations in the US Gulf Coast (Equation 5.5):

$$G_{FP} = K_o [G_{OB} - G_{PP}] + G_{PP}, \quad (5.5)$$

where G_{FP} is the fracture pressure gradient (psi/ft); G_{OB} is the overburden gradient (psi/ft); G_{PP} is the pore pressure gradient (psi/ft); K_o is the effective stress ratio. While Pennebaker (1968) recognized the dependency of effective stress ratio on the elastic constant of the rock (Poisson's ratio), effective stress ratio was expressed as a function of depth. The value of effective stress ratio can also be obtained by calibrating equation 5.5 to actual fracture pressure and pore pressure measurements in the field/region. Eaton (1969) modified Hubbert and Willis's model by incorporating the Poisson's ratio. Eaton's model is given by:

$$G_{FP} = \frac{v}{1-v} [G_{OB} - G_{PP}] + G_{PP}, \quad (5.6)$$

where G_{FP} is the fracture pressure gradient (psi/ft); G_{OB} is the overburden gradient (psi/ft); G_{PP} is the pore pressure gradient (psi/ft); v is the Poisson's ratio. Although initially developed for the US Gulf Coast area, Eaton's model is the most widely used empirical correlation to estimate the formation pressure (Parriag, 1976). Eaton's model allows the effect of lithology to be considered on formation fracture pressure. The Poisson's Ratio is usually back-calculated from the fracture/LOT data from the offset wells. Anderson et al. (1973) expressed formation fracture pressure as a function of overburden pressure (vertical stress), pore pressure, Poisson's ratio and Biot's constant for US Gulf Coast sands (equation 5.7):

$$FP = \left[\frac{2v}{1-v} \right] [\sigma_v - \alpha PP] + \alpha PP, \quad (5.7)$$

where FP is the fracture pressure (psi); σ_v is the vertical stress (psi); PP is the pore pressure (psi); v is the Poisson's ratio; α is the Biot's coefficient. Salz (1977) proposed an exponential relationship between fracture propagation gradient and pore pressure gradient based on instantaneous shut-in pressure data obtained during hydraulic fracture treatments performed on partially depleted and overpressure intervals for the Vicksburg formation in South Texas. Salz's model is given by:

$$G_{FP} = 0.75e^{(0.57G_{PP})}. \quad (3.8)$$

Daines (1982) introduced a superposed horizontal tectonic stress term into the fracture pressure prediction model proposed by Eaton (equation 5.9):

$$FP = \sigma_t + \left[\frac{v}{1-v} \right] [\sigma_v - PP] + PP, \quad (5.9)$$

where FP is the fracture pressure (psi); σ_v is the vertical stress (psi); PP is the pore pressure (psi); v is the Poisson's ratio; σ_t is the horizontal tectonic stress term (psi). Using hydraulic fracturing data from various sedimentary basins, Breckels & Van Eekelen (1982) proposed empirical relationships between minimum horizontal stress and depth for US Gulf Coast (equation 5.10: for $D < 11,500$ ft and equation 5.11 for $D > 11,500$ ft), Venezuela (equation 5.12: for $5,900 \text{ ft} < D < 9,200 \text{ ft}$) and Brunei (equation 5.13 for $D < 10,000 \text{ ft}$). These models are given by:

$$\sigma_h = 0.197Z^{1.145} + 0.46[OP], \quad (5.10)$$

$$\sigma_h = 1.167Z - 4596 + 0.46[OP], \quad (5.11)$$

$$\sigma_h = 0.210Z^{1.145} + 0.56[OP], \quad (5.12)$$

$$\sigma_h = 0.227Z^{1.145} + 0.49[OP], \quad (5.13)$$

where σ_h is the minimum horizontal stress (psi); OP is the overpressure (psi). Overpressure is the difference between the formation pore pressure and the normal pore pressure. The normal pore pressure gradient can vary between $0.433 - 0.515$ psi/ft depending on pore fluid type, formation temperature and concentration of dissolved salts in the formation water (Oloruntobi et al., 2018; Oloruntobi and Butt, 2019). The normal pore pressure corresponds to a gradient of 0.452 psi/ft in the North Sea (Holm, 1998). In the US Gulf Coast, the normal pore pressure corresponds to a gradient of 0.465 psi/ft (Harkins and Baugher, 1969). The normal pore pressure gradient is approximately 0.433 psi/ft in the Rocky Mountain regions in Canada and USA (Finch, 1969). A formation is said to be overpressure if it has a pore pressure gradient higher than the normal pore pressure gradient. Several Mechanisms that generate subsurface overpressure conditions have been reported in the literature (Dickey 1976; Swarbrick 1995, Swarbrick & Osborne 1998). Constant & Bourgoyn (1988) extended Eaton's work to deepwater settings by exponentially fitting effective stress ratio to depth for formations in the US Gulf Coast (equation 5.14):

$$FP = [1 - Ae^{(B*Z)}][\sigma_v - PP] + PP, \quad (5.14)$$

where FP is the fracture pressure (psi); σ_v is the vertical stress (psi); PP is the pore pressure (psi); Z is the true vertical depth (ft); A and B are constant parameters. Avasthi et al. (2000) then

introduced Biot's poroelastic constant into the fracture pressure model proposed by Eaton (1969) using the concept of uniaxial strain model (equation 5.15):

$$FP = \left[\frac{v}{1-v} \right] [\sigma_v - \alpha PP] + \alpha PP, \quad (5.15)$$

where FP is the fracture pressure (psi); σ_v is the vertical stress (psi); PP is the pore pressure (psi); v is the Poisson's ratio; α is the Biot's coefficient. Zhang and Zhang (2017) modified Avasthi's model to include minimum stress coefficient based on the generalized Hooke's law with coupling stresses and pore pressure (equation 5.16):

$$FP = \left[\frac{v}{1-v} \right] [\sigma_v - \alpha PP] + \alpha PP + \left[\frac{c}{1-v} \right] \sigma_v, \quad (5.16)$$

where FP is the fracture pressure (psi); σ_v is the vertical stress (psi); PP is the pore pressure (psi); v is the Poisson's ratio; α is the Biot's coefficient; c is the minimum stress coefficient. The minimum stress coefficient (c) can be obtained by calibrating equation 5.16 to the in-situ measured fracture/LOT data from the correlating offset wells. Zhang & Yin (2017) developed a fracture gradient model based on LOT data obtained from offshore wells in several sedimentary basins (equation 5.17):

$$G_{FP} = \left[A + \frac{B}{e^{Z/C}} \right] [G_{OB} - G_{PP}] + G_{PP}, \quad (5.17)$$

where G_{FP} is the fracture pressure gradient (psi/ft); G_{OB} is the overburden gradient (psi/ft); G_{PP} is the pore pressure gradient (psi/ft); Z is the true vertical depth (ft). The model incorporates a depth-dependent effective stress ratio and the variables A, B and C can be obtained by calibrating equation 5.17 to the fracture/LOT data obtained from the offset wells. There are other

popular fracture pressure prediction models in the literature that are not specific to the Niger Delta basin (Berry and Macpherson, 1972; Althaus, 1977; Brennan and Annis, 1984; Holbrook, 1989; Vuckovic, 1989; Schmitt and Zoback, 1989; Aadnoy and Larson, 1989; Akinbinu, 2010; Zhang, 2011).

Lowrey and Ottesen (1995) proposed an empirical correlation to estimate the in-situ minimum horizontal stress for offshore Niger Delta based on fracture closure pressures obtained from extended leak-off tests (equation 5.18):

$$FP = 0.1779Z^{1.1586}, \quad (5.18)$$

where FP is the fracture pressure (psi); Z is the true vertical depth (ft). Equation 5.18 is limited to normally pressured intervals and does not account for the effect of overpressure on fracture pressure. Ajienka and Nwokeji (1988) proposed a fracture gradient correlation for the onshore region of the Niger Delta basin based on 135 LOT measurements acquired from 93 onshore well covering a depth range of 2,159 ft to 13,070 ft (equation 5.19):

$$G_{FP} = 14.57595 + 0.0002193[Z] - 16.16777[G_{OB}] - 0.270395[K_i] + 0.6665068[G_{PP}], \quad (5.19)$$

$$K_i = 0.135726 + 0.0000366[Z], \quad (5.20)$$

where G_{FP} is the fracture pressure gradient (psi/ft); G_{OB} is the overburden gradient (psi/ft); G_{PP} is the pore pressure gradient (psi/ft); Z is the true vertical depth (ft); K_i is the stress ratio. The stress ratio (K_i) is expressed as a function of depth (Ajienka et al. 2009). Considering that Niger Delta basin operates under normal faulting regime where $S_v > \sigma_H > \sigma_h$, Ajienka and Nwokeji's model is fundamentally flawed because they suggested that formation fracture pressure decreases as overburden pressure increases. Hence, this model should not be used in predicting the formation

fracture pressure in the Niger Delta basin. Reginald-Ugwuadu et al. (2014) proposed the most calibrated fracture pressure prediction model for the Niger Delta sediments based on combined LOT data obtained from onshore, swamp and shallow offshore wells (equation 5.21):

$$FP = 0.000029[Z^2] + 0.46Z, \quad (5.21)$$

where FP is the fracture pressure (psi); Z is the true vertical depth (ft). However, the model fails to capture the effect of overpressure on fracture pressure. This limits its application to normally pressured intervals. Reginald-Ugwuadu's model was built from LOT measurements acquired at various wellbore inclinations and azimuths.

While few empirical models have been developed for the Niger Delta basin, none of the models were developed to work in High-Pressure High-Temperature (HPHT) environments. In fact, no fracture pressure prediction model exists in the Niger Delta that incorporates LOT measurements from the hard overpressure environments (pore pressure gradient > 0.70 psi/ft). The existing models were developed primarily from LOT measurements acquired from the normally and mildly pressured intervals. In this paper, an attempt is made to develop a new fracture pressure prediction model that can be applied to normal and overpressure intervals in the onshore, swamp and shallow offshore regions of the Niger Delta basin.

5.2 Field Data

The Niger Delta basin is an extensional rift basin located in the Niger Delta and the Gulf of Guinea along the west of central Africa. The basin covers an area of about 75,000 km² and consists of clastic sediments up to 12 km thick (Doust and Omatsola 1990; Evamy et al. 1978). The basin consists of three types of formations in descending order: Benin formations, Agbada

formations and Akata formations (Short and Stauble 1967; Avbovbo 1978a; Adewole et al. 2016). The Benin formations consist primarily of continental loose sands. The Agbada formations consist of an alternating sequence of sands and shales. The Akata formations consist of thick marine overpressure shales. The geothermal gradient varies across the Niger Delta basin between $1.2 - 3.0^{\circ}\text{F}$ per 100 feet (Avbovbo, 1978b). The structural trapping mechanisms in the basin are growth faults associated with rollover structures and the basin operates under normal faulting regime (Daukoru 1975; Weber 1987). The primary mechanism of subsurface overpressure conditions in the Niger Delta basin is compaction disequilibrium (Ugwu and Nwankwo, 2014; Oloruntobi et al., 2018; Oloruntobi and Butt, 2019).

For data analysis, all depths and pressures are referenced to a true vertical depth below the mean sea level. Figure 5.1 shows the location map for most of the wells used to build the new fracture pressure prediction model. Due to a large number of wells involved (> 100 wells), only 53 wells are displayed on the location map just to show the area extent of the LOT data. All other wells not shown on the map are scattered across the basin. Table 5.2 in the appendix provides a well data summary. A total of 141 LOT measurements from 109 wells were used to develop the new model. The well data cover the land, swamp and shallow offshore regions of the basin. The shallow offshore regions of the basin are limited to 500 ft water depth. The LOT data also cover a wide range of depth between 885 ft and 16,478 ft. The formation pore pressure gradient ranges between 0.433 psi/ft and 0.826 psi/ft. No existing fracture pressure prediction model in the Niger Delta covers this pore pressure range. Note that the normal pore pressure gradient in the Niger Delta ranges between 0.433 psi/ft to 0.472 psi/ft. In Table 5.2, any pore pressure value designated as “normal” will have a pore pressure gradient in this range. The fracture gradient ranges between 0.479 psi/ft and 1.018 psi/ft. Unexpectedly, the LOT measurements in the deep

overpressure zones have shown that fracture gradient can exceed 1.0 psi/ft in the Niger Delta. Most of the LOT data at depths shallower than 5000 ft were acquired in continental sands while LOT measurements at depths deeper than 5000 ft were mostly acquired in shale formations.

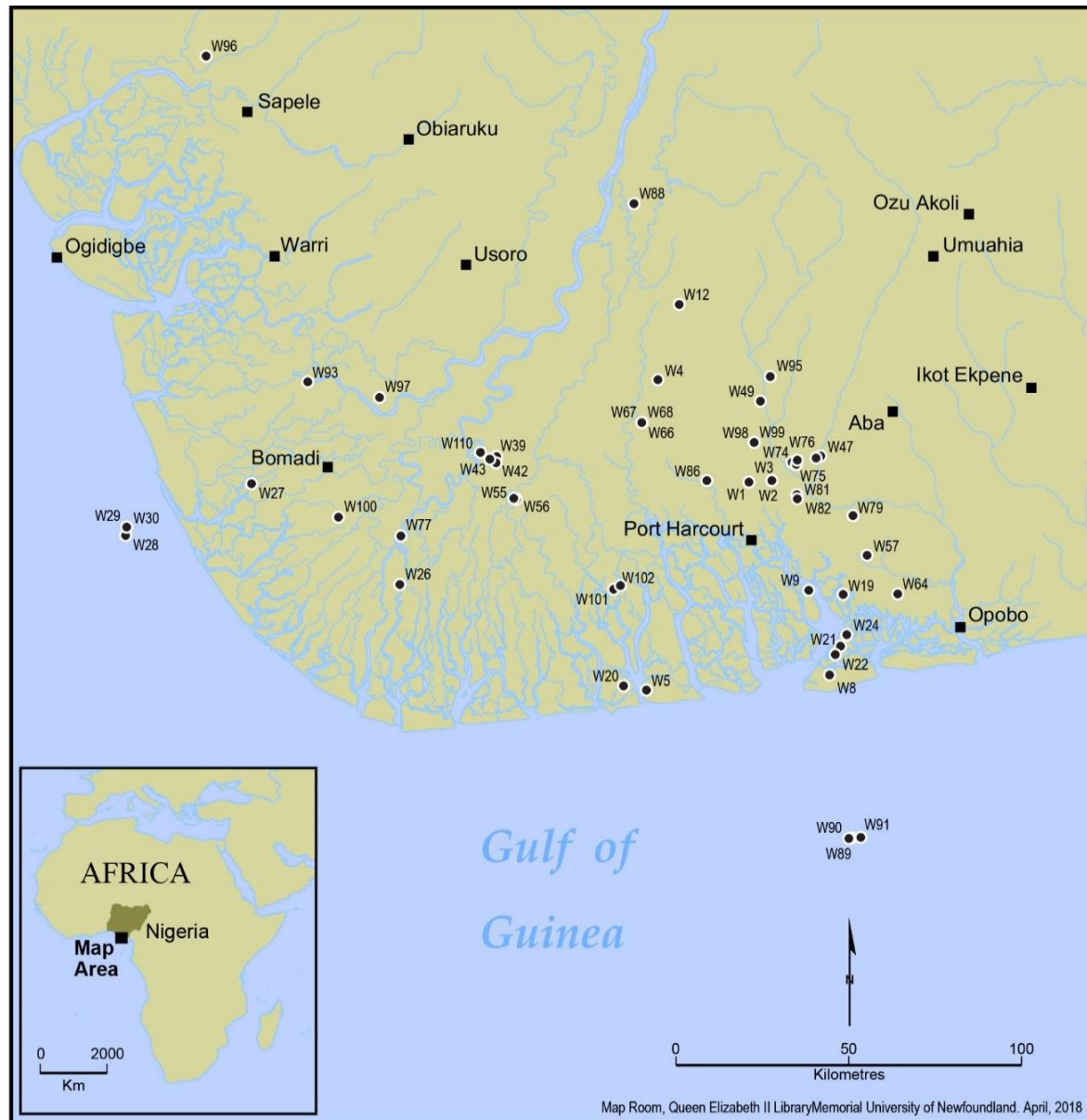


Figure 5 1: Location map for some wells used in model development.

To eliminate/minimize the effect of well inclination and azimuth on formation fracture pressure, only LOT measurements acquired in mostly vertical wells are considered with only few

slightly deviated wells. In the few slightly deviated wells, the wellbore inclinations at which LOT measurements were acquired are less than 18 degrees, thereby making the effect of well inclination and azimuth on formation fracture pressure insignificant in these wells. It should be noted that limit-test measurements across the Niger Delta basin are excluded from the data used to develop the new fracture pressure prediction model because they do not really provide any quantitative information about the formation strength

5.3 Model Development

To develop a single equation that can be used to describe the formation fracture pressure in normal and overpressure intervals, the LOT measurements acquired in overpressure intervals must be normalized for the effect of pore pressure. The procedures used to derive the new model are highlighted below.

- Measured fracture pressure data were plotted against depth.
- Trends corresponding to normal and overpressure intervals were identified.
- A model was fitted through the fracture pressure data acquired in normally pressured intervals. This is called normally pressured trendline model.
- Fracture pressure differentials were obtained across the overpressure intervals by computing the difference between the actual fracture pressure measurements and fracture pressure values estimated from the normally pressured trendline model.
- Pore pressure differentials were obtained across the overpressure intervals by computing the difference between the actual pore pressure and normal pore pressure.
- Fracture pressure differentials were plotted against the pore pressure differentials in the overpressure intervals to generate the new fracture pressure prediction model.

Figure 5.2 shows the plot of fracture pressure against depth using the LOT data presented in Table 5.2. While the pressure data are reported in gradient equivalent, pore and fracture pressure values are obtained by multiplying the pressure gradients by the corresponding vertical depth.

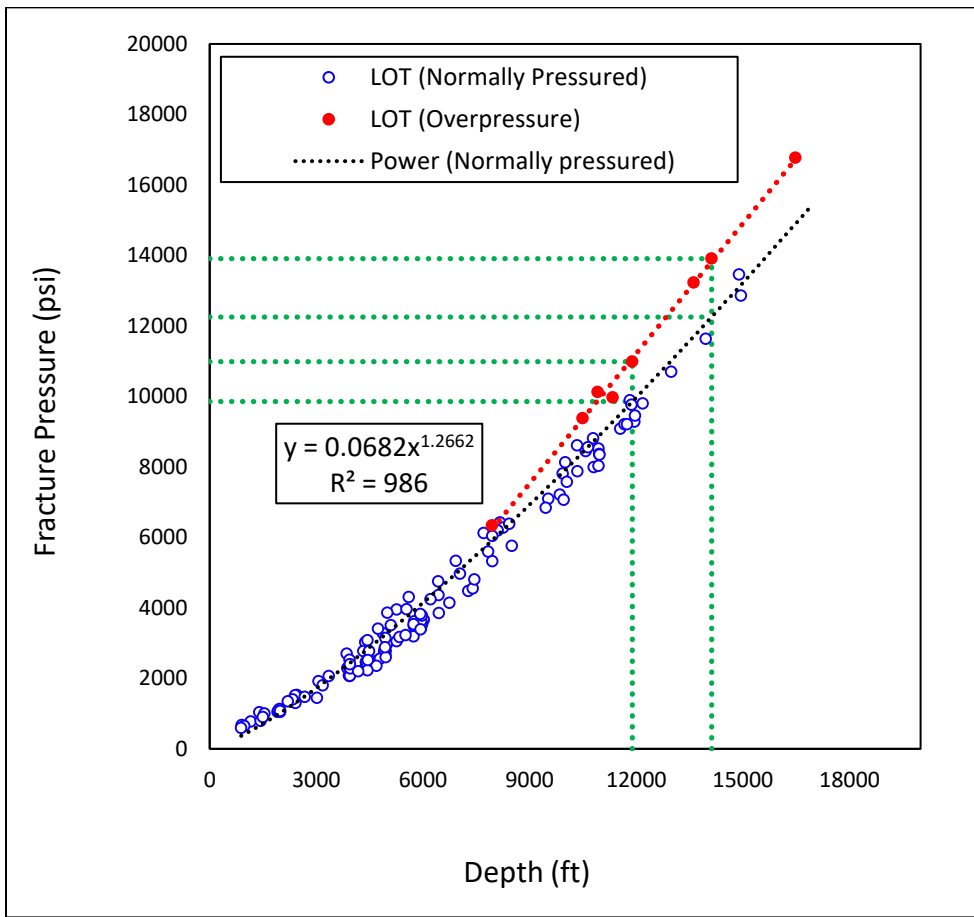


Figure 5.2: The plot of formation fracture pressure against depth

Although two distinct trends can be clearly identified from the plot (Figure 5.2), remarkable non-scattered trends are observed for each pressure regime despite the LOT measurements being acquired from various fields across the basin. A power law trend is observed between fracture pressure and depth for normally pressured intervals while a linear trend is observed for the overpressure intervals. As expected, formation fracture pressure values are higher in

overpressure intervals than the normally pressured intervals at the same depth. For instance, at the depth of 11,890 ft, the fracture pressure values in normally pressured and overpressure intervals are 9,854 psi and 10,986 psi respectively. This is an increase of 1,132 psi in formation fracture pressure when pore pressure increases by 2,378 psi from the normal. Likewise, at the depth of 14,122 ft, the formation fracture pressure values in normally pressured and overpressure intervals are 12,252 psi and 13,908 psi respectively. This is an increase of 1,657 psi in formation fracture pressure when pore pressure increases by 4,053 psi from the normal. These data indicate that formation fracture pressure increases at a rate proportional to but less than the rate of pore pressure increase. From Figure 5.2, at pore pressure value corresponding to a gradient of 0.515 psi/ft, the formation fracture pressure values for the normally pressured and overpressure intervals almost overlap. For non-depleting formations, overpressure has little effect on formation fracture pressure when pore pressure gradient falls below 0.515 psi/ft. A normally pressured trendline (NPT) is obtained by fitting a power-law model through the fracture pressure data acquired in the normally pressured intervals (equation 5.22). The formation fracture pressure in equation 5.22 is only a function of depth with no pore pressure term.

$$FP_{NPT} = 0.06817[D]^{1.2662} \quad (5.22)$$

Figure 5.3 shows the plot of fracture pressure differential (measured fracture pressure minus the corresponding fracture pressure computed from equation 5.22) versus the pore pressure differential (actual pore pressure (PP_a) minus normal pore pressure (PP_n)) in the overpressure intervals. Note that for all the normally pressured intervals, pore pressure differential will be zero. A normal pore pressure (PP_n) value with a gradient of 0.433 psi/ft with respect to mean sea level is used to derive the new model. From Figure 5.3, a polynomial relationship exists between

the fracture pressure differential and pore pressure differential (equation 5.23). The plot shows a good trend despite the overpressure LOT measurements were obtained from different fields.

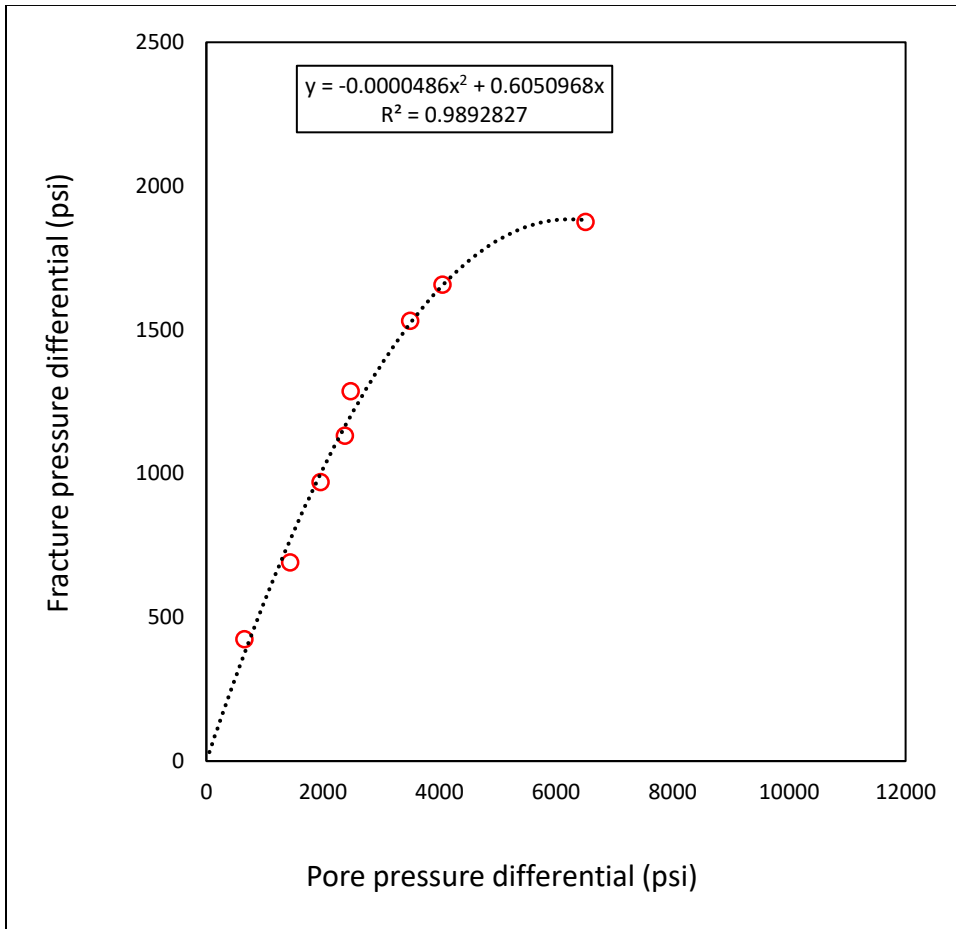


Figure 5.3: Fracture pressure differential versus pore pressure differential.

By rearranging equation 5.23 and substituting for the normally pressured trendline fracture pressure (equation 5.22), a new fracture pressure prediction model for the Niger Delta is obtained (equation 5.25). When operating in normally pressured intervals, the overpressure/pore pressure differential ($PP_a - PP_n$) term will go to zero and equation 5.25 will reduce to equation 5.22.

$$\Delta FP = 0.6051[\Delta PP] - 0.0000486[\Delta PP]^2 \quad (5.23)$$

$$FP - FP_{NPT} = 0.6051[PP_a - PP_n] - 0.0000486[PP_a - PP_n]^2 \quad (5.24)$$

$$FP = 0.06817[D]^{1.2662} + 0.6051[PP_a - PP_n] - 0.0000486[PP_a - PP_n]^2 \quad (5.25)$$

$$PP_n = 0.433[D] \quad (5.26)$$

5.4 Model Validation

To demonstrate the applicability of the new fracture pressure prediction technique, a recently drilled high-pressure high-temperature (HPHT) exploratory gas well (W 110) is considered as the case study. The well is located approximately 82 km northwest of Port Harcourt in the central region of the basin. The well is a slightly deviated well drilled to a total depth of 16,809 ft with a maximum inclination of 14.56°. The formation integrity tests were conducted at the 13 3/8" casing, 9 5/8" casing and 7" liner shoes. The 13 3/8" casing, 9 5/8" casing and 7" liner shoes were set at 9,382 ft, 15,087 ft and 16,404 ft respectively. The wellbore inclinations at the 13 3/8" casing, 9 5/8" casing and 7" liner shoes are 11°, 12° and 3° respectively. The types of formation integrity test performed at the 13 3/8" and 9 5/8" casing shoes were limit tests (no leak-off). The type of formation integrity test performed at the 7" liner shoe was the leak-off test. Although limit test measurements are not considered in the new model because they will not provide any quantitative information about the formation strength, they are included in this well to serve as control/calibrating data. The bottom-hole limit test pressure gradient at the 13 3/8" and 9 5/8" casing shoes are 0.717 psi/ft and 0.917 psi/ft respectively. The formation fracture gradient (bottom-hole leak-off pressure gradient) at the 7" liner shoe is 1.009 psi/ft. Table 5.1 shows the pore pressure data for the W 110 well. The formation pore pressures were obtained from the combination of formation pressure while drilling tool, wireline pressure

sampling tool, sonic logs and drilling kick data. The formation pore pressure is normal from 9,200 ft to 14,805 ft (onset of overpressure). The formation pore pressure gradient then increases gradually from 0.471 psi/ft at 14,805 ft to 0.856 psi/ft at 16,445 ft. Therefore, from 9,200 ft to 14,805 ft (normally pressured intervals), equation 5.25 will be used to estimate the formation fracture pressures with the overpressure/pore pressure differential ($PP_a - PP_n$) term being equal to zero. From 14,805 ft to 16,445 ft (overpressure intervals), full components of Equation 5.25 will be used to estimate the formation fracture pressure. Note that pore and fracture pressure terms are calculated by multiplying pressure gradient by depth.

Table 5. 1 The pore pressure data for the W 110 well.

S/N	Depth (ft)	PP (psi/ft)									
1	9200	0.432	7	10600	0.433	13	14235	0.462	19	15867	0.797
2	9382	0.432	8	11200	0.432	14	14546	0.470	20	15930	0.812
3	9562	0.432	9	12115	0.464	15	14805	0.471	21	16105	0.812
4	9722	0.432	10	12309	0.463	16	15087	0.610	22	16181	0.849
5	9943	0.435	11	12947	0.463	17	15122	0.665	23	16404	0.852
6	9988	0.433	12	13658	0.462	18	15407	0.722	24	16445	0.856

Figure 5.4 shows the comparison of predicted and measured fracture pressures for well W 110 using the new model and the most calibrated existing model for the Niger Delta basin (equation 5.21). At the 7" liner shoe (16,404 ft) where the actual leak-off test was conducted, a good agreement exists between the predicted and measured fracture pressure in overpressure interval. The newly proposed model predicts the formation fracture pressure within an accuracy of ± 125 psi which is typically less than the trip margin (200 psi) normally applied to formation fracture pressure as a safety factor. At the 13 3/8" and 9 5/8" casing shoes where limit tests were

conducted, the new model predicts fracture pressure values higher than the bottom-hole limit test pressures because limit tests are usually stopped prior to reaching the point where drilling fluid starts to invade the formation (leak-off point).

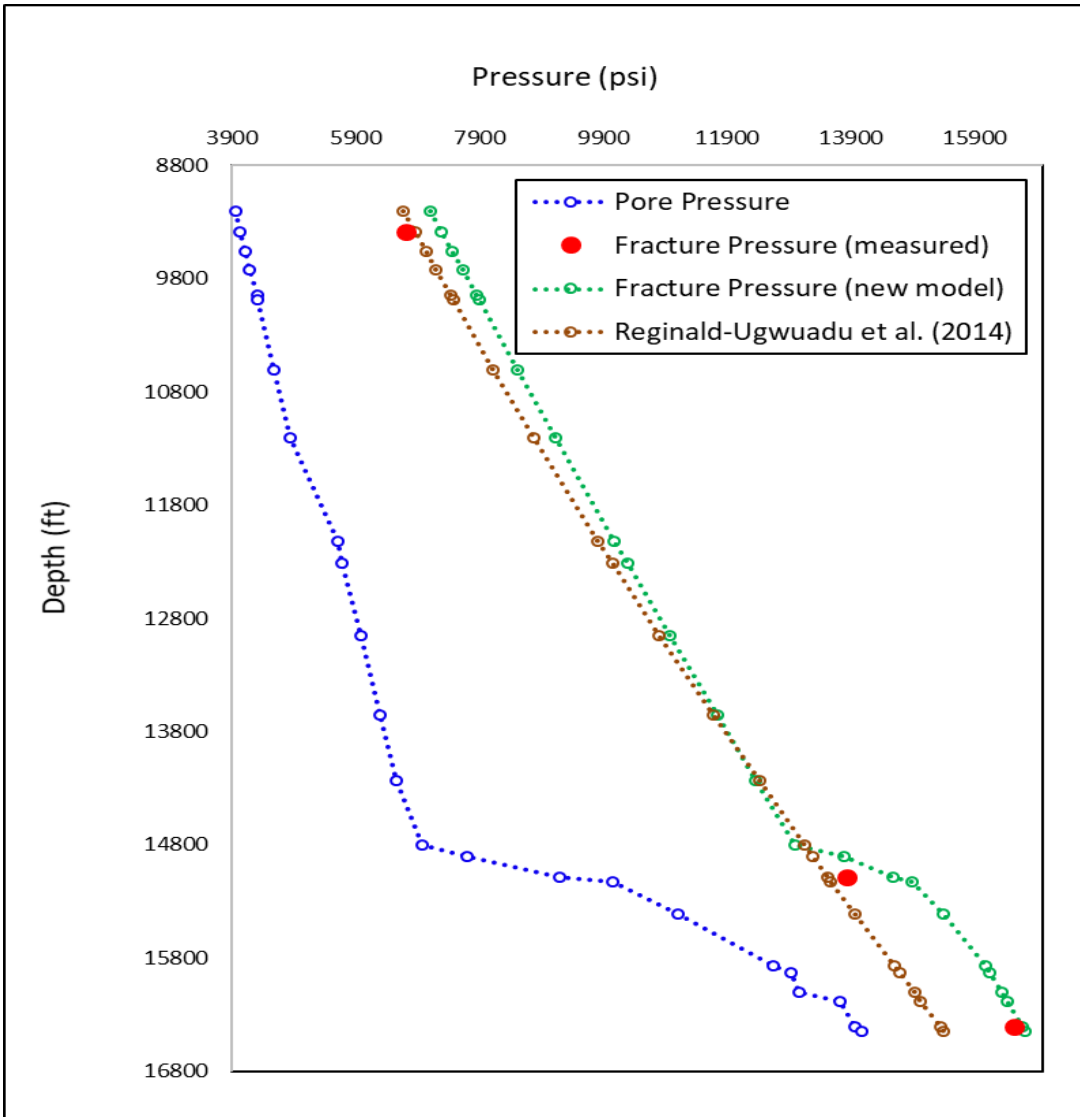


Figure 5 4: Comparison of predicted and measured fracture pressure for well W110

By using Reginald-Ugwuadu's model (equation 5.21), fairly accurate estimates of formation fracture pressures are observed in the normally pressured intervals (9,200 – 14,805 ft). However, in the transition and overpressure intervals, the model completely breaks down and underpredicts

the formation fracture pressures. At the 7" liner shoe, Reginald-Ugwuadu's model underpredicts the formation fracture pressure by 1,199 psi. Even at the 9 5/8" casing shoe, Reginald-Ugwuadu's model wrongly predicts the fracture pressure value that is less than the bottom-hole limit test pressure. Using such only depth-dependent model for pre-drill fracture pressure predictions in overpressure intervals will lead to expensive drilling campaign (more casing strings may be required than necessary).

5.5 Conclusion

A new robust fracture pressure prediction model that can be applied to a wide range of depths and subsurface pressure regimes (normal to very hard overpressure) has been developed. The new model establishes a relationship between fracture pressure, depth, and overpressure. The model covers land, swamp and shallow offshore sections of the Niger Delta basin. It is the first model to incorporate LOT measurements acquired in overpressure environments in the Niger Delta. The proposed model can form the new Niger Delta guideline for: (1) performing the limit tests at the wellsite during the actual drilling operations; (2) determining the pre-dill formation fracture pressure for well planning and design; and (3) establishing the injection pressure required for hydraulic fracturing. Although only one operator is currently drilling HPHT wells in the Niger Delta, the new model will find a useful application as more operating companies plan to embark on exploration drilling campaigns into the deeper HPHT sections of the basin.

5.6 Appendix

Table 5. 2 Well data summary

Well	Location	Depth (ft)	FP (psi/ft)	PP (psi/ft)
W 1	Land	4395	0.560	Normal
W 2	Land	4398	0.532	Normal
W 3	Land	1988	0.527	Normal
		7275	0.615	Normal
		11339	0.879	0.560
		13614	0.972	0.690
W 4	Land	4378	0.691	Normal
W 5	Land	4945	0.538	Normal
W 6	Swamp	4952	0.524	Normal
W 7	Swamp	4946	0.635	Normal
W 8	Land	4958	0.561	Normal
W 9	Swamp	4741	0.718	Normal
W 10	Swamp	5741	0.556	Normal
W 11	Swamp	2452	0.622	Normal
W 12	Land	1982	0.495	Normal
		7947	0.798	0.515
		10489	0.894	0.620
W 13	Land	9934	0.786	Normal
W 14	Swamp	11950	0.776	Normal
W 15	Swamp	5947	0.575	Normal
W 16	Swamp	6448	0.597	Normal
W 17	Swamp	5921	0.581	Normal
W 18	Swamp	5943	0.598	Normal
W 19	Swamp	1962	0.575	Normal
		5963	0.590	Normal
W 20	Swamp	4940	0.582	Normal
		8504	0.677	Normal
W 21	Swamp	3941	0.640	Normal
W 22	Swamp	9965	0.709	Normal
W 23	Swamp	8255	0.760	Normal
W 24	Swamp	10940	0.778	Normal
W 25	Offshore	2409	0.631	Normal
		5542	0.715	Normal
W 26	Land	1954	0.560	Normal

Well	Location	Depth (ft)	FP (psi/ft)	PP (psi/ft)
W 27	Swamp	3951	0.607	Normal
		10641	0.804	Normal
W 28	Offshore	3183	0.566	Normal
W 29	Offshore	2334	0.598	Normal
W 30	Offshore	2202	0.610	Normal
W 31	Land	3353	0.614	Normal
W 32	Land	9849	0.732	Normal
W 33	Swamp	4448	0.570	Normal
W 34	Swamp	3942	0.522	Normal
W 35	Swamp	4692	0.501	Normal
		7406	0.614	Normal
		11557	0.786	Normal
		13957	0.833	Normal
W 36	Swamp	5261	0.580	Normal
		10962	0.763	Normal
W 37	Swamp	8433	0.757	Normal
W 38	Land	3861	0.698	Normal
W 39	Land	6214	0.683	Normal
		11741	0.784	Normal
W 40	Land	7709	0.794	Normal
W 41	Land	16478	1.018	0.828
W 42	Land	12183	0.804	Normal
		14890	0.904	Normal
		6743	0.613	Normal
W 44	Offshore	1912	0.548	Normal
W 45	Offshore	1156	0.666	Normal
W 46	Offshore	1400	0.740	Normal
W 47	Land	3924	0.530	Normal
W 48	Land	3065	0.626	Normal
		5101	0.687	Normal
W 49	Land	8165	0.786	Normal
W 50	Offshore	902	0.745	Normal
W 51	Offshore	2412	0.539	Normal
W 52	Offshore	1433	0.548	Normal

Well	Location	Depth (ft)	FP (psi/ft)	PP (psi/ft)
W 53	Offshore	2681	0.549	Normal
		5340	0.593	Normal
W 54	Offshore	4999	0.771	Normal
W 55	Land	6022	0.607	Normal
		11826	0.836	Normal
W 56	Land	14122	0.985	0.720
W 57	Land	4585	0.518	Normal
		10341	0.832	Normal
		11890	0.924	0.633
W 58	Offshore	10786	0.816	Normal
W 59	Offshore	5931	0.645	Normal
		11670	0.789	Normal
W 60	Swamp	5955	0.610	Normal
W 61	Swamp	5970	0.632	Normal
W 62	Land	9531	0.744	Normal
W 63	Land	5754	0.603	Normal
W 64	Land	10580	0.799	Normal
W 65	Land	1926	0.560	Normal
W 66	Land	4439	0.694	Normal
W 67	Land	5746	0.608	Normal
W 68	Land	5752	0.628	Normal
W 69	Swamp	3946	0.577	Normal
W 70	Swamp	3945	0.600	Normal
W 71	Swamp	4491	0.617	Normal
W 72	Swamp	3948	0.524	Normal
W 73	Swamp	5739	0.616	Normal
W 74	Land	10810	0.739	Normal
W 75	Land	4908	0.557	Normal
W 76	Land	4990	0.596	Normal
W 77	Land	5981	0.592	Normal
W 78	Land	14945	0.860	Normal
W 79	Land	4324	0.641	Normal
W 80	Land	5259	0.751	Normal
W 81	Land	4184	0.526	Normal
W 82	Land	4690	0.530	Normal

Well	Location	Depth (ft)	FP (psi/ft)	PP (psi/ft)
W 83	Swamp	10943	0.733	Normal
W 84	Swamp	3955	0.576	Normal
W 85	Land	4793	0.532	Normal
W 86	Land	4922	0.570	Normal
W 87	Land	7951	0.669	Normal
		10004	0.813	Normal
		10912	0.928	0.660
W 88	Land	4430	0.545	Normal
W 89	Offshore	980	0.662	Normal
W 90	Offshore	1542	0.648	Normal
		6430	0.738	Normal
		11867	0.823	Normal
W 91	Offshore	885	0.670	Normal
W 92	Swamp	4446	0.500	Normal
W 93	Land	10051	0.754	Normal
W 94	Offshore	6440	0.677	Normal
W 95	Land	7833	0.714	Normal
W 96	Land	7046	0.705	Normal
W 97	Land	10970	0.760	Normal
W 98	Land	3876	0.589	Normal
W 99	Land	4872	0.674	Normal
W 100	Swamp	3023	0.479	Normal
		7451	0.645	Normal
		12988	0.824	Normal
W 101	Swamp	10352	0.761	Normal
W 102	Swamp	9452	0.724	Normal
		4447	0.566	Normal
W 103	Swamp	5932	0.571	Normal
		11967	0.790	Normal
W 104	Offshore	6925	0.769	Normal
W 105	Land	7951	0.760	Normal
W 106	Offshore	1501	0.600	Normal
		5605	0.768	Normal
W 107	Swamp	8109	0.763	Normal
W 109	Land	5510	0.585	Normal

5.7 Reference

- Aadnoy, B.S., 1988. Modeling of the Stability of Highly Inclined Boreholes in Anisotropic Rock Formations (includes associated papers 19213 and 19886). SPE Drill. Eng. 3, 259–268. <https://doi.org/10.2118/16526-PA>
- Aadnoy, B.S., Chenevert, M.E., 1987. Stability of Highly Inclined Boreholes (includes associated papers 18596 and 18736). SPE Drill. Eng. 2, 364–374. <https://doi.org/10.2118/16052-PA>
- Aadnoy, B.S., Larson, K., 1989. Method for Fracture-Gradient Prediction for Vertical and Inclined Boreholes. SPE Drill. Eng. 4, 99–103. <https://doi.org/10.2118/16695-PA>
- Adewole, E.O., Macdonald, D.I.M., Healy, D., 2016. Estimating density and vertical stress magnitudes using hydrocarbon exploration data in the onshore Northern Niger Delta Basin, Nigeria: Implication for overpressure prediction. J. African Earth Sci. 123, 294–308. <https://doi.org/10.1016/j.jafrearsci.2016.07.009>
- Ajienka, J., Nwokeji, B., 1988. Evaluating the performance of onshore fracture pressure gradient correlations in the Niger Delta. University of Port Harcourt.
- Ajienka, J., Egbon, F., Onwuemena, U., 2009. Deep Offshore Fracture Pressure Prediction in the Niger Delta - A New Approach. Niger. Annu. Int. Conf. Exhib. <https://doi.org/10.2118/128339-MS>
- Akinbinu, V.A., 2010. Prediction of fracture gradient from formation pressures and depth using correlation and stepwise multiple regression techniques. J. Pet. Sci. Eng. 72, 10–17.
- Alberty, M.W., McLean, M.R., 2004. A Physical Model for Stress Cages. SPE Annu. Tech. Conf. Exhib. <https://doi.org/10.2118/90493-MS>
- Althaus, V.E., 1977. A New Model For Fracture Gradient. J. Can. Pet. Technol. 16, 12. <https://doi.org/10.2118/77-02-10>
- Altun, G., Langlinais, J., Bourgoyn Jr., A.T., 2001. Application of a New Model To Analyze Leak-Off Tests. SPE Drill. Complet. 16, 108–116. <https://doi.org/10.2118/72061-PA>
- Anderson, E.M., 1951. The Dynamics of Faulting and Dyke Formation with Applications to Britain. Edinburgh, Oliver Boyd.
- Anderson, R.A., Ingram, D.S., Zanier, A.M., 1973. Determining Fracture Pressure Gradients From Well Logs. J. Pet. Technol. 25, 1259–1268. <https://doi.org/10.2118/4135-PA>

- Aston, M.S., Alberty, M.W., McLean, M.R., de Jong, H.J., Armagost, K., 2004. Drilling Fluids for Wellbore Strengthening. IADC/SPE Drill. Conf. <https://doi.org/10.2118/87130-MS>
- Avasthi, J.M., Goodman, H.E., Jansson, R.P., 2000. Acquisition, Calibration, and Use of the In Situ Stress Data for Oil and Gas Well Construction and Production, in: SPE Rocky Mountain Regional/Low-Permeability Reservoirs Symposium and Exhibition. Society of Petroleum Engineers.
- Avbovbo, A.A., 1978a. Tertiary lithostratigraphy of the Niger Delta. Am. Assoc. Pet. Geol. Bull. 62, 295–306.
- Avbovbo, A.A., 1978b. Geothermal gradients in the southern Nigeria basin. Bull. Can. Pet. Geol. 26, 268–274.
- Berry, L.N., Macpherson, L.A., 1972. Prediction of Fracture Gradients from Log Derived Elastic Moduli. Log Anal. 13.
- Breckels, I.M., Van Eekelen, H.A.M., 1982. Relationship between horizontal stress and depth in sedimentary basins. J. Pet. Technol. 34, 2–191.
- Brennan, R.M., Annis, M.R., 1984. A New Fracture Gradient Prediction Technique That Shows Good Results in Gulf of Mexico Abnormal Pressure. SPE Annu. Tech. Conf. Exhib. <https://doi.org/10.2118/13210-MS>
- Bybee, K., 2008. Wellbore Strengthening in Shale. J. Pet. Technol. 60, 71–72. <https://doi.org/10.2118/0108-0071-JPT>
- Chan, A.W., Ekbote, S., Hows, M.P., Wong, G.K., 2015. In Situ Stress Measurements during Well Abandonment. 49th U.S. Rock Mech. Symp.
- Chellappah, K., Kumar, A., Aston, M., 2015. Drilling Depleted Sands: Challenges Associated With Wellbore Strengthening Fluids. SPE/IADC Drill. Conf. Exhib. <https://doi.org/10.2118/173073-MS>
- Chellappah, K., Majidi, R., Aston, M., Cook, J., 2018. A Practical Model for Wellbore Strengthening. IADC/SPE Drill. Conf. Exhib. <https://doi.org/10.2118/189589-MS>
- Christman, S.A., 1973. Offshore Fracture Gradients. J. Pet. Technol. 25, 910–914. <https://doi.org/10.2118/4133-PA>
- Constant, D.W., Bourgoyne Jr, A.T., 1988. Fracture-gradient prediction for offshore wells. SPE Drill. Eng. 3, 136–140.
- Contreras, O., Hareland, G., Husein, M., Nygaard, R., Al-saba, M.T., 2014. Experimental

- Investigation on Wellbore Strengthening In Shales by Means of Nanoparticle-Based Drilling Fluids. SPE Annu. Tech. Conf. Exhib. <https://doi.org/10.2118/170589-MS>
- Couzens-Schultz, B.A., Chan, A.W., 2010. Stress determination in active thrust belts: An alternative leak-off pressure interpretation. *J. Struct. Geol.* 32, 1061–1069.
- Daines, S.R., 1982. Prediction of Fracture Pressures for Wildcat Wells. *J. Pet. Technol.* 34, 863–872. <https://doi.org/10.2118/9254-PA>
- Daneshy, A.A., Slusher, G.L., Chisholm, P.T., Magee, D.A., 1986. In-Situ Stress Measurements During Drilling. *J. Pet. Technol.* 38, 891–898. <https://doi.org/10.2118/13227-PA>
- Daukoru, J.W., 1975. PD 4(1) Petroleum Geology of the Niger Delta. *World Pet. Congr.*
- De Bree, P., Walters, J. V, 1989. Micro/Minifrac test procedures and interpretation for in situ stress determination, in: *International Journal of Rock Mechanics and Mining Sciences & Geomechanics Abstracts*. Elsevier, pp. 515–521.
- Doust, H., Omatsola, E., 1990. Niger Delta, in: *Divergent / Passive Margin Basins*. pp. 201–238.
- Eaton, B.A., 1969. Fracture Gradient Prediction and Its Application in Oilfield Operations. *J. Pet. Technol.* 21, 1353–1360. <https://doi.org/10.2118/2163-PA>
- Edwards, S.T., Meredith, P.G., Murrell, S.A.F., 1998. An investigation of leak-off test data for estimating in-situ stress magnitudes: application to a basinwide study in the North Sea, in: *SPE/ISRM Rock Mechanics in Petroleum Engineering*. Society of Petroleum Engineers.
- Engelder, T., Fischer, M.P., 1994. Influence of poroelastic behavior on the magnitude of minimum horizontal stress, S_h in overpressured parts of sedimentary basins. *Geology* 22, 949–952.
- Evamy, B.D., Haremboure, J., Kamerling, P., Knaap, W.A., Molloy, F.A., Rowlands, P.H., 1978. Hydrocarbon habitat of Tertiary Niger delta. *Am. Assoc. Pet. Geol. Bull.* 62, 1–39.
- Feng, Y., Gray, K.E., 2017. Review of fundamental studies on lost circulation and wellbore strengthening. *J. Pet. Sci. Eng.* 152, 511–522.
- Feng, Y., Gray, K.E., 2016. A comparison study of extended leak-off tests in permeable and impermeable formations, in: *50th US Rock Mechanics/Geomechanics Symposium*. American Rock Mechanics Association.
- Finch, W., 1969. Abnormal Pressure in the Antelope Field, North Dakota. *J. Pet. Technol.* 21.
- Gonzalez, M.E., Bloys, J.B., Lofton, J.E., Pepin, G.P., Schmidt, J.H., Naquin, C.J., Ellis, S.T., Laursen, P.E., 2004. Increasing Effective Fracture Gradients by Managing Wellbore

- Temperatures. IADC/SPE Drill. Conf. <https://doi.org/10.2118/87217-MS>
- Haimson, B., Fairhurst, C., 1967. Initiation and extension of hydraulic fractures in rocks. *Soc. Pet. Eng. J.* 7, 310–318.
- Harkins, L.K., Baugher, I.H., 1969. Geological significance of abnormal formation pressures. *J. Pet. Technol.* 961–966. <https://doi.org/10.2118/2228-PA>
- Hettema, M.H.H., Bostrøm, B., Lund, T., 2004. Analysis of Lost Circulation During Drilling in Cooled Formations. *SPE Annu. Tech. Conf. Exhib.* <https://doi.org/10.2118/90442-MS>
- Holbrook, P.W., 1989. A New Method for Predicting Fracture Propagation Pressure From MWD or Wireline Log Data. *SPE Annu. Tech. Conf. Exhib.* <https://doi.org/10.2118/SPE-19566-MS>
- Holm, G.M., 1998. Distribution and origin of overpressure in the Central Graben of the North Sea. Law, B.E., G.F. Ulmishek, V.I. Slavin eds., *Abnorm. Press. Hydrocarb. Environ.* AAPG Mem. 70, 123–144.
- Hubbert, M.K., Willis, D.G., 1957. Mechanics Of Hydraulic Fracturing.
- Kumar, A., Savari, S., Whitfill, D., Jamison, D.E., 2010. Wellbore Strengthening: The Less-Studied Properties of Lost-Circulation Materials. *SPE Annu. Tech. Conf. Exhib.*
- Kunze, K.R., Steiger, R.P., 1992. Accurate In-Situ Stress Measurements During Drilling Operations. *SPE Annu. Tech. Conf. Exhib.* <https://doi.org/10.2118/24593-MS>
- Li, G., Lorwongngam, A., Roegiers, J.-C., 2009. Critical Review Of Leak-Off Test As A Practice For Determination Of In-Situ Stresses. 43rd U.S. Rock Mech. Symp. 4th U.S. - Canada Rock Mech. Symp.
- Lowrey, J.P., Ottesen, S., 1995. An Assessment of the Mechanical Stability of Wells Offshore Nigeria. *SPE Drill. Complet.* 10, 34–41. <https://doi.org/10.2118/26351-PA>
- Matthews, W.R., Kelly, J., 1967. How to predict formation pressure and fracture gradient from electric and sonic logs. *Oil Gas.*
- Oloruntobi, O., Adedigba, S., Khan, F., Chunduru, R., Butt, S., 2018. Overpressure prediction using the hydro-rotary specific energy concept. *J. Nat. Gas Sci. Eng.* 55, 243–253.
- Oloruntobi, O., Butt, S., 2019. Energy-based formation pressure prediction. *J. Pet. Sci. Eng.* 173, 955–964.
- Parriag, E.R., 1976. Prediction of Fracture Gradients in Samaan Field, in: *SPE Petroleum and Exposition Conference*. Society of Petroleum Engineers.

- Pennebaker, E.S., 1968. An Engineering Interpretation of Seismic Data. Fall Meet. Soc. Pet. Eng. AIME. <https://doi.org/10.2118/2165-MS>
- Perkins, T.K., Gonzalez, J.A., 1984. Changes in Earth Stresses Around a Wellbore Caused by Radially Symmetrical Pressure and Temperature Gradients. *Soc. Pet. Eng. J.* 24, 129–140. <https://doi.org/10.2118/10080-PA>
- Raaen, A.M., Horsrud, P., Kjørholt, H., Økland, D., 2006. Improved routine estimation of the minimum horizontal stress component from extended leak-off tests. *Int. J. Rock Mech. Min. Sci.* 43, 37–48.
- Rai, U.B., Ghodke, N., Schutjens, P., Shete, K., 2014. Fracture Gradient From Leakoff Test: Pitfalls of Using LOT Data From Nonvertical Wells. IADC/SPE Drill. Conf. Exhib. <https://doi.org/10.2118/167963-MS>
- Reginald-Ugwuadu, O.G., Alabi, T.I., Eze, J.O., Ebisike, R.C., 2014. Fracture Gradient Estimation in the Niger Delta - A Practical and Statistical Approach. SPE Niger. Annu. Int. Conf. Exhib. <https://doi.org/10.2118/172481-MS>
- Salz, L.B., 1977. Relationship Between Fracture Propagation Pressure And Pore Pressure. SPE Annu. Fall Tech. Conf. Exhib. <https://doi.org/10.2118/6870-MS>
- Savari, S., Whitfill, D.L., Jamison, D.E., Kumar, A., 2014. A Method to Evaluate Lost Circulation Materials - Investigation of Effective Wellbore Strengthening Applications. IADC/SPE Drill. Conf. Exhib. <https://doi.org/10.2118/167977-MS>
- Schmitt, D.R., Zoback, M.D., 1989. Poroelastic effects in the determination of the maximum horizontal principal stress in hydraulic fracturing tests—a proposed breakdown equation employing a modified effective stress relation for tensile failure, in: International Journal of Rock Mechanics and Mining Sciences & Geomechanics Abstracts. Elsevier, pp. 499–506.
- Short, K., Stauble, A., 1967. Outline of Geology of Niger Delta. *Am. Assoc. Pet. Geol. Bull.* 51, 761–779.
- Song, J., Rojas, J.C., 2006. Preventing Mud Losses by Wellbore Strengthening. SPE Russ. Oil Gas Tech. Conf. Exhib. <https://doi.org/10.2118/101593-MS>
- Swarbrick, R.E., 1995. Distribution and Generation of the Overpressyre System, Eaastern Delaware BAsin, Western Texas and Southern New Mexico: Discussion. *Am. Assoc. Pet. Geol. Bull.* 12, 1386–1405.
- Swarbrick, R.E., Osborne, M.J., 1998. Mechanisms that generate abnormal pressures: an

- overview. Law, B.E., G.F. Ulmishek, V.I. Slavin eds., Abnorm. Press. Hydrocarb. Environ. AAPG Mem. 70 13–34.
- Taylor, D.B., Smith, T.K., 1970. Improved Fracture Gradient Estimates in Offshore Drilling Operations, in: Drilling and Production Practice. American Petroleum Institute.
- Thiercelin, M.J., Plumb, R.A., Desroches, J., Bixenman, P.W., Jonas, J.K., Davie, W.A.R., 1996. A New Wireline Tool for In-Situ Stress Measurements. SPE Form. Eval. 11, 19–25. <https://doi.org/10.2118/25906-PA>
- Ugwu, S.A., Nwankwo, C.N., 2014. Integrated approach to geopressure detection in the X-field, Onshore Niger Delta. J. Pet. Explor. Prod. Technol. 4, 215–231.
- van Oort, E., Vargo, R.F., 2008. Improving Formation-Strength Tests and Their Interpretation. SPE Drill. Complet. 23, 284–294. <https://doi.org/10.2118/105193-PA>
- Vuckovic, V., 1989. Prediction of Fracture Gradients Offshore Australia. SPE Asia-Pacific Conf.
- Wang, H., Soliman, M.Y., Shan, Z., Meng, F., Towler, B.F., 2011. Understanding the effects of leakoff tests on wellbore strength. SPE Drill. Complet. 26, 531–539.
- Wang, H., Soliman, M.Y., Towler, B.F., 2009. Investigation of Factors for Strengthening a Wellbore by Propping Fractures. SPE Drill. Complet. 24, 441–451.
- Weber, K.J., 1987. Hydrocarbon distribution patterns in Nigerian growth fault structures controlled by structural style and stratigraphy. J. Pet. Sci. Eng. 1, 91–104.
- Yassir, N.A., Addis, M.A., Hennig, A., 1998. Relationships between pore pressure and stress in different tectonic settings.
- Zhang, J., 2011. Pore pressure prediction from well logs: Methods, modifications, and new approaches. Earth-Science Rev. 108, 50–63.
- Zhang, J., Alberty, M., Blangy, J.P., 2016. A Semi-Analytical Solution for Estimating the Fracture Width in Wellbore Strengthening Applications. SPE Deep. Drill. Complet. Conf.
- Zhang, J., Yin, S.-X., 2017. Fracture gradient prediction: an overview and an improved method. Pet. Sci. 14, 720–730.
- Zhang, Y., Zhang, J., 2017. Lithology-dependent minimum horizontal stress and in-situ stress estimate. Tectonophysics 703, 1–8.
- Zoback, M.D., 2010. Reservoir geomechanics. Cambridge University Press

Chapter 6

6.0 Real-time Lithology Prediction Using Hydromechanical Specific Energy

Preface

*A version of this chapter has been published in the **Journal of Petroleum Science and Engineering, 2019**. I am the primary author. Co-author Dr. Stephen Butt reviewed the manuscript and provided technical assistance in the development of the concept. I formulated the initial concept and carried out most of the data analysis. I prepared the first draft of the manuscript and revised the manuscript based on the feedback from the co-author.*

Abstract

The previous applications of specific energy to drilling operations have focused mainly on drilling optimization and identification of inefficient drilling conditions. Recent advances in specific energy extend its applications to overpressure detection and pore pressure prediction. In this paper, an attempt is made to further extend the application of specific energy to real-time identification of subsurface lithology. The concept is based on the principle that the total energy required to break and remove a unit volume of rock is a function of lithology. The proposed methodology is tested using a recently drilled exploratory gas well in the tertiary deltaic system of the Niger Delta basin. In general, an excellent agreement is observed in trend between the traditional lithology identifiers (gamma ray and sonic velocity ratio) and the total energy consumed in breaking and removing the penetrated rocks. Unlike the logging while drilling (LWD) technique commonly employed in the industry (including the application of near bit sensors placed few feet behind the bit), the proposed methodology can provide a reliable means

of picking formation tops and identifying subsurface lithology at the bit with no extra cost since drilling parameters are routinely recorded at the wellsite during the drilling of a well. The proposed methodology will assist the drilling engineers and geologists in determining the casing setting depths and coring points without having to drill too deep into the formation of interest.

Keywords: Hydromechanical specific energy, Lithology, Rate of penetration, Drilling, Bit.

6.1 Introduction

Traditionally, real-time detection of lithological boundary and identification of lithology is performed at the wellsite during the drilling of a well using the logging while drilling (LWD) tools. However, there are some critical subsurface drilling conditions where the application of conventional LWD may prove inadequate. For instance, using the conventional LWD tools to determine the coring point of a thin reservoir. Under this condition, a large proportion of the reservoir thickness may be unknowingly penetrated before the conventional LWD is able to identify the formation top of interest, thereby jeopardizing the entire coring operations. The application of near bit LWD allows lithology identification a few feet behind the bit at an extremely high cost. In most cases, the high cost of the near bit sensors may be prohibitive to operating companies, especially the marginal operators. Moreover, while drilling at a great depth in an offshore environment with a floating rig, there is a possibility that the LWD tools may fail when approaching the casing setting depth or coring point with only a few feet remaining to be drilled before calling off the current operations. Under this prohibitive condition of extremely high operating cost, the drilling engineers and geologists will not likely pull out of hole to replace the LWD tools if subsurface lithology can be predicted from readily recorded drilling parameters except for the purpose of reservoir evaluation other than lithology identification. The

applications of cutting descriptions by mud loggers for lithology identification also have their limitations. The associated lag time required to move the drill cuttings from the bottom of the hole to surface and the possibility that the drill cuttings obtained at the shale shakers may not be coming from the bottom of the hole but rather somewhere higher up in the well (especially in unstable wellbore) can make the cutting descriptions unsuitable for determining the casing setting depths and coring points. At best, cutting descriptions are mostly used in conjunction with LWD for confirmation purposes.

Previous attempts to use drilling-related parameters (ROP and d-exponent) to identify subsurface lithology have produced mixed results. The ROP is influenced by several factors which include: the degree of rock compaction, lithology, rotary speed, bit type, weight on bit (WOB), bit size, bit wear, torque, bit hydraulics energy and differential pressure (Bourgoyn and Young, 1973). From an operational point of view, it may not always be possible to maintain the above factors constant during the drilling of a well (Oloruntobi and Butt, 2019a). Therefore, changes in ROP may not necessarily signify changes in subsurface lithology. Although the d-exponent is normalized for the effects of rotary speed, WOB and bit diameter on the ROP (Jorden and Shirley, 1966), one of its major limitations is that the model does not consider the effect of bit hydraulic energy on the ROP. This limits the application of d-exponent to hard rocks and makes it unsuitable to most unconsolidated sediments where the bit hydraulic energy assists in breaking the rock ahead of the bit. There are also instances when the driller decides to increase the flow rate for hole cleaning, reduces the flow rate to minimize loss circulation incidents, change the nozzle sizes for drilling optimization purposes or change the mud weight for well control and wellbore stability purposes. Under such circumstances of fluctuating bit hydraulic energy, the use of d-exponent for lithology identification may lead to wrong interpretation.

The mechanical specific energy was first defined by Teale (1965) as the amount of energy required to remove a unit volume of rock (the sum of axial and rotary energies):

$$MSE = \frac{WOB}{A_b} + \frac{120\pi NT}{A_b ROP} \quad (6.1)$$

where MSE is the mechanical specific energy (psi); WOB is the downhole weight on bit (lbs); A_b is the bit area (in^2); N is the rotary speed (rpm); T is the torque on bit (lb-ft); ROP is the rate of penetration (ft/hr). Because the majority of the field data are recorded by the surface sensors under normal circumstances, Pessier and Fear (1992) proposed a relationship among the downhole torque, bit diameter (D_b) and WOB:

$$T = \frac{\mu * D_b * WOB}{36}, \quad (6.2)$$

where T is the downhole torque (lb-ft); D_b is the bit diameter (in); WOB is the weight on bit (lbs); μ is the bit specific coefficient of sliding friction. The bit coefficient of sliding friction depends on several factors which include rock confined compressive strength, lithology, depth of cut, mud weight, cutter density/blade count (for PDC bits), cutter sizes and bit wear (Caicedo et al. 2005; Guerrero & Kull 2007). Pessier and Fear combined equations 6.1 and 6.2 to produce equation 6.3:

$$MSE = \frac{WOB}{A_b} + \frac{13.33\mu NWOB}{D_b ROP}. \quad (6.3)$$

The real-time application of MSE is a valuable tool for both drillers and drilling engineers (Koederitz and Weis, 2005). The MSE surveillance has proved to be an effective tool in identifying downhole drilling problems and optimizing drilling operations (Dupriest et al., 2005;

Dupriest, 2006; Amadi & Iyalla, 2012; Bevilacqua et al., 2013; Pinto & Lima, 2016). Rabia (1985) used the concept of modified specific energy for bit selection. Waughman et al. (2003) also used the specific energy concept to determine when to pull worn poly polycrystalline diamond compact (PDC) bit in oil-based mud. To improve the usefulness of MSE surveillance in field operations, the original mechanical specific energy equation as derived by Teale (1965) was adjusted to include a mechanical drilling efficiency factor (Dupriest & Koederitz, 2005). Armenta (2008) showed the importance of including the bit hydraulic energy term into the MSE model. The results of extensive experimental studies conducted by Rajabov et al. (2012) on three different rock types (Carthage marble, Mancos shale, and Torrey Buff sandstone) showed that the mechanical specific energy of PDC cutters increases with increasing back rake angle at both atmospheric and confining pressure conditions. Abbas et al. (2014) combined the bit dullness model (dimensionless torque and dimensionless rate of penetration) and MSE to determine the downhole drill bit conditions where torque data is unavailable. Abbott (2015) used the mechanical specific energy ratio (MSER) to optimize real-time drilling performance for underreaming operations. Menand and Mills (2017) used the combination of MSE and MSE-DS (drilling strength) ratio to detect vibration, bit balling, and bit wear. Wei et al. (2016) used the MSE plus hydraulic energy to identify abnormal conditions for pulsed-jet drilling. Zhou et al. (2017) proposed a model that relates MSE to the depth of cut for a circular cutter. Laboratory investigations have shown the dependency of MSE on differential/confining pressure (Rafatian et al. 2010; Akbari et al. 2013). Akbari et al. (2014) established a relationship among MSE, uniaxial compressive strength, differential pressure, and confining pressure:

$$\text{MSE} = \text{UCS} + \left[a + b^{\frac{\Delta P}{P_c}} \right] \ln \frac{P_c}{P_{\text{atm}}}, \quad (6.4)$$

where MSE is the mechanical specific energy (psi); UCS is the uniaxial compressive strength (psi); ΔP is the differential pressure between confining pressure and pore pressure (psi); P_c is the confining pressure (psi); P_{atm} is the atmospheric pressure (psi); a is the coefficient that is dependent on rock internal friction angle; b is the coefficient that is dependent on rock permeability, porosity, fluid viscosity, fluid compressibility, rotary speed and depth of the cut. The dependency of specific energy on differential pressure has been explored for pore pressure predictions (Cardona, 2011; Majidi et al., 2017; Oloruntobi et al., 2018).

Currently, the applications of specific energy to drilling operations can be classified into three categories: (1) drilling optimization; (2) identification of drilling problems; (3) pore pressure prediction. In this paper, an attempt is made to extend the application of specific energy to real-time detection of lithological boundaries and identification of subsurface lithology.

6.2 Methodology

The mechanical drilling efficiency factor (MDEF) is defined as the ratio between the rock's confined compressive strength (CCS) and the MSE:

$$MDEF = \frac{CCS}{MSE} \quad (6.5)$$

The value of MDEF is typically between 0.3 and 0.4 for most drilling conditions (Dupriest & Koederitz, 2005). Based on the Mohr-Coulomb criterion, the CCS is given by:

$$CCS = UCS + \Delta P \left[\frac{1 - \sin \theta}{1 + \sin \theta} \right] \quad (6.6)$$

where UCS is the unconfined compressive strength (psi); ΔP is the differential pressure between

the bottom-hole pressure and formation pore pressure (psi); θ is the angle of internal friction (degrees). Equations 6.5 and 6.6 can be combined to obtain equation 6.7:

$$MSE = \frac{1}{MDEF} \left[UCS + \Delta P \left[\frac{1 - \sin \theta}{1 + \sin \theta} \right] \right] \quad (6.7)$$

Equation 6.7 clearly demonstrates that the drilling response (specific energy) is a function of rock properties (UCS and θ) which are lithology dependent, differential pressure (ΔP) and bit conditions (MDEF). Therefore, changes in specific energy can be used to identify changes in lithology if the drilling environment is known or changes in lithological boundary if the drilling environment is not known. Note that changes in lithological boundary will also indicate variation in the stratigraphic unit. Moreover, changes in specific energy can also be used to identify downhole bit conditions and subsurface pressure regimes.

However, the MSE does not necessarily represent the total energy consumed in removing a unit volume of rock because it excludes the bit hydraulic energy (Oloruntobi et al., 2018). In soft rock environments, the bit hydraulic energy contributes to the total energy required to remove a unit volume of rock by weakening the rocks ahead of the bit. The hydromechanical specific energy (HMSE) is the total energy consumed during the drilling of a well (Mohan et al. 2015; Chen et al. 2016; Wei et al., 2016; Oloruntobi and Butt, 2019). The HMSE is the combination of the axial, rotary, and hydraulic energies (equation 6.8):

$$HMSE = Axial\ Energy + Rotary\ Energy + Hydraulic\ Energy \quad (6.8)$$

$$HMSE = MSE + Hydraulic\ Energy \quad (6.9)$$

In the expanded form, the hydromechanical specific energy is given by:

$$HMSE = \frac{WOB}{A_b} + \frac{120\pi NT}{A_b ROP} + \frac{1154\eta\Delta P_b Q}{A_b ROP} \quad (6.10)$$

where WOB is the downhole weight on bit (lbs); A_b is the bit area (in^2); N is the rotary speed (rpm); T is the torque on bit (lb-ft); ROP is the rate of penetration (ft/hr); ΔP_b is the bit pressure drop (psi); Q is the flow rate (gpm); η is the hydraulic energy reduction factor. Due to accelerated fluid entrainment immediately below the jet nozzles during drilling, only a portion (25 – 40%) of the available bit hydraulic energy actually reaches the bottom of the hole (Warren, 1987). The hydraulic energy reduction factor converts the jet hydraulic energy into the bottom-hole hydraulic energy. For polycrystalline diamond compact (PDC) bits, the hydraulic energy reduction factor ($\eta_{PDC\ Bit}$) can be expressed as a function of the junk slot area and total flow area (Oloruntobi et al., 2018):

$$\eta_{PDC\ Bit} = 1 - \left[\frac{JSA}{TFA} \right]^{-0.122} \quad (6.11)$$

where JSA is the junk slot area (in^2); TFA is the total flow area (in^2). For roller cone bits (RCB), the hydraulic energy reduction factor is expressed as a function of bit area and total flow area Warren (1987):

$$\eta_{RCB} = 1 - \left[\frac{0.15 \text{ Bit Area}}{TFA} \right]^{-0.122} \quad (6.12)$$

The pressure drop at the bit nozzle is expressed as a function of circulating fluid density, volumetric flow rate, and nozzle total flow area:

$$\Delta P_b = \frac{MW Q^2}{10858 TFA^2}, \quad (6.13)$$

where ΔP_b is the bit pressure drop (psi); MW is the mud weight (ppg); Q is the flow rate (gpm); TFA is the total flow area (in^2). The hydromechanical specific energy consumed while drilling with PDC bits can be obtained by combining equations 6.10, 6.11 and 6.13:

$$\text{HMSE}_{\text{PDC}} = \frac{\text{WOB}}{A_b} + \frac{120\pi NT}{A_b \text{ROP}} + \frac{1154 \text{ MW } Q^3 \left[1 - \left[\frac{\text{JSA}}{\text{TFA}} \right]^{-0.122} \right]}{10858 A_b \text{ROP TFA}^2} \quad (6.14)$$

The hydromechanical specific energy consumed while drilling with roller cone bits can be obtained by combining equations 6.10, 6.12 and 6.13:

$$\text{HMSE}_{\text{RCB}} = \frac{\text{WOB}}{A_b} + \frac{120\pi NT}{A_b \text{ROP}} + \frac{1154 \text{ MW } Q^3 \left[1 - \left[\frac{0.15 \text{ Bit Area}}{\text{TFA}} \right]^{-0.122} \right]}{10858 A_b \text{ROP TFA}^2} \quad (6.15)$$

It is acknowledged that the HMSE may be affected by several factors other than subsurface lithology. These factors include rock compaction, bit wear, bit type and the differential pressure between the bottom-hole pressure (dictated by equivalent circulating density: ECD) and the formation pore pressure. In normally pressured intervals, rock compaction typically increases with depth due to an increase in effective stress. Hence, the energy required to break and remove a unit volume of rock will also increase with depth. Generally, bit wear will cause an increase in the HMSE due to reduction in the rate of penetration. The application of different bit type in the same hole section will produce different HMSE signature due to variation in cutting structure. An increase in the strength of the surrounding rocks due to an increase in the downhole differential pressure will result in an increase in the HMSE. The effect of differential pressure on the ROP (hence, HMSE) is more pronounced at low values of overbalance than at high values of overbalance (Vidrine and Benit, 1968; Black et al. 1985; Bourgoyn et al., 1986). Although lithology is the major factor controlling the HMSE changes, if the effects of other factors on the

HMSE can be minimized, changes in the HMSE can be directly attributed to lithological changes due to changes in drillability corresponding to different rocks types.

Based on Athy (1930) porosity compaction model (equation 6.16), the HMSE can be normalized for rock compaction effect (equations 6.16 and 6.17):

$$\emptyset = \emptyset_o e^{-kZ} \quad (6.16)$$

$$HMSE_{PDC} = \left[\frac{WOB}{A_b} + \frac{120\pi NT}{A_b ROP} + \frac{1154 MW Q^3 \left[1 - \left[\frac{JSA}{TFA} \right]^{-0.122} \right]}{10858 A_b ROP TFA^2} \right] \emptyset_o e^{-kZ} \quad (6.17)$$

$$HMSE_{RCB} = \left[\frac{WOB}{A_b} + \frac{120\pi NT}{A_b ROP} + \frac{1154 MW Q^3 \left[1 - \left[\frac{0.15 \text{ Bit Area}}{TFA} \right]^{-0.122} \right]}{10858 A_b ROP TFA^2} \right] \emptyset_o e^{-kZ} \quad (6.18)$$

where \emptyset_o is the surface/mudline porosity (fraction); Z is the true vertical depth (ft); k is the compaction coefficient (1/ft). The value of \emptyset_o ranges between 0.40 and 0.70, depending on the lithology and environment of deposition (Meade, 1966; Burrus, 1998; Swarbrick and Osborne, 1998; Zoback, 2010). It is widely known that different lithologies will compact at different rates and from contrasting surface/mudline porosities (Swarbrick, 2001). Therefore, a line of best fit through an offset well data that consists of several stratigraphic units can be used to calibrate the compaction coefficient and surface/mudline porosity.

For practical purposes, the effects of bit wear and bit type on the HMSE can be minimized by analyzing the HMSE over short intervals drilled with a single bit. The short intervals will ensure that the bit dulling is within tolerable range and the single bit will ensure the effect of bit type on the HMSE is eliminated. Interval of analysis to minimize bit wear effect should be obtained from the offset data. Therefore, over the intervals where the bit dulling is

within an acceptable range, any changes in the HMSE trend will either indicate changes in lithology or changes in differential pressure. The changes caused by differential pressure are more gradual: gradual decrease in the HMSE may indicate drilling through the pressure transition zones as formation pore pressure increases while the gradual increase in the HMSE may indicate the amount of overbalance is becoming excessive. However, the changes caused by lithology are typically abrupt and easily identified. Since lithology identification is the objective; any sudden changes in the HMSE trend will indicate changes in lithology. When plotted against depth on semi-log, the HMSE computed using equation 6.17 or 6.18 should be able to identify the various stratigraphic units being penetrated.

If available, downhole measurements of torque and WOB from the measurement while drilling (MWD) tools should be used to estimate the HMSE. Using the drilling parameters obtained from surface measurements to estimate the HMSE can introduce significant errors especially in moderately to highly deviated wells ($> 20^\circ$ inclination) due to the presence of friction between the drill string and the borehole walls. The application of drilling data obtained from surface measurements to compute the HMSE is possible in vertical wells since the friction between the drill string and the walls of the borehole is usually negligible.

6.3 Field Example

To demonstrate the usefulness of the proposed methodology, an exploratory gas well (Well A) located approximately 83 km northwest of Port Harcourt in the central swamp region of the Niger Delta basin is considered as the case study. Well A is a slightly deviated well with a maximum inclination of 14.6° . Figure 6.1 shows the location of the well under consideration. The Niger Delta is an extensional rift basin system that consists of three types of formations in

descending order: (1) Benin formation - this formation consists of mostly continental loose sands, (2) Agbada formation - this formation consists of alternating sequence of sands and shales where commercial accumulation of hydrocarbons are found, and (3) Akata formation - this formation consists of thick marine shales. (Oloruntobi and Butt, 2019b; Oloruntobi et al., 2019; Yusuf et al., 2019). The detailed geology and hydrocarbon system of the basin can be obtained from the literature (Short and Stauble, 1967; Burke, 1972; Daukoru 1975; Avbovbo, 1978; Evamy et al., 1978; Nwachukwu and Chukwura, 1986; Weber 1987; Doust, 1990; Doust and Omatsola, 1990; Reijers 2011).

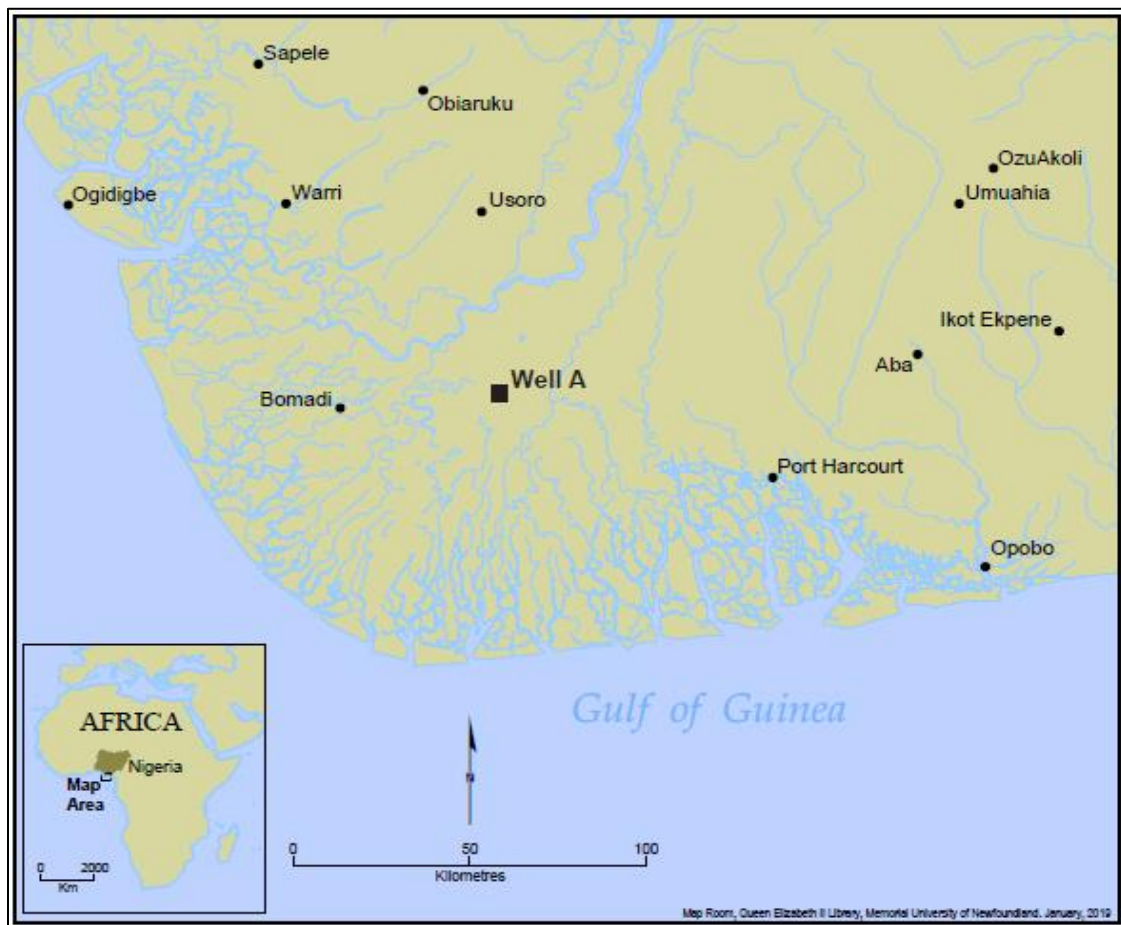


Figure 6 1: The location map for Well A.

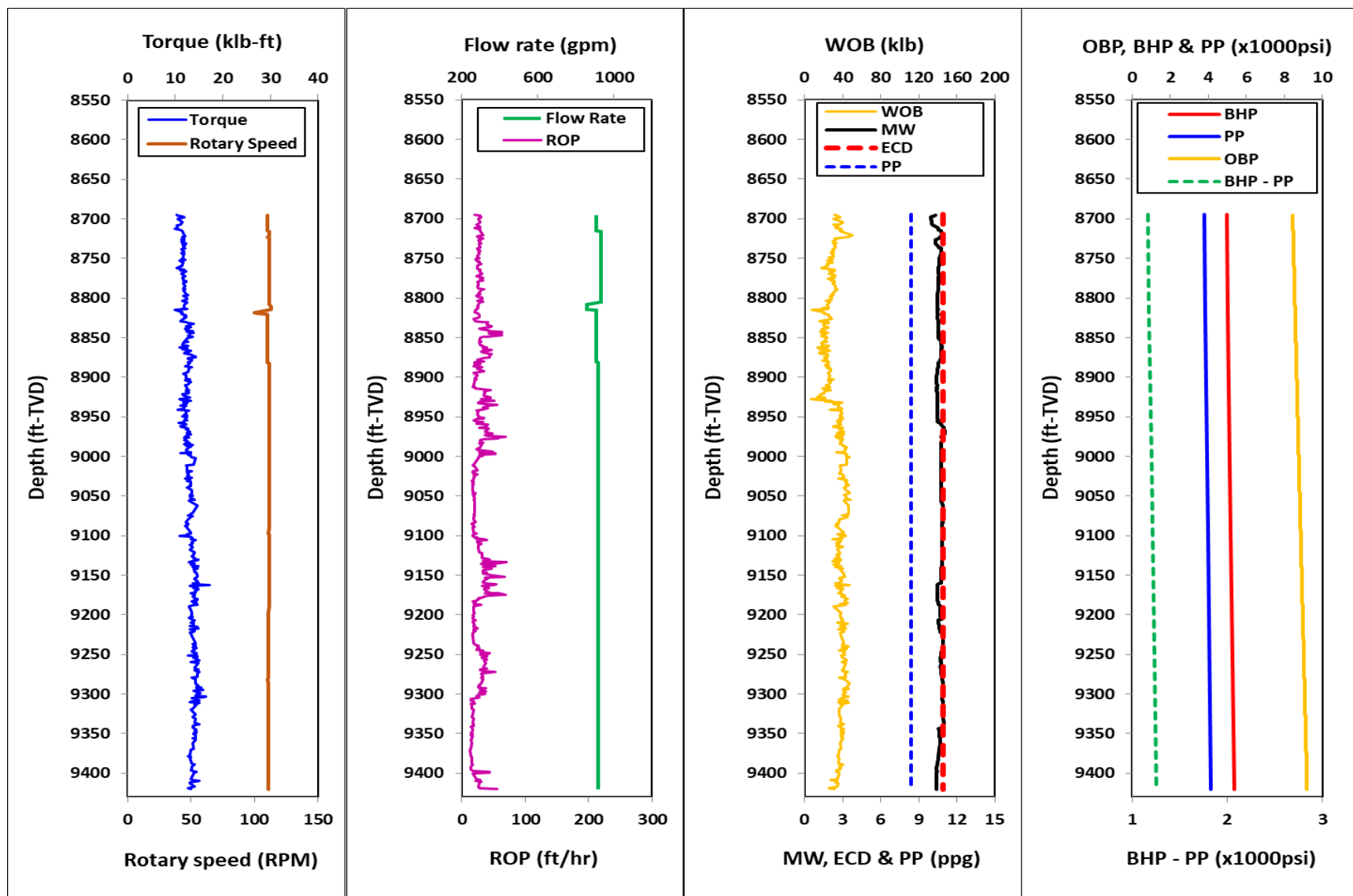


Figure 6 2: The plots of drilling parameters and wellbore pressures versus depth for Well A (Interval 1).

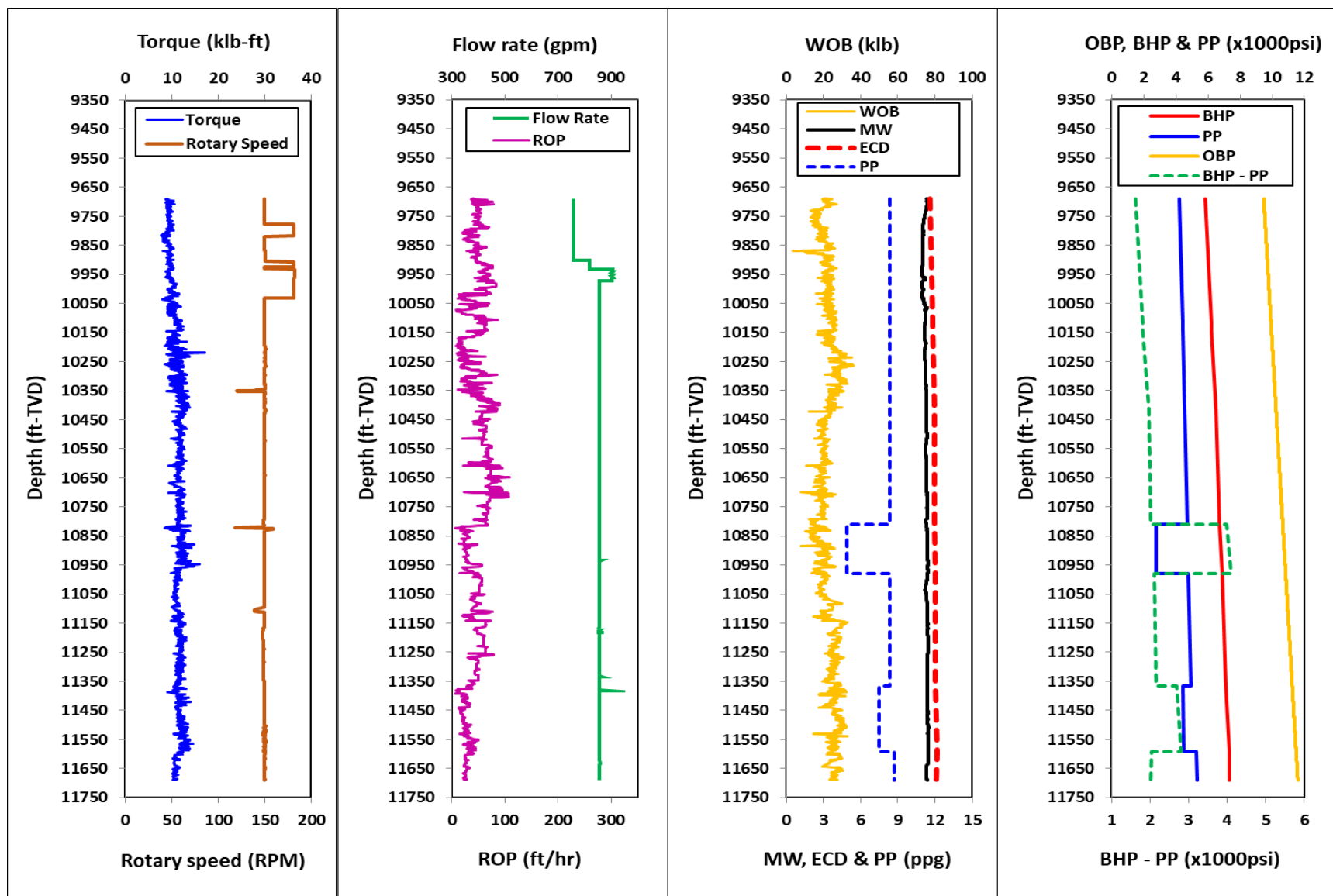


Figure 6 3: The plots of drilling parameters and wellbore pressures versus depth for Well A (Interval 2).

Figures 6.2 and 6.3 display the recorded drilling parameters and wellbore pressures for two separate intervals in Well A. The recorded data include torque, rotary speed, flow rate, rate of penetration (ROP), weight on bit (WOB), equivalent circulating density (ECD), mud weight (MW) and pore pressure (PP). The bottom-hole pressure (BHP) is obtained from the ECD. The recorded drilling parameters were obtained from surface measurements. These data were then checked for identification and elimination of outliers. The errors associated with using the drilling data obtained from surface measurements to compute the HMSE in this well may be negligible because the well maximum inclination is low ($< 15^\circ$), the intervals under consideration are short (≤ 2000 ft), the kick-off point is deep (7,878 ft) and the dogleg severities (DLS) do not exceed $1.5^0/100$ ft anywhere across the intervals. Over short intervals in low inclination wells at low DLS, changes in friction forces between the drill string and the borehole walls can be negligible.

In interval 1 (Figure 6.2), the recorded drilling parameters were acquired in the 16" hole section drilled with a single roller cone (milled tooth) bit from 8,695 ft to 9,420 ft. The interval was drilled with water-based mud and the total flow area (TFA) of the roller cone bit is 1.1689 in². The formation pore pressure is normal across all the penetrated rocks with an average gradient of 0.435 psi/ft. In interval 2 (Figure 6.3), the recorded drilling parameters were acquired in the 12 1/4" hole section drilled with a single PDC bit from 9,690 ft to 11,690 ft. The total flow area (TFA) of the PDC bit is 1.2003 in² and its junk slot area (JSA) is 21.28 in². The interval was drilled with oil-based mud and the formation pore pressure varies across the penetrated rocks between 0.254 psi/ft and 0.455 psi/ft. This interval consists of both normally pressured zones and two depleted sands.

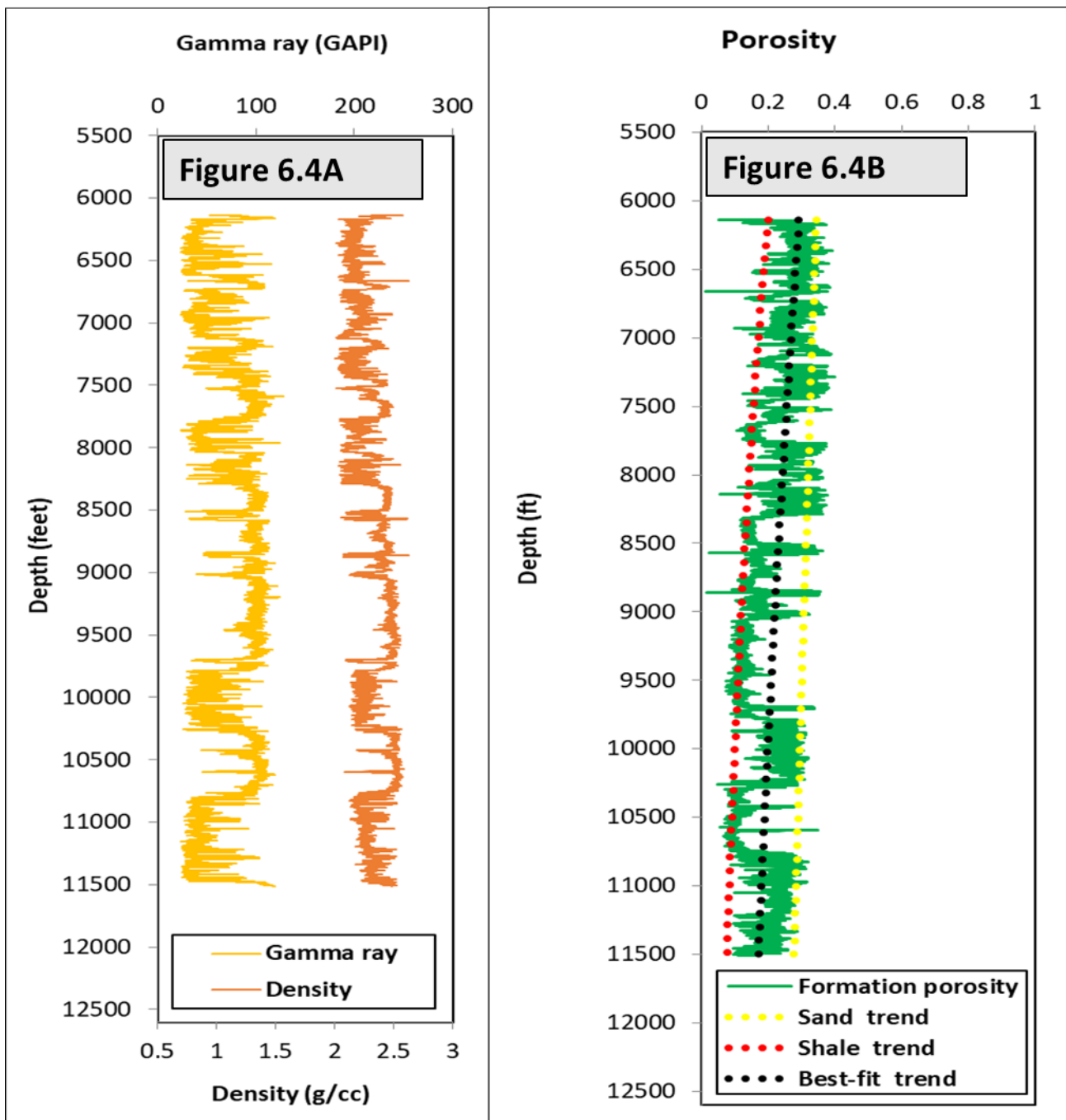


Figure 6.4: The offset well data used to calibrate ϕ_0 and k.

To obtain the rock compaction coefficient (k) and the surface porosity (ϕ_0), equation 6.16 is calibrated to an offset well in the basin. Figure 6.4B shows the plot of porosity against depth.

The red dotted line corresponds to the shale compaction trend (equation 6.19). The yellow dotted line corresponds to the sand compaction trend (equation 6.20). The black dotted line corresponds to a line of best fit through the various stratigraphic units (equation 6.21).

$$\emptyset = 0.60e^{-0.00018*Z} \quad (6.19)$$

$$\emptyset = 0.448e^{-0.00004*Z} \quad (6.20)$$

$$\emptyset = 0.54e^{-0.0001*Z} \quad (6.21)$$

In this paper, equation 6.21 is used to normalize the HMSE for rock compaction effect for all the lithologies with the rock compaction coefficient and the surface porosity being 0.0001 1/ft and 0.54 (fraction) respectively. Using equation 6.21 to normalize the HMSE for all the lithologies will only introduce small error which can be acceptable. The formation porosity (\emptyset) is estimated using equation 6.22:

$$\emptyset = \left[\frac{\rho_{ma}}{\rho_{ma} - \rho_{fl}} \right] - \left[\frac{1}{\rho_{ma} - \rho_{fl}} \right] \rho_b - \left[\frac{\rho_{ma} - \rho_{sh}}{\rho_{ma} - \rho_{fl}} \right] V_{sh} \quad (6.22)$$

where \emptyset is the formation porosity (fraction); ρ_{ma} is the sand matrix density (g/cc); ρ_{sh} is the shale matrix density (g/cc); ρ_{fl} is the saturating fluid density which is typically assumed to be 1.00 g/cc; ρ_b is the measured formation bulk density (g/cc) V_{sh} is the shale volume (fraction). In the Niger Delta, the values of sand matrix density and shale matrix density are 2.65 g/cc and 2.68 g/cc respectively. For the Niger Delta sediments, field observations have shown that a linear relationship exists between shale volume and gamma ray index (I_{GR}). Therefore, shale volume is obtained using equation 6.23:

$$V_{sh} = I_{GR} = \frac{GR_{log} - GR_{min}}{GR_{max} - GR_{min}} \quad (6.23)$$

where GR_{log} is the gamma ray reading at any given depth; GR_{min} is the sand line gamma ray reading; GR_{max} is the shale line gamma ray reading. However, other non-linear empirical responses between shale volume and gamma ray index exist depending on the formation age and geographic area (Larionov, 1969; Stieber, 1970; Clavier et al., 1971; Assaad, 2008).

6.4 Discussion

Figure 6.5A shows the GR-depth and HMSE-depth plots for interval 1. The HMSE is computed using equation 6.18 because the interval was drilled with a roller cone bit. An excellent agreement in trend is observed between the gamma ray (GR) and the HMSE. This clearly demonstrates the applicability of the HMSE to lithology identification. Abrupt changes in the HMSE trend indicate lithological changes. In shale formations as indicated by high GR, higher specific energy is consumed in removing the rocks. However, in sand formations as indicated by low GR, lower specific energy is consumed in removing the rocks. A shale baseline drawn through the interval indicates that the shale formation between 8,695 ft and 8,826 ft required lower energy to drilled than the remaining deeper shale formations. This is probably due to bit dulling effects on the HMSE.

Figure 6.5B shows the GR-depth, velocity ratio-depth and HMSE-depth plots for interval 2. The velocity ratio is derived from the ratio of compressional to shear velocities. Note that the display unit of velocity ratio is in 1/100 for ease of interpretation.

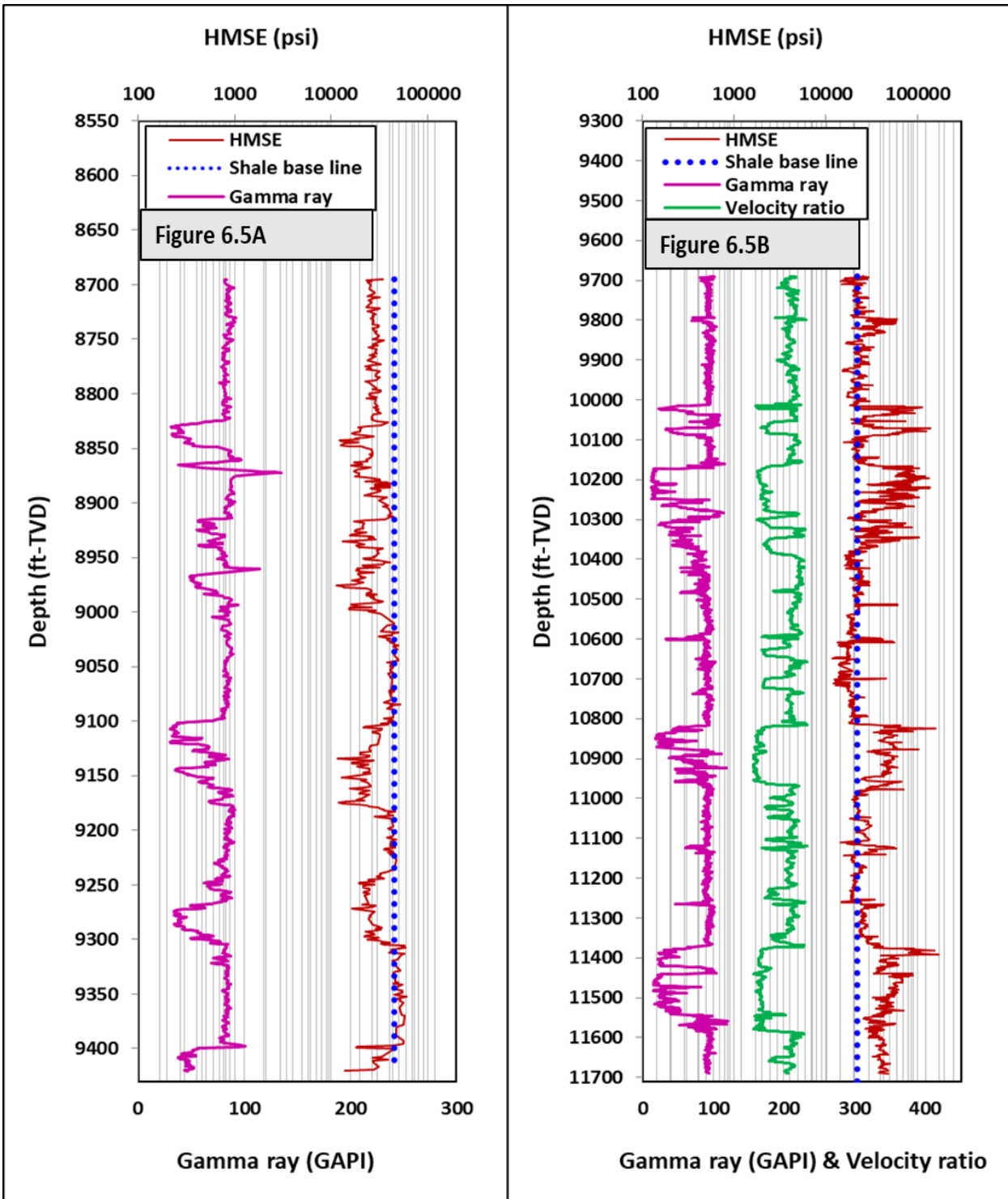


Figure 6.5: The GR-depth, VR-depth and HMSE-depth plots for Well A.

The HMSE is computed using equation 6.17 because the interval was drilled with PDC bit. A good agreement exists between the conventional lithology identifiers and the HMSE. In shale formations as indicated by high GR and high velocity ratio, lower specific energy is consumed in breaking the rocks. In sand formations as indicated by low GR and low velocity ratio, higher specific energy is consumed in breaking the rocks. The formation tops are clearly visible with abrupt changes in the HMSE. Remarkably, the HMSE is able to identify the very tiny sands (minor reservoirs), confirming the accuracy of the proposed methodology. The HMSE values in the shale intervals trail the shale baseline except at depths greater than 11,600 ft where the HMSE values in the bottom shale interval begin to shift from the shale baseline possibly due to bit dulling effects. If the longer interval of analysis is considered, the effects of bit dulling on the HMSE may be more pronounced, making evaluations more complex and difficult. The conflicting responses of roller cone and PDC bits in the same lithology are mainly due to their cutting actions. Each bit type drills hole in a different manner. The roller cone bit crushes the formations while the PDC bit shears the formations. The abrupt changes in the HMSE at the formation tops indicate that the effect of lithology on the HMSE dominates the drilling process.

6.5 Conclusions

In addition to drilling optimization and identification of drilling problems, the applications of HMSE have been extended to real-time identification of lithology. Lithology identification using the HMSE concept is based on observing trend changes. Any abrupt change in the HMSE trend can be directly attributed to lithological change. The proposed methodology can provide a reliable means of picking formation tops and identifying the various stratigraphic units being penetrated at a relatively low cost. The proposed methodology can serve as an excellent

correlation tool in wells where petrophysical data are either not available or poorly acquired. To ease interpretation, the drill bit responses (HMSE signatures) in different lithologies may be predicted in advance by applying the HMSE concept to the offset data. Since PDC and roller cone bits produce different HMSE responses, intervals drilled with two different types of bits should not be analyzed together. The HMSE-depth plot for each bit run should be entirely separated from the other bit runs.

The ability of the proposed methodology to be able to accurately identify subsurface lithology will depend on the quality of the input data. Computation of HMSE using drilling parameters that are subjected to severe vibrations will produce inaccurate results. The quality of the input data can be improved in several ways: (1) measured parameters should be compared to model parameters; (2) surface/downhole sensors should be calibrated before use; (3) If possible, measurements should be taken using different sensors for comparison purposes; (4) Noise in the data transmission system should be minimized; (5) Shocks and vibrations can be controlled by incorporating the shock sub into the bottom-hole assembly (BHA), optimizing drilling parameters (weight on bit and rotary speed) and selecting the right bit/BHA.

6.6 Reference

- Abbas, K.R., Hassanpou, A., Hare, C., Ghadiri, M., 2014. “Instantaneous Monitoring of Drill Bit Wear and Specific Energy as a Criteria for the Appropriate Time for Pulling Out Worn Bits.” Soc. Pet. Eng. (SPE 172269).
- Abbott, A., 2015. The MSE Ratio: The New Diagnostic Tool to Optimize Drilling Performance in Real-Time for Under-Reaming Operations. SPE Annu. Tech. Conf. Exhib. <https://doi.org/10.2118/178724-STU>
- Akbari, B., Miska, S., Mengjiao, Y., Ozbayoglu, E., 2013. Effect of Rock Pore Pressure on

- Mechanical Specific Energy of Rock Cutting Using Single PDC Cutter, in: 47th US Rock Mechanics/Geomechanics Symposium. American Rock Mechanics Association.
- Akbari, B., Miska, S., Yu, M., Ozbayoglu, M., 2014. Experimental Investigations of the Effect of the Pore Pressure on the MSE and Drilling Strength of a PDC Bit. Soc. Pet. Eng. (SPE 169488). <https://doi.org/10.2118/169488-MS>
- Amadi, W.K., Iyalla, I., 2012. Application of Mechanical Specific Energy Techniques in Reducing Drilling Cost in Deepwater Development, in: SPE Deepwater Drilling and Completions Conference. Society of Petroleum Engineers.
- Armenta, M., 2008. Identifying Inefficient Drilling Conditions Using Drilling-Specific Energy. Soc. Pet. Eng. (SPE 116667). <https://doi.org/10.2118/116667-MS>
- Assaad, F.A., 2008. Field methods for petroleum geologists: A guide to computerized lithostratigraphic correlation charts case study: Northern Africa. Springer Science & Business Media.
- Athy, L.F., 1930. Density, Porosity, and Compaction of Sedimentary Rocks. Am. Assoc. Pet. Geol. Bull. 14, 194–200. <https://doi.org/10.1306/3D93289E-16B1-11D7-8645000102C1865D>
- Avbovbo, A.A., 1978. Tertiary lithostratigraphy of the Niger Delta. Am. Assoc. Pet. Geol. Bull. 62, 295–306.
- Bevilacqua, M., Ciarapica, F.E., Marchetti, B., 2013. Acquisition, processing and evaluation of down hole data for monitoring efficiency of drilling processes. J. Pet. Sci. Res.
- Black, A.D., Dearing, H.L., DiBona, B.G., 1985. Effects of Pore Pressure and Mud Filtration on Drilling Rates in a Permeable Sandstone. J. Pet. Technol. 37, 1671–1681. <https://doi.org/10.2118/12117-PA>
- Bourgoine, A.T., Millheim, K.K., Chenevert, M.E., Young, F.S., 1986. Applied Drilling Engineering (SPE Textbook Series, Vol. 2). Soc. Pet. Eng. Richardson, TX.
- Bourgoine, J.A.T., Young, J.F.S., 1973. Formation Evaluation and Abnormal Pressure Detection. SPWLA Fourteenth Annu. Logging Symp. MAY 6-9,. <https://doi.org/10.1016/B978-0-323-04184-3.50079-0>
- Burke, K., 1972. Longshore drift, submarine canyons, and submarine fans in development of Niger Delta. Am. Assoc. Pet. Geol. Bull. 56, 1975–1983.

- Burrus, J., 1998. Memoir 70, Chapter 3: Overpressure models for clastic rocks, their relation to hydrocarbon.
- Caicedo, H.U., Calhoun, W.M., Ewy, R.T., 2005. Unique ROP Predictor Using Bit-specific Coefficient of Sliding Friction and Mechanical Efficiency as a Function of Confined Compressive Strength Impacts Drilling Performance. Soc. Pet. Eng. (SPE/IADC 92576). <https://doi.org/10.2118/92576-MS>
- Cardona, J., 2011. Fundamental Investigation of Pore Pressure Prediction during Drilling from the Mechanical Behaviour of Rocks. PhD Thesis, Texas A&M Univ. Mech. Eng.
- Chen, X., Gao, D., Guo, B., Feng, Y., 2016. Real-time optimization of drilling parameters based on mechanical specific energy for rotating drilling with positive displacement motor in the hard formation. *J. Nat. Gas Sci. Eng.* 35, 686–694.
- Clavier, C., Hoyle, W., Meunier, D., 1971. Quantitative interpretation of thermal neutron decay time logs: part I. Fundamentals and techniques. *J. Pet. Technol.* 23, 743–755.
- Daukoru, J.W., 1975. PD 4(1) Petroleum Geology of the Niger Delta. World Pet. Congr.
- Doust, H., 1990. Petroleum geology of the Niger Delta. *Geol. Soc. London, Spec. Publ.* 50, 365.
- Doust, H., Omatsola, E., 1990. Niger Delta, in: Divergent / Passive Margin Basins. pp. 201–238.
- Dupriest, F.E., 2006. Comprehensive Drill-Rate Management Process To Maximize Rate of Penetration. Soc. Pet. Eng. (SPE 102210). <https://doi.org/10.2118/102210-MS>
- Dupriest, F.E., Koederitz, W.L., 2005. Maximizing drill rates with real-time surveillance of mechanical specific energy, in: SPE/IADC Drilling Conference. Society of Petroleum Engineers.
- Dupriest, F.E., Witt, J.W., Remmert, S.M., 2005. Maximizing ROP with real-time analysis of digital data and MSE, in: International Petroleum Technology Conference. International Petroleum Technology Conference.
- Evamy, B.D., Haremboure, J., Kamerling, P., Knaap, W.A., Molloy, F.A., Rowlands, P.H., 1978. Hydrocarbon habitat of Tertiary Niger delta. *Am. Assoc. Pet. Geol. Bull.* 62, 1–39.
- Guerrero, C.A., Kull, B.J., 2007. Deployment Of An SeROP Predictor Tool For Real-Time Bit Optimization. SPE/IADC Drill. Conf. <https://doi.org/10.2118/105201-MS>
- Jorden, J.R., Shirley, O.J., 1966. Application of Drilling Performance Data to Overpressure Detection. *J. Pet. Technol.* 18, 1387–1394. <https://doi.org/10.2118/1407-PA>

- Koederitz, W., Weis, J., 2005. A Real-Time Implementation of MSE, American Association of Drilling Engineers. AADE-05-NTCE-66.
- Larionov, V. V., 1969. Radiometry of boreholes. Nedra, Moscow 127.
- Majidi, R., Albertin, M., Last, N., 2017. Pore-Pressure Estimation by Use of Mechanical Specific Energy and Drilling Efficiency. SPE Drill. Complet. 32, 97–104.
- Meade, R.H., 1966. Factors influencing the early stages of the compaction of clays and sands-- review. J. Sediment. Res. 36.
- Menand, S., Mills, K., 2017. Use of Mechanical Specific Energy Calculation in Real-Time to Better Detect Vibrations and Bit Wear While Drilling. Am. Assoc. Drill. Eng.
- Mohan, K., Adil, F., Samuel, R., 2015. Comprehensive Hydromechanical Specific Energy Calculation for Drilling Efficiency. J. Energy Resour. Technol. 137, 012904. <https://doi.org/10.1115/1.4028272>
- Nwachukwu, J.I., Chukwura, P.I., 1986. Organic matter of Agbada Formation, Niger Delta, Nigeria. Am. Assoc. Pet. Geol. Bull. 70, 48–55.
- Oloruntobi, O., Adedigba, S., Khan, F., Chunduru, R., Butt, S., 2018. Overpressure prediction using the hydro-rotary specific energy concept. J. Nat. Gas Sci. Eng. 55, 243–253.
- Oloruntobi, O., Butt, S., 2019a. Energy-based formation pressure prediction. J. Pet. Sci. Eng. 173, 955–964.
- Oloruntobi, O., Butt, S., 2019b. The New Formation Bulk Density Predictions for Siliciclastic Rocks. J. Pet. Sci. Eng. 180, 526–537. <https://doi.org/https://doi.org/10.1016/j.petrol.2019.05.017>
- Oloruntobi, O., Onalo, D., Adedigba, S., James, L., Chunduru, R., Butt, S., 2019. Data-driven shear wave velocity prediction model for siliciclastic rocks. J. Pet. Sci. Eng. 106293. <https://doi.org/https://doi.org/10.1016/j.petrol.2019.106293>
- Pessier, R.C., Fear, M.J., 1992. Quantifying Common Drilling Problems With Mechanical Specific Energy and a Bit-Specific Coefficient of Sliding Friction. Soc. Pet. Eng. (SPE 24584). <https://doi.org/10.2118/24584-MS>
- Pinto, C.N., Lima, A.L.P., 2016. Mechanical Specific Energy for Drilling Optimization in Deepwater Brazilian Salt Environments. Soc. Pet. Eng. (IADC/SPE 180646). <https://doi.org/10.2118/180646-MS>

- Rabia, H., 1985. Specific energy as a criterion for bit selection. *J. Pet. Technol.* 37, 1225–1229.
<https://doi.org/10.2118/12355-PA>
- Rafatian, N., Miska, S.Z., Ledgerwood, L.W., Yu, M., Ahmed, R., Takach, N.E., 2010. Experimental study of MSE of a single PDC cutter interacting with rock under simulated pressurized conditions. *SPE Drill. Complet.* 25, 10–18.
- Rajabov, V., Miska, S.Z., Mortimer, L., Yu, M., Ozbayoglu, M.E., 2012. The Effects of Back Rake and Side Rake Angles on Mechanical Specific Energy of Single PDC Cutters with Selected Rocks at Varying Depth of Cuts and Confining Pressures. *IADC/SPE Drill. Conf. Exhib.* <https://doi.org/10.2118/151406-MS>
- Reijers, T., 2011. Stratigraphy and sedimentology of the Niger Delta. *Geologos* 17, 133–162.
- Short, K., Stauble, A., 1967. Outline of Geology of Niger Delta. *Am. Assoc. Pet. Geol. Bull.* 51, 761–779.
- Stieber, S.J., 1970. Pulsed neutron capture log evaluation-louisiana gulf coast, in: Fall Meeting of the Society of Petroleum Engineers of AIME. Society of Petroleum Engineers.
- Swarbrick, R.E., 2001. Pore-Pressure Prediction: Pitfalls in Using Porosity, in: Offshore Technology Conference. Offshore Technology Conference.
- Swarbrick, R.E., Osborne, M.J., 1998. Memoir 70, Chapter 2: Mechanisms that Generate Abnormal Pressures: an Overview.
- Teale, R., 1965. The Concept of Specific Energy in Rock Drilling. *Int. J. Rock Mech. Min. Sci.* 2, 57–73. [https://doi.org/10.1016/0148-9062\(65\)90022-7](https://doi.org/10.1016/0148-9062(65)90022-7)
- Vidrine, D.J., Benit, E.J., 1968. Field Verification of the Effect of Differential Pressure on Drilling Rate. *J. Pet. Technol. (SPE 1859)* 20, 676–682. <https://doi.org/10.2118/1859-PA>
- Warren, T.M., 1987. Penetration Rate Performance of Roller Cone Bits. *SPE Drill. Eng.* 2, 9–18.
<https://doi.org/10.2118/13259-PA>
- Waughman, J.R., Kenner, V.J., Moore, A.R., 2003. Real-Time Specific Energy Monitoring Enhances the Understanding of When To Pull Worn PDC Bits. *SPE Drill. Complet. (SPE 81822)* 59–68.
- Weber, K.J., 1987. Hydrocarbon distribution patterns in Nigerian growth fault structures controlled by structural style and stratigraphy. *J. Pet. Sci. Eng.* 1, 91–104.
- Wei, M., Li, G., Shi, H., Shi, S., Li, Z., Zhang, Y., 2016. Theories and applications of pulsed-jet

- drilling with mechanical specific energy. *SPE J.* 21, 303–310.
- Yusuf, B., Oloruntobi, O., Butt, S., 2019. The formation bulk density prediction for intact and fractured siliciclastic rocks. *Geod. Geodyn.* <https://doi.org/https://doi.org/10.1016/j.geog.2019.05.005>
- Zhou, Y., Zhang, W., Gamwo, I., Lin, J.S., 2017. Mechanical specific energy versus depth of cut in rock cutting and drilling. *Int. J. Rock Mech. Min. Sci.* 100, 287–297. <https://doi.org/10.1016/j.ijrmms.2017.11.004>
- Zoback, M.D., 2010. Reservoir geomechanics. Cambridge University Press.

Chapter 7

7.0 Summary and Recommendations

7.1 Summary

The works presented in this manuscript have demonstrated the application of specific energies (HRSE and HMSE) to pore pressure prediction. The new techniques allow the formation pore pressure to be reliably predicted at the bit at relatively low cost. The field data required for the computation of these energies allow the formation pore pressure to be monitored real-time. Unlike the previous pore pressure prediction models from the drilling parameters, the inclusion of the bit hydraulic energy term in the new models allows accurate prediction of formation pore pressure under any subsurface drilling conditions (soft and hard rock environments). Pore pressure prediction from the new methods is based on the concept that overpressure intervals with lower effective stress will require less energy to drill than the normally pressured intervals at the same depth. In normally pressured intervals, the values of the specific energy computed over a uniform stratigraphic unit will increase with depth due to an increase in rock density and degree of rock compaction. In overpressure intervals, the specific energy values start to gradually deviate from the normal compaction trend to lesser values. The amount of deviation from the normal compaction trend at any given depth is generally related to the magnitude of overpressure. The higher the deviation, the greater the formation pore pressure. The concept of specific energy has also been extended to real-time identification of subsurface lithology. The accuracy of formation pore pressure prediction can be improved by improving the accuracy of overburden pressure computation via improvement in formation bulk density prediction. This thesis also presents a novel, simple and accurate techniques of estimating the formation bulk

density in areas where density logs are unavailable or unreliable. The new bulk density prediction models can be applied to a wide range of lithologies in siliciclastic environments. Finally, since pore and fracture pressures are closely related, this thesis presents a new fracture pressure prediction model that can be applied to normal and overpressure intervals in the Niger Delta basin. The main contributions of this thesis are highlighted below:

1. The development of a new pore pressure prediction technique from drilling parameters that incorporates the bit hydraulic energy term based on the concept of total energy consumed while drilling using downhole measurements.
2. The development of a new pore prediction technique from drilling parameters that incorporates the bit hydraulic energy term based on the concept of total energy consumed while drilling using only surface measurements.
3. The development of the new bulk density prediction models for siliciclastic rocks.
6. The application of specific energy concept to real-time lithology identification.
7. The development of a new fracture pressure prediction model for the Niger Delta.

7.2 Recommendations

Although the works in this thesis present new techniques of predicting pore pressure, fracture pressure (Niger Delta), bulk density and lithology, many knowledge gaps still exist, and future works can be used to address some of these gaps. These include but not limited to:

1. Excessive bit wear can mask the reversal in the specific trend when drilling through the overpressure and pressure transition zones. Therefore, specific energy models that incorporate wear factor term can be developed.

2. Just like the previous empirical relationships, the newly proposed formation bulk density prediction models in this thesis may not be applicable to rocks that contain microcracks/fractures. In consolidated formations that contain microcracks, changes in effective stress will cause substantial changes in compressional wave velocity with little or no changes in formation bulk density until all the microcracks are closed. The newly proposed models should be extended to rocks that contain microcracks/fractures by incorporating an additional parameter (shear sonic velocity) that will negate the effect of microcracks/fractures on compressional sonic velocity.
3. The newly proposed formation bulk density prediction models do not cover carbonate and evaporite environments. Similar models should be developed for these environments.